UNIVERSITY OF MODENA AND REGGIO EMILIA
PhD SCHOOL IN MOLECULAR AND REGENERATIVE MEDICINE
XXVI cycle

# *Unravelling new regulatory mechanisms and activities of the transcription factor NF-Y: implications for cancer therapy.*

***Thesis work by***
*Silvia Belluti*

***Supervisor***
Dr. Carol Imbriano

***PhD School coordinator***
Prof. Rossella Tupler

ACADEMIC YEAR 2012/2013

# TABLE OF CONTENTS

# 1. ABSTRACT

The transcription factor NF-Y is a heterotrimeric complex composed by three highly conserved subunits, NF-YA, NF-YB and NF-YC, all necessary for sequence-specific DNA binding. NF-Y is a fundamental regulator of cell proliferation and cell cycle progression, controlling particularly the transcription of G2/M genes, but also genes associated to DNA replication and repair.

Numerous findings highlight that NF-Y is involved in cancer. Although mutations in NF-Y subunits have never been specifically identified in tumours, systematic examination of protein expression profiles indicates that NF-YA is upregulated in different types of cancer. In addition, the analysis of global regulatory perturbations across human cancers pointed at NF-Y as one of the transcription factors responsible for oncogenic transcriptional changes.

Increased levels of the NF-Y-target gene Topoisomerase-IIα (TOP2A) have been identified in various cancer cells. TOP2A enzyme plays a fundamental role in DNA metabolism and chromatin organization. It is the target of many successful anti-cancer drugs, such as TOP2A poisons, which stabilize TOP2A-DNA cleavage complexes and create DNA double strand breaks (DSBs), leading to cell death. Here we show that the Curcumin-derivative bis-DemethoxyCurcumin (bDMC) irreversibly induces DSBs and apoptotic cell death selectively in cancer cells by targeting TOP2A activity and expression. Short-term exposure to bDMC induces retention of TOP2A-DNA intermediates, impairing TOP2A decatenating activity, while longer exposure inhibits TOP2A transcription by reducing the recruitment of NF-Y on its promoter, thus altering its chromatin status. Indeed, bDMC clearly impairs expression and sub-cellular localization of NF-Y subunits. Our findings suggest that the dual activity of bDMC on TOP2A represents a novel therapeutic strategy to induce persistent apoptosis in cancer cells and identify NF-Y regulation as a promising approach in anti-cancer therapy.

With the aim of developing NF-Y-targeted therapy, we investigated the molecular mechanisms controlling NF-Y subunits expression in cancer. Our studies highlight a complex autoregulatory loop which controls proper NF-Y expression, both at the level of gene transcription and of protein stabilization *via* protein-protein interactions.

Finally, taking into account that NF-YA nuclear levels increase at the onset of S phase and its inactivation affects the progression of cells through S phase, we investigated the role of NF-Y in DNA replication. Transcription and DNA replication are fundamental DNA metabolic processes that need to be finely regulated to preserve genome integrity and accumulating evidences suggest the involvement of transcription factors in the regulation of DNA replication. We exploited the *Xenopus*

*laevis* cell-free system to study cell-cycle regulated DNA replication in the absence of transcription, unravelling a novel non-transcriptional role of NF-Y in DNA replication. In human cells, silencing of NF-YA confirms that NF-Y is involved in DNA replication and further studies will better characterize which are the underlying molecular mechanisms.

All together, our results highlight that NF-Y plays both a transcriptional and non-transcriptional role in controlling cell proliferation, making NF-Y an attractive target for the development of anti-proliferative therapy in cancer cells.

# 2. INTRODUCTION: Nuclear Factor-Y (NF-Y)

## 2.1 Structure

Gene transcription is initiated by efficient sequence-specific binding of transcription factors (TFs) to DNA elements in promoters and enhancers, regulating chromatin structures.

NF-Y (Nuclear Factor-Y) was identified as a nuclear protein that recognize the CCAAT box with high affinity [Hatamochi et al.,1988; Chodosh et al.,1988]. NF-Y is a heterotrimeric complex composed of NF-YA, NF-YB, and NF-YC subunits, which are all required for binding to the CCAAT pentanucleotide [Dolfini et al.,2012a; Gnesutta et al.,2013]. Each subunit is characterized by a core region that is required for trimer interactions and DNA-binding and that is highly conserved throughout evolution. Indeed, the C-terminal domain of human NF-YA, the central part of NF-YB and the N-terminal domain of NF-YC display a sequence homology greater than 70% among species, while flanking regions are less conserved. The N-terminus of NF-YA and the C-terminus of NF-YC subunits contain Q-rich domains, enriched in glutamines and hydrophobic amino acids, which are more loosely conserved but include important transactivation functions [de Silvio et al.,1999; Mantovani,1999; Dolfini et al.,2012a].



NF-YB and NF-YC core regions show sequence homology to histones H2B and H2A, respectively, and are necessary for their heterodimerization, a prerequisite for NF-YA association and CCAAT box recognition [Baxevanis et al.,1995; Sinha et al.,1995; Romier et al.,2003; Gnesutta et al.,2013]. Indeed, functional mutagenesis studies of several residues in NF-YB and NF-YC histone fold motifs (HFMs) proved that these domains are important for dimer formation and DNA-binding [Xing et al.,1993; Sinha et al.,1996; Kim et al.,1996; Zemzoumi et al.,1999]. Romier et al. first characterized the structure of NF-Y, solving by x-ray crystallography the structure of the dimer formed by human NF-YB/NF-YC conserved regions, that are required for complex formation. The structure refined at 1.6 Å resolution highlighted that the two subunits interact through their histone fold motifs in a head-to-tail fashion ***(Figure 2.1A)***. HFMs are composed of three helices (α1, α2, and α3), separated by two loops (L1 and L2) and NF-YB/NF-YC structure is actually very close to that of the HFD-protein-pairs H2A/H2B ***(Figure 2.1B and 2.2A)*** and NC2α/NC2β, the TBP/TATA-binding negative cofactor 2 [Romier at al.,2003; Gnesutta et al.,2013].

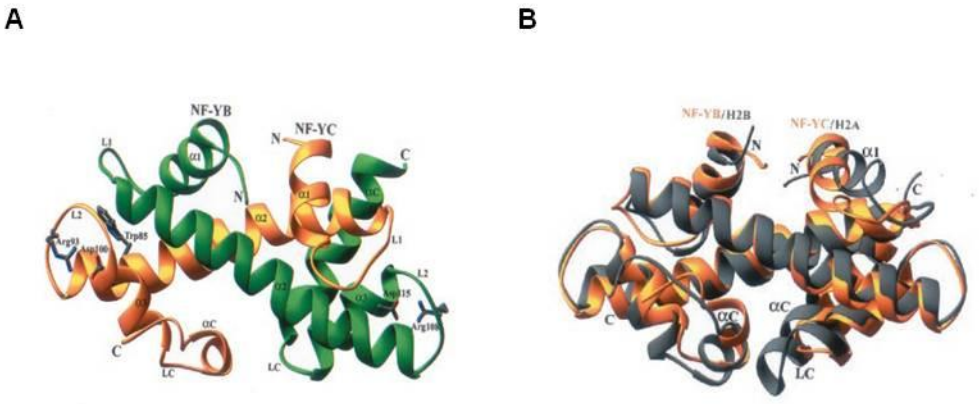


**Figure 2.1|** (A) Ribbon representation of NF-YB/NF-YC dimer structure and (B) comparison between the structures of NF-YB/NF-YC (in orange) and H2B/H2A (in grey) histone pairs. (Romier et al.,2003)

Nevertheless, differences in sequences and secondary structures account for diverse functional roles played by these histone-like proteins. NF-Y combines the ability to form stable (though aspecific) complexes with DNA of the HFM, with the capacity to target key functional locations. Photocross-linking experiments have demonstrated that all three subunits of NF-Y directly interact with DNA (Liang and Maity,1998). The general stability of the NF-Y/DNA complex is due to favourable van der Waals and electrostatic interactions, created between the highly basic surface of the NF-YB/NF-YC dimer and the negatively charged DNA sugar-phosphate backbone (Romier et al.,2003). Nevertheless, these interactions are not DNA sequence specific. In order to gain the distinctive affinity for the CCAAT pentanucleotide, NF-YA must stabilize the complex and only when the trimeric factor is assembled, it binds DNA with very high specificity (Mantovani,1999; Romier et al.,2003; Nardini et al.,2013). NF-YA provides sequence recognition potential through a relatively short protein segment. Within the evolutionarily conserved C-terminus of NF-YA, different domains have been identified (Romier et al., 2003; Nardini et al., 2013): an N-terminal A1 helix (residues 243–258) and a C-terminal A2 helix (272–280), with a 15-residue linker loop between them (A1A2 linker), followed by a loop containing a GxGGRF domain (284–289; x=any residue) ***(Figure 2.2A)***. Recognition of the CCAAT box is based on the insertion of the A2 helix in the DNA minor groove and the presence of the GxGGRF motif in the subsequent loop ***(Figure 2.2B)***. In the beginning, the A1 helix of NF-YA (positively charged) interacts with the predominantly negatively charged scaffold of HFM-subunits dimer. In particular, the NF-YC αC and α1 helices, together with NF-YB α2, are on one side of the NF-YC/NF-YB dimer and form a wide and negatively charged surface to which the NF-YA A1 helix can bind (Romier et al., 2003; Nardini et al., 2013) .

Consistently, NF-YA binding is influenced by mutations in NF-YB α2 helix [Sinha et al., 1996], as well as in both helices α1 and αC of NF-YC [Kim et al., 1996; Zemzoumi et al., 1999].

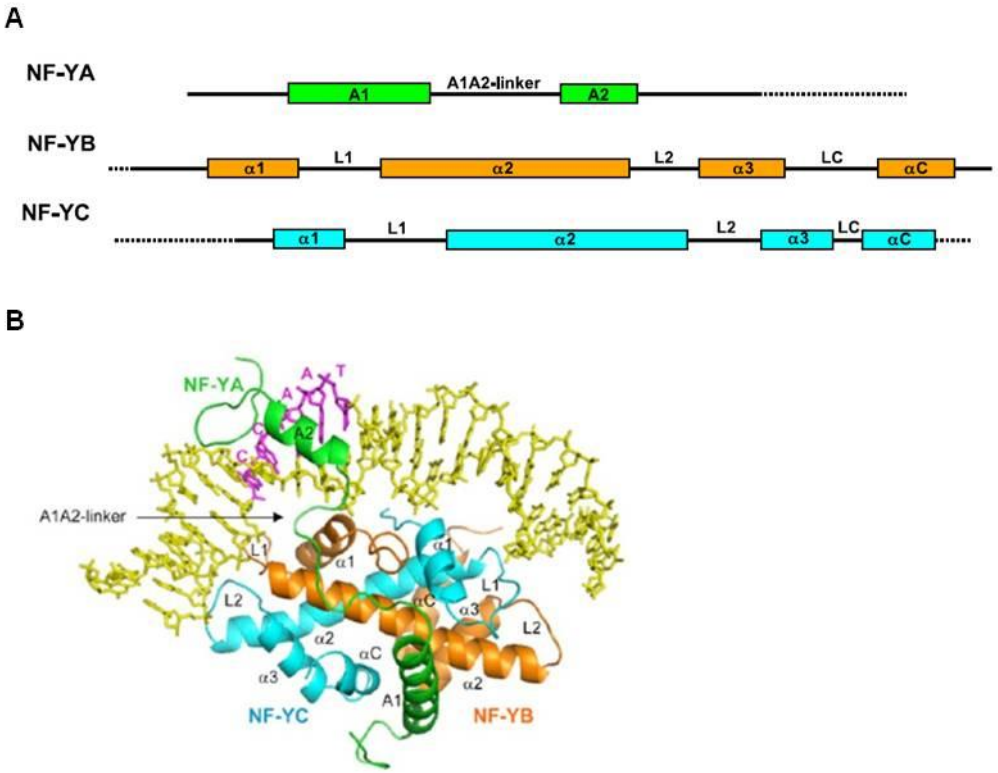


**Figure 2.2|** (A) schematic representation of the conserved domains of NF-Y subunits required for DNA interactions and (B) Ribbon representation of NF-YA/NF-YB/NF-YC trimer structure in complex with a 25bp NF-Y-target DNA, containing the CCAAT box (Nardini et al.,2013).



An interesting structural feature of the NF-Y/DNA complex is that the insertion of NF-YA A2 helix into the DNA minor groove determines a global DNA bending of ~80° centred on the CCAAT box [Liberati et al., 1999; Nardini et al., 2013] ***(Figure 2.2B)***. Most importantly, this distortion of the DNA, together with the active recruitment operated by NF-YA and NF-YC trans-activation domains [Roeder,1996; Izumi et al.,2001], allow the binding of other regulatory factors to the adjacent DNA, thus mediating transcriptional regulation. Notably, NF-YA seems to be the limiting subunit for NF-Y functionality, since HFM subunits are more abundant *in vivo*.

## 2.2 The CCAAT box and genomic binding of NF-Y

As mentioned above, the eukaryotic transcription factor NF-Y specifically binds the regulatory CCAAT motif, that is found in ~30% of the promoters.

All bases of the pentanucleotide are crucial for NF-Y recruitment, and in all promoters tested, mutations of the CCAAT motif impair gene transcription. Nevertheless, also the flanking sequences on both sides of CCAAT are important for successful DNA binding *in vitro* and *in vivo* (Kim et al.,1990; Mantovani,1999; Testa et al.,2005; Ceribelli et al.,2008; Dolfini et al.,2009).***(Figure 2.3)***


**Figure 2.3|** (A) Sequence Logo of NF-Y consensus sequence optimized with ChIP on chip data (Dolfini et al.,2009) and (B) sequence logo of the NF-Y DNA-binding site identified with 12655 NF-YB peaks from ChIP-seq performed in K562 cells (Fleming et al.,2013).



At many promoters, the CCAAT element is found ~80 bp upstream of the transcriptional start site (TSS), in either CCAAT or ATTGG orientation, indicating that its location is important for gene expression.

NF-Y has been associated to the control of G2/M progression by several studies (Bolognese et al.,1999; Elkon et al.,2003; Linhart et al.,2005). In fact, NF-Y modulates the transcription of a number of key regulators of this phase, such as Cdc2, CyclinB1 and CyclinB2, but it also controls promoters active in G0/G1 phase (e.g., PDGFβ-R, c-Jun and JunB), G1/S (as E2F1, PCNA, CyclinA) and S/G2 phases (e.g., TopoisomeraseIIα, Cdc25C) (Caretti et al.,2003; Salsi et al.,2003) ***(Figure 2.4)*.**

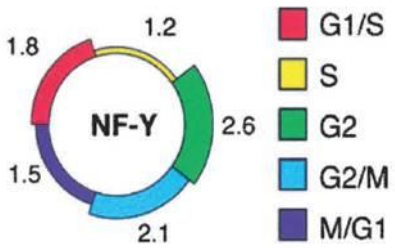


**Figure 2.4|** Representation of the prevalence of NF-Y binding motif in promoters of cell-cycle-regulated genes *versus* a background set of promoters (Elkon et al.,2003).

*In vivo*, chromatin immunoprecipitation (ChIP) experiments determined that the precise transcriptional activity of NF-Y across the cell cycle results from its timely-

regulated binding to specific cell cycle promoters [Caretti et al.,2003]. Additionally, NF-Y is an important player in the control of G2/M genes during the DNA-damage response, by mediating the p53-dependent repression of G2/M genes [Imbriano et al.,2005]. Recently, the growing informations derived from transcriptome studies, bioinformatics analyses and ENCODE genome-wide data have expanded the knowledge about genomic binding of NF-Y [Dolfini et al.,2009; Benatti et al.,2011; Wang et al.,2012; Fleming et al.,2013].

When NF-Y dependent CCAAT genes were analyzed in relation to Gene Ontology (GO) categories, the most significant terms were Cell division and M phase, in line with the fact that NF-Y motifs were the most abundant signal in G2/M phase promoters [Linhart et al.,2005; Dolfini et al.,2009]. These data were confirmed by the gene expression profiles obtained after NF-Y inactivation [Benatti et al.,2008,2011], which included additional categories such as DNA metabolism, cell cycle, chromatin and endoplasmic reticulum genes.

Bioinformatic and ChIP on chip experiments [Ceribelli et al.,2008; Dolfini et al.,2009] highlighted that multiple CCAAT are present in the majority of NF-Y-dependent promoters, especially G2/M ones (e.g., the triple CCAAT Cyclin B2 promoter)[Bolognese et al.,1999; Salsi et al.,2003]. Analyses of the respective distances between CCAAT sequences showed peaks at 32, 42 and 53 nucleotides, corresponding to 3, 4 and 5 turns of the double helix, respectively. Only a few CCAAT are more distant than 80 bp or closer than 24 bp, that is the minimum allowed distance so that sites are not mutually exclusive [Liberati et el.,1999; Salsi et al.,2003].



Very recently, Fleming et al. investigated the genome-wide binding of NF-Y in three tumour cell lines (K562, GM12878 and HeLa S3). This study confirmed that NF-YA binds directly on the CCAAT pentanucleotide, while NF-YB binding is about 15 bp downstream from the CCAAT box, indicating that NF-Y binds asymmetrically at its target sites [Romier et al.,2003; Nardini et al.,2013].

Broad ChIP-sequencing analyses of NF-Y further validated its presence at proximal promoters, particularly in growth controlling genes. GO analysis of NF-Y sites in different cancer cell lines revealed a strong enrichment of genes involved in cell-signalling pathways, cell cycle (G2/M checkpoints and regulation of DNA replication), DNA repair (homologous recombination and base excision), and metabolism (cholesterol biosynthesis and polyamines). In addition, NF-Y regulates genes involved in transcription, mRNA splicing, processing and transport, together with a large number of TFs, including the NF-Y genes themselves. Accordingly, NF-Y seems to be a regulator of gene expression regulators [Fleming et al.,2013].

Even though NF-Y has been generally identified as a factor that binds to gene promoters, only 22% of NF-Y sites are within 1 kbp upstream of a RefSeq Transcription Start Site (TSS) and ~30% of NF-Y sites co-localize with histone modifications characteristic of promoters. More generally, only one third of NF-Y binding is linked to active promoters, as determined by high levels of di- and trimethylated H3K4, acetylated H3K27 and H3K9, RNA PolymeraseII and depletion of nucleosomes. When bound to proximal promoters, NF-Y is essentially positioned at -40 to -100 bp upstream of the TSS, similar to the position of the CCAAT motif (Dolfini et al.,2009; Fleming et al.,2013). ***(Figure 2.5)***.

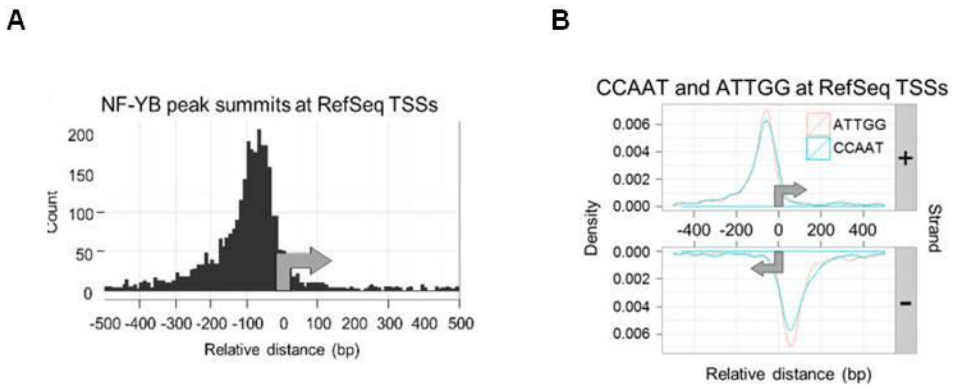


**Figure 2.5|** (A) Frequency distribution plot of K562 NF-YB peak summits at RefSeq TSSs and (B) Gaussian kernel density distribution in positive and negative strand of CCAAT and ATTGG sequences at K562 NF-YB-bound RefSeq TSSs. (Fleming et al.,2013).



Interestingly, also novel NF-Y functions have emerged, related to its recruitment at tissue-specific enhancers and also in "closed" chromatin regions, including LTRs (Fleming et al.,2013).

It is noteworthy that cell-type-specific NF-Y loci are enriched in enhancers, if compared with NF-Y sites common to all cell types. This suggests that experimental depletion of NF-Y through RNAi can affect both promoters and enhancers relevant for transcription of neighbouring genes.

Unexpectedly, in K562 cells 40% of NF-Y binding sites overlap an LTR, the promoter elements of endogenous retroviruses: these loci maintain considerable NF-Y occupancy, although they appear to be inactive.

Differently from other TFs, such as E2Fs and MYC, NF-Y is not excluded from any chromatin state. However, while CCAAT motifs located within "open" chromatin regions shows near-saturated levels of NF-Y binding (about 80% occupancy), ~20% of CCAAT motifs into "closed" chromatin or transcription elongation states are bound by NF-Y.

Only a small number of "pioneer" transcription factors can efficiently bind to their DNA consensus sequences located in closed chromatin, thus recruiting chromatin-modifying factors and partner TFs to enhance transcription. *In vitro,* NF-Y can associate with a CCAAT motif after nucleosome assembly, and the NF-YB/NF-YC dimer can interact with H3/H4 histones both in solution and on DNA (Caretti et al.,1999; Nardini et al.,20113). This means that NF-Y could be pioneer TF, with histone-like features and high-sequence specificity, that is able to access its motif irrespective of the chromatin state.

## 2.3 NF-Y interactions with other TFs and coregulators

Bioinformatic analysis of CCAAT promoters showed a co-occurrence with SP1, E2F, CREB motifs (Dolfini et al.,2009). *In vivo*, from the large number of available ChIP-seq data in K562, it was evident that NF-Y co-associates with 44 factors at promoters and 50 factors at enhancers (Fleming et al.,2013). Indeed, multiple TFs are usually required for transcription in mammalian cells. In promoter regions, NF-Y is associated with factors including FOS, CHD2, TBP, PolymeraseII, HMGB2, MYC and E2F4/6, although mainly FOS seems to be specifically associated with NF-Y. Differently, at enhancers NF-Y interacts with FOS, USF1/2, MAX, CHD2, and E2F4. ***(Figure 2.6)***. All these TFs interact with either NF-YA or the HFD dimer and, in most cases, these relationships lead to synergistic activation of transcription (Dolfini et al.,2012a).



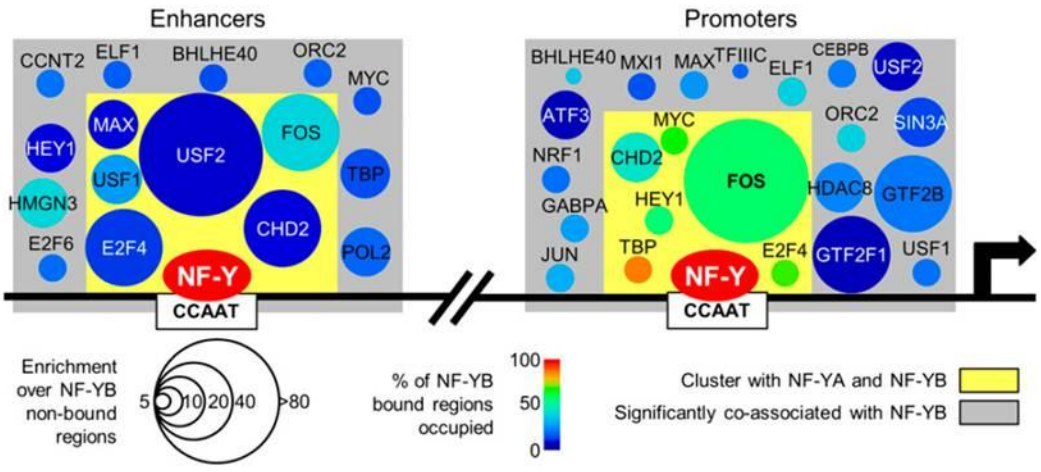


**Figure 2.6|** Illustration of the factors that significantly associate with NF-YB-bound promoters and enhancers (Fleming et al.,2013).

The identified partnership of NF-Y with TFs that control cell proliferation and play important roles in cancer, points at the importance of NF-Y in regulating cell growth and proliferation.

Besides, NF-Y is generally required to establish the chromatin environment in proximity of the TSS, allowing further activators/coactivators recruitment. As demonstrated by functional inactivation of NF-Y subunits or the use of a dominant-negative NF-YA, NF-Y influences the pattern of histone post-translational modifications at CCAAT promoters. Different histone post-translational modifications have been associated to specific chromatin states (Kouzarides,2007): for instance, accessible chromatin that is active or poised to rapid induction, is marked by acetylations of H3 and H4 and methylation of H3K4 (H3K4me3), H3K36 (H3K36me3) and H3K79 (H3K79me2). On the contrary, other methylations, such as H3K9me3, H3K27me3 and H4K20me3, are associated with heterochromatin, both constitutive or facultative.

NF-Y timely-regulated binding to cell cycle promoters provides a DNA-binding platform that allows interactions with the histone acetyltransferases (HATs) hGCN5, P/CAF and p300 (Currie,1998; Uramoto et al.,2004). Recruitment of p300 appears to be mediated by NF-Y and correlates with activation of transcription (Gurtner et al.,2008), while PCAF/hGCN5 are often found before NF-Y association. A hierarchy of PCAF-NF-Y-p300 connections are then required for acetylation of H3 and H4 histones and for activation of cell cycle promoters (Caretti et al.,2003; Salsi et al.,2003).



Moreover, positive histone methylations, including H3K4me3, H3K36me3 and H3K79me2 are dependent on NF-Y binding (Donati et al.,2008; Gurtner et al.,2008), while negative heterochromatic marks (H3K9me3 and H4K20me3) are imparted to silenced cell cycle genes upon NF-YA removal (Gurtner et al.,2008). Fine tuning of H3K4 methylations is particularly intriguing: NF-Y is required for mono– and tri-methylation, but not di-methylation of H3K4 (Donati et al.,2008). Indeed, NF-Y is able to recruit the Lysine-demethylase KDM1 (LSD1) and coREST cofactor, thus supporting the di- to mono-methylation switch of H3K4. Furthermore, NF-Y binding is necessary to recruit key components of the MLL methylating complex (MLL1, Menin and hASH2L) and for deposition of H3K4me3 and H3K79me2 (Donati et al.,2008; Fossati et al.,2011). Interestingly, Lys138 of NF-YB is a site of monoubiquitination structurally related to histone H2B Lys120, that has been characterized as one of the earliest marks in transcribed genes. This raised the hypothesis that NF-YB-K138 could play an important role in establishing the chromatin environment at gene promoters, by allowing the deposition of H3 methylations and H2B ubiquitination (Dolfini et al.,2012a; Nardini et al.,2013).

Notably, an emerging theme is the mechanism of transcriptional repression mediated by NF-Y. Genome-wide studies pointed out several NF-Y sites associated to the negative histone marks H3K27me3 and H4K20me3 (Ceribelli et al.,2008). Moreover, negative regulation through histone deacetylation was associated to NF-Y: in particular, the histone deacetylases HDAC1, HDAC4 and the corepressive complex

HDAC1/SIN3A can be recruited to target promoters *via* NF-Y (Imbriano et al.,2005; Basile et al.,2006; Peng et al.,2007; De Amicis et al.,2011). Besides, in growth regulating genes, such as G2/M promoters, NF-Y can interact with MYC and p53 family members, which thus repress transcription from CCAAT sites (Jung et al.,2001; Uramoto et al.,2004; Imbriano et al.,2005; Testoni and Mantovani,2006).

As a result, NF-Y is a bifunctional CCAAT-binding factor, that is important for the assembly of either activating or repressive complexes on its target promoters (Park et al.,2002; Peng at al.,2007; Ceribelli et al.,2008; De Amicis et al.,2011).

## 2.4 Regulation of NF-Y subunits

*Expression and post-translational modifications*

NF-Y is fundamental for activation of growth-controlling and growth–promoting genes and all immortalized and transformed cell-lines described so far express all of the three subunits. However, certain types of normal cells lack of NF-YA: in myocytes, the protein level drops during terminal differentiation to myotubes (Gurtner et al.,2003,2008), while it is absent in circulating monocytes but it increases when cells are activated towards antigen-presenting macrophages (Marziali et al.,1999). Moreover, NF-YA levels are progressively decreased in primary cells undergoing senescence (Matuoka and Chen,2002).



While NF-YB and NF-YC expression is essentially constant throughout the cell cycle, NF-YA protein levels are high in G1, further raise in S, and then decline in the G2/M phase. Interestingly, these variations seem to be controlled at the post-transcriptional level, because NF-YA mRNA levels are relatively constant in growing cells (Bolognese et al.,1999). A competition between ubiquitynation and acetylation of neighbouring Lysine residues might represent a mechanism to regulate NF-YA protein stability (Manni et al.,2008). Indeed, NF-YA can be ubiquitynated at Lysines 283, 289, 292, and 296, and two of these ubiquitynated lysines (K283, K289) can also be acetylated by p300 (Manni et al.,2008) ***(Figure 2.7A)***. Therefore, NF-YA acetylation could restrain its ubiquitynation, interfering with the ubiquitin–proteasome pathway and eventually with protein degradation. As for post-translational modifications, NF-YA also undergoes cell cycle-dependent phosphorylation, overlapping with periodic activation of CDK2 kinase (Yun et al.,2003; Chae et al.,2004). NF-YA protein can be phosphorylated in two Serines (S292 and S298) close to the DNA binding domain: this is not required for its interaction with the NF-YB/NF-YC heterodimer, but it is important for efficient binding to DNA.

*Splicing*

It is known that the majority of mammalian genes are differentially spliced and NF-Y is not an exception. Specifically, NF-YA has two isoforms, namely "long" (NF-YAl) and "short" (NF-YAs) [Li et al.,1992]. NF-YAs derives from alternative splicing of exon3 and lacks 28 amino acids in the Q-rich transactivation domain ***(Figure 2.7A)***.

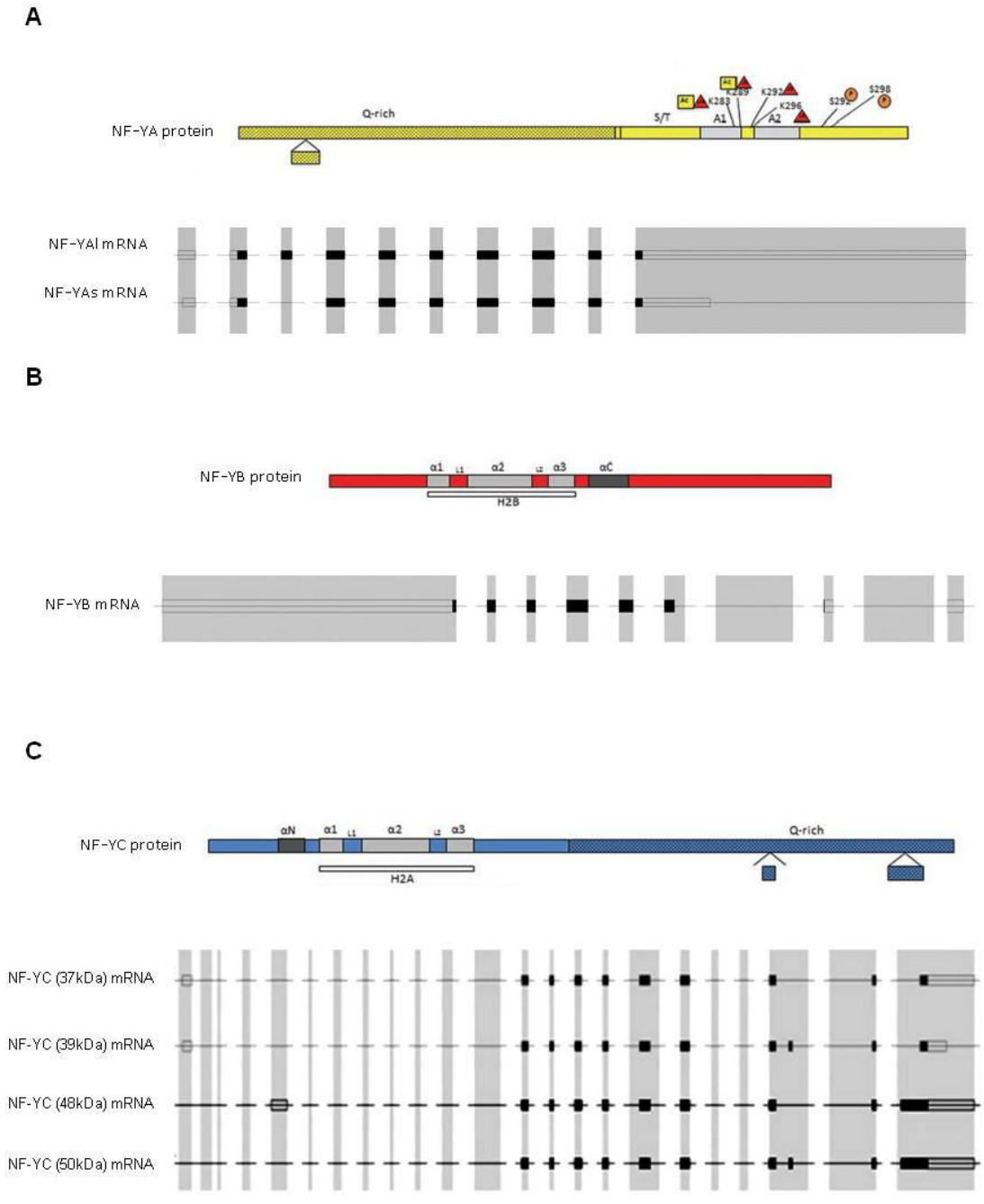


**Figure 2.7|** Schematic representation of (A) NF-YA, (B) NF-YB and (C) NF-YC proteins and mRNAs, indicating differentially spliced regions/exons, protein domains and residues involved in post-translational modifications. In mRNA annotations, empty boxes indicate untranscribed exons, full boxes represents coding exons (Dolfini et al.,2012a; Flicek et al.,2013).

It is not clear whether the expression of one or the other NF-YA transcript affects the expression of NF-Y target genes. However, the relative abundance of the two variants is different among cell types and it seems to regulate cell proliferation and differentiation. In particular, NF-YAs is the transcript isoform responsible for proliferation of stem cells in different tissues. A switch from the NF-YAs isoform to NF-YAl was recently observed during differentiation of mouse embryonic stem cells towards embryoid bodies [(Dolfini et al.,2012b)]. Besides, NF-YAs is also necessary for maintenance of stem cells in the hematopoietic system [(Zhu at al.,2005)], supporting the hypothesis of a functional diversification of the two NF-YA isoforms.

NF-YB subunit is ubiquitously expressed and no differential splicing events have been described in mammals ***(Figure 2.7B)***. NF-YB can be acetylated and ubiquitynated, but the specific roles of these modifications have not yet been elucidated [(Li et al.,1998; Salsi et al.,2003; Manni et al.,2008)].

As far as NF-YC is concerned, a first indication that this subunit is differentially spliced was the discovery of a shorter mRNA lacking 62 amino acids inside the HFD, named NF-YCb [(Chen et al.,2002)]. However, this isoform is largely localized in the cytoplasm and is not assembled into functional NF-Y trimers. Ceribelli et al. then described many NF-YC isoforms, as a consequence of alternative splicing and of the presence of two alternative promoters (P1 and P2). At least four NF-YC splicing variants were identified in human cell lines, that are translated into the canonical 37 kDa protein rather than into polypeptides of 39, 48 and 50 kDa [(Ceribelli et al.,2009)]. The region affected by alternative splicing events is in the Q-rich transactivation domain of NF-YC. The new transcripts coding for NF-YC (48kDa) and NF-YC (50kDa) retain an additional 312bp exon downstream of exon 9 (named exon 9bis), while NF-YC (39kDa) has an extra 57bp exon downstream of exon 8 (named exon 8bis). The longer NF-YC (50kDa) isoform includes both exon 8bis and 9bis ***(Figure 2.7C)***. Analysis of 13 human cell lines showed that the different NF-YC mRNAs coexist inside the cell, with the 37kDa transcript being the prevalent one. In addition, a second promoter (P2) has been identified into the first intron of the RefSeq NF-YC (37kDa) mRNA [(Ceribelli et al.,2009)]. P1 promoter seems to be the housekeeping promoter in various cell lines, while P2 promoter has a lower basal activity, but can be activated depending on the cellular environment. Both promoters contain CCAAT boxes, and ChIP experiments confirmed that NF-Y is bound to both promoters.



*Localization*

Besides gene and protein expression, subcellular compartmentalization is another important level of regulation for DNA-binding proteins. Immunofluorescence experiments showed that NF-YA has predominant nuclear localization in

proliferating cells, whereas NF-YC and NF-YB are also present in the cytoplasm (Frontini et al.,2004), even though in S phase they seem to relocate inside the nucleus as well. NF-YA has a nonclassical Nuclear Localization Signal (NLS) in the conserved C-terminal region of the protein, which allows Importinβ-mediated transfer inside the nucleus. Therefore, NF-YA is imported inside the nucleus separately from the other subunits.

Differently, the HFM-subunits take part in the nuclear localization of the histone fold partner: nuclear localization of NF-YC depends on its interaction with NF-YB. NF-YB and NF-YC do not contain any autonomous NLS and their nuclear transport as a heterodimer depends on Importin13. (Frontini et al.,2004; Kahle et al.,2005)

## 2.5 NF-Y and disease

Although mutations in genes coding for NF-Y subunits have never been described, several reports indicated that alterations of NF-Y functions may contribute to the pathogenesis of various diseases. Systematic evaluation of protein expression profiles of cancer cells indicated that NF-YA is often upregulated in lymphomas, gliomas, breast and endometrial cancers, as well as in some cervical, lung and ovarian cancers (Uhlen et al.,2010; Garipov et al.,2013). Moreover, NF-Y binding-sites are enriched in promoters of genes overexpressed in cancers, such as in the breast, colon, thyroid and prostate tumours, as well as in leukemia, as described in a recent review (Ly et al.,2013). Besides, a number of key regulators of the cell cycle, such as Topoisomerase IIα, Cdc2, Cyclins and Cdc25C, and anti-apoptotic genes, among which Bcl-2 and BI-1, are under the transcriptional control of NF-Y (Hu et al.,2002; Caretti et al.,2003, Benatti et al.,2008). On the whole, NF-Y controls both cell cycle-related genes and human disease-related genes.



*Polyglutamine diseases* offer a few good examples of NF-Y-associated human diseases. Huntington disease is a neurodegenerative disorder caused by mutations in Huntingtin (HTT) protein which lead to expansion of polyglutamine tracts. In post-mitotic neurons of striatum and cortex, mutant HTT binds many TFs and cofactors with Q-rich activating domains, thus restricting their activity. Recent analyses performed on mice models of HD highlighted that the subunits containing a Gln-rich domain, that are NF-YA and NF-YC, can form complexes with HTT (Yamanaka et al.,2008). Their accumulation into cytosolic aggregates depleted the nuclear compartment, reducing CCAAT-binding activity in neurons: this determines a downregulation of Heat Shock Proteins HSP40 and HSP70 and worsen the effects of misfolded protein aggregates, increasing neurologic toxicity.

Another polyglutamine disease which involves NF-Y is the SpinoCerebellar Ataxia Type 17 (SCA17), caused by Gln expansion in the TBP factor. TBP and NF-Y co-

activate a few genes, including those of HSP chaperones. Huang et al. recently reported that, *in vivo*, polyglutamine-TBP determines NF-YA aggregates, and results in degeneration of cerebellar Purkinje cells (Huang et al.,2011). The exact contribution of NF-Y to the pathogenesis of HD and SCA17 has not been well established, but initial analyses suggest that it could be worth to define that mechanisms.

A different category of pathologies that could be linked to NF-Y misfunctions is that of *Hematopoietic disorders.* Indeed, NF-Y orchestrates the tissue- and developmental stage- specific expression of human γ-globin genes (HBG1 and HBG2) (Zhu et al.,2012), recruiting either transcription activators or repressors, that are GATA-2 and BCL11A, respectively. Expression of γ-globin should be limited to fetal liver, bone marrow and spleen, but in some β-thalassemias γ-chain production persists until adulthood.

In a different study, specific expression of Hoxb4 was found to be dependent on NF-Y (Gilthorpe et al.,2002), given that the transcriptional activator NF-Y and the repressor protein YY1 mediate opposing transcriptional effects through the same site. This is a relevant finding, since expression of Hoxb4 determines the expansion of hematopoietic stem and progenitor cells *in vivo* and *in vitro*. This makes of NF-Y a prospective candidate for therapeutic stem cell expansion in leukemia therapy.



Finally, NF-Y also plays a role in regulation of the MHC gene. This is a cell surface molecule which allows interactions of leukocytes, determining susceptibility to autoimmune diseases *via* cross-reacting immunization (Villard et al.,2000).

Moreover, current studies in the Drosophila system demonstrate novel roles of NF-Y in *eye development* and apoptosis (Ly et al.,2013).

*Apoptosis* (programmed cell death) is a vital cellular process which allows to remove damaged cells: a deficiency in apoptosis often results in development of tumours and/or autoimmune diseases, while excess of cell death is associated with neurodegenerative diseases.

As concerns the role of NF-Y in apoptosis and DNA-damage processes, NF-Y controls cell cycle promoters in response to DNA damage, through p53-dependent transcriptional inhibition (Imbriano et al.,2005; Imbriano et al.,2012). p53 is indirectly bound to CCAAT-promoters through NF-Y and, upon DNA damage, the NF-Y/p53 complex recruits histone-deacetylases (HDACs) and releases acetyltransferases (HATs), thus converting the chromatin structure into a repressive non-transcriptional state.

Interestingly, it is well-known that more than 50% of tumours are associated to p53 mutations, many of which are Gain-of-function (GOF) mutations. One of the most prevalent GOF mutants, R175H, is able to convert the repressive wt-p53 attitude at CCAAT boxes, into activation of growth promoting genes (Di Agostino et al.,2006; Imbriano et al.,2011).

A growing number of gene expression profile experiments support the notion that activation of CCAAT-dependent genes is crucial in cell transformation ***(Figure 2.8)***. NF-Y cooperates with neighbouring transcription factors and oncogenic factors [(Wang et al.,2012)], consistently with the enrichment of CCAAT motifs in the promoters of genes overexpressed in *cancer* [(Goodarzi et al.2009; Dolfini et al.,2012a)].

**Analysis of TFBS in promoters of genes overexpressed in human cancers.**

| CANCER TYPE | ENRICHED TFBS | REFERENCE |
|---|---|---|
| Human embryonic lung fibroblasts (WI-38) and *in vitro* cancerous transformation process | **NF-Y, E2F,** CDE, ELK1, CHR, CHR-**NF-Y**-CDE | Tabach et al., 2005 |
| Small Cell lung Cancer, Leukemia, Lymphoma<br>DLBCL<br>Squamous Cell Lung Carcinoma<br>Lung adenocarcinoma<br>Breast Cancer, Prostate Cancer<br>Hepatocellular Carcinoma<br>Adrenocorticoal Carcinoma | **NF-Y** | Rhodes et al., 2005 |
| Brest Cancer<br>Estrogen treatment | **NF-Y, E2F**, NRF1 | Scafoglio et al., 2005 |
| Anaplastic Thyroid Carcinoma | **NF-Y, E2F** | Salvatore et al., 2007 |
| U87, A549, LAN1, SHEP, NCIH929<br>Ras inhibitor S-farnesylthiosalicylic treatment | **NF-Y, E2F,** FOS | Blum et al., 2007 |
| Brest Cancer cell metastasis | **NF-Y,** YY1, **E2F** | Thomassen et al., 2008 |
| Brest Cancer Cell<br>Malignant progression | **NF-Y**, ELK1, E2F, NRF1 | Niida et al., 2008 |
| Hormone Refractory Prostate Cancer | **NF-Y**, SP1, **E2F1**, CREB1, TFAP2A | Calvo et al., 2009 |
| Burkitt's Lymphoma | **NF-Y, E2F,** ELK4, NF-AT, MYB, Let7, SP1 | Goodarzi et al., 2009 |
| Prostate Cancer<br>Fetal Prostate stem cell | **NF-Y, E2F,** ETF/TEAD2, AP2, AhR/Arnt | Blum et al., 2009 |
| HCT116 (colorectal cancer)<br>P27 target genes<br>P27 and P16 targets | **NF-Y, E2F** | Yamanaka et al., 2009 |
| Normal Hematopoietic Stem Cell (HSC) | **NF-Y**, Evi-1, ATF4, IRF1, NF1, Ik1, CMYC/MAX, MAZ | Fosberg et al., 2010 |
| Colorectal Cancer<br>MER/ERK pathway regulated genes | **NF-Y, E2F** | Jurchott et al., 2010 |
| Follicular Lymphoma<br>Breast Cancer<br>HCV infected liver cancer<br>Leukemia<br>Diffuse large B-cell lymphoma (DLBCL)<br>CNS tumor<br>Liver/Lung Cancer<br>GC-DLBCL<br>B lymphoma | **NF-Y**<br><br><br><br><br>**NF-Y, E2F** | Sinha et al., 2010 |

**Figure 2.8|** The studies in which NF-Y binding site was reported to be enriched in genes overexpressed in cancer are listed, together with the other signicant TFs (Dolfini et al.,2012a).

The assessment of 46 microarray studies of cancer *versus* normal tissues identified the role of many known transcription factors and miRNAs in cancer, taking a step forward in the knowledge of regulatory perturbations in cancer [(Goodarzi et al.2009)]. As expected, pathways involved in cell growth and proliferation, such as mitotic cell

cycle, DNA replication and chromatin-assembly genes, are upregulated in tumour samples as compared to normal data sets ***(Figure 2.9)***. Metabolic pathways, such as glycolysis, are also upregulated in many malignancies, whereas stress responses that lead to cell-cycle arrest, such as "negative regulation of progression through cell cycle" are often downregulated. As shown in the pathway-regulatory interaction map ***(Figure 2.9)***, genes with a NF-Y-binding site are significantly associated with sterol biosynthetic process, antigen processing and presentation, chromatin assembly and modification and mitotic cell cycle. As this last GO term concerns, it is already known that NF-Y can promote tumorigenesis through cyclin B2 overexpression, for instance (Park et al.,2007).

Taken together, these results suggest that targeting NF-Y interactions with DNA could be a potential strategy for blocking proliferation of cancer cells.

# 3. AIM OF THE WORK

Although mutations of NF-Y genes have never been identified in human diseases, it is increasingly accepted that NF-Y activity is involved in the development of different pathologies. Misregulated transcriptional activity of NF-Y can be determined by altered binding at promoters or association with mutated proteins. Since NF-Y-dependent genes and NF-Y itself play a key role in tumour formation and/or progression, targeting NF-Y interactions with DNA could be a potential strategy for blocking proliferation of malignant cells. With the aim to deepen our knowledge of NF-Y biology and to develop new NF-Y targeted therapies, we studied three different aspects of NF-Y activity:

I. The inhibition of NF-Y binding to DNA as a valid strategy to block proliferation of cancer cells;
II. The complex regulation of NF-Y subunits expression, both at the transcriptional and post-translational levels;
III. The non-transcriptional role of NF-Y in controlling cell proliferation.

# 4. TASK I:
# TARGETING NF-Y IN CANCER CELLS

## 4.1 Background

### 4.1.1 Topoisomerase IIα

Expression of human DNA topoisomerase IIα gene (TOP2A) is highly regulated by the binding of NF-Y to its promoter (Benatti et al.,2008 and 2011). TOP2A is a homodimeric nuclear protein that solves the DNA topological problems throughout the cell cycle (Vos et al.,2011). Indeed, transcription and replication of DNA imply topological modifications in its double-stranded conformation: TOP2A can reduce supercoiling of DNA during DNA synthesis and also decatenates sister-chromatids entanglements at mitosis. TOP2A performs its activity through a double-stranded break in the DNA backbone, the passage of another portion of the duplex through the break, and the religation of the cleaved DNA(Deweese et al.,2008). While TOP2A is carrying out the decatenation cycle, the enzyme establishes covalent interactions with the cleaved DNA strand, producing a transient TOP2-DNA cleavable complex (TOP2-cc).



TOP2A is an ubiquitous enzyme, but its expression fluctuates throughout the cell cycle: its level is low in G1 phase, increases during S phase and peaks at the G2/M phase interface (Woessner et al.,1991), consistently with the importance of TOP2A for DNA replication, mitosis and cell proliferation. Interestingly, Topoisomerases are part of the chromosome scaffold in mitosis (Wang,2002; Cortès et al.,2003; Nitiss,2009a) and TOP2A has been associated to the decatenation checkpoint. Catenations between sister chromatids need to be eliminated prior to mitosis, to permit accurate chromosome condensation and segregation: TOP2A plays a crucial role in delaying the onset of mitosis until complete disentanglement has occurred (Luo et al.,2009).

Expression of TOP2A seems to be mainly regulated at the transcriptional level (Magan et al.,2003): within the first 617bp of the promoter there are several *cis*-acting elements (Hochhauser et al.,1992), specifically two Sp proteins consensus sites (GC1and GC2) and four inverted CCAAT boxes (ICB1–ICB4). An additional ICB (ICB5) is present in the 5'UTR, into the first exon of TOP2A gene. NF-Y is the main transcriptional activator of TOP2A (Benatti et al.,2008 and 2011): the binding of NF-Y to four of five ICBs present in TOP2A regulatory region has a positive effect on transcription. Conversely, NF-Y binding to ICB2 has been associated to confluence-

induced repression of TOP2A [Isaacs et al.,1996]. Moreover, NF-Y is involved both in p53-dependent and -independent negative regulation of TOP2A, whose transcriptional levels can be reduced by decreasing NF-Y binding to ICB1 or by the recruitment of p53 at ICB sites [Joshi et al.,2003].

Due to its central role in cell proliferation, TOP2A is actually an important target for clinically useful anticancer agents [Nitiss 2009b; Pommier 2013], since rapidly growing cancer cells often express high levels of TOP2A.

Drugs targeting TOP2A can be classified as either TOP2 catalytic inhibitors or TOP2 poisons [Nitiss 2009a and b]. TOP2 poisons trap TOP2-cc intermediates, generating enzyme-mediated DNA damage: these agents include both DNA-intercalating (such as Doxorubicin and other Anthracyclines, Mitoxantrone, mAMSA) and non-intercalating agents (such as Etoposide and Teniposide). As concerns these latters, it has been suggested that protein-drug interactions have a crucial role in trapping TOP2-cc. Differently, several groups of compounds can inhibit TOP2 activity without affecting DNA cleavage, by blocking the enzyme in a non-covalent clamp around DNA. DNA damage can subsequently be generated when DNA/RNA polymerases collide with these trapped complexes, triggering nucleolytic and/or proteolytic processing. Catalytic inhibitors are either non-hydrolysable ATP analogues or, mostly, non-competitive ATPase inhibitors, as the Bisdioxopiperazines ICRF-187 and ICRF-159 [Nittis,2009a and b].



DNA lesions resulting from TOP2A inhibition can be detected by the DNA damage checkpoint, that arrests cell cycle progression in order to repair DNA: if this is not possible, the cell undergoes programmed cell death [Sancar et al.,2004 ; Branzei et al.,2008]. Two DNA damage checkpoints can be activated, one in late G1, which prevents entry into S phase, and the other in late G2, which prevents entry into mitosis. Furthermore, if DNA damage occurs during S phase, an intra-S checkpoint can be elicited [Caldwell et al.,2008].

Despite the use of TOP2-targeting drugs in clinical practice, unfortunately some of the intercalating poisons, especially Anthracyclines, trigger side effects that are independent of their action against TOP2. On the contrary, Bisdioxopiperazines show poor anti-tumour activity, but their clinical usage aims to reduce cardiotoxicity in patients treated with anthracyclines.

Even though several TOP2A inhibitors already exist, the positive results obtained in clinical practice prompted the scientific community to search for new effective drugs with lower side effects. Curcumin, the pigment derived from the rhizome *Curcuma longa*, showed promising anticancer properties, with selective cell death-inducing ability in tumour cells. The apoptotic process seems to be related to TOP2 poisoning and consequent DNA damage induction [Martin-Cordero et al.,2003; López-Lázaro et al.,2007]. Indeed, *in vitro* experiments have demonstrated that Curcumin can directly interact

with purified TOP2A and DNA, inducing TOP2A-cc. However, a recent bioinformatic blind docking study predicted that the derivative bis-DemethoxyCurcumin has higher binding affinity with TOP2A than Curcumin or Demethoxycurcumin (Kesharwani and Misra,2011).

### 4.1.2 Curcumin and its derivatives

Phytochemicals from dietary agents, especially herbs and spices, are currently under investigation for the prevention and therapy of various diseases, thanks to their pleiotropic properties and very low toxicity. The polyphenol Curcumin is the major active compound obtained from the dried rhizome of *Curcuma longa*, together with smaller quantities of the Curcumin-derivatives DemethoxyCurcumin, bis-DemethoxyCurcumin and the recently identified CycloCurcumin. The yellow powder obtained from the plant was traditionally used not only as food spice and colouring agent, but also in cosmetics and traditional Asian medicine (Goel et al.,2008), for treatment for example of inflammations, hepatic disorders, wound healing and rheumatism (Singh,2007). Present studies confirmed that Curcumin has anti-inflammatory, anti-oxidant, chemopreventive and chemotherapeutic activities. The wide range of activities of Curcumin are likely correlated to its ability to affect many cellular pathways, by regulating many transcription and growth factors, cytokines, protein kinases and other enzymes. Microarray analysis of mRNA expression revealed a genome wide effect of Curcumin treatment (Teiten et al.,2009). Additional informations about the mechanism of activity are still required, but new perspectives emerged from the identification of Curcumin as an inhibitor of p300-mediated epigenetic regulation (Marcu et al.,2006 ; Balasubramanyam et al.,2004).



Besides the promising effects observed both in cellular and animal models, numerous clinical trials verified the safety and efficacy of Curcumin in different types of human cancers. Early clinical trials showed that Curcumin is well tolerated up to 12 g/day (Goel et al.,2008 ; Lao et al.,2006) and that a maximum daily intake of Curcumin of 1 mg/kg body weight has no adverse effects. In addition, positive results of Curcumin efficacy were obtained in the treatment of multiple myeloma, post-operative inflammation, pancreatic and colon cancers (Shehzad et al.,2010). Unfortunately, regardless of its safety and efficacy, Curcumin is characterized by poor absorption, rapid metabolism and systemic elimination (Anand et al.,2007).

In order to overcome these limitations, Curcumin derivatives/analogues with improved anti-tumour potential or bioavailability are under investigations (Ohori et al.,2006).

In our previous studies, we demonstrated that bis-DemethoxyCurcumin (bDMC) is more stable in physiological conditions than its lead compound, overcoming one of

the most limiting factors for clinical applications of Curcumin [Basile et al.,2009]. While Curcumin triggers a G2/M arrest, due to impairment of microtubule spindle formation, bDMC is able to induce a concomitant and more stable G1/S and mitotic block in HCT116 cells ***(Figure 2.10)***. Our results pointed out that DNA-damage is concomitant to cell cycle arrest in bDMC treated-cells, whereas it is likely the result of severe mitotic arrest after Curcumin incubation [Basile et al.,2009]. p53 and p21 are both necessary for Curcumin-induced post-mitotic G1/S cell cycle arrest (mitotic slippage), while a p53-independent p21 upregulation is involved in G1/S arrest directly activated by bDMC. Moreover, bDMC exhibited higher cytotoxicity in ovarian cancer cells and greater anti-carcinogenic and anti-metastatic activities than Curcumin [Anand et al.,2008].

These previous studies drew our attention on bDMC. Our current analyses focus on the activity of bDMC as DNA-damaging agent and TOP2A inhibitor. We highlight that bDMC leads colon cancer cells to apoptosis by targeting TOP2A. Indeed, bDMC affects both enzymatic activity and NF-Y-mediated transcription of TOP2A.



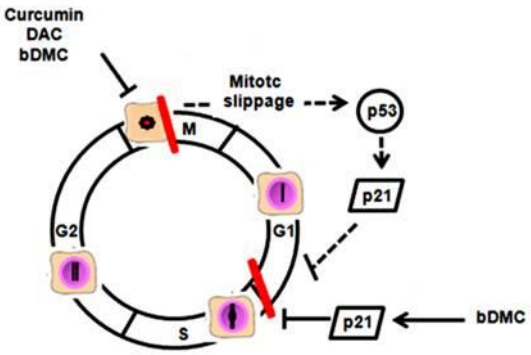


**Figure 2.10|** Graphical abstract representing Curcumin, bis-DemethoxyCurcumin (bDMC) and DiacetylCurcumin (DAC) activities in HCT116 cells. [Basile et al.,2009].

## 4.2 Results

### 4.2.1 bDMC triggers irreversible cell death in colorectal carcinoma cells, but not in healthy cells

We already demonstrated that bDMC administration has a cytostatic effect on HCT116 cells, inducing a concomitant G1/S and G2/M arrest of the cell cycle [Basile et al.,2009]. Time-course experiments of bDMC administration for up to 24 hours, followed by release in drug-free medium, not only confirmed our previous findings, but highlighted an additional cytotoxic activity. Indeed, PI cytofluorimetric analyses

pointed out that SubG1 events increase in a time-dependent way ***(Figure 4.1A and B)***, from 0.6% in DMSO-treated cells to 7.5% after 24h of bDMC.

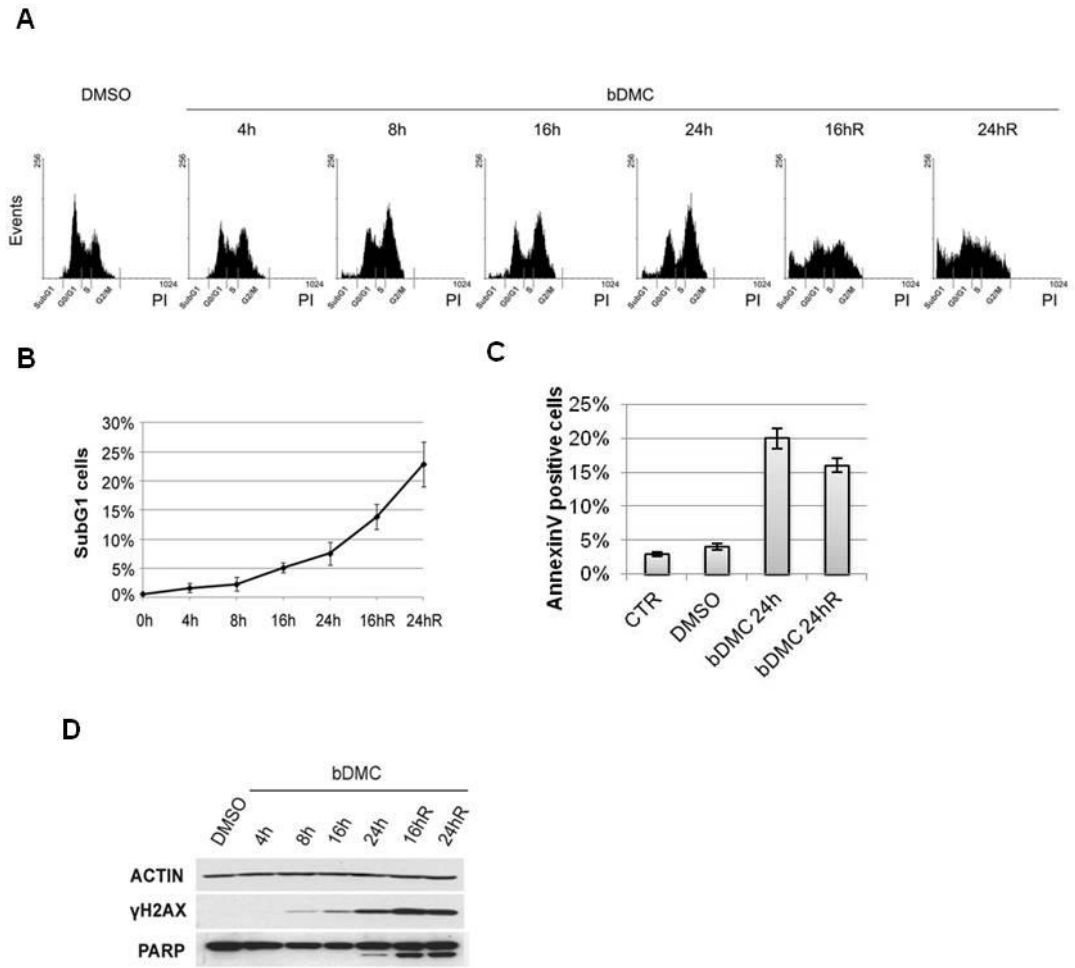


**Figure 4.1| bDMC triggers irreversible cell death in HCT116 cells.** (A) PI-Cytometric cell-cycle analysis of HCT116 cells treated with bDMC for 4, 8, 16, 24h and released in drug-free medium for further 16 and 24h (16hR and 24hR), following 24 h of bDMC treatment. (B) Graphical quantification of SubG1 events detected by PI-cytofluorimetric analysis after incubation with bDMC for the indicated times. (C) Percentage of Annexin V-positive cells after 24h treatment with bDMC is compared with Control (CTR) and DMSO-treated cells and with cells released for additional 24h into fresh medium (24hR). (D) Western blot analysis of γH2AX and PARP1 following time-dependent treatment of HCT116 cells. Actin was used as loading control.



Interestingly, the release of cells from bDMC into fresh medium further increased SubG1 events to 14% and 23% after 16h and 24h from release, respectively. Flow cytometric quantification of AnnexinV positive cells showed that after 24h of bDMC incubation already 20% of cells are positive to the staining ***(Figure 4.1C)***, hinting that bDMC irreversibly commits cells to apoptosis. Consistently, we detected time-dependent cleavage of PARP-1 and phosphorylation of H2AX Ser139 (γH2AX) ***(Figure 4.1D)***, which continued to increase after release from bDMC. The same

results were obtained in colorectal carcinoma Lovo cells, with bDMC triggering time-dependent increase of SubG1 events (up to 18% after 24h release into fresh medium) ***(Figure 4.2A and B)*** and activation of γH2AX ***(Figure 4.2C)***.

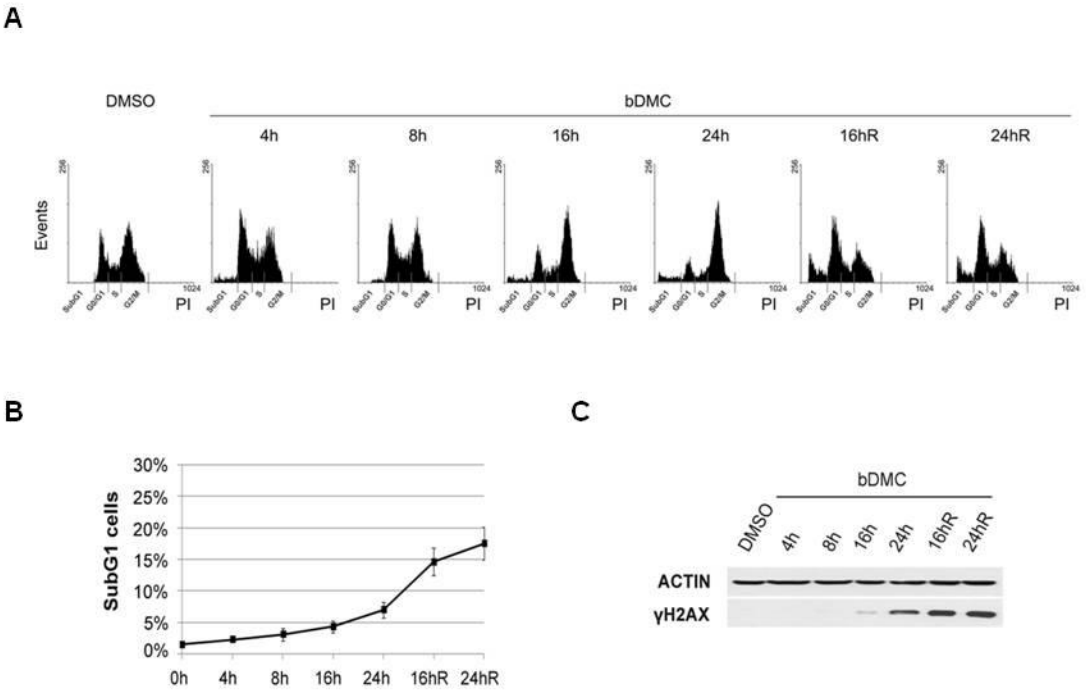




**Figure 4.2| bDMC triggers irreversible cell death in Lovo cells.** (A) PI-Cytometric cell-cycle analysis of Lovo cells treated with bDMC for 4, 8, 16, 24h and released in drug-free medium for further 16 and 24h (16hR and 24hR) following 24 h of bDMC treatment. (B) Graphical quantification of SubG1 events detected by PI-cytofluorimetric analysis after incubation with bDMC for the indicated times. (C) Western blot analysis of γH2AX following time-dependent treatment of Lovo cells. Actin was used as loading control.

In order to characterize the cytotoxic effects of bDMC, we performed the same treatments with 30μM bDMC in human normal fibroblasts (HF) and hepatic fetal epithelial cells (WRL-68). We could not detect any increase of SubG1 events ***(Figure 4.3A and B)*** nor γH2AX activation in WRL-68 cells treated for up to 24h ***(Figure 4.3C)***, even after release from bDMC.

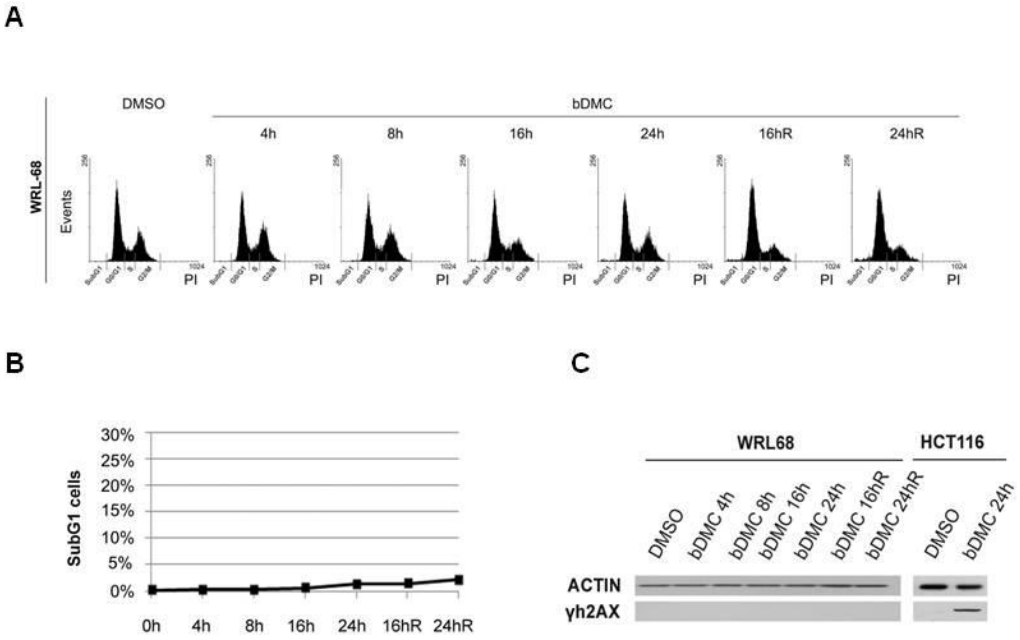


**Figure 4.3| bDMC does not elicit cell death in WRL-68 cells.** (A) PI-Cytometric cell-cycle analysis of WRL-68 cells treated with bDMC for 4, 8, 16, 24h and released in drug-free medium for further 16 and 24h (16hR and 24hR) following 24h of bDMC treatment. (B) Graphical quantification of SubG1 events detected by PI-cytofluorimetric analysis after incubation with bDMC for the indicated times. (C) Western blot analysis of γH2AX following time-dependent treatment of WRL-68 cells, in comparison to HCT116 cells treated for 24h. Actin was used as loading control.



Due to the longer doubling-time of HF cells compared to HCT116 or WRL-68 cells, we performed time-course analyses after 24 and 48 hours from bDMC administration, and released cells in fresh medium for additional 24/48h. Nevertheless, the lack of a significant increase of SubG1 events ***(Figure 4.4A and B)*** and γH2AX phosphorylation was confirmed also in HF cells ***(Figure 4.4C)***. Furthermore, we performed dose-response analyses comparing cancer cells *versus* healthy cells ***(Figure 4.5A and B)***: as expected, IC50 concentrations are lower in HCT116 and Lovo cells (~30 μM) than in HF and WRL-68 cells (>320 μM and 55 μM, respectively), further corroborating the tumour selectivity of bDMC activity.

In order to better characterize bDMC activity, we then performed cellular and molecular experiments in HCT116 as model cell line.

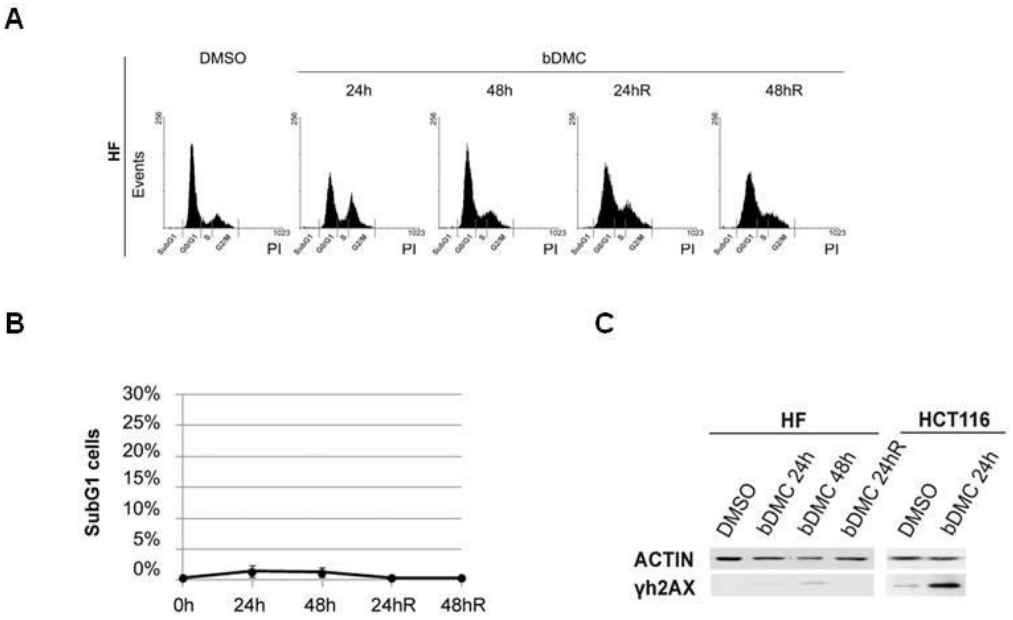


**Figure 4.4| bDMC does not induce cell death in HF cells.** (A) PI-Cytometric cell-cycle analysis of HF cells treated with bDMC for 24 and 48h and released in drug-free medium for further 24 and 48h (24hR and 48hR) following 48h of bDMC treatment. (B) Graphical quantification of SubG1 events detected by PI-cytofluorimetric analysis after incubation with bDMC for the indicated times. (C) Western blot analysis of γH2AX following time-dependent treatment of HF cells, in comparison to HCT116 cells treated for 24h. Actin was used as loading control.



**Figure 4.5| Cancer cells are more sensitive to bDMC than healthy cells.** Percentage of cell survival of (A) HCT116 and LOVO tumor cells compared to (B) HF and WRL-68 normal cells, following administration of increasing concentrations of bDMC for 24h

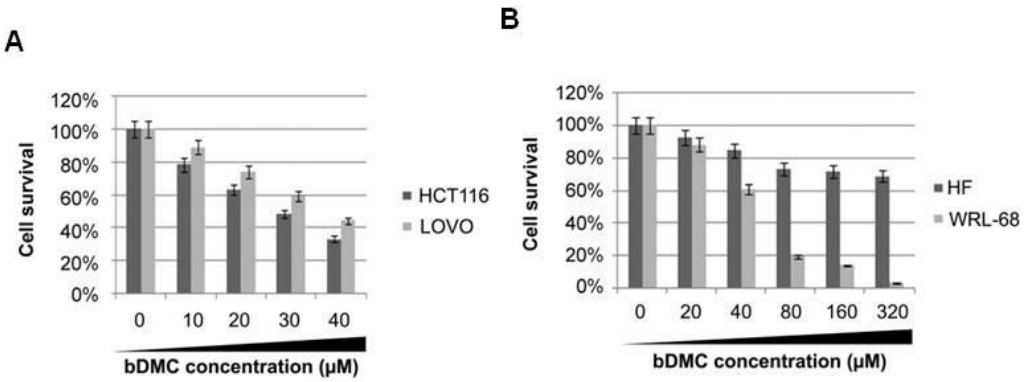


### 4.2.2 bDMC induces DNA damage in HCT116 cells

H2AX Ser139 phosphorylation is an important molecular marker both of apoptosis and of DNA double-strand breaks (DSBs). Therefore, we wondered if the increase of

γH2AX observed after bDMC treatment of cancer cells could be the result of DNA damage rather than apoptosis. To discriminate between these two possibilities, we co-treated HCT116 cells with bDMC and the pan-caspase inhibitor Z-VAD.

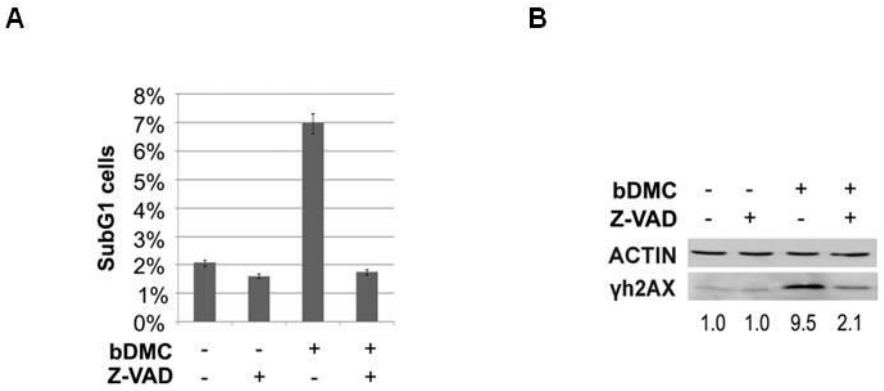


**Figure 4.6| bDMC induce DNA damage.** (A) Graphical quantification of SubG1 events detected by PI-cytofluorimetric analysis after incubation with bDMC and Z-VAD alone or in combination for 24h. (B) Western blot quantification of γH2AX expression levels versus actin following bDMC and Z-VAD rteatments for 24h, alone or in combination.



Cytofluorimetric analysis highlighted that Z-VAD blocked the accumulation of SubG1 cells induced by bDMC ***(Figure 4.6A)***, but a partial activation of γH2AX was still detectable in Western Blot ***(Figure 4.6B)***, suggesting that bDMC can induce DNA damage. When DSBs occur, the cell activates a complex pathway composed of sensor, mediator, transducer and effector proteins (Bakkenist and Kastan,2004). DSBs are thus recognized, transducers such as ATM/ATR/DNA-PK are activated and, in turn, they phosphorylate sensors, mediators (as H2AX, BRCA1) and distal transducers and effectors (as Chk1 and Chk2). We previously demonstrated that 24h bDMC determines activation of ATM (Basile et al.,2009), which is the major transducer of DSBs response pathway. Western Blot experiments demonstrate that a DNA-damage response is actually elicited in bDMC-treated cells, since ATM, BRCA1, Chk1 and H2AX are phosphorylated ***(Figure 4.7)***.

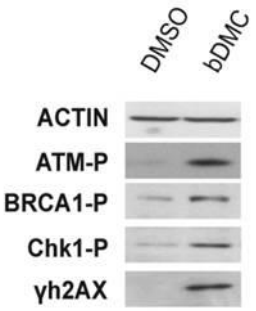


**Figure 4.7| bDMC elicit a DNA damage response.** Western blot analysis of expression levels of the indicated phospho-proteins after 24h-bDMC.

In order to further support this hypothesis, we pre-treated cells with Wortmannin (WORT), an inhibitor of PI3-Kinases involved in DNA damage and repair mechanisms, namely ATM and DNA-PK [Sarkaria et al.,1998]. WORT decreased γH2AX activation ***(Figure 4.8A)*** and reduced G2/M population, from 47% in bDMC-cells to 31% in WORT-bDMC-cells, with a concomitant increase in G1 events ***(Figure 4.8B)***.

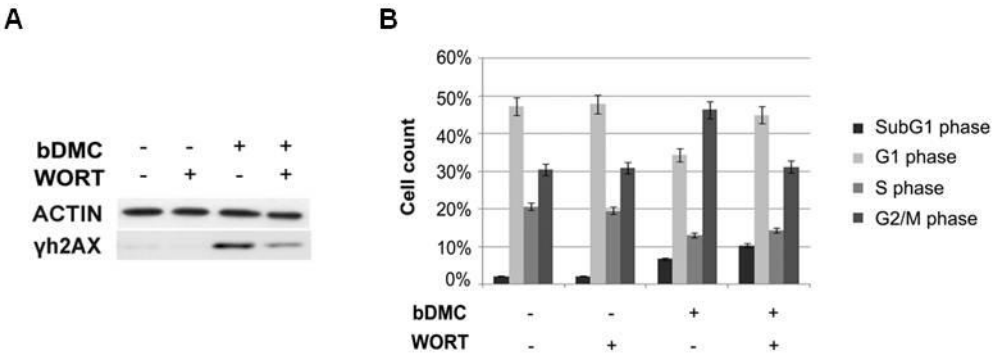


**Figure 4.8| bDMC elicits a G2/M DNA damage checkpoint.** (A) Western blot analysis of γH2AX expression and (B) graphical distribution of events detected by PI-cytometric analysis after 24h treatment of HCT116 with Wortmannin (WORT) and bDMC, alone or in co-treatment.



These data indicate that bDMC elicits a G2/M DNA damage checkpoint, which probably prevents cells from entering the next G1 phase. Cytofluorimetric evaluation of cell populations expressing γH2AX confirmed that after 24h treatment with bDMC there is an increase of positive cells with a 4N DNA content, most likely G2/M arrested cells ***(Figure 4.9A)***. We then sought to understand if bDMC cause chromosome aberrations in these mitotic DNA-damaged cells. Chromosome spreads of HCT116 ***(Figure 4.9B)*** treated for 24h with bDMC were analyzed by Giemsa staining: we detected chromatid-gaps and -breaks in bDMC-cells, supporting the hypothesis that G2/M-arrested cells are damaged and presumably committed to apoptotic death.

We already showed that in HCT116/E6 cells, lacking p53, bDMC induces an even more robust arrest in G2/M phase compared to HCT116 [Basile et al.,2009]: also in these cells, bDMC triggers a time-dependent increase of SubG1 events and of γH2AX ***(Figure 4.9C and D)***, corroborating that damaged cells are G2/M cells subsequently committed to cell death.

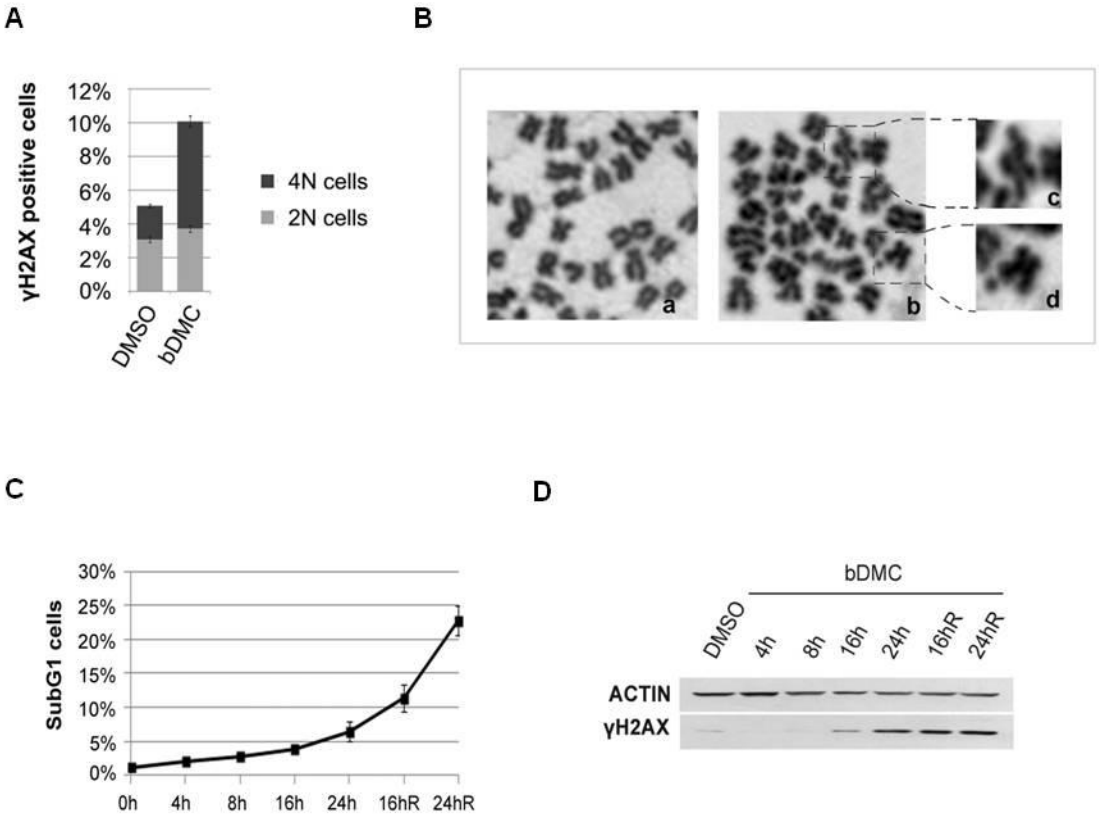




**Figure 4.9| bDMC accumulates DNA-damaged cells in G2/M phase.** (A) Percentages of γH2AX-positive cells in 2N and 4N cells after bDMC treatments for 24h. (B) Representative Giemsa-stained mitotic chromosome spread of HCT116 treated with DMSO (a) or bDMC (b) for 24 h. Enlargements (box c and d) show chromosome aberrations of bDMC-cells. (C) Graphical quantification of SubG1 events detected by PI-cytofluorimetric analysis after incubation of HCT116/E6 with bDMC for the indicated times. (D) Western blot analysis of γH2AX after time-dependent treatment of HCT116/E6. Actin was used as loading control.

### 4.2.3 bDMC as a TOP2A poison

It has been demonstrated that Curcumin can induce Topoisomerase I and Topoisomerase II complexes with DNA (López-Lázaro et al.,2007) and recent studies revealed that bDMC has a stronger binding affinity for TOP2A than Curcumin (Kesharwani and Misra,2011). Taking into account these results and the ability of bDMC to induce DNA-damage and chromosome breaks, we speculated that bDMC could inhibit TOP2A activity in HCT116 cells.

We performed an *in vitro* TOP2 activity assay with a commercial kit, quantifying the ability of TOP2 to decatenate a specific substrate, kinetoplast DNA (kDNA), in the presence of DMSO or bDMC. As shown in ***Figure 4.10A***, 30 μM bDMC reduced to 50% TOP2 activity and besides, bDMC showed a significant inhibitory ability when compared to the known TOP2 poison Etoposide (ETP). We thus assessed if bDMC

was able to trap TOP2A-DNA covalent complexes in cells, by a band-depletion assay. Indeed, the enzyme covalently linked to DNA cannot enter SDS-polyacrylamide gels, resulting in a loss of the respective immunoreactive band in Western Blots of whole cell lysates, unless Micrococcal Nuclease (MNase) digestion allows the release of TOP2A from DNA complexes. We performed a bDMC time-course experiment and for each time point we prepared protein extracts and compared TOP2A levels before and after digestion with MNase. Western Blots in

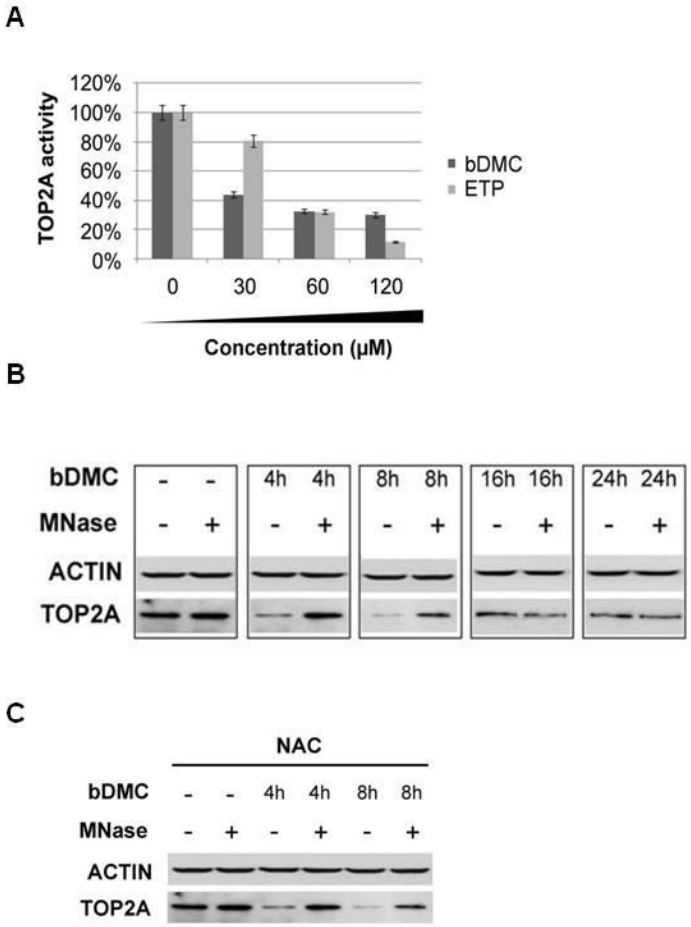


**Figure 4.10| bDMC inhibits TOP2A activity.** (A) Inhibition of TOP2A-dependent decatenation of kDNA with increasing concentrations of bDMC and Etoposide (ETP) versus DMSO (arbitrarily set at 100%). (B) Western blot of TOP2A immunoreactive bands after 4, 8, 16 and 24h bDMC addition, with or without MNase digestion. (C) Expression of TOP2A in untreated and MNase-treated samples upon bDMC-NAC treatment



***Figure 4.10B*** shows that MNase digestion restored TOP2A levels (at least partially) only after 4h and 8h of incubation with bDMC, consistently with the presence of TOP2A-DNA complexes. Conversely, after 16 and 24 hours of bDMC treatment no increase in TOP2A levels was observed after MNase incubation.

Since poisoning of TOP2A can be an indirect effect (López-Lázaro et al.,2007), due to an increase of reactive oxygen species (ROS), we performed a band-depletion assay with extracts of cells pre-treated and co-treated with the antioxidant N-acetylcisteine (NAC). This assay ***(Figure 4.10C)*** demonstrated that bDMC can trap

enzyme-DNA complexes also in the presence of NAC, ruling out that this phenomenon could be indirectly mediated by ROS production. All together, these data clearly suggest that bDMC acts as a TOP2A poison up to 8h of treatment.

### 4.2.4 bDMC induces transcriptional repression of TOP2A by affecting NF-Y binding to its promoter region

Western Blot analysis of MNase-digested extracts highlighted that TOP2A expression levels decrease in a time-dependent way, being reduced by 60-70% after 24h of bDMC ***(Figure 4.11A and B)***. In order to understand whether this could be ascribed to increased protein degradation, we co-treated cells with bDMC and the proteasome inhibitor MG132. The graphical quantification of Western Blot experiments in ***Figure 4.11B*** clearly suggests that proteasomal degradation is not the

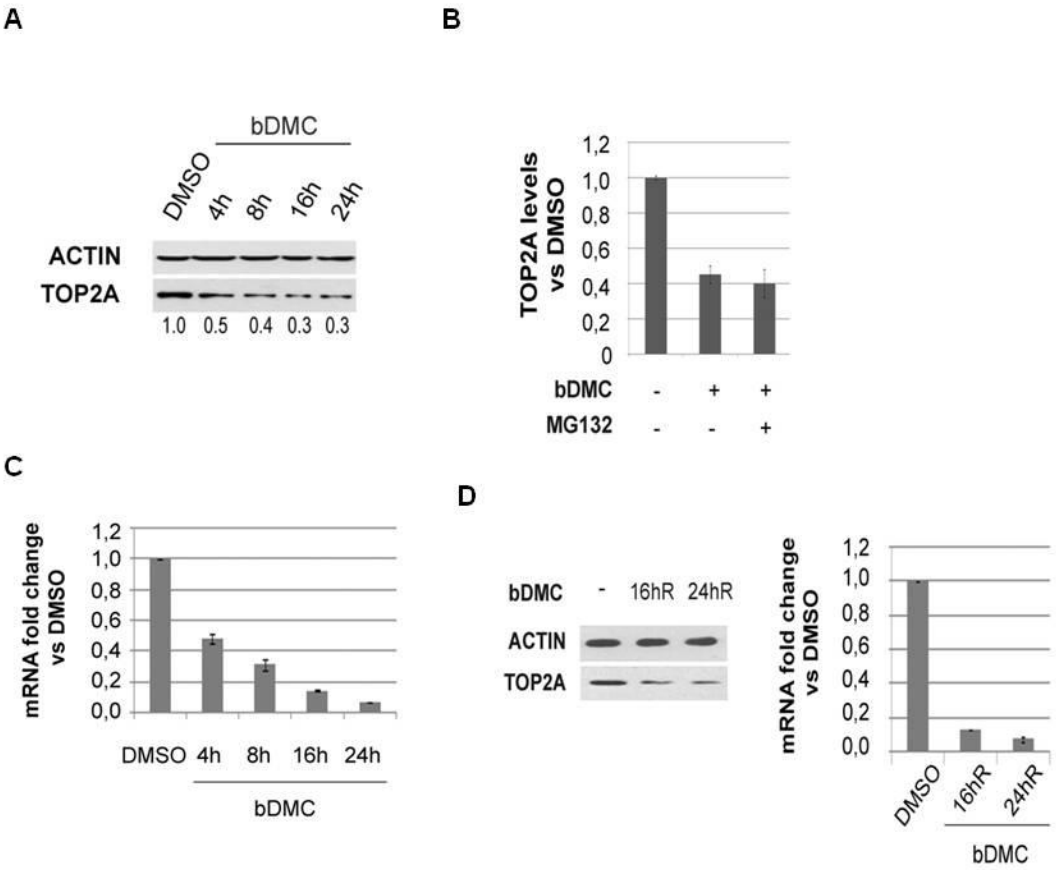


**Figure 4.11| TOP2A expression is downregulated by bDMC.** (A) Quantification of TOP2A protein levels in MNase-treated extracts after 4, 8, 16 and 24h of incubation with bDMC. The indicated values are quantifications of TOP2A immunoreactive bands normalized vs actin levels. (B) Quantification of TOP2A expression (normalized to actin) following bDMC and bDMC-MG132 administration for 24h versus DMSO (arbitrarily set at 1). (C) Real-time PCR analysis of TOP2A mRNA in bDMC-cells, represented as mRNA fold change versus DMSO (arbitrarily set at 1). GAPDH has been used as internal control. (D) Analysis of protein and mRNA levels of TOP2A after incubation with bDMC for 24h, followed by release for 16h (16hR) and 24h (24hR) in fresh medium.

cause of TOP2A halving.

Consequently, we analyzed the level of TOP2A transcription after incubation with bDMC: real-time RT-PCRs ***(Figure 4.11C)*** clearly show time-dependent downregulation of TOP2A gene transcription. Furthermore, even after the release of cells into fresh medium, both protein and mRNA levels of TOP2A continue to be reduced ***(Figure 4.11D)***.

NF-Y is the major transcription factor controlling the activation of TOP2A transcription, through direct binding to the CCAAT boxes in its promoter region. Therefore, we assessed NF-Y binding to TOP2A gene regulatory region after 24h bDMC treatment, by Chromatin Immunoprecipitations (ChIP). Interestingly, NF-YA and NF-YB binding was reduced by 40% and 30%, respectively ***(Figure 4.12A and B).*** Furthermore, epigenetic markers associated to transcriptionally active chromatin

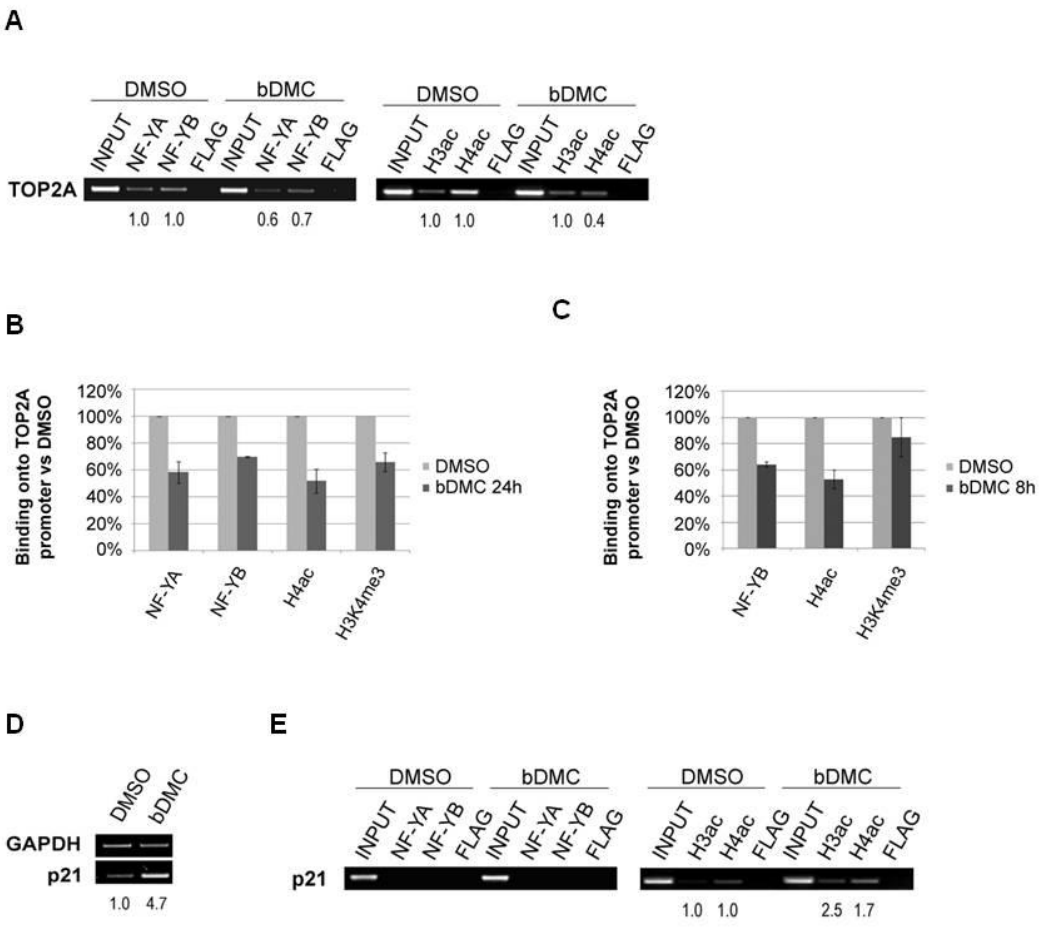


**Figure 4.12| Inhibition of NF-Y-mediated TOP2A transcription by bDMC** (A) Semi-quantitative ChIP analysis of NF-YA, NF-YB, acetyl-H3 (H3ac) and acetyl-H4 (H4ac) binding to TOP2A promoter in HCT116 treated with DMSO or 24h-bDMC. (B and C) ChIP real-time PCR analysis of chromatin-associated NF-Y, H4ac and H3K4me3 to TOP2A promoter following 24h (B) or 8h (C) of incubation with bDMC. Image (D) shows mRNA expression levels of p21 in 24h bDMC-treated cells and (E) shows semi-quantitative PCR analysis of the recruitment of NF-Y and acetylated histones on p21 regulatory region, in cells treated for 24h with DMSO and bDMC.

and associated to NF-Y binding[Fossati et al.,2011], such as acetylation of histone H4 (H4ac) and tri-metylathion of histone H3 Lys4 (H3K4me3), are cut by about 40%. ChIP analyses performed at an earlier time-point of bDMC incubation, pointed out that NF-YB and H4ac are already maximally depleted from TOP2A promoter after 8h of treatment, whereas H3K4me3 is only slightly decreased after 8h and further decreases at 24 hours ***(Figure 4.12B and C)***. These results hint that NF-Y reduction, together with early and late NF-Y-dependent epigenetic modifications of the promoter can be responsible for the observed downregulation of TOP2A transcription.

In order to rule out global, non-specific effects on histone acetylation, we analysed the transcription of 21, that is transcriptionally upregulated ***(Figure 4.12D)*** and therefore associated to increased H3ac and H4ac ***(Figure 4.12E)***.

### 4.2.5 bDMC treatment affects the levels of NF-Y subunits inside the nucleus

The decrease of NF-Y recruitment onto TOP2A promoter raised the question whether this was dependent on reduced expression levels of NF-Y. Western Blots of whole cell extracts ***(Figure 4.13A)*** and RT-PCRs ***(Figure 4.13B)*** of cells treated with DMSO or bDMC for 24h highlighted a decrease of ~50% of NF-YA subunit, both at the mRNA and protein levels. Conversely, no significant variations were observed in NF-YB and NF-YC expression levels.



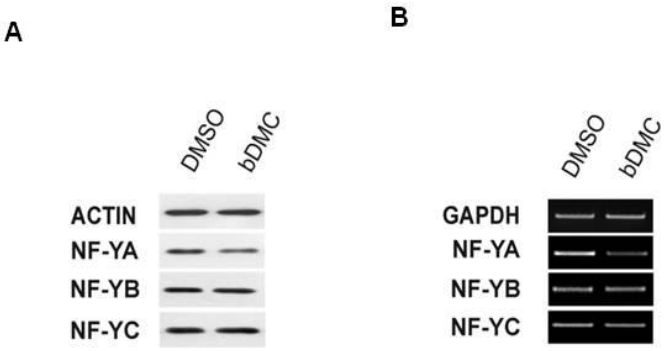


**Figure 4.13| bDMC affects NF-Y subunits expression.** (A) Western blot of whole cell extracts of DMSO and bDMC-treated cells (24h) with NF-Y antibodies and (B) Semi-quantitative RT-PCRs of NF-YA, NF-YB and NF-YC subunits after bDMC administration for 24h.

Differently from NF-YA, that is mostly localized into the nucleus, NF-YB and NF-YC can shuttle between cytoplasm and nucleus [Frontini et al.,2004]. For this reason, we assessed the localization of the subunits by Western Blot analysis of nuclear and

cytosolic protein extracts. ***Figure 4.14A*** shows a time-dependent accumulation of NF-YC and –YB into the cytosol following bDMC administration, which is maximum after 24h-treatment. However, a clear decrease is observed in nuclear extracts already after 8h of incubation with bDMC. To investigate whether this was related to alterations in nuclear export or nuclear import, we co-treated cells with bDMC and an inhibitor of nuclear export CRM1-mediated, Leptomycin B (LMB).

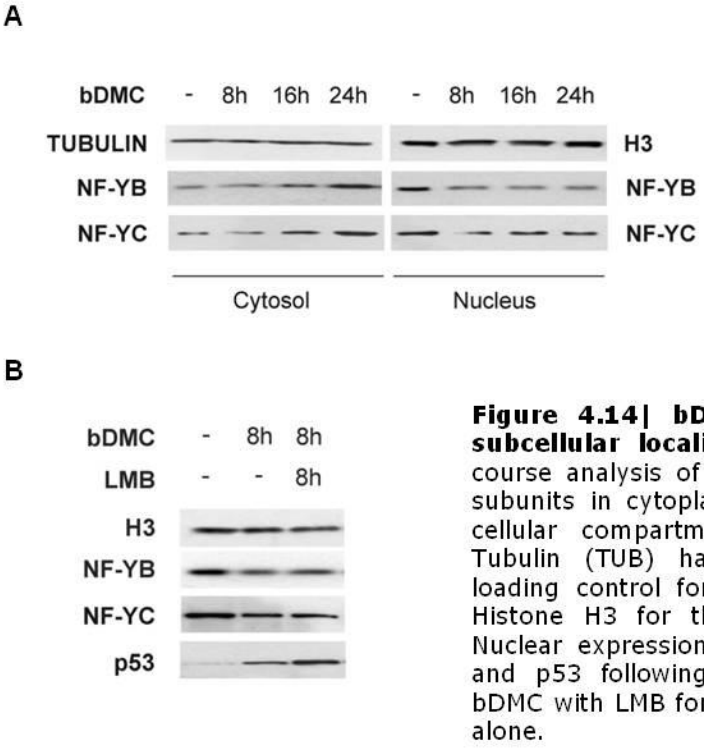


**Figure 4.14| bDMC alters NF-Y subcellular localization.** (A) Time course analysis of NF-YB and NF-YC subunits in cytoplasmic and nuclear cellular compartments of HCT116. Tubulin (TUB) has been used as loading control for the Cytosol and Histone H3 for the Nucleus. (B) Nuclear expression of NF-YB, NF-YC and p53 following co-incubation of bDMC with LMB for 8 h versus bDMC alone.



Western Blots performed on nuclear extracts ***(Figure 4.14B)*** highlighted that NF-YB and NF-YC levels do not rise in co-treated cells compared with bDMC alone, while p53 increase confirmed the efficiency of LMB treatment. These data indicate that bDMC triggers NF-YB/NF-YC retention into the cytosol, together with NF-YA reduction, thus determining TOP2A transcriptional downregulation.

Since it is known that TOP2A can be cooperatively regulated by NF-Y and Sp1 (Magan et al.,2003), we checked if also Sp1 expression could be affected by bDMC treatment. Western Blot experiments carried out with chromatin-enriched and whole cell extracts of HCT116 ***(Figure 4.15)*** pointed out that Sp1 levels decrease already after 8h of bDMC treatment, while its recruitment onto chromatin is mainly reduced after 24h bDMC, consistent with a time-dependent release of Sp1 from TOP2A promoter, which could be secondary to the release of NF-Y binding.

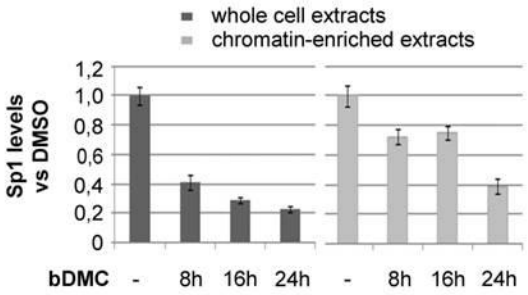


**Figure 4.15| bDMC also affects Sp1 function.** Quantification of Sp1 protein levels in whole cell extracts and chromatin-enriched extracts after bDMC treatment of HCT116 for 8, 16 and 24h, compared to DMSO-cells (-), arbitrarily set at 1.

### 4.2.6 Both enzymatic and transcriptional TOP2A targeting contributes to bDMC cytotoxic activity

With the aim of determining the role played by TOP2A in the cytotoxic activity of bDMC, we knocked down TOP2A by siRNA transfection. Protein levels were reduced by about 70% after 48h from transfection, and TOP2A could be further decreased by bDMC treatment ***(Figure 4.16A)***.



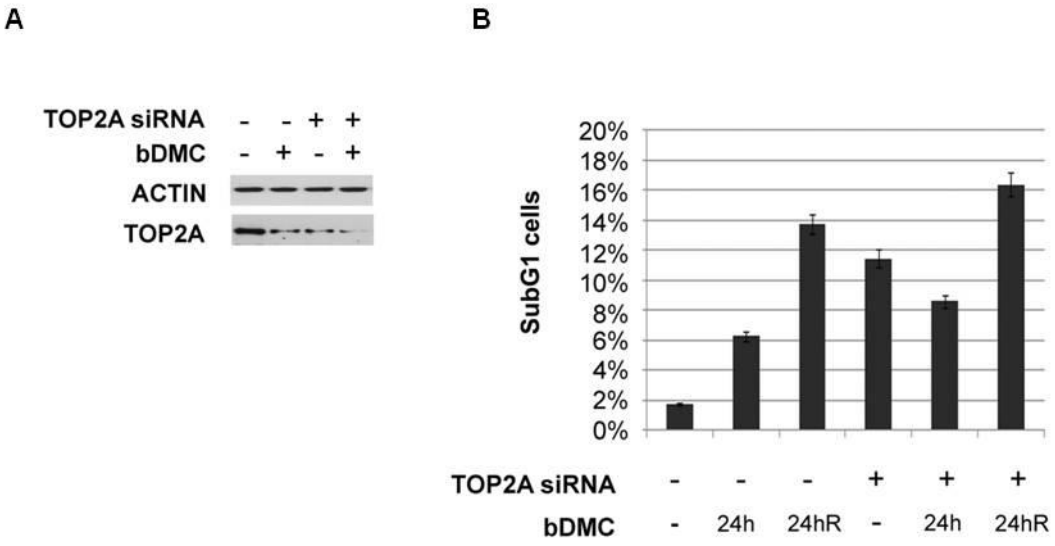


**Figure 4.16| bDMC activity is mediated by dual targeting of TOP2A at the transcriptional and enzymatic levels.** (A) Western blot of TOP2A after siRNA-mediated knockdown and bDMC treatment for 24h. (B) Quantification of SubG1 events detected by PI-Cytofluorimetric analysis after bDMC treatment for 24h and release for additional 24h in control and TOP2A-inactivated cells.

After RNAi, SubG1 events increased from 1.8% to 11.5%, that is indicative of the important role played by TOP2A in HCT116 cell viability ***(Figure 4.16B)***. Interestingly, 24h bDMC administration was not able to further increase SubG1 events in knocked-down cells, hinting that the initial inhibition of TOP2A enzymatic activity is important for cytotoxicity. On the other hand, when cells are released into fresh medium for additional 24h, SubG1 events doubled both in control and silenced cells ***(Figure 4.16B)***, suggesting that long-term apoptosis relies on TOP2A transcriptional downregulation rather than TOP2A poisoning.

## 4.3 Discussion

High expression levels of TOP2A have been associated to high proliferation and malignancy of cancer cells. As expected, these TOP2A-overexpressing tumours are particularly sensitive to TOP2-targeting drugs. For this reason, therapy-induced downregulation of TOP2A has been associated to a positive response to chemotherapy and longer relapse free survival, but also to subsequent drug resistance (Tinari et al.,2006). Nonetheless, TOP2A is the target of many effective chemotherapeutic drugs currently used in clinical practice, such as Etoposide. Our analyses pointed out that bDMC has a cytostatic and cytotoxic activity in cancer cells, which can be ascribed, at least in part, to its dual effect on TOP2A activity and expression. Indeed, bDMC acts as TOP2A inhibitor, as demonstrated by *in vitro* decatenation and band-depletion assays performed in HCT116 ***(Figure 4.10)***. bDMC induces persistent and irreversible DNA damage in cancer but not in normal cells, which are less sensitive to bDMC treatment, as highlighted by higher IC50 concentrations ***(Figure 4.5)***. Curcumin and its derivatives were already demonstrated to be tumour-selective agents, due to their lower uptake in healthy cells or to increased sensitivity of cancer cells (Basile et al.,2013). Taking into account that various tumours are characterized by increased TOP2A levels compared to their normal counterpart, it could be that TOP2A-targeting is at the basis of bDMC cancer selectivity.



TOP2A has an important role in DNA replication and in cell cycle progression, especially in G2/M phase. bDMC administration delays cells in the passage from early- to late-S phase (Basile et al.,2009) and, moreover, it triggers G2/M accumulation of damaged-cells harbouring chromosome aberrations and H2AX phosphorylation (γH2AX) ***(Figure 4.9A and C)***. In fact, bDMC triggers a DNA-damage response and activates the G2/M checkpoint, as demonstrated by the reduction of G2/M cells after pre-treatment with the PI3-K inhibitor WORT ***(Figures 4.7 and 4.8).*** Indeed, in the absence of an effective G2/M checkpoint, bDMC-cells are accumulated in the

following G1 phase rather than in SubG1, indicating that the prolonged activation of the checkpoint in G2/M is important to commit cells towards apoptosis.

We demonstrated that short-term exposure to bDMC (4h and 8h) determines the concomitant inhibition of TOP2A transcription and activity, while longer incubation (16h and 24h) mainly downregulates TOP2A expression ***(Figures 4.10 and 4.11)***. We should bear in mind that bDMC undergoes a rapid cell metabolism, and its concentration inside the cell is reduced to 7.5% and 6.2% after 4h and 8h of incubation, respectively, and to <0.5% after 24h [(Basile et al.,2009)]. All together, these data indicate that bDMC exerts its main direct activity by 8h from incubation, when we observed enzymatic inhibition of TOP2A and the maximal reduction of NF-Y function. Nevertheless, bDMC activates long-term transcriptional inhibition of TOP2A. Both of these aspects are important for bDMC anti-cancer activity, as demonstrated by TOP2A siRNA experiments ***(Figure 4.16)***: TOP2A poisoning is important for first-line induction of cell death (within 24h bDMC), but inhibition of TOP2A transcription plays a role in long-term, irreversible activation of cell death, even after drug release.

TOP2A transcriptional inhibition is determined by reduction of NF-YA protein, which is the limiting-subunit of the complex, and retention of NF-YB/NF-YC into the cytosol ***(Figures 4.13 and 4.14)***. Although bDMC treatment doesn't result in an impressive reduction of NF-YA and NF-YB binding to TOP2A promoter (of about 30-40%),we already know that TOP2A promoter activity is highly sensitive to small variations in NF-Y binding [(Benatti et al.,2011)]. Moreover, another transcription factor that is tightly related to NF-Y and is involved in the control of TOP2A, Sp1, undergoes a reduction in protein expression and chromatin association following bDMC treatment. In addition to the NF-Y/Sp1 cooperation in the regulation of gene transcription of multiple targets, the interplay between NF-Y and Sp1 is also due to the NF-Y-mediated transcriptional control of the Sp1 gene. ChIP-seq ENCODE data show NF-Y binding on Sp1 promoter [(Rosenbloom et al.,2013)] and, consistently, its mRNA levels decrease in NF-Y-inactivated cells [(Benatti et al.,2011)].

Taken together, we identified TOP2A as an important target for bDMC tumour-selective cytostatic and cytotoxic activity. Moreover, we pointed out that the regulation of NF-Y activity can be a good and interesting strategy in cancer therapy. Bearing in mind that NF-Y has been identified among the regulators of oncogenic transcriptional changes and that upregulation of NF-Y target-genes correlates to poor clinical prognosis [(Goodarzi et al.,2009; Yamanaka et al.,2009)], this study can pave the way to new strategies to fight cancer cell proliferation.

In order to achieve this goal, we still need to deepen our knowledge about the regulation of NF-Y subunits expression and activity.

# 5. TASK II: REGULATION OF NF-Y EXPRESSION

## 5.1 Background

Large-scale analyses of gene expression profiles indicated that NF-YA is upregulated in different kinds of tumour [Uhlen et al.,2012; Garipov et al.,2013]. However, NF-Y subunits transcriptional regulation has not yet been extensively studied, and it will be interesting to understand how NF-YA, -YB and –YC are controlled. Previous works of our group pointed out that after NF-YA knock down in HCT116 cells, expression levels of NF-YB are increased, and silencing of NF-YB determines an upregulation of NF-YA and NF-YC transcripts [Benatti et al.,2008 and 2011]. Since available ENCODE ChIP-Seq data indicate that NF-Y ***(Figure 5.1)*** and NF-Y-dependent



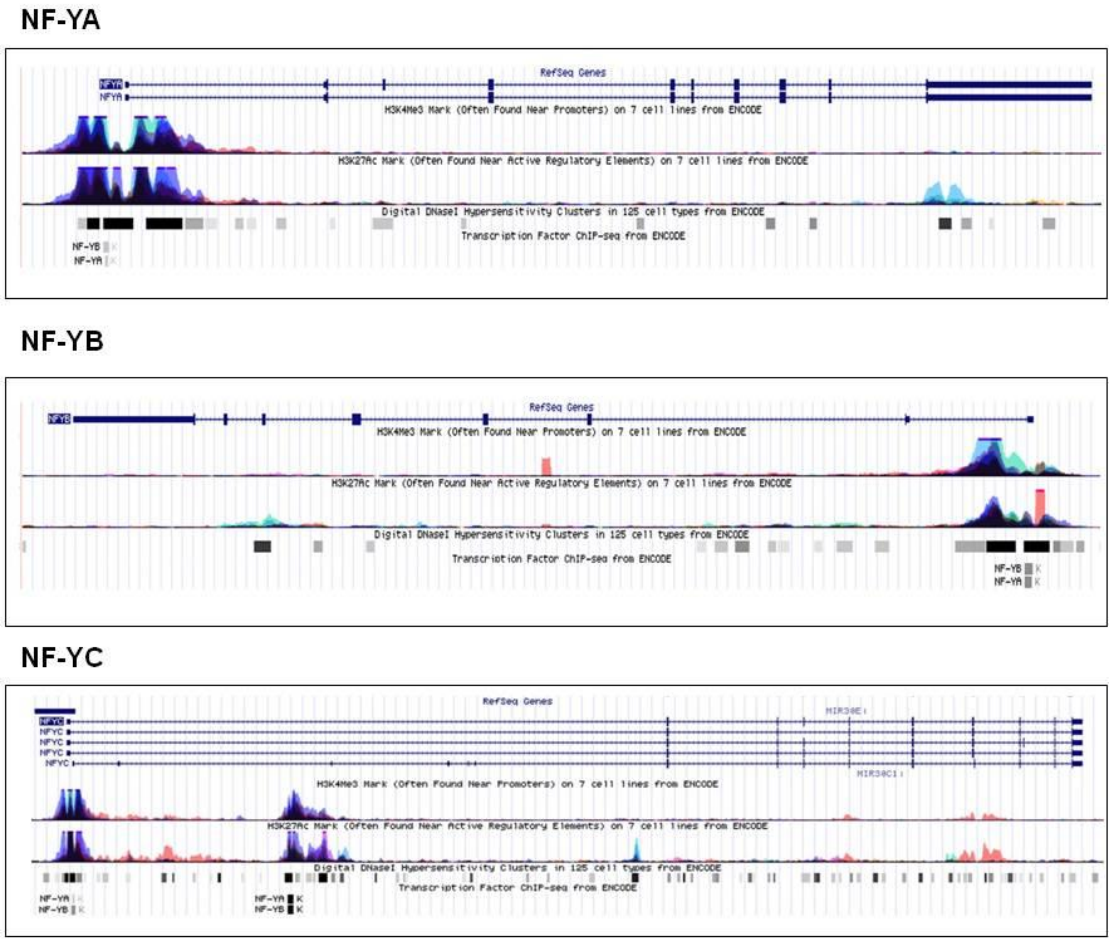


**Figure 5.1| NF-Y is recruited on its own gene promoters.** ChIP-seq and ENCODE data obtained from UCSC Genome Browser (Feb. 2009 GRCh37/hg19 assembly). Figures highlight *in vivo* binding sites of NF-YA and NF-YB and promoter regions are identified by a peak of the histone marks trimethyl-H3k4 (H3K4me3) and acetyl-H3K27 (H3K27Ac).

transcriptional regulators are bound on NF-Y subunits' promoter regions [Rosenbloom et al.,2013], it is likely that NF-Y regulates its own expression: understanding how and to what extent is the aim of the second task of my studies.

## 5.2 Results

### 5.2.1 Abrogation of NF-YA subunit by RNAi positively regulates NF-YB and NF-YC expression

As described above (§2.4), two major NF-YA isoforms have been described, a "long" and a "short" one, whose relative abundance varies in different cell types. Moreover, NF-YC mRNA can undergo various alternative splicing events, leading to expression of 37-, 39-, 48- and 50-kDa NF-YCs, as well as a shorter NF-YC, named

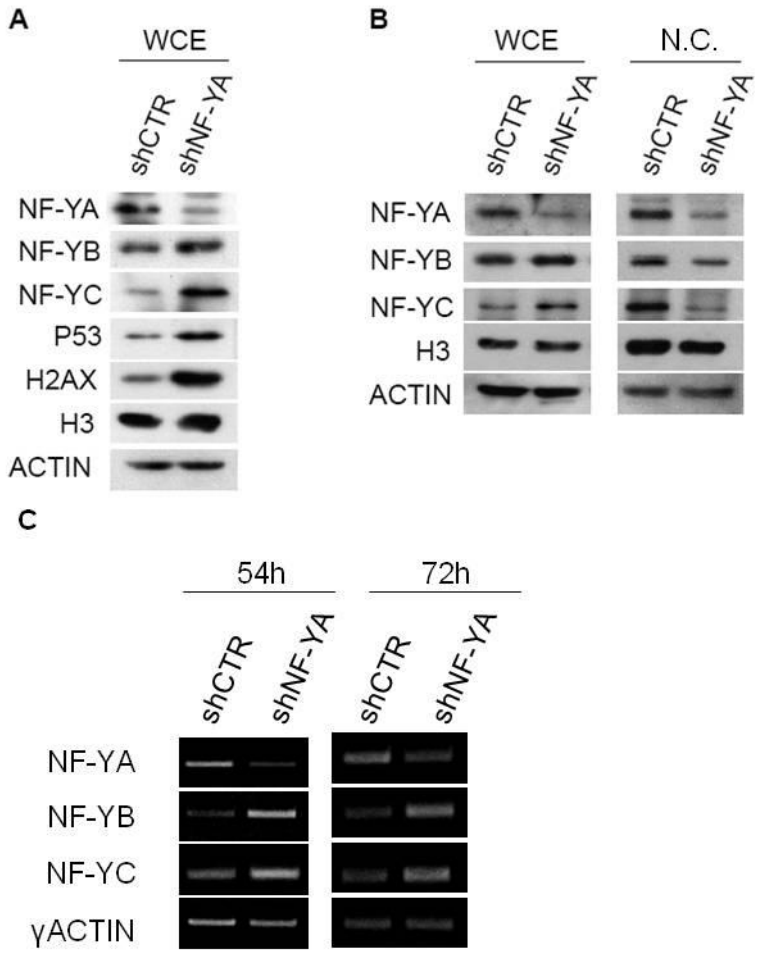


**Figure 5.2| NF-YA depletion leads to upregulation of NF-YB and NF-YC.** (A) Western Blot analysis performed with the indicated antibodies on Whole Cell Extracts (WCE) after 54h of shRNA lentiviral infection of HCT116 cells. Actin was used as loading control. (B) Protein levels of NF-YA, -YB and –YC in WCE and Nuclear Chromatin-enriched extracts (N.C.) after 72h shRNA infection. Histone H3 was used as normalizer. (C) Transcriptional levels of NF-Y subunits following 54h and 72h from lentiviral infection with shCTR and shNF-YA.

NF-YCb, that is mainly cytoplasmic [Ceribelli et al.,2009]. As described for NF-YA, also NF-YC splice variants are differentially expressed depending on cell type. HCT116 cells express NF-YA short and mainly the NF-YC (37kDa) variant, with the other isoforms being detected about 6 PCR cycles later.

In order to understand the biological relevance of NF-Y for its own regulation, we knocked-down the limiting subunit of the trimer, NF-YA, by lentiviral delivery of shRNAs. A vector containing a non-targeted shRNA was used as control (shCTR). Protein levels of NF-YA are reduced of about 70% after 54h ***(Figure 5.2A)*** and 72h ***(Figure 5.2B)*** from HCT116 infection, while NF-YB and NF-YC protein expression is clearly upregulated (two- and three-fold, respectively). Nevertheless, silencing of NF-YA determines ~80% reduction of all of the three NF-Y subunits in chromatin-enriched extracts ***(Figure 5.2B)***, that is consistent with the depletion of the DNA-binding and limiting subunit of the complex. As previously demonstrated [Benatti et al.,2011], the knock-down of NF-YA induces DNA damage, as indicated by activation of γH2AX, and triggers an upregulation of p53 protein ***(Figure 5.2A)***.

To ascertain whether increased protein amounts of NF-YB and NF-YC were due to higher levels of transcription, we performed RT-PCR analyses on shCTR and shNF-YA cells. As shown in ***Figure 5.2C,*** NF-YB and NF-YC mRNA levels have an average three-fold increase in shNF-YA cells compared to shCTR cells. As concerns minor NF-YC splice variants, they show only a slight increase in shNF-YA cells ***(Figure 5.3)***, ruling out that specific isoforms different from the constitutive NF-YC (37kDa) could be activated in response to NF-YA depletion.



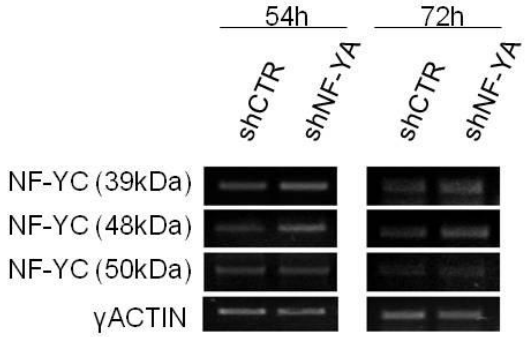


**Figure 5.3| Silencing of NF-YA has little effects on minor NF-YC splice-variants.** Semi-quantitative RT-PCR of NF-YC (39, 48 and 50 kDa) after 54h and 72h from lentiviral infection of HCT116 with shCTR and shNF-YA constructs.

With the aim to confirm the negative role played by NF-Y in the transcriptional regulation of NF-YB and NF-YC, we exploited HCT116 cells stably transfected with wild-type NF-YA or the well characterized dominant negative NF-YAm29 (NF-YA-DN) [Imbriano et al.,2005]. In this NF-YA mutant, three amino acids in the DNA-binding domain have been mutated, allowing proper association with the NF-YB/NF-YC dimer, but not the recognition of the CCAAT box. Western Blot analyses pointed out that NF-YA overexpression leads to downregulation of NF-YB and NF-YC protein

levels compared to cells transfected with a control vector (CTR) ***(Figure 5.4)***. On the contrary, expression of NF-YA-DN determined a slight increase of the two HFM-subunits, as expected.

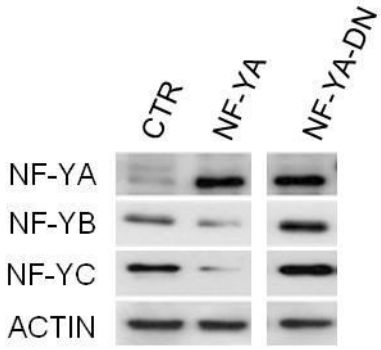


**Figure 5.4| Overexpression of NF-YA or a dominant negative mutant (NF-YA-DN).** Protein levels of NF-Y subunits in Whole Cell Extracts of HCT116 stably transfected with NF-YA, a dominant negative NF-YA mutant (NF-YA-DN) or an empty control vector (CTR).

### 5.2.2 Impairment of NF-Y activity affects chromatin structure in the promoters of NF-Y subunits

The *in vivo* binding of NF-Y on NF-YA, NF-YB and NF-YC promoters has been identified by ChIP-Sequencing experiments performed in K562, HelaS3 and GM12878 cell lines [(Rosenbloom et al.,2013)]. First, we validated NF-Y binding to promoters of NF-YB, NF-YC P1 and NF-YC P2 in HCT116 cells, and as already observed by Ceribelli et al., NF-YC P2 regulatory region showed higher NF-Y enrichment compared to P1 [(Ceribelli et al.,2009)]. Furthermore, ChIP real-time PCRs highlighted that the histone marks acetyl-H3 (H3ac), acetyl-H4 (H4ac) and acetyl-H3K56 (H3K56ac), indicative of an active chromatin state, were higher in P1 promoter rather than in P2 ***(Figure 5.5)***, hinting that the constitutive NF-YC promoter in HCT116 cells is P1.

We therefore carried out Chromatin Immunoprecipitation (ChIP) experiments in



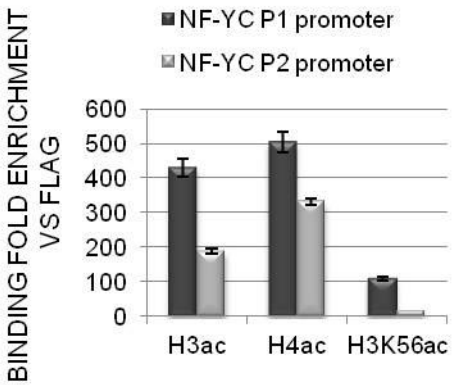


**Figure 5.5| NF-YC P1 is the active basal promoter in HCT116 cells.** Quantification of the active chromatin marks acetyl-H3 (H3ac), acetyl-H4 (H4ac) and acetyl-H3K56 (H3K56ac) in the two NF-YC promoters in shCTR-HCT116 cells, as detected by ChIP real-time PCR. Data are expressed as the fold enrichment of the percentage of immunoprecipitated sample over a non-correlated FLAG antibody.

HCT116 cells after lentiviral infection with shNF-YA or shCTR, to assess if differential NF-Y binding could be responsible for variations in NF-YB and NF-YC transcription ***(Figure 5.6)***. NF-Y binding to NF-YB and NF-YC promoters was cut by at least 80% after 54h from shNF-YA infection ***(Figure 5.6A)***. Conversely, when we analysed histone marks indicative of an active chromatin state, we observed a striking rise in acetyl-H3 (H3ac) and acetyl-H3K56 (H3K56ac) in NF-YB and NF-YC P1 regulatory regions, together with a slight increase of acetyl-H4 (H4ac). On the contrary, knock-down of NF-YA had little effects on global acetylation of NF-YC P2 promoter ***(Figure 5.6B)***. These data prompted us to speculate that NF-Y takes part in

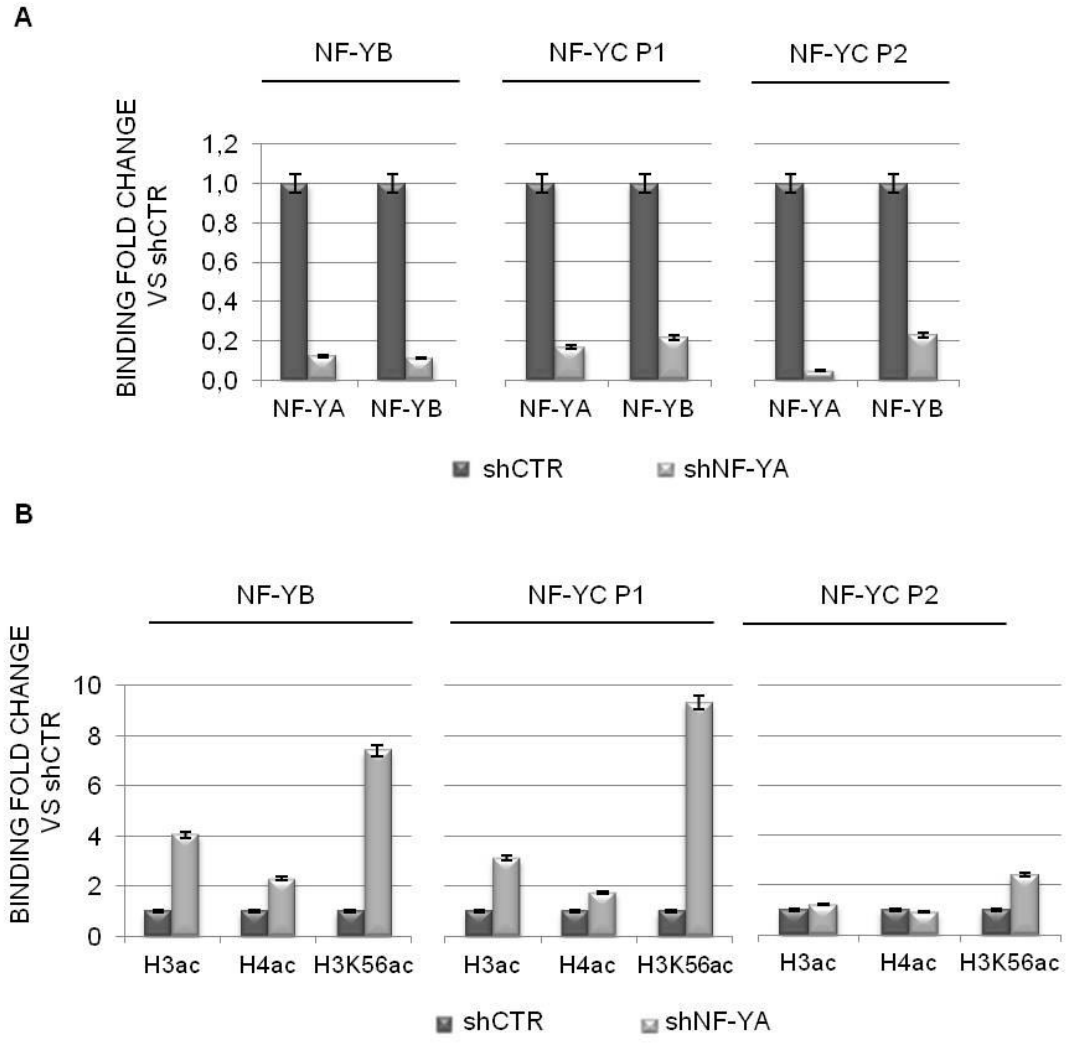


**Figure 5.6| NF-Y binding to NF-YB and NF-YC promoters is impaired after shNF-YA, while positive histone acetyl-marks are increased.** Quantification of (A) NF-YA and NF-YB and (B) of the active chromatin marks acetyl-H3 (H3ac), acetyl-H4 (H4ac) and acetyl-H3K56 (H3K56ac) to the indicated promoters, as detected by ChIP real-time PCR. Data are expressed as fold change of binding in shNF-YA (54h) cells over shCTR cells. Specific antibody immunoprecipitations were normalized to FLAG antibody.

the housekeeping activity of NF-YB and NF-YC P1 promoters, being able to maintain restricted basal levels of transcription.

In NF-YB and NF-YC P1 regulatory regions, an inverse correlation between NF-Y recruitment and open chromatin marks was confirmed also 72h post-infections ***(Figure 5.7)***, hinting at a sensible and persistent molecular mechanism that leads to NF-Y subunits upregulation when NF-Y transcriptional activity is impaired.

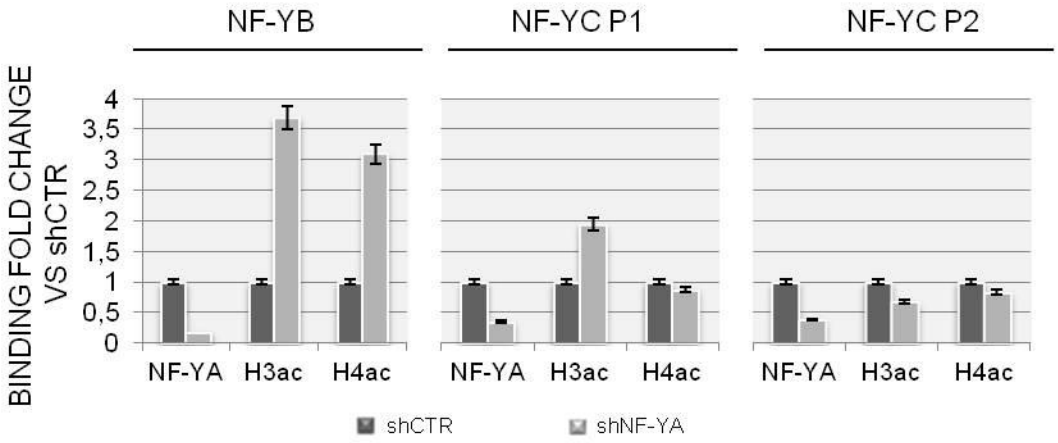




**Figure 5.7| Alterations in NF-Y binding and chromatin structure at NF-YB and NF-YC promoters is maintained 72h post-shRNAs infections.** Quantification of NF-YA and of the active chromatin marks acetyl-H3 (H3ac) and acetyl-H4 (H4ac) in the indicated NF-Y promoters, as detected by ChIP real-time PCR. Data are expressed as fold change of binding in shNF-YA (72h) cells over shCTR cells. Specific antibody immunoprecipitations were normalized to FLAG antibody.

### 5.2.3 NF-YB and NF-YC proteins are necessary for NF-Y trimer stability

To strengthen our findings about a negative autoregulatory loop in NF-Y subunits expression, we assessed their mRNA levels in HCT116 after shRNAs-mediated depletion of NF-YB or NF-YC. As expected, NF-YB and NF-YC were completely inactivated by 48h post-infection ***(Figure 5.8)***. Conversely, we observed a two-fold increase of NF-YA transcript levels. Surprisingly, only a slight increase of NF-YC was detected after silencing of NF-YB and no significant changes were detected in NF-YC mRNA after silencing of the corresponding histone-fold partner, compared to shCTR. This lack of evident transcriptional effects could be ascribed to the lower efficiency of shNF-YB and shNF-YC in depleting NF-Y complex from chromatin, as compared to shNF-YA [(Benatti et al.,2011)].

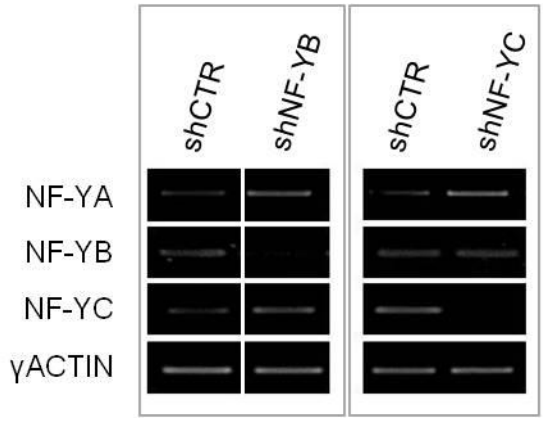


**Figure 5.8| Silencing of NF-YB or NF-YC slightly increased NF-YA transcription.** mRNA levels of NF-Y subunits following 48h from lentiviral infection with shCTR, shNF-YB and shNF-YC.

Unexpectedly, Western Blot analyses ***(Figure 5.9A and B, left panels)*** showed a severe NF-YA protein downregulation (of 80%) in shNF-YB and shNF-YC cells compared to shCTR samples. Furthermore, knock-down of NF-YB triggers a comparable depletion of both NF-YB and NF-YC proteins. The same phenomenon is observed following shNF-YC infection ***(Figure 5.9A and B, left panels)***.



Since these results were in contrast with the data obtained at the transcriptional level, we hypothesized that enhanced NF-Y degradation could occur in shNF-YB- and shNF-YC-cells, due to the lack of NF-YB/NF-YC dimer assembly. Therefore, we inhibited protein degradation pathways by treating HCT116 cells with the lysosomal inhibitor Chloroquine (CQ) together with the proteasomal inhibitors MG132 and LLnL. Under this experimental conditions, doubling of NF-YA protein levels is detected in NF-YB or NF-YC silenced cells, compared to shCTR cells. Moreover, the expression of the dimerization partner is completely restored ***(Figure 5.9A and B, right panels)***.

These data suggest that the loss of one of the two HFM subunits, that hampers the formation of a stable NF-YB/NF-YC complex, leads the respective HFM partner to protein degradation.

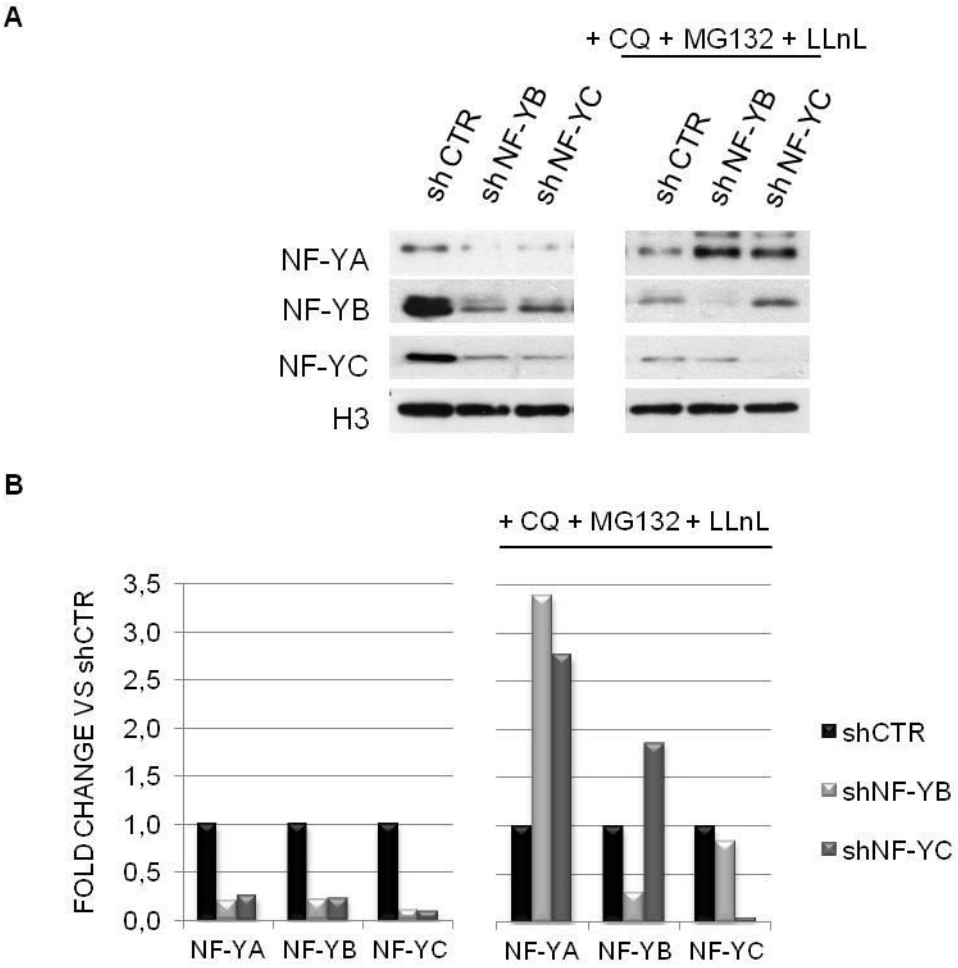


**Figure 5.9| NF-YB/NF-YC dimer confers stability to the complex.** (A) Protein levels of NF-Y subunits following 48h from lentiviral infection with shCTR, shNF-YB and shNF-YC. In right panel, cells have been treated for 18h with inhibitors of lysosomal degradation (Chloroquine, CQ) and of proteasomal degradation (MG132 and LLnL). (B) Quantification of NF-YA, -YB and –YC expression levels in shNF-Y versus control cells, with and without administration of CQ, MG132 and LLnL.



## 5.3 Discussion

In the last years a multitude of studies pointed out that expression of NF-Y-dependent genes and NF-Y itself are deregulated in cancers [(Goodarzi et al.,2009, Uhlen et al.,2010; Garipov et al.,2013)]. NF-Y has a crucial role in cell cycle progression and it could be a useful target for controlling aberrant hyper-proliferation of cancer cells. Therefore, besides NF-Y activities and target-genes, we need to know the mechanisms regulating the expression of NF-Y subunits. This subject has not been extensively studied so far. Our previous works indicated that after NF-YA knock

down in HCT116 cells, NF-YB and NF-YC are up-regulated. Moreover, public ChIP-Seq data reveal that NF-Y is bound onto NF-Y subunits' promoters. We thus hypothesized that NF-Y transcription could be controlled through a negative self-regulatory loop. To evaluate this model, we either silenced the different NF-Y subunits through lentiviral delivery of specific shRNAs or we overexpressed a wild-type and a dominant-negative form of NF-YA, that is the limiting subunit of the complex. Our studies highlighted that the presence of active NF-Y complexes in the cell has an inverse correlation with the transcription of NF-YA, NF-YB and NF-YC ***(Figures 5.2C, 5.3, 5.8)***. Chromatin Immunoprecipitations confirmed that in front of reduced NF-Y binding to the constitutive NF-YB and NF-YC promoters, histone acetylation is increased ***(Figures 5.6 and 5.7)***, supporting higher transcriptional levels of the HFM-subunits. Conversely, the P2 promoter, which was previously postulated to be an inducible promoter in response to genotoxic stress (Ceribelli et al.,2009), showed low levels of activity either in shCTR or shNF-YA cells ***(Figures 5.5-5.7)***, indicating that it is not involved in the steady-state control of NF-YC expression.

Since it is known that NF-Y can exert a negative function by recruiting transcriptional co-repressors, it will be of great interest to identify the precise molecular machinery involved in this negative feedback control of NF-Y transcription. One possibility is that NF-Y serves as a platform for p53-mediated repression, since a biochemical and functional link has already been demonstrated between NF-Y and the tumour suppressor p53 (Di Agostino et al.,2006; Benatti et al.,2008; Imbriano et al.,2005 and 2012). Indeed, NF-Y can mediate the binding on CCAAT promoters of p53, which in turn recruits histone deacetylases and other repressive complexes. This is a common mechanism which controls, for example, G2/M promoters activity in response to DNA damage (Basile et al.,2006; Bansal et al.,2011; De Amicis et al.,2011). It is thus possible that the NF-Y-p53 complex maintains low basal levels of NF-YB and NF-YC, and functions as a sensor which enables an increase of transcription when NF-Y protein is absent. Moreover, it is already known that NF-YC P2 promoter is under negative regulation by p53 in growing conditions, while binding is lost following genotoxic treatment with Doxorubicin (Ceribelli et al.,2009). Further investigations are needed to validate this hypothesis, which could open new attractive questions about the correlation between increased NF-Y levels in cancer cells and the expression of mutant p53.

On the other hand, NF-Y can directly interact with several histone deacetylases (HDACs) to mediate transcriptional repression (Peng et al.,2003; Imbriano et al.,2005; Basile et al.,2006). In particular, NF-Y can recruit on target promoters (both directly o *via* p53) HDAC1 or a Sin3/HDAC co-repressor complex, that mediates gene repression by chromatin compaction. Interestingly, these factors have been identified on promoter regions of NF-YA, NF-YB and NF-YC genes by ChIP-Seq analyses (Rosenbloom

et al.,2013). Furthermore, ENCODE and Microarray data indicated that both HDAC1 and Sin3A expression are regulated by NF-Y (Benatti et al.,2011; Rosenbloom et al.,2013). This could contribute to create an interesting regulatory mechanism which senses the amount of cellular NF-Y and increases its transcription when it is not sufficient to exploit its cellular functions.

In addition, knock down of NF-YB and NF-YC in HCT116 cells evidenced that the two histone-fold subunits can mutually stabilize each other at the protein level ***(Figure 5.9)***. In fact, NF-YB and NF-YC mRNA levels were roughly unperturbed after silencing of the partner subunit ***(Figure 5.8)***, most likely due to lower efficiency in displacing NF-Y from chromatin compared to NF-YA knock-down (Benatti et al.,2011). However, a comparative analysis of the stability of NF-Y proteins after shRNAs-mediated silencing of single HFM-subunits, demonstrated that the formation of NF-YB/NF-YC dimer is required for the stability of the complex.

Taken together, our results demonstrate that NF-Y expression is controlled by a complex autoregulatory loop, which involves both gene transcription and protein stabilization of NF-Y subunits.

# 6. TASK III: NON-TRANSCRIPTIONAL ROLE OF NF-Y IN DNA REPLICATION

**(Collaboration with Prof. J.Julian Blow, University of Dundee, UK)**

## 6.1 Background

### 6.1.1 NF-Y and cell proliferation: insights from silencing experiments

The role of NF-Y in gene transcription and cell cycle control has been evaluated either by expression of NF-YA mutants with impaired functions or by knock-down of each of the three NF-Y subunits. Recent investigations demonstrated that the major effect of NF-YB inactivation is a delay in G2/M progression, while a few cells are impaired in S-phase progression (Benatti et al.,2008 and 2011). Indeed, transcriptome analyses indicated that G2/M-phase genes are repressed, as well as genes of microtubule/cytoskeleton and spindle formation GO categories, ascribing the major function of NF-Y in cell-cycle progression to its activity in gene transcription. Consistently, NF-YC inactivation determined similar effects and also the expression of a NF-YA-Bdbd mutant, that lacks the C-terminal transcription activation domain, arrested cells at the G2/M boundary (Hu et al.,2006). Unexpectedly, the lack of NF-YA subunit has been demonstrated to elicit a different cellular response. Expression of NF-YA-DN mutant in mouse fibroblasts slowed down cell proliferation, delaying especially S-phase progression (Hu et al.,2000), while deletion of NF-YA in primary cultures of mouse embryonic fibroblasts (MEFs) caused a complete S-phase arrest, leading cells to apoptosis (Bhattacharya et al.,2003). Moreover, NF-YA-depleted HCT116 cells had a very severe phenotype, with a strong increase of cell death due to the presence of DNA replication defects (Benatti et al.,2011). The different phenotypes observed after depletion of NF-YB/NF-YC rather than NF-YA can be attributed to the higher ability of NF-YA-silencing to impair the occupancy of CCAAT promoters. In fact, NF-YB and -YC depletion only reduces NF-Y binding to its target sequences, thus leading to repression of highly dynamic NF-Y-dependent genes, in particular G2/M genes. Conversely, the loss of NF-YA implies almost no occupancy of CCAAT boxes and determines changes also in the expression of G1/S genes (Bhattacharya et al.,2003), which could account for DNA damage. Nevertheless, it has been suggested that either NF-YA subunit alone or NF-Y complex could have additional functions in

the cell: NF-YA depletion originates spontaneous DSBs and NF-Y itself could be fundamental for the DNA-replication process or the intra-S damage checkpoint.

### 6.1.2 DNA replication

The DNA double helix must be accurately duplicated at each cell cycle. The DNA synthesis machinery copies each DNA strand starting from opening sites, called replication origins, and then progresses from these sites in a bidirectional way. In mammals, up to 50000 origins are activated every cell cycle, following a strict time-regulation. Replication origins are primed by a three-step process: recognition of origins, assembly of a pre-replication complex (pre-RC) during G1 phase and activation of the pre-RC (Méchali,2010; Takeda et al.,2005). In eukaryotes, the heterohexameric origin recognition complex (ORC) directly recognizes DNA origins, recruiting the initiation factors Cdc6 and Cdt1; these proteins then allow the binding of two MCM2-7 complexes ***(Figure 6.1)***. This MCM complex is an ATPase-dependent DNA helicase, which forms a ring around the DNA (Remus et al.,2009): after loading of the helicase, the pre-RC is completely assembled and the origin is licensed. pre-RCs are thus assembled in a highly ordered manner, to be subsequently activated at the onset of S-phase, promoting origin unwinding and recruitment of DNA polymerases.



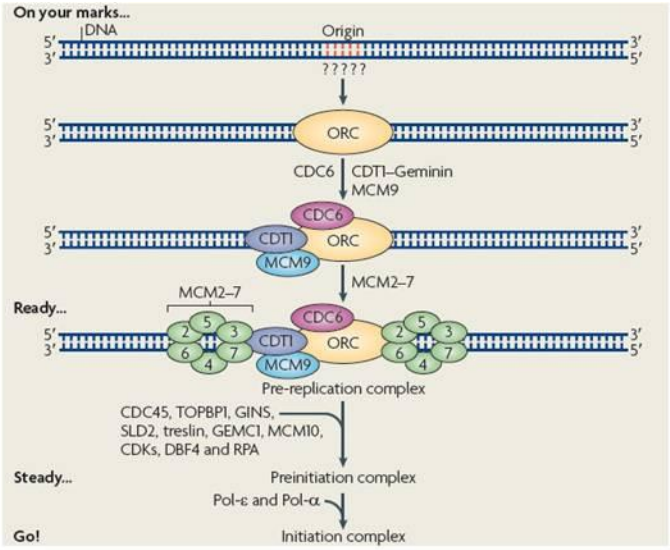


**Figure 6.1|** Grafical representation of the process of DNA replication initiation in eukaryotic cells. (Méchali, 2010).

This process needs to be tightly controlled as any origin can be activated only once per cell cycle. Furthermore, pre-RCs are activated at different times during S phase, identifying early-, mid- and late-origins. It has been recently proved that potential

replication start-sites are in excess and that only a small subset is used at each cell cycle: this guarantees that the entire genome can be duplicated even if some pre-RCs fail to fire, as neighbouring dormant origins can be activated (Méchali,2010; Blow et al.,2011). In a similar way, dormant origins might also rescue DNA replication when forks are stalled due to replicative stress: indeed, when DNA synthesis or the DNA-damage pathways are impaired, an intra-S phase checkpoint is activated to prevent late-origins firing and allow DNA repair. Furthermore, under poor cell-growth conditions, such as low nucleotides concentration, late-origins are inhibited by the checkpoint activity and the use of dormant origins is increased to rescue under-replicated regions (Luciani et al.,2004; Branzei et al.,2005; Woodward et al.,2006; Karnani et al.,2011).

Pre-RCs are converted into replication forks at the onset of S phase. Initiation of DNA replication requires the activity of two kinases, CDK2 (Cyclin Dependent Kinase 2) and DDK (Dbf Dependent Kinase), and the recruitment of another series of replication factors temporally regulated during S phase, MCM10, Cdc45 and the GINS complex (consisting of Sld5 and Psf1–3): this is necessary for the following unwinding of origins and loading of replicative polymerases (Uchiyama et al.,2001; Sawyer et al.,2004; Méchali,2010). Cdc45 represents a link between initiation and elongation factors, interacting with both pre-RC and DNA-polymerases (Masuda et al.,2003). Cdc45 binds origins in a CDK- and DDK-dependent way and is loaded at early-origins in early S phase, and at late-origins in late S phase. After origin firing, Cdc45 proceeds with the components of the active replicating fork, since it is important also for the elongation phase of replication (Tercero et al.,2000). At least three polymerases are essential for replication, performing specialized functions. After origin unwinding, DNA polymerase α (DNApol α) is loaded onto origins and synthesizes short RNA primers, allowing *de novo* synthesis of DNA. After that, DNApol α is replaced by DNApol δ and/or DNApol ε: these have proofreading exonuclease activity and also an increased processivity, thanks to their association with the processivity factor PCNA (Takeda et al.,2005).



Transcription and replication are highly interconnected processes, since transcription may influence either the choice of replication origins or the chromatin conformation around them. Indeed, in mammal cells a link has been established between early-origins and highly transcribed genes, whereas late-origins have been associated with non-transcribed domains (Donaldson, 2005; Schwaiger et al.,2006). Even though active transcription exerts a negative function in firing of potential origins, the high chromatin accessibility of gene promoters may facilitate the selection of a nearby origin. This phenomenon could be ascribed either to the open chromatin organization at promoters, or to a crosstalk between replication and transcription factors (Ghosh et al.,2004; Dominguez-Sola et al.,2007). Recently, increasing evidences have emerged showing that transcription factors can have a role also in other cellular

processes associated to chromatin structure. For example, the transcription factor E2F1 is able to promote the assembly of repair factors to sites of DNA-damage (Biswas et al.,2012), whereas Myc interacts with the pre-RC and modulates the activation of replication origins through a non-transcriptional mechanism (Dominguez-Sola et al.,2007).

## 6.2 Results

### 6.2.1 NF-Y is recruited onto actively replicating chromatin

Although all of the three NF-Y subunits are required for its transcriptional activity, the conditional inactivation of NF-YB/NF-YC triggered different cell cycle defects from NF-YA silencing (Benatti et al.,2011). In particular, the lack of NF-YA leads to a delay in S-phase progression and a severe DNA-damage, while silencing of NF-YB or NF-YC arrests cells in G2/M phase. These discrepancies could be ascribed to different efficiencies in depleting NF-Y from chromatin, with the silencing of NF-YA showing the greatest efficacy. However, taking into account that NF-Y is accumulated inside the nucleus at the beginning of S-phase, we hypothesized that NF-YA could have a direct uncharacterized role during S phase.



Previous works indicated that NF-Y is highly conserved from *Xenopus* to human, with *Xenopus* NF-YB and NF-YC showing a 90% amino acid identity with human protein, while sequence homology between *Xenopus* NF-YA and human is about 75% (Li et al.,1998). For this reason, to shed light on the possible non-transcriptional role of NF-Y in DNA replication, we took advantage of a *Xenopus laevis* cell-free system, which supports cell-cycle-regulated DNA replication in the absence of transcription and new protein synthesis (a comprehensive description of the principles and procedures about the use of *Xenopus* egg extracts to study DNA replication is provided in Gillespie et al.,2012). In this assay, a template DNA (demembranated *X. laevis* sperm chromatin) is added to an activated low-speed cytosolic extract derived from *Xenopus* eggs. DNA added to the extract is first assembled into chromatin, then into structures analogues to interphase nuclei: after nuclear assembly, the DNA can be efficiently duplicated, under the same cell-cycle controls that are present *in vivo*.

First of all, we assessed the dynamics of replication factors association with chromatin during replication, in order to understand if NF-Y is specifically recruited on DNA during replication. Time-course Western Blot analysis of chromatin-extracts demonstrated that NF-YA is actually bound to chromatin during replication and its binding peaks just after the recruitment of the replication initiation factors MCM10, Cdc45 and DNApol α ***(Figure 6.2).***

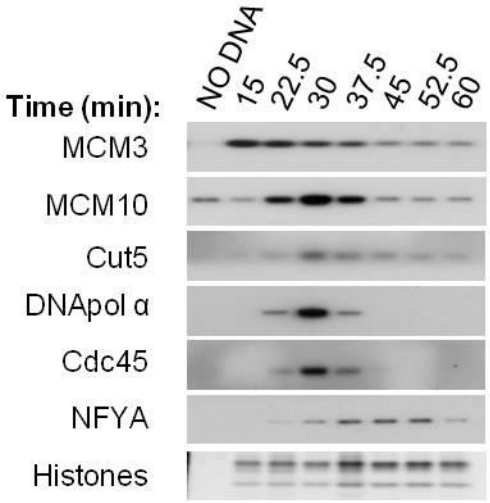


**Figure 6.2| NF-YA associates to replicating chromatin.** Chromatin was isolated from a replication reaction at the indicated times, separated by SDS-PAGE and immunoblotted with the indicated antibodies against replication proteins. Histones were stained with Comassie as a loading control.

In order to understand if the presence of active replicating forks is a prerequisite for the binding of NF-YA, we repeated the same time-course experiments in the presence of either the CDK inhibitor p27, which allows assembly of the pre-RC but not its activation, or Geminin, that prevents pre-RC assembly. Western blots in ***Figure 6.3*** clearly point out that NF-YA cannot bind to chromatin unless origins have already been licensed and replication forks have been activated.



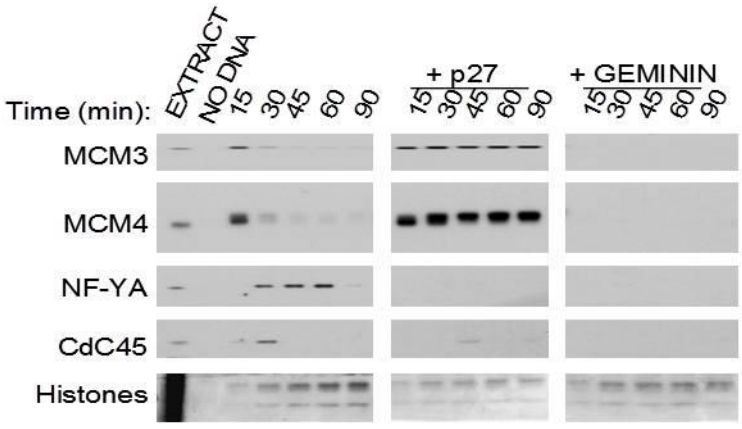


**Figure 6.3| NF-YA requires active forks to assemble to chromatin.** Chromatin was isolated at the indicated times from a replication reaction assembled plus or minus the CDK inhibitor p27 or the licensing inhibitor Geminin. Western Blot were performed with the indicated antibodies. Histones were stained with Comassie and used as a loading control.

### 6.2.2 NF-Y is required for efficient DNA replication in *Xenopus* egg extracts

In order to understand whether NF-Y has a functional role in the process of DNA duplication, we immunodepleted endogenous NF-YA and NF-YB from the extracts that we used in replication assays. The high level of protein sequence homology allowed us to efficiently immunoprecipitate *Xenopus* proteins with antibodies raised against mouse NF-Y subunits.

Analysis of DNA replication kinetics in NF-Y depleted (ΔNF-YA and ΔNF-YB) compared to a mock depleted extracts (ΔIgG), highlighted a 30% decrease in nucleotide incorporation into genomic DNA ***(Figure 6.4A)***, both by depleting NF-YA or

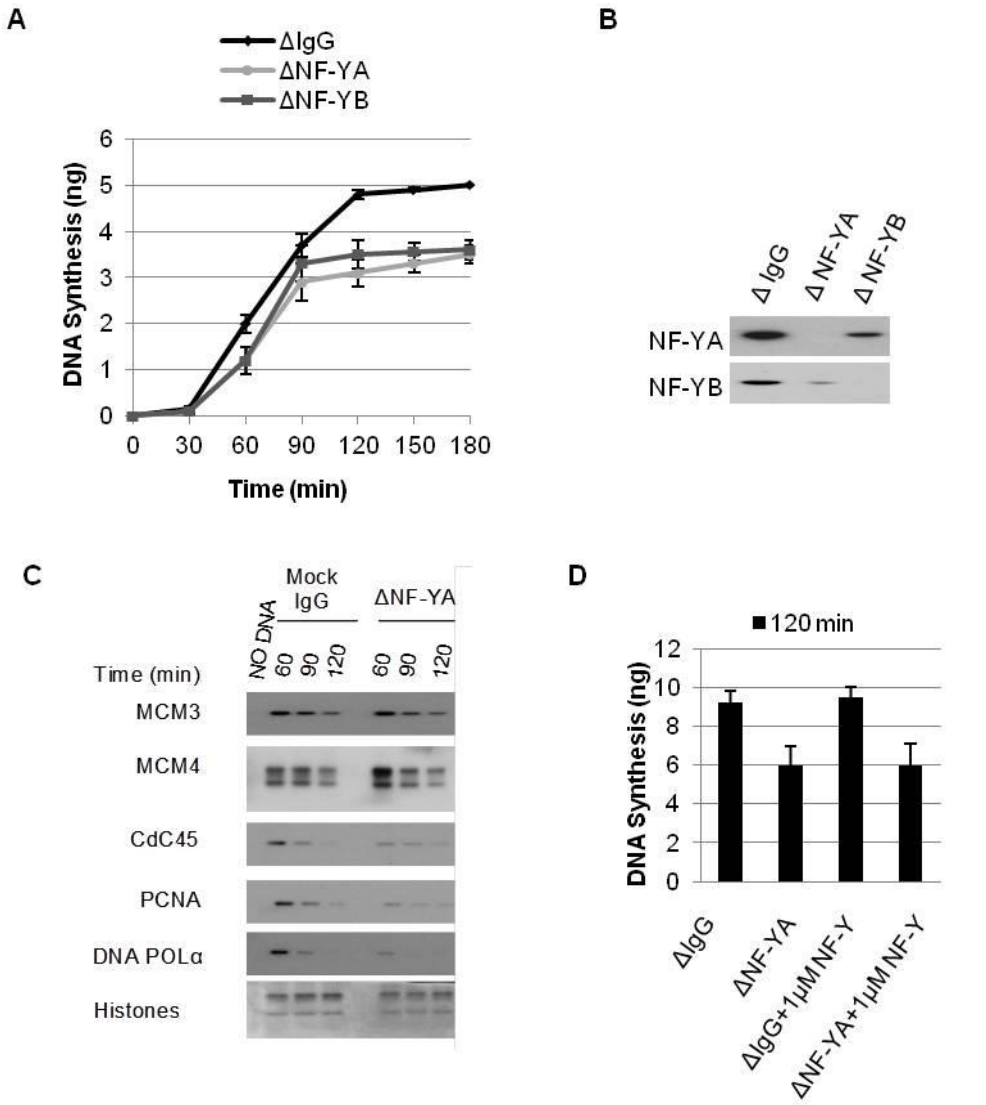


**Figure 6.4| NF-Y modulates DNA replication efficiency.** (A) DNA synthesis was monitored in a time-course experiment based on the incorporation of $\alpha^{32}$P-dATP, in mock (ΔIgG) or NF-Y depleted (ΔNF-Y) extracts. (B) Western Blot analysis of NF-YA and NF-YB in ΔIgG and ΔNF-Y extracts used in Replication assays. (C) Time-course of replication factors association to chromatin in mock and NF-YA depleted extracts. (D) Quantification of global DNA replication after addition of recombinant NF-Y protein complex to ΔIgG or ΔNF-YA extracts.

NF-YB. Western blot analyses carried out with the same extracts, demonstrated that the procedure completely removed *Xenopus* NF-YA or NF-YB from the corresponding immunodepleted extract ***(Figure 6.4B)***. Moreover, it is to be noted that a single immunoprecipitation eliminates both the subunits from the extract, consistently with the formation of NF-Y heterotrimeric complexes also in *Xenopus* cells (Li et al.,1998). As a consequence, we were not able to attribute the observed impairment of DNA synthesis to NF-YA alone, rather than to NF-Y complex. Nevertheless, we focused our attention on ΔNF-YA extracts. Investigations on the binding of replication proteins to chromatin after NF-YA immunodepletion ***(Figure 6.4C)***, pointed out that active replication fork proteins are diminished in comparison with mock-depleted extracts, confirming that NF-Y is necessary for proper DNA replication to take place. Surprisingly, the observed replicative defects could not be rescued by addition of recombinant NF-Y heterotrimer ***(Figure 6.4D)***, hinting that I) by depleting NF-Y, we are removing from the extracts one or some NF-Y interactors that are fundamental for DNA replication or II) the minor differences between *Xenopus* and *mouse* protein sequences could account for a reduced activity of mouse proteins in *Xenopus* extracts.

To overcome these limitations, *in vitro* DNA synthesis assays were performed on extracts supplemented with a dominant-negative NF-YA mutant (indicated hereafter as NF-YA mutant), that hampers the DNA binding activity of NF-Y without removing any of the endogenous *Xenopus* proteins from the experimental system.



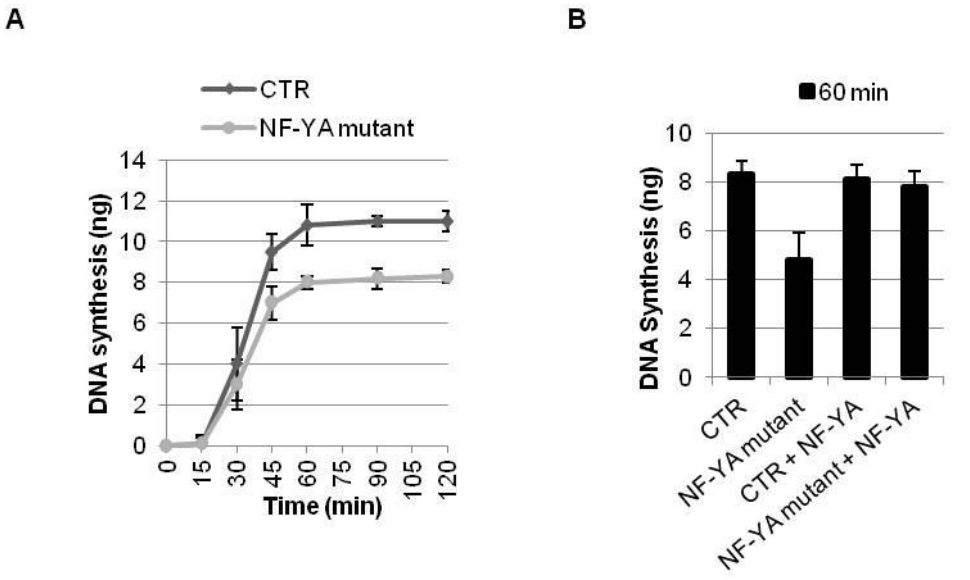


**Figure 6.5| NF-Y is required for proper DNA replication.** (A) DNA synthesis was monitored in a time-course experiment based on the incorporation of $\alpha^{32}$P-dATP, in extracts with or without addition of a Dominant Negative-NF-YA mutant. (B) Quantification of global DNA replication after addition of recombinant NF-YA proteins to control extracts or extracts containing mutant dominant-negative NF-YA .

The presence of NF-YA mutant triggered a decrease of about 30% in the rate of DNA replication ***(Figure 6.5A)***, consistently with the results obtained from NF-Y immunodepletion. However, in this case replication defects were fully rescued by addition of recombinant wild-type NF-YA protein (indicated as NF-Y) ***(Figure 6.5B)***.
Overall, these results prove that NF-Y has a non-transcriptional role in the control of DNA replication, and suggest that it executes its function after assembly of the pre-RC and activation of the replication fork.

## 6.3 Discussion

It was previously proposed that NF-Y regulates timely progression of cells through G2/M and S phase by the specific transcription of factors promoting cell growth and proliferation (Elkon et al.,2003). Transcriptional control of target genes associated to DNA replication and repair, such as Cdc45L, MCMs or Cdt1 (Benatti et al.,2011), may be an important component in the global NF-Y-dependent regulation of DNA replication. However, our novel results show that NF-Y has a direct non-transcriptional role that ensures efficient duplication of the genome ***(Figures 6.4 and 6.5)***. Interestingly, the DNA binding domain of NF-YA seems to be crucial not only to mediate transcriptional functions, but also replicative ones, hinting that NF-Y could exploit similar molecular mechanisms to direct both DNA-dependent pathways. For example, this mechanism could involve NF-Y-dependent epigenetic remodelling, since epigenetic modifications can account for differential replication origins timing and replication fork progression (Casas-Delucchi et al.,2011; Sims and Wade,2011). As an example, it was recently revealed an important role for HDAC1 and 2 in the proper chromatin reassembly following DNA replication, which is a relevant step that modulates fork velocity (Bhaskara et al.,2013) Due to the fact that NF-YA depletion delays cell progression through S-phase and prevents efficient DNA synthesis, it is possible that NF-Y-mediated recruitment of HDAC1 to chromatin plays a significant role also in DNA replication, rather than in transcription. Moreover, known NF-Y-related co-factors, such as p300, are known to have a function in DNA-damage response (Hasan et al.,2001; Vempati et al.,2010).



Our results clearly demonstrate for the first time that NF-Y has a non-transcriptional activity during S-phase.
Further studies will be required to define its precise molecular function and our data open a few different possibilities: NF-Y could I) bind and stabilize the replicative fork, II) be involved in the proper reassembly of chromatin behind the fork or III) participate to the poorly characterized DNA replication elongation checkpoint (Conti et al.,2007), which controls the velocity of replication forks under normal and stress conditions.

Our findings can also give further insights into the consequences of NF-Y over-expression in cancer cells, which can contribute to higher proliferation rates. On the contrary, DNA-damage and apoptosis observed after knock-down of NF-YA are the global result of transcriptional inhibition together with replication defects.

# 7. CONCLUSIONS

Mutations of NF-Y have never been observed in transformed cells, thus reducing the interest of scientists addressing cancer problems in understanding the biology of this transcription factor. Although, NF-Y has emerged as an important factor involved in oncogenic transcriptional changes (Goodarzi et al.,2009), which could be triggered by NF-Y hyper-activity in cancer cells. In agreement with this hypothesis, NF-YA seems to be upregulated in many malignant lymphomas, gliomas, breast cancer and endometrial cancers, as well as a few cervical, lung and ovarian cancers. Despite these data available from Human Protein Atlas database (http://www.proteinatlas.org/cancer), an exhaustive study on NF-Y expression and regulation has never been done in cancer *versus* normal cells.

Our data provide evidence for the complex mechanism which regulates NF-Y subunits, suggesting that their controlled expression is fundamental for proper cell proliferation. In particular, NF-YA deregulation seems to trigger more evident biological consequences than NF-YB or NF-YC. Consistently, both overexpression and depletion of NF-YA lead to cell death with the activation of a common p53-dependent apoptotic pathway (Benatti et al.,2008; Gurtner et al.,2010). We demonstrated that a transcriptional autoregulatory loop occurs in order to maintain controlled housekeeping expression levels, and to increase or decrease NF-Y synthesis when cellular levels of its subunits are lowered or raised, respectively. Besides, we showed that the assembly of NF-YB/NF-YC dimer is necessary to stabilize the NF-Y complex. This contributes to reinforce the self-regulatory loop which regulates NF-Y intracellular concentrations: if even only one of the subunits is lacking, the whole trimer is depleted from the cell, strongly stimulating an increase of NF-Y expression.



This fine tuning is indicative of the essential role of NF-Y for cell survival Indeed, we demonstrated that the modulation of NF-YB/NF-YC subcellular localization by the anti-tumor drug bDMC has a positive anti-proliferative effect on cancer cells, contributing to cell death both *via* transcriptional mechanisms (TOP2A downregulation) and probably non-transcriptional activities (delay in S-phase progression an replicative stress).

Our results point out that NF-Y not only orchestrates cell proliferation through its transcriptional activity, but it also plays a direct role in DNA replication, suggesting that it could have a double function in promoting hyper-proliferation of malignant cells

Gene transcription and DNA replication are essential prerequisites for cell proliferation. Coordination of these processes is a key determinant of gene organization and of the complex architecture of mammalian genomes [(Huvet et al.,2007)], being implicated in genome stability and tumorigenesis. The activation of replication origins in early S-phase could result from i) a particular genomic context involving transcription factor binding-sites or ii) the transcription of neighboring housekeeping genes. Indeed, early replication origins are associated with an open chromatin structure, which is permissive to both replication and gene expression [(Chakalova et al.,2005)]. The effect of this open conformation is to promote the expression of nearby genes, but this is progressively weakened with the increasing distance from the putative replication origin.

In the last years various transcription factors and their binding sites were shown to play an important role in DNA replication. Our data clearly suggest that NF-Y can be one of these transcription factors regulating S phase progression, presumably through its activity of pioneer factor ***(Figure 7.1)*** [(Fleming et al.,2013)]. NF-Y not only performs a genetic function early in the activation of transcription, but also binds DNA in condensed chromatin prior to other factors, thus allowing the recruitment of other proteins involved in gene transcription and/or replication.



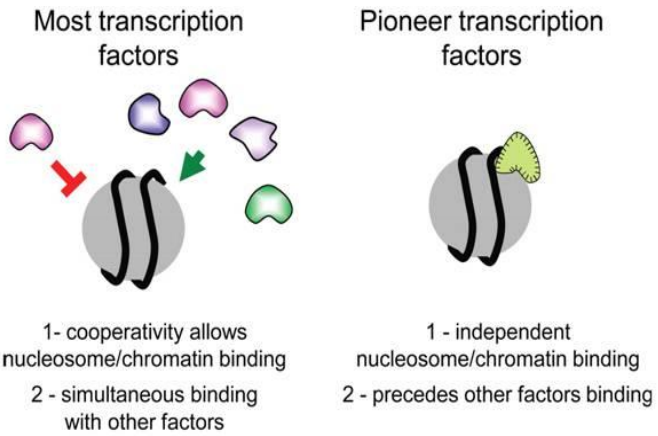


**Figure 7.1 |** Properties that distinguish pioneer factors from other transcription factors[(Zaret and Carroll,2011)].

# 8. MATERIALS AND METHODS

## 8.1 Cell lines and treatments

HCT116 colorectal carcinoma cells were grown in Iscove's modified Dulbecco's medium (IMDM) supplemented with 10% heat inactivated fetal calf serum (FCS). Human hepatic fetal epithelial WRL-68 cells and colon carcinoma Lovo cells were cultured in Dulbecco's modified Eagle's medium (DMEM) supplemented with 10% FCS. Primary human fibroblasts (HF) were grown in DMEM with 10% FCS, 2mM Glutamine and 55mg/l Gentamicin. Stable expressing NF-YA cells were obtained by lentiviral infection of HCT116 cells with pSIN-NF-YAs or pSIN-NF-YAs-DN particles (gift of R. Mantovani, University of Milano) for 48 hours. Infected cells were then selected using puromycin and maintained in medium supplemented with puromycin (1µg/ml). All cell lines were cultured at 37°C with 5% $CO_2$. Doubling time has been estimated of about 16 h for HCT116, LOVO and WRL68 cells, and 24 h for HF cells.
bis-DemethoxyCurcumin (bDMC) [1,7-bis[4-hydroxyphenyl]hepta-1,6-diene-3,5-dione] was synthesized as previously reported (Basile et al.,2009) by the Chemistry laboratory of Prof. Saladini and Dr. Ferrari, University of Modena and Reggio Emilia. As determined by NMR and combustion analyses, the purity was >98%. bDMC was added to warm medium at 30 µM concentration, when not differently specified. Dimethyl Sulfoxide (DMSO, Sigma-Aldrich) was used as control, as it is the solvent in which bDMC is dissolved.
For pharmacological inhibitions, cells were pre-treated for 1 h and then co-incubated with bDMC or treated only with the inhibitors for the indicated times, with 25 µM Z-VAD-fmk (Enzo Life Sciences), 10 µM Wortmannin (WORT; Enzo Life Sciences), 1 µM *Z-Leu-Leu-Leu-H* (MG132; Sigma-Aldrich), 5µM *N-Ac-Leu-Leu-norleucinal* (LLnL; Sigma Aldrich), 20mM N-acetylcisteine (NAC; Sigma-Aldrich), 10 ng/ml Leptomycin B (LMB; Enzo Life Sciences) and 50 µM Chloroquine (Sigma Aldrich).



## 8.2 Flow cytometric analysis

### 8.2.1 Cell cycle analysis

Cells were harvested after drug treatments by trypsinization, collected in culture medium and washed in 1X Phosphate Buffered Saline (1X PBS: 137 mM NaCl, 2.7 mM KCl, 4.3 mM Na2HPO4, 7.7 mM KH2PO4, pH7.4) to get rid of serum proteins. Cells were then resuspended in 500 µl of Propidium Iodide (PI) staining solution (50 µg/ml PI, 0.1% sodium citrate, 0.1% Triton X-100, 0.1 µg/µl RNAseA in 1X PBS) and incubated for 30 minutes at 4°C in the dark. DNA distribution analysis was then performed by an Epics cytofluorimeter (Beckman Coulter).
Apoptotic cells were detected by FACS using Annexin V-PE conjugate (BD Biosciences, Becton Dickinson Italia) following the protocol of the manufacturer.

### 8.2.2 Indirect immunofluorescence staining

Cells were harvested after drug treatments, washed twice in 1X PBS and fixed in 1% formaldehyde for 10 minutes at 37°C, followed by post-fixation with 90% methanol for 30 minutes on ice. After two washes in blocking solution (0.5% BSA in 1X PBS) and permeabilization with 0.25% Triton X-100 for 5 minutes, cells were stained with anti-phospho-H2AX(S139) primary antibody (Millipore, #05-636) over-night at 4°C, and then incubated with rabbit anti-mouse FITC-conjugated secondary antibody (Dako, #0313) for 2h at 4°C in the dark. Cells were subsequently washed, treated with RNAseA for 10 minutes and incubated in PI solution (30 µg/ml PI in blocking solution) for additional 30 minutes at 4°C in the dark. Samples were then analyzed by an Epics cytofluorimeter (Beckman Coulter).

## 8.3 siRNA transfection

HCT116 cells were transfected (Metafectene SI$^+$, Biontex Laboratories GmbH) with 300 nM of paired TOP2A and non-targeting control siRNAs obtained from Sigma-Aldrich. TOP2A sense strand sequence: 5'-AAGACTGTCTGTTGAAAGAA-3'. Cells were analyzed or treated with bDMC 36 h after transfection.

## 8.4 Short hairpin RNA (shRNA)



pLKO.1 non-targeted short hairpin RNA (shCTR), shRNA-NF-YA targeting exon 6 (CCATCGTCTATCAACCAGTTA), shRNA-NF-YB targeting exon 5 (GCTATGTCTACTTTAGGCTTT) and shRNA-NF-YC targeting exon 5 (GCCTGGATTCACACAGAAGAT) were designed by Sigma-Aldrich. Puromycin resistance cassette was replaced with EGFP cassette [(Benatti et al.,2011)]. For lentivirus production, the shRNA vector plasmid (20 mg) and second-generation packaging plasmids (5 mg of pMD2-VSVG and 15 mg of pCMVΔR8.91) were co-transfected in HEK293T cells. Lentivirus-containing supernatant was collected 24h after transfection, centrifuged at 3000 rpm to remove cell debris for 5 min, 0.45 µm-filtered and frozen at -80°C until use. The titer of lentiviral shRNA particles was determined by use of Fluorescent Activated Cell Sorter (FACS) counting of transduced GFP-positive cells. HCT116 cells were infected by spinoculation (1800 rpm for 45 min at 30°C) at MOI 5. Cells were harvested at the indicated times post-infection.

## 8.5 Growth assay based on Crystal Violet staining

The inhibition of proliferation was evaluated by Crystal Violet staining following 24 h treatment with bDMC at the indicated concentrations. Briefly, cells were methanol-fixed and stained with 0.05% Crystal Violet solution in 20% methanol for 1 h. After washes, cells were allowed to dry and the incorporated dye was solubilised in acidic isopropanol and quantified spectrophotometrically at 540 nm wavelength. The extracted dye is proportional to cell number and percentage of cell survival was calculated by comparing the absorbance of treated *versus* untreated cells.

## 8.6 Chromosome spreads

DMSO- and bDMC-treated cells were collected, swollen in 0.075 M KCl solution and incubated 10 minutes at room temperature. Cells were then centrifuged at 1000xg, washed in Fix solution (3:1(vol/vol) methanol:acetic acid) and resuspended in 150 µl of Fix solution. ~20 µl of cell suspension were dropped on a wet ice-cold slide. Excess liquid was drained on a paper towel and slides were stained for 15 minutes in Giemsa stain (Sigma-Aldrich, #32884). Slides were washed in distilled water, air-dried and mounted with DPX mountant (Sigma-Aldrich, #44581). Chromosomes were analysed with a Nikon Eclipse 90i microscope.

## 8.7 Protein extraction and Immunoblotting

Cells were harvested by trypsinization, collected in culture medium and washed in 1X PBS. Whole cell protein extracts (WCE) were obtained by resuspending cells in 1X SDS sample buffer (25mM Tris–HCl pH 6.8, 1.5mM EDTA, 20% glycerol, 2% SDS, 5% b-mercaptoethenol, 0.0025% Bromophenol blue).
For subcellular protein fractionation, cells were resuspended in 100 µl of Solution A (10 mM HEPES pH7.9, 10 mM KCl, 1.5 mM $MgCl_2$, 0.34 M sucrose, 10% glycerol, protease and phosphatase inhibitors), then 0.1% Triton X-100 was added. After incubating 10 minutes on ice, the supernatant containing cytoplasmic proteins was collected by centrifugation at 1300xg, 4 minutes at 4°C. The remaining nuclear pellet was washed twice in Solution A and either directly disrupted in 1X SDS sample buffer (nuclear extract) or lysed in 100 µl of Solution B (3 mM EDTA, 0.2 mM EGTA, 1 mM DTT, protease and phosphatase inhibitors) for 30 minutes, centrifuged at 10000xg, 4 minutes at 4°C and the pellet was dissolved in 1X SDS sample buffer, followed by brief sonication (chromatin-enriched extract).
Protein concentration was determined by Bradford dye assay, then equal protein amounts of each sample were fractionated by SDS-PAGE, transferred to a PVDF membrane (GE Healthcare) by electroblotting, then non-specific protein interactions were blocked by incubation in a solution of 5% non-fat dry milk in 1X TBS-T (0.15 M NaCl, 50 mM Tris-HCl pH7.5 at 25°C, 0.1% Tween-20). For Immunoblotting, the following primary antibodies were used (1:1000 in TBS1X-BSA 1 mg/ml): anti-NF-YB and anti-NF-YC, purified in our laboratory from polyclonal rabbit serum; anti-phospo-H2AX (sc-101696), anti-H3 (C16) (sc-8654), anti-p53 (DO1) (sc-126), anti-TOP2A (K19) (sc-5347), anti-PARP1 (F2) (sc-8007), anti-NF-YA (sc-10779), anti-Sp1 (sc-420 X) and anti-actin (I19) (sc-1616) from Santa Cruz Biotecnology; antiphospho-ATM Ser1981 (No. 4526), anti-phospho-BRCA1 Ser1524 (No. 9009), anti-phospho-Chk1 Ser296 (No. 2349) from Cell Signaling Technology; and anti-α-tubulin (T6074) from Sigma-Aldrich. Secondary antibodies HRP-conjugated were from Santa Cruz and chemiluminescent detection reagent has been purchased from Millipore (Luminata Classico and Forte Western HRP).



## 8.8 Immuno-band depletion assay

$6x10^5$ cells were lysed in 50 µl of alkaline lysis solution (200 mM NaOH, 2 mM EDTA), and the lysate was neutralized by 8 µl of neutralization buffer (1 M HCl, 600 mM Tris pH 8.0). The neutralized lysate was mixed with 6.6 µl of 10xMNase

reaction buffer (50 mM MgCl2, 50mM CaCl2, 5 mM DTT, 1 mM EDTA, 1 mM PMSF, protease inhibitors) and incubated or not with 60 units of MNase. After 20 min digestion, 60 µl of 2xSDS sample buffer were added to each sample, and the lysates were separated on 8% SDS-PAGE gels and immunoblotted.

## 8.9 TOP2 decatenation assay

TOP2 activity was assayed in vitro through the Topoisomerse II assay kit (No. TG1001, TopoGEN Inc), following the instructions of the manufacturer. Nuclear extracts containing TOP2 activity were obtained from HCT116 cells following the suggestions and protocol of the manufacturer, and the ability to decatenate kDNA was analyzed in the presence of DMSO, bDMC and Etoposide (ETP) at the indicated concentrations. Reaction products were loaded directly onto a 1% agarose gel containing ethidium bromide (0.5 mg/ml) and TOP2 activity was measured by the appearance of decatenated minicircular products and determined as the percentage of DMSO by ImageJ software (Image J, U.S. National Institutes of Health, Bethesda, MD, USA).

## 8.10 Reverse-Transcription PCR (RT-PCR)

RNA was extracted from cells treated with the described drugs or transduced with the indicated lentiviral vectors, by using Purelink RNA mini kit (Invitrogen, Life Technologies) according to the manufacturer's protocol. For cDNA synthesis, 3 µg of RNA were retro-transcribed with a *Moloney* murine leukemia virus reverse transcriptase (MMLV-RT) (Promega). RNAs were denatured at 65°C for 5 minutes and placed on ice for 3 minutes. Then the following cDNA synthesis mix was added: 1 µl MMLV-RT (200 U/µl), 0.5 µl RNAsin (40 U/µl), 6 µl RT buffer (250 mM Tris-HCl pH 8.3, 300 mM KCl, 15 mM $MgCl_2$, 50 mM DTT), 0.5 µl oligonucleotide dT primers (0,5 µg/µl), 3 µl BSA (bovine serum albumine) (1 µg/µl), 1.5 µl dNTPs (10 mM), 2.5 µl bi-distilled sterile water. The negative control (RT-) was obtained by adding the above reaction mix lacking MMLV-RT: this control is necessary to identify possible contaminations by genomic DNA. The samples were incubated at 42°C for 1h to allow cDNA synthesis, then the enzyme was inactivated at 95°C for 3 minutes.



Semi-quantitative PCRs were carried out by using the following reaction mix: 2 µl DNA, 1 µl dNTPs (10 mM), 0.5 µl *forward* primer (1 µg/µl), 0.5 µl *reverse* primer (1 µg/µl), 0.2 µl Taq polymerase (5 U/µl), 10 µl 5X Taq buffer, 35.8 µl bi-distilled water.

Quantitative real-time PCRs were performed using DyNAmo ColorFlash SYBR Green Master mix (Thermo Scientific). 20 µl reactions were setup with 10 µl of 2x master mix, 2 µl DNA, 0.2 µl forward+reverse primers (50 µM each), 7.8 µl bi-distilled water.

Semi-quantitative and real-time PCRs were performed with the following oligonucleotides designed to amplify the cDNA of:

GAPDH (f 5'-acagtcagccgcatcttctt-3'; r 5'-gcccaatacgaccaaatcc-3'),
TOP2A (f 5'-tggcagaggcagagagagtt-3'; r 5'-tcaaaaagcaccatagagttgc-3'),
p21 (f 5'-tgaccctgaagtgagcacag-3'; r 5'-gggaaaaggctcaacactga-3'),
G-ACTIN (f 5'-gccaacagagagaagatgactc-3'; r 5'-agaggcgtagagggacagc-3'),
NF-YA (f 5'- ggaggccagctaatcacatc -3'; r 5'-gccgagactcatgcaggtat-3'),

NF-YB (f 5'-aggtgccatcaagagaaact-3'; r 5'-tgttgttgaccgtctgtggt-3').
For amplification of NF-YC isoforms in semi-quantitative PCR, the following primer sets were used ***(Figure 8.1)***: exon8 f (5'-cagcctgtatcaggcactca-3'); exon8bis f (5'-cctcgaaggtgcctgaaaga-3'); exon9bis r (5'-gaagaggtgcagggagttga-3'); exon10 r (5'-ggtgacttgctggatctggt-3').

A

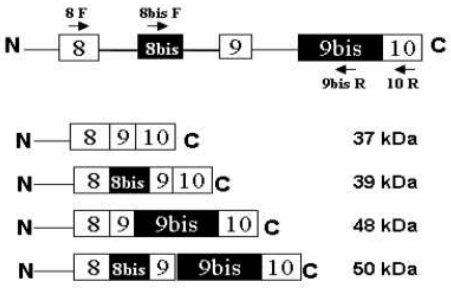


B

| Primers | NF-YC isoforms |
|---|---|
| 8F– 10R | 37 kDa, 39 kDa, 48 kDa, 50 kDa |
| 8F– 9bisR | 48 kDa, 50 kDa |
| 8bisF – 10R | 39 kDa, 50 kDa |
| 8bisF – 9bisR | 50 kDa |

**Figure 8.1|** (A) Schematic representation of the NF-YC C-terminus genomic structure. White boxes indicate exons coding for NF-YC (37kDa) protein, while in black are shown alternative spliced exons in the NF-YC (39, 48, 50 kDa) proteins. Primers used in RT-PCR experiments are mapped within the NF-YC C-terminus. (B) Different primers pairs which have been used to detect NF-YC splice variants are indicated.

Semi-quantitative PCR products were analysed through Agarose Gel Electrophoresis in a 2% agarose gel in TAE (40 mM Tris pH8.0, 20 mM acetic acid, 1 mM EDTA), visualized by Ethidium Bromide (EtBr) and analyzed by ImageJ software.
In real-time PCRs, relative fold change enrichments of the samples were calculated with: $2^{-(\Delta\Delta Ct)}$, where $-(\Delta\Delta Ct) = -((Ct_{target}-Ct_{GAPDH})_{bDMC}-(Ct_{target}-Ct_{GAPDH})_{DMSO})$.



## 8.11 Chromatin Immunoprecipitation (ChIP)

Cells were cross-linked with formaldehyde to a final concentration of 1%, then the reaction was quenched with 0.125 M glycine. Cells were lysed in Lysis buffer (1% SDS, 10 mM EDTA pH8.0, 50 mM Tris-HCl pH8.0, with protease inhibitors) for 10 minutes on ice. Sonication was then used to disrupt cell and nuclear membranes and to fragment cross-linked chromatin fibres to 500bp average length. Then the protein concentration of the lysate was measured and 400 µg of each sample were diluted 10 times in a mixture 9:1 Dilution buffer:Lysis buffer (Dilution buffer: 1% Triton X-100, 150 mM NaCl, 2mM EDTA pH8.0, 20 mM Tris-HCl pH8.0, protease inhibitors) and used for immunoprecipitation with 4 µg of the following, over-night at 4°C, on a rotating wheel: anti-H3ac (Millipore, No. 06-599); anti-H4ac (Millipore, No. 06-866); anti-NF-YA (Santa Cruz, sc-10779); anti-NF-YB (purified in our laboratory from polyclonal rabbit serum); anti-H3K59ac (Active Motif, No. 39281); anti-FLAG (Sigma Aldrich, No. F3165) used as control for non-specific interactions. Simultaneously, proteinG beads (KPL) were diluted 10 times in a solution 9:1 Dilution buffer:Lysis buffer and pre-absorbed with 100 µg/ml BSA, 500 µg/ml salmon sperm DNA. Pre-absorbed beads were washed twice in Dilution buffer and resuspended in 1 ml of 9:1 Dilution buffer:Lysis buffer. 110 µl of beads solution were added to each sample and incubated for 2h at 4°C, on a rotating wheel. After gentle centrifugation (2000 rpm), 1 ml from anti-FLAG samples' supernatant was

collected as INPUT and the beads were washed 4 times in Wash buffer (1% Triton X-100, 0.1% SDS, 150 mM NaCl, 2 mM EDTA pH8.0, 20 mM Tris-HCl pH8.0, protease inhibitors) and finally once in Final wash buffer (1% Triton X-100, 0.1% SDS, 500 mM NaCl, 2 mM EDTA pH8.0, 20 mM Tris-HCl pH8.0, protease inhibitors). Immunocomplexes were then eluted in 450 µl of Elution buffer (1% SDS, 100 mM $NaHCO_3$). Samples and Input were added with 0.25 µg/µl proteinase K, 0.25 µg/µl RNAseA and incubated first for 1h at 37°C, then for 4h at 65°C. DNAs were finally extracted by adding an equal volume of phenol:chlorophorme:isoamylalcohol (25:24:1): the aqueous phases were collected and an additional back extraction was performed on the phenolic phase, by addition of an equal volume of TE buffer (10 mM Tris-HCl pH8.0, 1 mM EDTA, protease and phosphatase inhibitors). The aqueous phase collected from each sample was put together with the previous one. The purified DNAs were precipitated over-night at -20°C with 0.3 µg/µl glycogen, 1/10th of the volume of 3M sodium acetate and 3 volumes of 100% ethanol. After 30 minutes centrifugation at 14000 rpm at 4°C, the pellets were washed with 70% ethanol and air-dried. DNAs were resuspended in 60 µl sterile TE buffer (120 µl for Inputs) and stored at -20°C until PCR analysis.
Semi-quantitative and real-time PCRs were performed as described above, with the following primers amplifying the promoter region of:
p21 (f 5'-gtaaatccttgcctgccagagtg-3'; r 5'-gctgcccagcgccgagccag-3'),
TOP2A (f 5'-cgtcagaacagaggacagttttt-3'; r 5'-tggaagagatgggctttgg-3'),
NF-YB (f 5'-gttccttcgcagccatttt-3'; r 5'-gcgagacacaaacctccaat-3'),
NF-YC P1 (f 5'-gacctggcaccttattggac-3'; r 5'-cctctcttccccttaaagc-3'),
NF-YC P2 (f 5'-ccctgttctgcttctcaagg-3'; r 5'-ctgcagcctccttccacttt-3').
In real-time PCRs, the relative sample enrichment was calculated with the following formula: $2^{\Delta Ctx}$-$2^{\Delta Ctb}$, where ΔCtx=Ct input-Ct sample and ΔCtb=Ct input-Ct flag Ab.



## 8.12 Preparation and use of *Xenopus* egg extracts

I performed all the experiments with the *Xenopus laevis* cell-free system in the Laboratory of Prof. J.J. Blow, University of Dundee, UK. The procedures used to prepare *Xenopus* egg extracts, demembranated sperm nuclei and to study DNA replication and chromatin associated proteins are described extensively in Gillespie et al.,2012.

### 8.12.1 Use of *Xenopus* egg extracts

Metaphase-arrested *Xenopus* egg extract and demembranated *Xenopus* sperm nuclei were obtained from Dr. Julia Neusiedler, Blow Laboratory, University of Dundee. Briefly, extracts were supplemented with 250 µg/ml cycloheximide, 25 mM phosphocreatine and 15 µg/ml creatine phosphokinase, in order to maintain high ATP levels throughout the duration of DNA synthesis reaction and supply high-energy phosphate. Moreover, extracts were incubated with 0.3 mM $CaCl_2$ for 15 min to release from metaphase arrest.
When indicated, recombinant NF-Y trimer (Imbriano et al.,2005), NF-YA or NF-YA dominant negative mutant (NF-YA mutant, kind gift of R. Mantovani) were added to the extracts at the indicated concentrations.
For immunodepletion, Protein A–magnetic beads were incubated with anti-NF-YA (sc-10779, Santa Cruz), NF-YB (purified in Imbriano Lab) or rabbit IgGs as a

control, extensively washed and then *Xenopus* egg extracts were incubated with beads for 30 min at 4 °C. After removal of the beads, the process was repeated another time.

### 8.12.2 TCA replication assay

For DNA synthesis assays, sperm nuclei were incubated at 5–10 ng DNA /µl in activated extracts, supplemented with $^{32}$P-dATP. Reactions were terminated by addition of a solution containing 0.5% SDS and protease K, then cold 10% Trichloroacetic acid solution (TCA) was added to facilitate precipitation of the DNA. DNA synthesis was assayed by measuring incorporation of $^{32}$P-dATP into acid-insoluble material followed by scintillation counting.

### 8.12.3 Chromatin isolation from egg extract

Briefly, a synthesis reaction has been set up, with or without addition of 100 nM recombinant p27 or 100 µg/ml recombinant geminin. At each timepoint, 10 µl of reaction were diluted with ice-cold Nuclear Isolation Buffer (NIB) (50 mM KCl, 50 mM HEPES–KOH pH 7.6, 5 mM $MgCl_2$, 0.5 mM spermidine, 0.15 mM spermine, 2 mM DTT) containing phosphatase inhibitors, under-laid with NIB + 20% sucrose (w/v) and centrifuged in a swinging bucket rotor at 2100*g* for 5 min at 4°C. Following a wash of the cushion, chromatin was compacted by spinning at 13 000*g* for 2 min in a fixed angle rotor. The resulting pellet was resuspended in 1X SDS sample buffer, separated on 4–12% Bis–Tris gradient SDS–PAGE gels (Invitrogen) and proteins were electrotransferred to PVDF membranes (GE Healthcare). After blocking in PBS/0.2% Tween-20/5% non-fat milk, and after incubation with primary and secondary antibodies, membranes were developed using enhanced chemiluminescence detection (SuperSignal West Pico Chemiluminescent; Thermo Scientific). The lower portion of each gel was typically cut and stained with Coomassie to visualize histones. The following antibodies were used: anti-NF-YA (sc-10779) from Santa Cruz Biotecnology; anti-NF-YB, purified in our laboratory from polyclonal rabbit serum; anti-MCM3, anti-MCM4, anti-MCM10, anti-Cut5, anti-PCNA, anti-DNA polymerase α and anti-Cdc45, provided by J.J. Blow Laboratory, University of Dundee

# 9. REFERENCES CITED


Anand P, Kunnumakkara AB, Newman RA, Aggarwal BB. (2007). Bioavailability of curcumin: problems and promises. *Mol Pharm.*;4(6):807-18.

Anand P, Thomas SG, Kunnumakkara AB, Sundaram C, Harikumar KB, Sung B, Tharakan ST, Misra K, Priyadarsini IK, Rajasekharan KN, Aggarwal BB. (2008). Biological activities of curcumin and its analogues (Congeners) made by man and Mother Nature. *Biochem Pharmacol.*;76(11):1590-611.

Bakkenist CJ, Kastan MB. (2004). Initiating cellular stress responses. *Cell*; 118: 9–17.

Balasubramanyam K, Varier RA, Altaf M, Swaminathan V, Siddappa NB, Ranga U, Kundu TK. (2004). Curcumin, a novel p300/CREB-binding protein-specific inhibitor of acetyltransferase, represses the acetylation of histone/nonhistone proteins and histone acetyltransferase-dependent chromatin transcription. *J Biol Chem.*;279(49):51163-71.

Bansal N, Kadamb R, Mittal S, Vig L, Sharma R, Dwarakanath BS, Saluja D. (2011). Tumor suppressor protein p53 recruits human Sin3B/HDAC1 complex for down-regulation of its target promoters in response to genotoxic stress. *PLoS One*.;6(10):e26156.

Basile V, Ferrari E, Lazzari S, Belluti S, Pignedoli F, Imbriano C. (2009). Curcumin derivatives: molecular basis of their anti-cancer activity. *Biochem Pharmacol*; 78: 1305–1315.





Basile V, Mantovani R, Imbriano C. (2006). DNA damage promotes histone deacetylase 4 nuclear localization and repression of G2/M promoters, via p53 C-terminal lysines. *J Biol Chem.*; 281(4):2347-57

Basile V, Belluti S, Ferrari E, Gozzoli C, Ganassi S, Quaglino D, Saladini M, Imbriano C. (2013). bis-Dehydroxy-Curcumin triggers mitochondrial-associated cell death in human colon cancer cells through ER-stress induced autophagy. *PLoS One*;8(1):e53664.

Baxevanis AD, Arents G, Moudrianakis EN, Landsman D. (1995). A variety of DNA-binding and multimeric proteins contain the histone fold motif. *Nucleic Acids Res*; 23:2685–2691.

Benatti P, Basile V, Merico D, Fantoni LI, Tagliafico E, Imbriano C. (2008). A balance between NF-Y and p53 governs the pro- and anti-apoptotic transcriptional response. *Nucleic Acids Res*; 36:1415-28.

Benatti P, Dolfini D, Viganò A, Ravo M, Weisz A, Imbriano C. (2011). Specific inhibition of NF-Y subunits triggers different cell proliferation defects. *Nucleic Acids Res.*; 39(13):5356-68.

Bhaskara S, Jacques V, Rusche JR, Olson EN, Cairns BR, Chandrasekharan MB. (2013). Histone deacetylases 1 and 2 maintain S-phase chromatin and DNA replication fork progression. *Epigenetics Chromatin.*; 6(1):27.

Bhattacharya A, Deng JM, Zhang Z, Behringer R, de Crombrugghe B, Maity SN. (2003). The B subunit of the CCAAT box binding transcription factor complex (CBF/NF-Y) is essential for early mouse development and cell proliferation. *Cancer Res.*;63:8167-8172.

Biswas AK, Johnson DG. (2012). Transcriptional and nontranscriptional functions of E2F1 in response to DNA damage. *Cancer Res.*; 72(1):13-7.

Blow JJ, Ge XQ, Jackson DA. (2011). How dormant origins promote complete genome replication. *Trends Biochem Sci.*;36(8):405-14.

Bolognese F, Wasner M, Dohna CL, Gurtner A, Ronchi A, Muller H, Manni I, Mossner J, Piaggio G, Mantovani R, Engeland K. (1999). The cyclin B2 promoter depends on NF-Y, a trimer whose CCAAT-binding activity is cell-cycle regulated. *Oncogene*;18(10):1845-53.

Branzei D, Foiani M. (2008). Regulation of DNA repair throughout the cell cycle. *Nat Rev Mol Cell Biol.*;9(4):297-308.

Branzei, D. & Foiani, M. (2005). The DNA damage response during DNA replication. *Curr. Opin. Cell Biol.;* 17, 568–575.

Caldwell JM, Chen Y, Schollaert KL, Theis JF, Babcock GF, Newlon CS, Sanchez Y. (2008). Orchestration of the S-phase and DNA damage checkpoint pathways by replication forks from early origins. *J Cell Biol.*;180(6):1073-86.

Caretti G, Motta MC, Mantovani R. (1999). NF-Y associates with H3-H4 tetramers and octamers by multiple mechanisms. *Mol Cell Biol*; 19: 8591–8603.

Caretti G, Salsi V, Vecchi C, Imbriano C, Mantovani,R. (2003). Dynamic recruitment of NF-Y and histone acetyltransferases on cell-cycle promoters. *J. Biol. Chem.*; 278,30435–30440.

Casas-Delucchi CS, Cardoso MC. (2011). Epigenetic control of DNA replication dynamics in mammals. *Nucleus*.;2(5):370-82.



Ceribelli M, Benatti P, Imbriano C, Mantovani R. (2009). NF-YC complexity is generated by dual promoters and alternative splicing. *J Biol Chem*; 284:34189–34200.

Ceribelli M, Dolfini D, Merico D, Gatta R, Vigano AM, Pavesi G, Mantovani R. (2008). The histone-like NF-Y is a bifunctional transcription factor. *Mol Cell Biol*; 28: 2047–2058.

Chae HD, Yun J, Bang YJ, Shin DY. (2004). Cdk2-dependent phosphorylation of the NF-Y transcription factor is essential for the expression of the cell cycle-regulatory genes and cell cycle G1/S and G2/M transitions. *Oncogene*; 23:4084–4088.

Chakalova L, Debrand E, Mitchell JA, Osborne CS, Fraser P. (2005). Replication and transcription: shaping the landscape of the genome. *Nat Rev Genet*.; 6(9):669-77.

Chen F, Ogawa K, Liu X, Stringfield TM, Chen Y. (2002). Repression of Smad2 and Smad3 transactivating activity by association with a novel splice variant of CCAAT-binding factor C subunit. *Biochem J*.; 364(Pt 2):571-7.

Chodosh LA, Baldwin AS, Carthew RW, Sharp PA. (1988). Human CCAAT-binding proteins have heterologous subunits. *Cell*; 53:11-24.

Conti C, Seiler JA, Pommier Y. The mammalian DNA replication elongation checkpoint: implication of Chk1 and relationship with origin firing as determined by single DNA molecule and single cell analyses. *Cell Cycle.*;6(22):2760-7.

Cortés F, Pastor N, Mateos S, Domínguez I. (2003). Roles of DNA topoisomerases in chromosome segregation and mitosis. *Mutat Res*.;543(1):59-66.

Currie, R. A. (1998). NF-Y is associated with the histone acetyltransferases GCN5 and P/CAF. *J. Biol. Chem.*; 273, 1430-1444

De Amicis F, Giordano F, Vivacqua A, Pellegrino M, Panno ML, Tramontano D, Fuqua SA, Andò S. (2011). Resveratrol, through NF-Y/p53/Sin3/HDAC1 complex phosphorylation, inhibits estrogen receptor alpha gene expression via p38MAPK/CK2 signaling in human breast cancer cells. *FASEB J*.;25(10):3695-707.

de Silvio A, Imbriano C, Mantovani R. (1999) Dissection of the NF-Y transcriptional activation potential. *Nucleic Acids Res.*; 27(13):2578-84.

Deweese JE, Osheroff MA, Osheroff N. (2008). DNA Topology and Topoisomerases: Teaching a "Knotty" Subject. *Biochem Mol Biol Educ*.;37(1):2-10.

Di Agostino S, Strano S, Emiliozzi V, Zerbini V, Mottolese M, Sacchi A, Blandino G, Piaggio G. (2006). Gain of function of mutant p53: the mutant p53/NF-Y protein complex reveals an aberrant transcriptional mechanism of cell cycle regulation. *Cancer Cell*.;10(3):191-202.

Dolfini D, Gatta R, Mantovani R. (2012a). NF-Y and the transcriptional activation of CCAAT promoters. *Crit Rev Biochem Mol Biol*; 47:29-49.

Dolfini D, Zambelli F, Pavesi G, Mantovani R. (2009). A perspective of promoter architecture from the CCAAT box. *Cell Cycle*; 8, 4127–4137.

Dolfini D, Minuzzo M, Pavesi G, Mantovani R. (2012b). The short isoform of NF-YA belongs to the embryonic stem cell transcription factor circuitry. *Stem Cells*; 30(11):2450-9. doi: 10.1002/stem.1232.



Dominguez-Sola D, Ying CY, Grandori C, Ruggiero L, Chen B, Li M, Galloway DA, Gu W, Gautier J, Dalla-Favera R. (2007). Non-transcriptional control of DNA replication by c-Myc. *Nature*; 448(7152):445-51.

Donaldson A.D. (2005). Shaping time: chromatin structure and the DNA replication programme. *Trends Genet.*; 21, 444–449.

Donati G, Gatta R, Dolfini D, Fossati A, Ceribelli M, Mantovani R. (2008). An NF-Y-dependent switch of positive and negative histone methyl marks on CCAAT promoters. *PLoS ONE* 3:e2066.

Elkon R, Linhart C, Sharan R, Shamir R, Shiloh Y.(2003). Genome-wide in silico identification of transcriptional regulators controlling the cell cycle in human cells. *Genome Res.*;13(5):773-80.

Fleming JD, Pavesi G, Benatti P, Imbriano C, Mantovani R, Struhl K. (2013). NF-Y coassociates with FOS at promoters, enhancers, repetitive elements, and inactive chromatin regions, and is stereo-positioned with growth-controlling transcription factors. *Genome Res.*; 23(8):1195-209.

Flicek P, Ahmed I, Amode MR, Barrell D, Beal K, Brent S, Carvalho-Silva D, Clapham P, Coates G, Fairley S, Fitzgerald S, Gil L, García-Girón C, Gordon L, Hourlier T, Hunt S, Juettemann T, Kähäri AK, Keenan S, Komorowska M, Kulesha E, Longden I, Maurel T, McLaren WM, Muffato M, Nag R, Overduin B, Pignatelli M, Pritchard B, Pritchard E, Riat HS, Ritchie GR, Ruffier M, Schuster M, Sheppard D, Sobral D, Taylor K, Thormann A, Trevanion S, White S, Wilder SP, Aken BL, Birney E, Cunningham F, Dunham I, Harrow J, Herrero J, Hubbard TJ, Johnson N, Kinsella R, Parker A, Spudich G, Yates A, Zadissa A, Searle SM. (2013). Ensembl 2013. *Nucleic Acids Res.*;41(Database issue):D48-55.

Fossati A, Dolfini D, Donati G, Mantovani R. (2011). NF-Y recruits Ash2L to impart H3K4 trimethylation on CCAAT promoters. *PLoS ONE*; 6:e17220.

Frontini M, Imbriano C, Manni I, Mantovani R. (2004). Cell cycle regulation of NF-YC nuclear localization. *Cell Cycle*; 3:217–222.

Garipov A, Li H, Bitler BG, Thapa RJ, Balachandran S, Zhang R. (2013). NF-YA underlies EZH2 upregulation and is essential for proliferation of human epithelial ovarian cancer cells. *Mol Cancer Res*.;11(4):360-9.

Gatta R, Mantovani R. (2011). NF-Y affects histone acetylation and H2A.Z deposition in cell cycle promoters. *Epigenetics* 6:526–534.

Ge Y, Matherly LH, Taub JW. (2001). Transcriptional regulation of cell-specific expression of the human cystathionine beta –synthase gene by differential binding of Sp1/Sp3 to the -1b promoter. *J Biol Chem*; 276:43570–43579.

Ghosh M, Liu G, Randall G, Bevington J, Leffak M. (2004). Transcription factor binding and induced transcription alter chromosomal c-myc replicator activity. *Mol Cell Biol.*; 24(23):10193-207.

Gillespie PJ, Gambus A, Blow JJ. (2012). Preparation and use of Xenopus egg extracts to study DNA replication and chromatin associated proteins. *Methods*.;57(2):203-13.

Gilthorpe J, Vandromme M, Brend T, Gutman A, Summerbell D, Totty N and Rigby PW. (2002). Spatially specific expression of Hoxb4 is dependent on the ubiquitous transcription factor NFY. *Development*; 129: 3887-3899.

Gnesutta N, Nardini M, Mantovani R. (2013). The H2A/H2B-like histone-fold domain proteins at the crossroad between chromatin and different DNA metabolisms. *Transcription;* May 16;4(3).



Goel A, Kunnumakkara AB, Aggarwal BB. (2008). Curcumin as "Curecumin": from kitchen to clinic. *Biochem Pharmacol*.;75(4):787-809.

Goodarzi H, Elemento O, Tavazoie S. (2009). Revealing global regulatory perturbations across human cancers. *Mol Cell* 36: 900–911.

Gurtner A, Fuschi P, Magi F, Colussi C, Gaetano C, Dobbelstein M, Sacchi A, Piaggio G. (2008). NF-Y dependent epigenetic modifications discriminate between proliferating and postmitotic tissue. *PLoS ONE* 3:e2047.

Gurtner A, Manni I, Fuschi P, Mantovani R, Guadagni F, Sacchi A, Piaggio G. (2003). Requirement for down-regulation of the CCAATbinding activity of the NF-Y transcription factor during skeletal muscle differentiation. *Mol Biol Cell;* 14:2706–2715.

Gurtner A, Fuschi P, Martelli F, Manni I, Artuso S, Simonte G, Ambrosino V, Antonini A, Folgiero V, Falcioni R, Sacchi A, Piaggio G. (2010). Transcription factor NF-Y induces apoptosis in cells expressing wild-type p53 through E2F1 upregulation and p53 activation. *Cancer Res.*;70(23):9711-20.

Hasan S, Hassa PO, Imhof R, Hottiger MO. (2001). Transcription coactivator p300 binds PCNA and may have a role in DNA repair synthesis. *Nature.*;410(6826):387-91.

Hatamochi A, Golumbek PT, Van SE, de CB. A. (1988). CCAAT DNA binding factor consisting of two different components that are both required for DNA binding. *J Biol Chem*; 263:5940-7.

Hochhauser D, Stanway CA, Harris AL, Hickson ID. (1992) Cloning and characterization of the 5_-flanking region of the human topoisomerase IIα gene. *J. Biol. Chem.*; 267, 18961–18965

Hu Q, Bhattacharya C and Maity SN. (2002). CCAAT binding factor (CBF) binding mediates cell cycle activation of topoisomerase IIalpha. Conventional CBF activation domains are not required. *J Biol Chem*; 277: 37191-37200.

Hu Q, Lu JF, Luo R, Sen S, Maity SN. (2006). Inhibition of CBF/NF-Y mediated transcription activation arrests cells at G2/M phase and suppresses expression of genes activated at G2/M phase of the cell cycle. *Nucleic Acids Res.*;34:6272-6285.

Hu Q, Maity SN. (2000). Stable expression of a dominant negative mutant of CCAAT binding factor/NF-Y in mouse fibroblast cells resulting in retardation of cell growth and inhibition of transcription of various cellular genes. *J. Biol. Chem.*;275:4435-4444.

Huang S, Ling JJ, Yang S, Li XJ, Li S. (2011). Neuronal expression of TATA box-binding protein containing expanded polyglutamine in knock-in mice reduces chaperone protein response by impairing the function of nuclear factor-Y transcription factor. *Brain*; 134:1943–1958.

Huvet M, Nicolay S, Touchon M, Audit B, d'Aubenton-Carafa Y, Arneodo A, Thermes C. (2007). Human gene organization driven by the coordination of replication and transcription. Genome Res.;17(9):1278-85.

Imbriano C, Gnesutta N, Mantovani R. (2011). The NF-Y/ p53 liaison: well beyond repression. *Biochim Biophys Acta*; 1825:131-39.

Imbriano C, Gnesutta N, Mantovani R. (2012) The NF-Y/p53 liaison: well beyond repression. *Biochim Biophys Acta*.;1825(2):131-9. doi: 10.1016/j.bbcan.2011.11.001.



Imbriano C, Gurtner A, Cocchiarella F, Di Agostino S, Basile V, Gostissa M, Dobbelstein M, Del Sal G, Piaggio G, Mantovani R. (2005). Direct p53 transcriptional repression: In vivo analysis of CCAAT-containing G2/M promoters. *Mol Cell Biol*; 25:3737-51.

Isaacs RJ, Harris AL, Hickson ID. (1996). Regulation of the human topoisomerase IIalpha gene promoter in confluence-arrested cells. *J Biol Chem*; 271: 16741–16747.

Joshi AA, Wu Z, Reed RF, Suttle DP. (2003). Nuclear factor-Y binding to the topoisomerase IIalpha promoter is inhibited by both the p53 tumor suppressor and anticancer drugs. *Mol Pharmacol.*;63(2):359-67.

Jung MS, Yun J, Chae HD, Kim JM, Kim SC, Choi TS, Shin DY. (2001). p53 and its homologues, p63 and p73, induce a replicative senescence through inactivation of NF-Y transcription factor. *Oncogene*; 20:5818–5825.

Kahle J, Baake M, Doenecke D, Albig W. (2005). Subunits of the heterotrimeric transcription factor NF-Y are imported into the nucleus by distinct pathways involving importin beta and importin 13. *Mol Cell Biol*; 25:5339–5354.

Karnani N, Dutta A. (2011). The effect of the intra-S-phase checkpoint on origins of replication in human cells. *Genes Dev.*; 25(6):621-33.

Kesharwani KR, Misra K. (2011). Prediction of binding site for curcuminoids at human toposomerase II a protein; an in silico approach. *Curr Sci*; 101: 1060–1065.

Kim CG, Swendeman SL, Barnhart KM, Sheffery M. (1990). Promoter elements and erythroid cell nuclear factors that regulate a-globin gene transcription in vitro. *Mol Cell Biol;* 10: 5958–5966.

Kim IS, Sinha S, de Crombrugghe B, Maity SN. (1996). Determination of functional domains in the C subunit of the CCAAT-binding factor (CBF) necessary for formation of a CBF-DNA complex: CBF-B interacts simultaneously with both the CBF-A and CBF-C subunits to form a heterotrimeric CBF molecule. *Mol Cell Biol*; 16:4003–4013.

Kouzarides T. (2007). Chromatin modifications and their function. *Cell.*; 23;128(4):693-705. Review.

Lao CD, Ruffin MT 4th, Normolle D, Heath DD, Murray SI, Bailey JM, Boggs ME, Crowell J, Rock CL, Brenner DE. (2006). Dose escalation of a curcuminoid formulation. *BMC Complement Altern Med.*;6:10.

Li Q, Herrler M, Landsberger N, Kaludov N, Ogryzko VV, Nakatani Y, Wolffe AP. (1998). Xenopus NF-Y pre-sets chromatin to potentiate p300 and acetylation-responsive transcription from the Xenopus hsp70 promoter in vivo. *EMBO J.*; 17(21):6300-15.

Li XY, Hooft van Huijsduijnen R, Mantovani R, Benoist C, Mathis D. (1992). Intron-exon organization of the NF-Y genes. Tissuespecific splicing modifies an activation domain. *J Biol Chem;* 267:8984–8990.

Liang SG, Maity SN. (1998). Pathway of complex formation between DNA and three subunits of CBF/NF-Y. Photocross-linking analysis of DNA-protein interaction and characterization of equilibrium steps of subunit interaction and dna binding. *J. Biol. Chem.;* 273, 31590–31598

Liberati C, di Silvio A, Ottolenghi S, Mantovani, R. (1999). NF-Y binding to twin CCAAT boxes: role of Q-rich domains and histone fold helices. *J. Mol.Biol.;* 285, 1441–1455.



Linhart C, Elkon R, Shiloh Y, Shamir R. (2005). Deciphering transcriptional regulatory elements that encode specific cell cycle phasing by comparative genomics analysis. *Cell Cycle*; 4:1788-97.

López-Lázaro M, Willmore E, Jobson A, Gilroy KL, Curtis H, Padget K, Austin CA. (2007). Curcumin induces high levels of topoisomerase I- and II-DNA complexes in K562 leukemia cells. *J Nat Prod*; 70: 1884–1888.

Luciani MG, Oehlmann M, Blow JJ. (2004). Characterization of a novel ATR-dependent, Chk1-independent, intra-S-phase checkpoint that suppresses initiation of replication in Xenopus. *J Cell Sci.*; 117(Pt 25):6019-30

Luo K, Yuan J, Chen J, Lou Z. (2009). Topoisomerase IIalpha controls the decatenation checkpoint. *Nat Cell Biol.*;11(2):204-10.

Ly LL, Yoshida H, Yamaguchi M. (2013). Nuclear transcription factor Y and its roles in cellular processes related to human disease. *Am J Cancer Res*;3(4):339-46.

Magan N, Szremska AP, Isaacs RJ, Stowell KM. (2003). Modulation of DNA topoisomerase II alpha promoter activity by members of the Sp (specificity protein) and NF-Y (nuclear factor Y) families of transcription factors. *Biochem J.*;374(Pt 3):723-9.

Mantovani R. (1999). The molecular biology of the CCAAT-binding factor NF-Y. *Gene*; 239(1):15-27.

Marcu MG, Jung YJ, Lee S, Chung EJ, Lee MJ, Trepel J, Neckers L. (2006). Curcumin is an inhibitor of p300 histone acetylatransferase. *Med Chem.*;2(2):169-74.

Martin-Cordero C, Lopez-Lazaro M, Galvez M, Ayuso MJ. (2003). Curcumin as a DNA topoisomerase II poison. *J Enzyme Inhib Med Chem*; 18: 505–509. 32.

Marziali G, Perrotti E, Ilari R, Coccia EM, Mantovani R, Testa U, Battistini A. (1999). The activity of the CCAAT-box binding factor NF-Y is modulated through the regulated expression of its A subunit during monocyte to macrophage differentiation: Regulation of tissue-specific genes through a ubiquitous transcription factor. *Blood*; 93:519–526.

Masuda T, Mimura S, Takisawa H. (2003). CDK- and Cdc45-dependent priming of the MCM complex on chromatin during S-phase in Xenopus egg extracts: possible activation of MCM helicase by association with Cdc45. *Genes Cells.*;8(2):145-61.

Matuoka K, Chen KY. (2002). Transcriptional regulation of cellular ageing by the CCAAT box-binding factor CBF/NF-Y. *Ageing Res Rev;* 1:639–651.

Méchali M. (2010). Eukaryotic DNA replication origins: many choices for appropriate answers. *Nat Rev Mol Cell Biol.*;11(10):728-38. doi: 10.1038/nrm2976.

Nardini M, Gnesutta N, Donati G, Gatta R, Forni C, Fossati A, Vonrhein C, Moras D, Romier C, Bolognesi M, Mantovani R. (2013). Sequence-specific transcription factor NF-Y displays histone-like DNA binding and H2B-like ubiquitination. *Cell*; 152:132- 43.

Nitiss JL. (2009a). DNA topoisomerase II and its growing repertoire of biological functions. *Nat Rev Cancer.*;9(5):327-37.

Nitiss JL. (2009b). Targeting DNA topoisomerase II in cancer chemotherapy. *Nat Rev Cancer.*; 9(5):338-50.

Ohori H, Yamakoshi H, Tomizawa M, Shibuya M, Kakudo Y, Takahashi A, Takahashi S, Kato S, Suzuki T, Ishioka C, Iwabuchi Y, Shibata H. (2006). Synthesis and biological analysis of new curcumin analogues bearing an enhanced potential for the medicinal treatment of cancer. *Mol Cancer Ther.*;5(10):2563-71.



Park SH, Yu GR, Kim WH, Moon WS, Kim JH, Kim DG. (2007). NF-Y-dependent cyclin B2 expression in colorectal adenocarcinoma. *Clin Cancer Res.*;13(3):858-67.

Park SH, Lee SR, Kim BC, Cho EA, Patel SP, Kang HB, Sausville EA, Nakanishi O, Trepel JB, Lee BI, Kim SJ. (2002). Transcriptional regulation of the transforming growth factor beta type II receptor gene by histoneacetyltransferase and deacetylase is mediated by NF-Y in human breast cancer cells. *J Biol Chem*; 277(7):5168-74.

Peng Y, Stewart D, Li W, Hawkins M, Kulak S, Ballermann B, Jahroudi N. (2007). Irradiation modulates association of NF-Y with histone-modifying cofactors PCAF and HDAC. *Oncogene*;26(54):7576-83. Epub 2007 Jun 18.

Peng Y, Jahroudi N. (2003). The NFY transcription factor inhibits von Willebrand factor promoter activation in non-endothelial cells through recruitment of histone deacetylases. *J Biol Chem.*;278(10):8385-94. Epub 2003 Jan 2.

Pommier Y. (2013). Drugging topoisomerases: lessons and challenges. *ACS Chem Biol.*;8(1):82-95.

Remus D, Beuron F, Tolun G, Griffith JD, Morris EP, Diffley JF. (2009). Concerted loading of Mcm2-7 double hexamers around DNA during DNA replication origin licensing. *Cell.*; 139(4):719-30.

Roeder RG. (1996). The role of general initiation factors in transcription by RNA polymerase II. *Trends Biochem. Sci*; 21, 327–335

Romier C, Cocchiarella F, Mantovani R., Moras, D. (2003). The NF-YB/NF-YC structure gives insight into DNA binding and transcription regulation by CCAAT factor NF-Y. *J. Biol. Chem;* 278, 1336–1345.

Rosenbloom KR, Sloan CA, Malladi VS, Dreszer TR, Learned K, Kirkup VM, Wong MC, Maddren M, Fang R, Heitner SG, Lee BT, Barber GP, Harte RA, Diekhans M, Long JC, Wilder SP, Zweig AS, Karolchik D, Kuhn RM, Haussler D, Kent WJ. (2013). ENCODE data in the UCSC Genome Browser: year 5 update. *Nucleic Acids Res.*;41(Database issue):D56-63.

Salsi V, Caretti G, Wasner M, Reinhard W, Haugwitz U, Engeland K, Mantovani R. (2003). Interactions between p300 and multiple NF-Y trimers govern cyclin B2 promoter function. *J Biol Chem* ;278(9):6642-50.

Sancar A, Lindsey-Boltz LA, Unsal-Kaçmaz K, Linn S. (2004). Molecular mechanisms of mammalian DNA repair and the DNA damage checkpoints. *Annu Rev Biochem.*;73:39-85.

Sarkaria JN, Tibbetts RS, Busby EC, Kennedy AP, Hill DE, Abraham RT. (1998). Inhibition of phosphoinositide 3-kinase related kinases by the radiosensitizing agent wortmannin. *Cancer Res.*;58(19):4375-82.

Sawyer SL, Cheng IH, Chai W, Tye BK. (2004). Mcm10 and Cdc45 cooperate in origin activation in Saccharomyces cerevisiae. *J Mol Biol.*;340(2):195-202.

Schwaiger M, Schubeler D. (2006). A question of timing: emerging links between transcription and replication. *Curr. Opin. Genet. Dev.;* 16, 177–183.



Shehzad A, Wahid F, Lee YS. (2010). Curcumin in Cancer Chemoprevention: Molecular Targets, Pharmacokinetics, Bioavailability, and Clinical Trials. *Arch Pharm (Weinheim).*;343(9):489-499.

Sims JK, Wade PA. (2011). Mi-2/NuRD complex function is required for normal S phase progression and assembly of pericentricheterochromatin. Mol Biol Cell.;22(17):3094-102.

Singh S. (2007). From exotic spice to modern drug? *Cell.*;130(5):765-8.

Sinha S, Kim IS, Sohn KY, de Crombrugghe B, Maity SN. (1996). Three classes of mutations in the A subunit of the CCAAT-binding factor CBF delineate functional domains involved in the three-step assembly of the CBF-DNA complex. *Mol Cell Biol;* 16:328–337.

Sinha S, Maity SN, Lu J, de Crombrugghe B. (1995) Recombinant rat CBF-C, the third subunit of CBF/NFY, allows formation of a protein-DNA complex with CBF-A and CBF-B and with yeast HAP2 and HAP3. *Proc.Natl.Acad.Sci. U.S.A.* 92, 1624–1628

Takeda DY, Dutta A. (2005). DNA replication and progression through S phase. *Oncogene*; 24(17):2827-43. Review.

Teiten MH, Eifes S, Reuter S, Duvoix A, Dicato M, Diederich M. (2009). Gene expression profiling related to anti-inflammatory properties of curcumin in K562 leukemia cells. *Ann N Y Acad Sci.*;1171:391-8.

Tercero JA, Labib K, Diffley JF. (2000). DNA synthesis at individual replication forks requires the essential initiation factor Cdc45p. *EMBO J.*;19(9):2082-93.

Testa A, Donati G, Yan P, Romani F, Huang TH, Vigano MA, Mantovani R. (2005). Chromatin immunoprecipitation (ChIP) on chip experiments uncover a widespread distribution of NF-Y binding CCAAT sites outside of core promoters. *J Biol Chem*; 280: 13606–13615.

Testoni B, Mantovani R. 2006. Mechanisms of transcriptional repression of cell-cycle G2/M promoters by p63. *Nucleic Acids Res;* 34:928–938.

Tinari N, Lattanzio R, Natoli C, Cianchetti E, Angelucci D, Ricevuto E, Ficorella C, Marchetti P, Alberti S, Piantelli M, Iacobelli S. (2006). Changes of topoisomerase IIalpha expression in breast tumors after neoadjuvant chemotherapy predicts relapse-free survival. *Clin Cancer Res.*;12(5):1501-6.

Uchiyama M, Griffiths D, Arai K, Masai H. (2001). Essential role of Sna41/Cdc45 in loading of DNA polymerase alpha onto minichromosome maintenance proteins in fission yeast. *J Biol Chem.*; 276(28):26189-96.

Uhlen M, Oksvold P, Fagerberg L, Lundberg E, Jonasson K, Forsberg M, Zwahlen M, Kampf C, Wester K, Hober S, Wernerus H, Björling L, Ponten F. (2010). Towards a knowledge-based Human Protein Atlas. *Nat Biotechnol.*; 28(12):1248-50.

Uramoto H, Wetterskog D, Hackzell A, Matsumoto Y, Funa K. (2004). p73 competes with co-activators and recruits histone deacetylase to NF-Y in the repression of PDGF beta-receptor. *J Cell Sci;* 117:5323–5331.

Vempati RK, Jayani RS, Notani D, Sengupta A, Galande S, Haldar D. (2010). p300-mediated acetylation of histone H3 lysine 56 functions in DNA damage response in mammals. *J Biol Chem.*;285(37):28553-64.

Villard J, Peretti M, Masternak K, Barras E, Caretti G, Mantovani R, Reith W. (2000). A functionally essential domain of RFX5 mediates activation of major histocompatibility complex class II promoters by promoting cooperative binding between RFX and NF-Y. *Mol Cell Biol.*; 20(10):3364-76.



Vos SM, Tretter EM, Schmidt BH, Berger JM. (2011). All tangled up: how cells direct, manage and exploit topoisomerase function. *Nat Rev Mol Cell Biol.*;12(12):827-41.

Wang J, Zhuang J, Iyer S, Lin X, Whitfield TW, Greven MC, Pierce BG, Dong X, Kundaje A, Cheng Y, Rando OJ, Birney E, Myers RM, Noble WS, Snyder M, Weng Z. (2012). Sequence features and chromatin structure around the genomic regions bound by 119 human transcription factors. *Genome Res*; 22:1798-812.

Wang JC. (2002). Cellular roles of DNA topoisomerases: a molecular perspective. *Nat Rev Mol Cell Biol.*;3(6):430-40.

Woessner RD, Mattern MR, Mirabelli CK, Johnson RK, Drake FH (1991). Proliferation- and cell cycle-dependent differences in expression of the 170 kilodalton and 180 kilodalton forms of topoisomerase II in NIH-3T3 cells. *Cell Growth Differ;* 2:209–214.

Woodward AM, Göhler T, Luciani MG, Oehlmann M, Ge X, Gartner A, Jackson DA, Blow JJ. (2006). Excess Mcm2-7 license dormant origins of replication that can be used under conditions of replicative stress. *J Cell Biol.*;173(5):673-83.

Xing Y, Fikes JD, Guarente L. (1993). Mutations in yeast HAP2/HAP3 define a hybrid CCAAT box binding domain. *EMBO J*; 12:4647–4655.

Yamanaka K, Mizuarai S, Eguchi T, Itadani H, Hirai H, Kotani H. (2009). Expression levels of NF-Y target genes changed by CDKN1B correlate with clinical prognosis in multiple cancers. *Genomics*; 94: 219–227.

Yamanaka T, Miyazaki H, Oyama F, Kurosawa M, Washizu C, Doi H, Nukina N. (2008). Mutant Huntingtin reduces HSP70 expression through the sequestration of NF-Y transcription factor. *EMBO J*; 27:827–839.

Yun J, Chae HD, Choi TS, Kim EH, Bang YJ, Chung J, Choi KS, Mantovani R, Shin DY. (2003). Cdk2-dependent phosphorylation of the NF-Y transcription factor and its involvement in the p53-p21 signaling pathway. *J Biol Chem*; 278:36966–36972.

Zaret KS, Carroll JS. (2011). Pioneer transcription factors: establishing competence for gene expression. *Genes Dev*.;25(21):2227-41.

Zemzoumi K, Frontini M, Bellorini M, Mantovani R. (1999). NF-Y histone fold alpha1 helices help impart CCAAT specificity. *J Mol Biol*; 286:327–337.

Zhu J, Zhang Y, Joe GJ, Pompetti R, Emerson SG. (2005). NF-Ya activates multiple hematopoietic stem cell (HSC) regulatory genes and promotes HSC self-renewal. *Proc Natl Acad Sci USA*; 102:11728–11733.

Zhu X, Wang Y, Pi W, Liu H, Wickrema A, Tuan D. (2012). NF-Y recruits both transcription activator and repressor to modulate tissue- and developmental stage-specific expression of human gamma-globin gene. *PLoS One*; 7: e47175.

# 10. APPENDIX

## 10.1 Acknowledgments

I would like to express my sincere gratitude to my supervisor, *Dr. Carol Imbriano*, for the constant support during my PhD research project, for her enthusiasm, meticulous advices and her brilliant ideas.

I would like to thank also Prof. Julian Blow for offering me the opportunity to learn new techniques based on the *Xenopus laevis* cell-free system in his laboratory (Dundee University, UK) and for his generous support to the project.

I thank my fellow labmates in Imbriano Group, University of Modena and Reggio Emilia (Dr. Valentina Basile, Dr. Paolo Benatti) and in J.J. Blow Group, University of Dundee (Dr. Julia Neusiedler, Dr. Gaganmeet Singh Chadha) for the stimulating discussions and advices and for the nice time we spent together in the lab.

Besides, I would like to thank my thesis committee, Dr. Susanna Molinari, Dr. Serena Carra and Prof. Rossella Tupler, for their insightful comments during the last three years.



## 10.2 Publications

The results shown in chapter 4 of this thesis have been published in the attached paper:

> **Belluti S**, Basile V, Benatti P, Ferrari E, Marverti G, Imbriano C. *Concurrent inhibition of enzymatic activity and NF-Y-mediated transcription of Topoisomerase-IIα by bis-DemethoxyCurcumin in cancer cells.* Cell Death Dis. 2013 Aug 8;4:e756.

During my PhD, I also contributed to the analysis of bis-DeHydroxyCurcumin activity on human cancer cells, and the results have been published in the attached paper:

> Basile V, **Belluti S**, Ferrari E, Gozzoli C,Ganassi S,Quaglino D,Saladini M,Imbriano C. *bis-dehydroxy-curcumin triggers mitochondrial-associated cell death in human colon cancer cells through ER-stress induced autophagy.* PLoS One. 2013;8(1):e53664.

OPEN

Citation: Cell Death and Disease (2013) 4, e756; doi:10.1038/cddis.2013.287

www.nature.com/cddis

# Concurrent inhibition of enzymatic activity and NF-Y-mediated transcription of Topoisomerase-IIα by *bis*-DemethoxyCurcumin in cancer cells

S Belluti[1], V Basile[1], P Benatti[1], E Ferrari[2], G Marverti[3] and C Imbriano*[,1]

**Topoisomerases-IIα (TOP2A) enzyme is essential for cell viability due to its fundamental role in DNA metabolism and in chromatin organization during interphase and mitosis. TOP2A expression is finely regulated at the transcriptional level through the binding of the CCAAT-transcription factor NF-Y to its promoter. Overexpression and/or amplification of TOP2A have been observed in many types of cancers. For this reason, TOP2A is the target of the most widely successful drugs in cancer chemotherapy, such as TOP2A poisons, which stabilize TOP2A-DNA cleavage complexes and create DSBs, leading to chromosome damage and cell death. We previously reported that the Curcumin-derivative *bis*-DemethoxyCurcumin (bDMC) is an anti-proliferative agent that inhibits cell growth by concomitant G1/S and G2/M arrest. Here we showed that bDMC irreversibly induces DSBs in cancer cells, but not in normal cells, by targeting TOP2A activity and expression. TOP2A ablation by siRNA corroborates its contribution to apoptosis induced by bDMC. Short-term exposure to bDMC induces retention of TOP2A-DNA intermediates, while longer exposure inhibits TOP2A transcription by affecting expression and sub-cellular localization of NF-Y subunits. ChIP analysis highlighted reduced recruitment of NF-Y to TOP2A regulatory regions, concomitantly to histone deacetylation and decreased gene transcription. Our findings suggest that the dual activity of bDMC on TOP2A represents a novel therapeutic strategy to induce persistent apoptosis in cancer cells and identify NF-Y regulation as a promising approach in anti-cancer therapy.**

*Cell Death and Disease* (2013) **4,** e756; doi:10.1038/cddis.2013.287; published online 8 August 2013
**Subject Category:** Cancer

Mammalian cells express two Topoisomerase II (TOP2) enzymes, TOP2A and TOP2B, but only the first is essential for cellular viability.[1,2] TOP2A has a key physiological function in DNA metabolism of eukaryotic cells and has a structural role in chromatin organization during interphase and mitosis.[3,4] The development of TOP2A-depleted mice terminates at the four- or eight-cell stage because of chromosome segregation defects.[5] TOP2A expression is low in quiescent cells and increases when cells are stimulated to re-enter the growth phase of the cell cycle: its levels rise throughout the S phase and peak during G2/M phase.[6–8] The expression of human TOP2A mRNA is controlled by its promoter region, whose activity is regulated through cis-acting elements within the first 617 base pairs.[9] Among multiple transcription factors controlling TOP2A transcription throughout the cell cycle, Sp and NF-Y have been shown to bind GC consensus sites and four inverted CCAAT boxes (ICB1–ICB4), respectively.[10–12]

NF-Y is a heterotrimeric complex composed of three conserved subunits, NF-YA, NF-YB and NF-YC.[13] NF-YA interacts with the NF-YB/NF-YC heterodimer and determines specific NF-Y binding to the CCAAT box. Although NF-Y acts as a transcriptional activator of TOP2A, its binding to ICB2 has been described to downregulate the promoter activity by confluence arrest.[14]

TOP2A transcription can be inhibited by wt p53 and the disruption of ICBs abolishes the p53-dependent downregulation of TOP2A.[15,16] In addition, p53-independent mechanisms can lead to decreased TOP2A mRNA levels through reduced NF-Y binding to ICB1.[15]

Increased TOP2A protein levels have been detected in cancer cells compared with non-malignant cells, although a strong heterogeneity of TOP2A expression within different cancer cells has been observed.[17] For this reason, TOP2A is the target for some of the most widely successful drugs used to treat human cancers.[18,19]

Two different classes of drugs targeting TOP2A have been described: the first one, referred to as TOP2A poisons, increases the concentration of covalent enzyme-cleaved DNA complexes and generates DNA strand breaks. The second class is composed by catalytic TOP2 inhibitors, compounds that prevent TOP2 from carrying out its physiological enzymatic activity.[18]

TOP2-DNA covalent complexes have severe effects on cell proliferation and viability: TOP2 poisons block both replication

[1]Dipartimento di Scienze della Vita, Università di Modena e Reggio Emilia, via Campi 213/D, Modena 41125, Italy; [2]Dipartimento di Scienze Chimiche e Geologiche, via Campi 283, Modena 41125, Italy and [3]Dipartimento di Scienze Biomediche, Metaboliche e Neuroscienze, via Campi 287, Modena 41125, Italy
*Corresponding author: C Imbriano, Dipartimento di Scienze della Vita, Università di Modena e Reggio Emilia, via Campi 213/D, Modena 41125, Italy. Tel: +39 059 2055542; Fax: +39 059 2055548; E-mail: cimbriano@unimo.it
**Keywords:** NF-Y; CCAAT box; gene transcription; TOP2A; curcuminoids
**Abbreviations:** TOP2, Topoisomerase II; bDMC, bis-DemethoxyCurcumin; DSB, double-strand break; PI, propidium iodide; LMB, Leptomycin B; NAC, *N*-acetylcisteine; WORT, Wortmannin
Received 03.5.13; revised 03.7.13; accepted 04.7.13; Edited by A Stephanou

and transcription processes and lead to the activation of apoptosis by inducing DNA strand breaks.[20–23]

Although the great potential of TOP2 targeting drugs towards multiple type of human cancers, TOP2 poisons can lead to secondary malignancies. In particular, etoposide and teniposide administration in chemotherapy regimens have a high potential of generating translocations, responsible for secondary malignancies,[24,25] while anthracyclines generate free radicals in both normal and tumor tissues, leading to bone marrow and cardiac toxicity.[26,27]

Curcumin, the pigment derived from the rhizome *Curcuma longa*, has demonstrated anticancer properties, attributed to its selective cell death-inducing ability in tumor cells.[28–30] The apoptotic process seems to be initiated by DNA damage triggered by TOP2 poisoning.[31,32] Despite the possible side effects of Curcumin on fertility and immune functions,[33–35] in the majority of normal and primary cells, it does not elicit a cytotoxic response.

We demonstrated that the Curcumin derivative bis-DemethoxyCurcumin (bDMC) is more stable in physiological condition than its lead compound, circumventing one of the most limiting facets of Curcumin in clinical applications.[36] bDMC exhibits improved cytotoxicity in ovarian cancer cells and shows higher anti-oxidant, anti-mutagenic, anti-carcinogenic and anti-metastatic activities than Curcumin.[37,38] While Curcumin delays the mitotic exit as a consequence of microtubule poisoning, bDMC is able to induce a concomitant and long-lasting G1/S and mitotic cell cycle block in human colon cancer cells. Concurrently to the cell cycle impairment, bDMC activates a DNA-damage response, which can be responsible for the slower kinetic in re-entering the cell cycle after the release.[36]

Our present investigations focus on the activity of bDMC as DNA-damaging agent and inhibitor of TOP2A. We highlight that bDMC triggers DNA damage in cancer cells by targeting TOP2A, both through inhibition of its enzymatic activity and through repression of its NF-Y-dependent transcription.

## Results

**Effect of bDMC on proliferation and cell cycle distribution in cancer and normal human cells.** We have already shown that bDMC treatment induces a concomitant G1/S and long-lasting mitotic arrest of the cell cycle of human colon cancer cells HCT116. In particular, the passage from early to late S is delayed when bDMC is added to synchronized G0/G1 cells.[36]

In addition to cytostatic effects, cytotoxicity was observed following bDMC administration at IC50 concentration (30 $\mu$M) to HCT116. A time-dependent increase of SubG1 events was detected by PI cytofluorimetric analysis in bDMC-treated cells (from 0.6% in control cells to 5.1 and 7.5% after 16 and 24 h, respectively) (Figures 1a and b). The presence of AnnexinV-positive cells (from 4% in dimethyl sulfoxide (DMSO) to 20% in bDMC cells) clearly suggested that bDMC triggers apoptotic cell death (Figure 1c). Interestingly, when HCT116 were released from bDMC into the fresh medium, SubG1 events raised up to about 14 and 23% after 16 and 24 h, hinting that bDMC irreversibly commits cells to apoptotic death (Figures 1a and b). Cleavage of PARP-1 and H2AX Ser139 phosphorylation ($\gamma$H2AX) followed the time-dependent increase of SubG1 events and further grew when cells were released from bDMC (Figure 1d). Exposure to bDMC induced the same effects on colorectal carcinoma Lovo cells (Supplementary Figures S1a–c).

To investigate the cytotoxicity of bDMC against tumor *versus* healthy cells, human normal fibroblasts (HF) and hepatic fetal epithelial cells (WRL-68) were treated with 30 $\mu$M bDMC (Figures 2a and b). No increase of SubG1 events was detected, also when cells were released from drug incubation (Figures 2c and e). The lack or very low expression of $\gamma$H2AX in treated and released cells further corroborates the tumor selectivity of bDMC (Figures 2d and f). Moreover, dose–response experiments highlighted that IC50 is significantly higher in HF ($>320\,\mu$M) and WRL68 (55 $\mu$M) cells, compared with HCT116 and LOVO tumor cells (Figures 2g and h).

**bDMC induces double-strand breaks (DSBs) and chromosome aberrations in HCT116 cells.** H2AX phosphorylation has an important role not only in apoptosis but also in response to DSBs.[39] To examine the relationship between $\gamma$H2AX and DNA damage rather than apoptosis, we co-treated cells with bDMC and the pan-caspase inhibitor Z-VAD. Although Z-VAD was able to completely abolish the accumulation of SubG1 events, $\gamma$H2AX was only partially reduced compared with bDMC-treated cells, coupling its expression to DNA damage (Figures 3A and B).

We previously demonstrated that bDMC administration for 24 h resulted in ATM (ataxia telangiectasia mutated) activation.[36] ATM has a major role in signal transduction in response to DSBs,[40] and once activated, it is able to phosphorylate different proteins associated with the DNA damage response, such as sensors, mediators, as H2AX and BRCA1, transducers and effectors of DSB, among which are ChK2, ChK1 and p53.[41] Western blot analysis with Phospho-BRCA1 (Ser1524) and Phospho-ChK1 (Ser296) antibodies further demonstrated the activation of a DNA damage response induced by bDMC (Figure 3C). Pre-treatment with Wortmannin (WORT), which is able to disrupt multiple DNA damage and DNA repair mechanisms via inhibition of PI3K-kinases (ATM and DNA-PK),[42–44] resulted in a clear reduction of H2AX phosphorylation (Figure 3D). In addition, WORT determined a robust decrease of G2/M population (from 46.3% in bDMC-treated cells to 31.2% in WORT-bDMC-treated cells) and an increase of G0/G1 events (from 34.4 to 44.9%), hinting that the activation of the DNA damage checkpoint occurs in G2/M and prevents cells from entering the next G1 phase (Figure 3E).

Fluorescent-activated cell sorting (FACS) was used to quantify the levels of H2AX phosphorylation in 2N and 4N populations. Following 24 h treatment with bDMC, we observed the accumulation of $\gamma$H2AX-positive cells with a 4N DNA content (Figure 3F), presumably G2/M arrested cells. Also HCT116/E6 cells, in which the lack of p53 causes a robust arrest in G2/M and prevents the G1/S block following bDMC administration,[36] showed an evident time-dependent increase of $\gamma$H2AX, corroborating that DNA damaged cells are

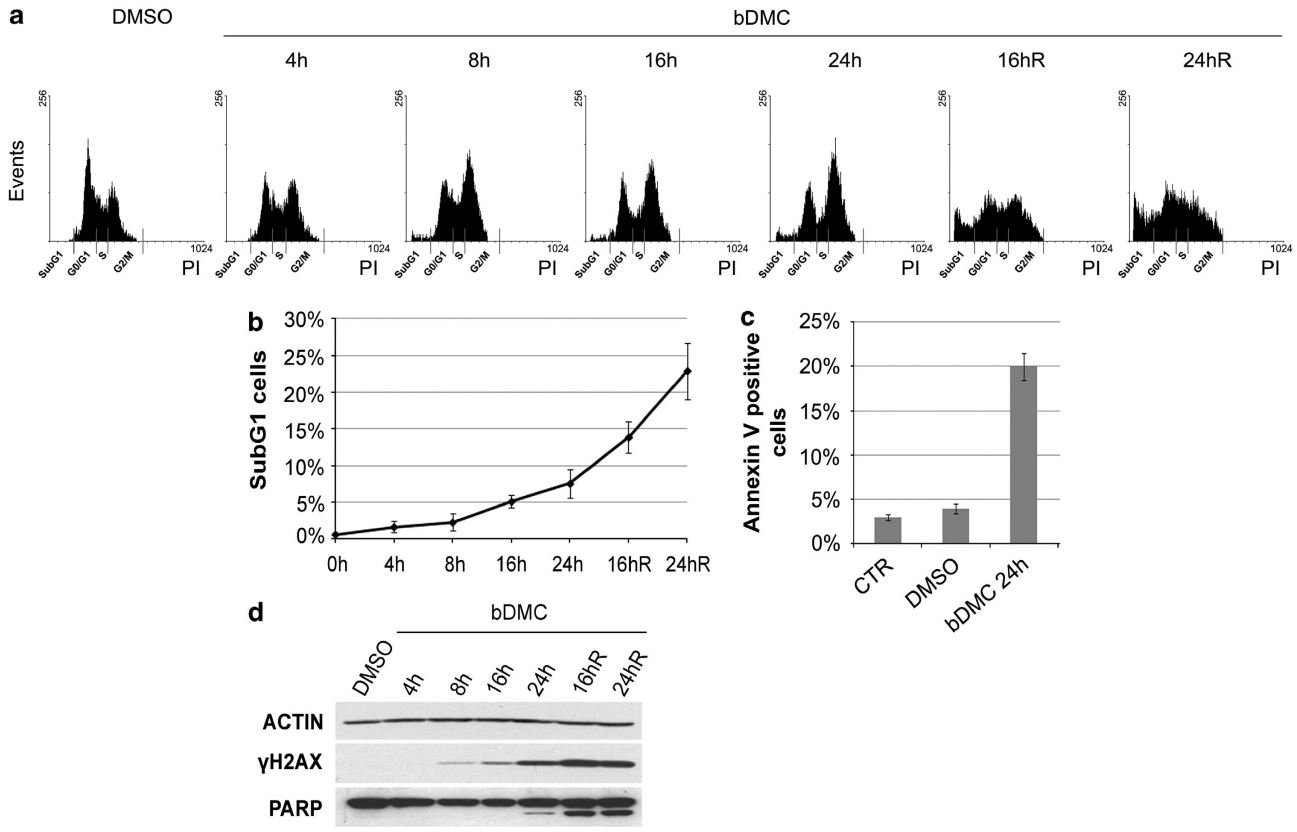


**Figure 1** bDMC triggers irreversible cell death in HCT116 cells. (**a**) Cytometric cell-cycle analysis of HCT116 cells treated with 30 $\mu$M bDMC for 4, 8, 16, 24 h and released in drug-free medium for additional 16 and 24 h (16hR and 24hR) following 24 h of bDMC treatment. (**b**) Percentages of SubG1 events detected by PI cytometric analysis following the indicated time exposure to bDMC. Reported values are an average of 10 independent experiments ± S.D. (**c**) The percentage of Annexin V-positive cells after 24 h treatment with 30 $\mu$M bDMC is compared with Control (CTR) and DMSO-treated cells. Data are means of three independent experiments ± S.D. (**d**) Western blot expression analysis of $\gamma$H2AX and cleaved PARP1 following time-dependent administration of 30-$\mu$M bDMC to HCT116 cells. Actin was used as loading control

mainly distributed in the G2/M phase of the cell cycle (Supplementary Figures S1d and e).

We then evaluated the ability of bDMC to cause chromosome aberrations. Cells were treated with DMSO or bDMC for 24 h, and Giemsa-stained metaphases were analyzed: while control cells did not show chromosome abnormalities, we detected an average of two chromatid-type aberrations per cell, in particular gaps and breaks, following bDMC administration (Figure 3G). The same defects were detected in HCT116/E6 cells (data not shown).

All together these data suggest that bDMC induces DNA damage in G2/M cells, which are prevented from entering the next G1 phase and presumably are then committed to apoptosis.

**bDMC inhibits TOP2α activity.** TOP1 and TOP2-DNA complexes have been observed following Curcumin administration to K562 cells.[32] Considering that bDMC has a predicted stronger binding affinity to TOP2A compared with Curcumin,[45] we hypothesized that DNA damage and chromosome aberrations induced by bDMC could be due to the inhibition of TOP2A in HCT116 cells.

To test TOP2A inhibitory activity of bDMC, we performed a cell-free TOP2A relaxation assay (Figure 4a). The kinetoplast DNA (kDNA) was used as a specific substrate for TOP2 enzymes. In accordance with its known activity as TOP2A poison, etoposide inhibited TOP2A-dependent decatenation. bDMC was found to halved DNA decatenation at lower concentrations than etoposide.

To assess whether bDMC could act as TOP2A poison, we verified the formation of TOP2A-DNA complexes through a band-depletion assay.[46] We compared the levels of TOP2A in the samples of each bDMC time point with or without Micrococcal Nuclease (MNase) addition, which allows the release of TOP2A from DNA complexes possibly induced by bDMC. MNase digestion partially restored TOP2A levels in cellular extracts from HCT116 treated with bDMC for 4 and 8 h, consistently with the presence of TOP2A-DNA complexes. Differently, no increase was observed following MNase addition in 16 and 24 h bDMC samples, hinting at a different mechanism triggering TOP2A depletion (Figure 4b).

Increase of cellular levels of reactive oxygen species (ROS) could have a role in the formation of TOP2-DNA complexes induced by Curcumin.[32] Therefore, a band-depletion assay was performed with extracts from cells pre-treated with the antioxidant *N*-acetylcisteine (NAC). Figure 4c shows that NAC did not abolish TOP2A band depletion, ruling out that ROS could mediate TOP2A-DNA complexes.

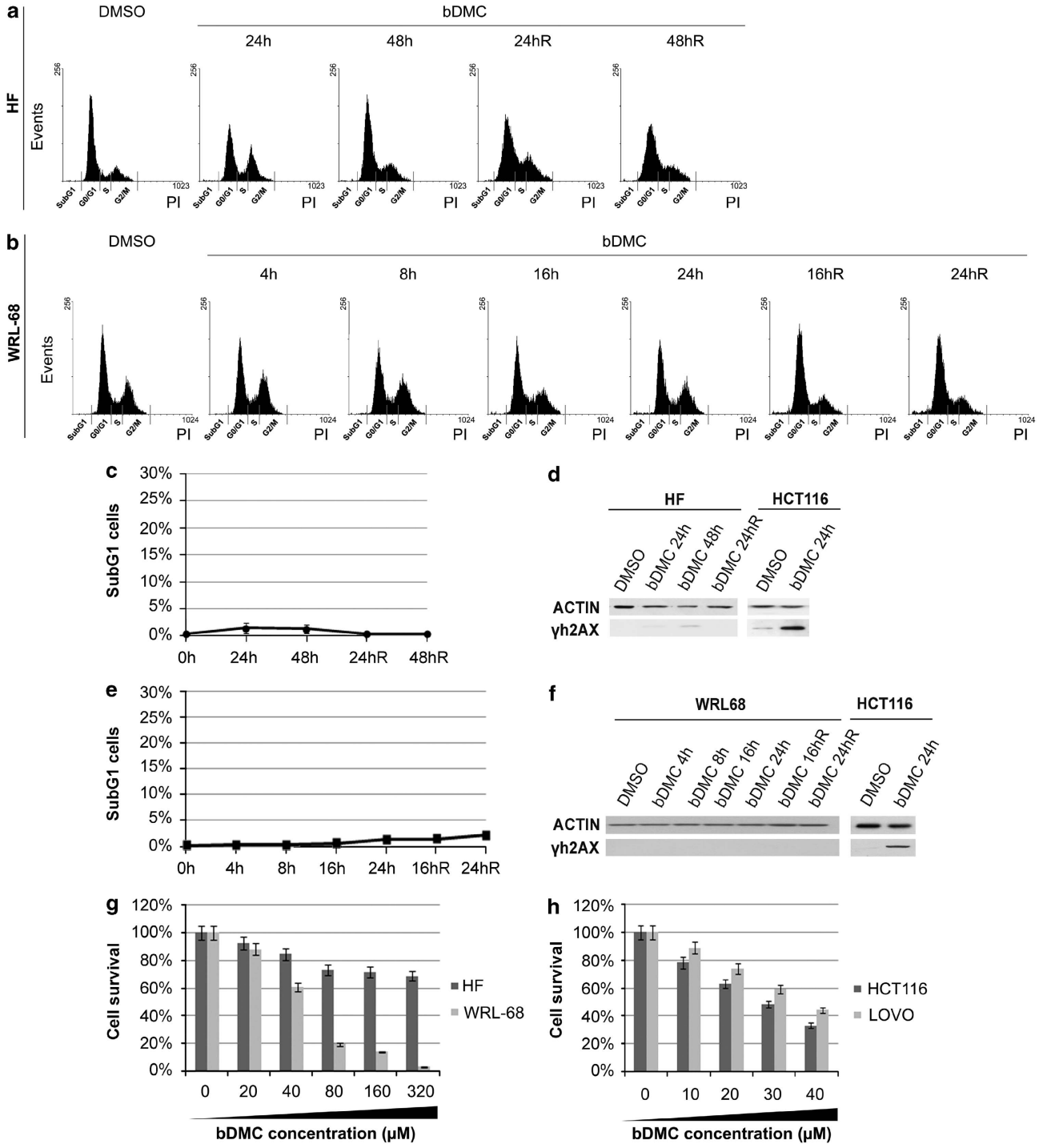


**Figure 2** bDMC does not induce cell death in human healthy cells. (**a** and **b**) Cell-cycle analysis of HF (**a**) and WRL-68 (**b**) cells treated with 30 $\mu$M bDMC for the indicated time points and released into fresh medium for additional 16, 24 or 48 h. (**c**) Quantification in percentage of SubG1 population in HF cells treated with bDMC and released into fresh medium for 24 and 48 h (24hR and 48hR). Values are means of three independent experiments ± S.D. (**d**) Expression levels of $\gamma$H2AX in DMSO- and bDMC-treated and released (R) HF cells. (**e**) Percentage of SubG1 population in WRL-68 cells following bDMC administration and released into drug-free medium (16hR and 24hR). Values are means of three independent experiments ± S.D. (**f**) Western blot analysis with anti-$\gamma$H2AX and anti-actin antibodies in WRL-68 cells treated and released from bDMC for the indicated time points. (**g** and **h**) Percentage of cell survival of HF and WRL-68 normal cells (**g**) and HCT116 and LOVO tumor cells (**h**) following administration with increasing concentrations of bDMC for 24 h

These data clearly suggest that bDMC induced retention of TOP2A-DNA intermediates up to 8 h, after which reduced protein levels cannot be ascribed to bDMC activity as TOP2 poison.

**bDMC impairs NF-Y-dependent gene transcription of TOP2α.** Despite MNase digestion, a time-dependent decrease of TOP2A levels was observed following bDMC

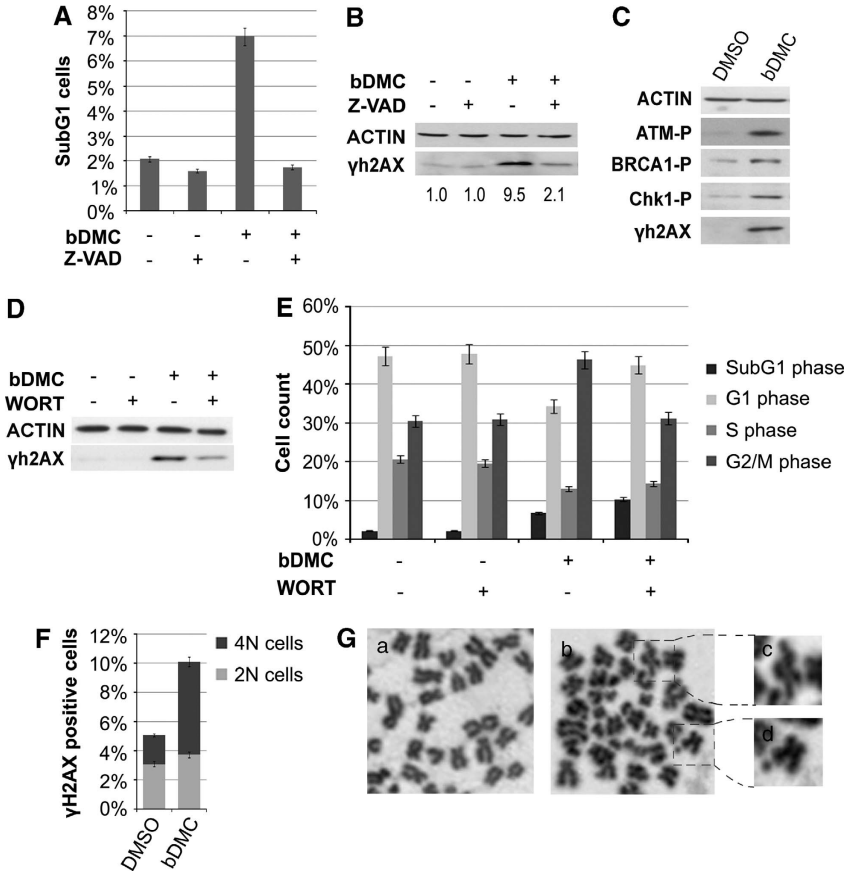


**Figure 3** bDMC induces DNA damage and activates the DNA-damage response in HCT116 cells. (**A**) Quantification of SubG1 phase cell number following Z-VAD/bDMC co-treatment or bDMC (30 $\mu$M) alone for 24 h. Data represent the average of three independent experiments ± S.D. (**B**) Western blot and quantification of $\gamma$H2AX expression levels *versus* actin following bDMC and bDMC-Z-VAD 24-h treatments. (**C**) Western blot analysis of total extracts of 24-h 30-$\mu$M bDMC-treated cells with the indicated antibodies. (**D**) Changes of $\gamma$H2AX expression levels in cells pre-treated with WORT compared with cells treated for 24 h with bDMC. (**E**) Percentage of cells throughout the different phases of the cell cycle of bDMC-treated cells before and after WORT pre-incubation. The indicated events are means of three independent experiments ± S.D. (**F**) Percentages of $\gamma$H2AX-positive cells in 2N and 4N populations after 30-$\mu$M bDMC treatments for 24 h. (**G**) Representative Giemsa-stained mitotic chromosome spread of cells treated with 30 $\mu$M DMSO (a) or bDMC (b) for 24 h. Enlargement of dashed box (c and d) shows chromosome aberrations of bDMC-cells

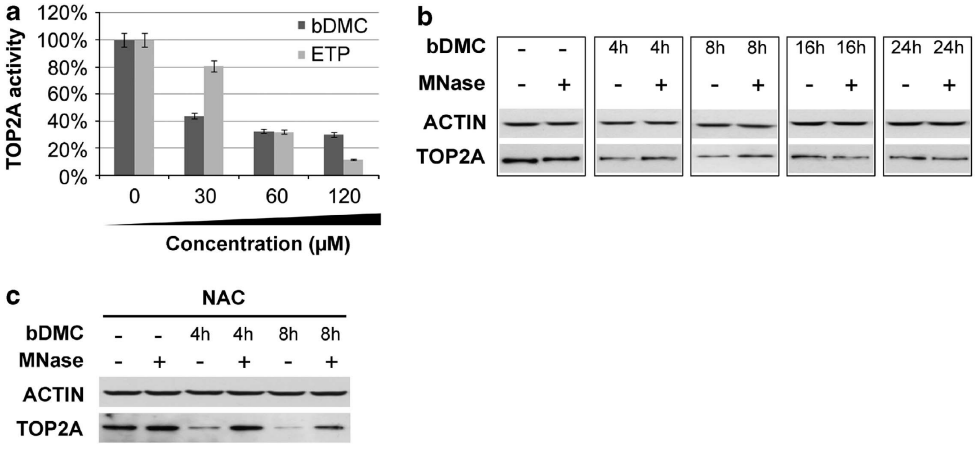


**Figure 4** bDMC inhibits TOP2$\alpha$ enzymatic activity. (**a**) Inhibition of TOP2A-dependent decatenation of kDNA following increasing concentrations of bDMC and Etoposide (ETP) *versus* DMSO (arbitrarily set at 100%). (**b**) Western blot analysis of TOP2A expression after 4, 8, 16 and 24 h after 30 $\mu$M bDMC addition, with or without MNase digestion. (**c**) TOP2A expression analysis of untreated and MNase-treated samples upon bDMC-NAC treatment

administration (Figure 5a). In addition, proteasome inhibition by MG132 did not raise TOP2A levels (Figure 5b), suggesting that neither the formation of TOP2A-DNA complexes or protein degradation were responsible for TOP2A halved levels. For this reason, we analyzed TOP2A mRNA levels after time course incubation with bDMC. Real-time RT-PCR analysis revealed that bDMC induced a clear time-dependent decrease of TOP2A gene transcription, with maximal inhibition after 24 h (Figure 5c). The release from bDMC for 16 and 24 h did not restore TOP2A mRNA and protein levels (Supplementary Figures S2a and b).

The transcription factor NF-Y is the key activator of TOP2A and specifically binds the CCAAT boxes of its regulatory regions. Chromatin immunoprecipitation (ChIP) experiments were performed to investigate NF-Y binding to TOP2A promoter after 24 h of bDMC administration. Compared with DMSO, the binding of NF-YA and NF-YB subunits was reduced by about 40 and 30%, respectively (Figure 5d). A strong correlation between NF-Y binding and epigenetic marks has been described, therefore we investigated by ChIP the levels of acetylated histones H3 and H4 (H3ac and H4ac) and H3K4me3, an epigenetic marker associated with active

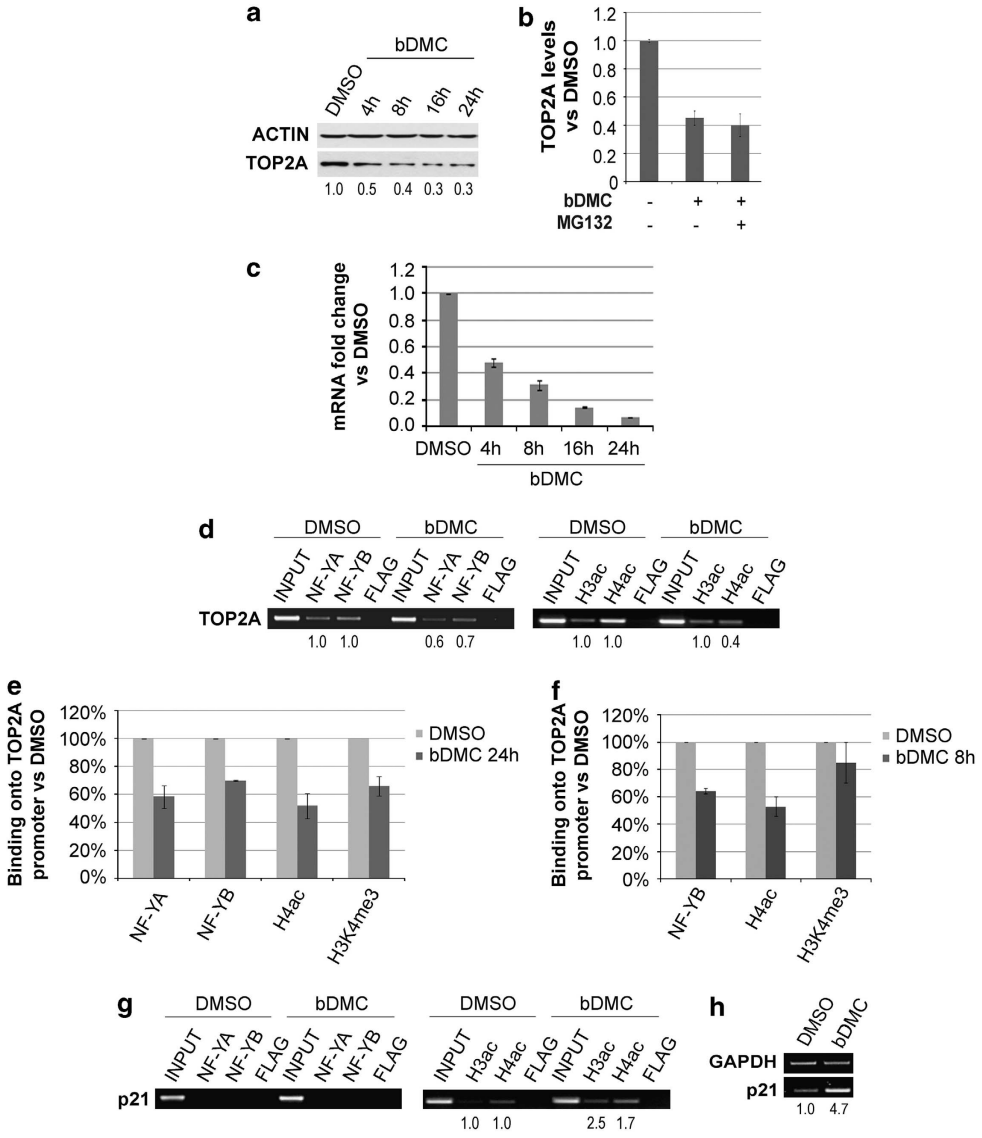


**Figure 5** Inhibition of NF-Y-mediated TOP2A transcription by bDMC. (**a**) TOP2A protein analysis in MNase-treated extracts following time course incubation with bDMC (30 $\mu$M). The indicated values represent the quantification of TOP2A immunoreactive bands of two independent experiments normalized to actin levels. (**b**) Quantification of TOP2A expression levels (normalized to actin) following bDMC and bDMC-MG132 administration for 24 h *versus* DMSO (arbitrarily set at 1). (**c**) Real-time analysis of TOP2A transcripts in cells treated with 30 $\mu$M bDMC, represented as mRNA fold change *versus* DMSO (arbitrarily set at 1). GAPDH has been used as internal control. The indicated values are mean of four independent experiments $\pm$ S.D. (**d**) ChIP semi-quantitative PCR analysis of NF-YA, NF-YB, acetyl-H3 and acetyl-H4 binding to TOP2A promoter in cells treated with DMSO or bDMC (30 $\mu$M) for 24 h. (**e** and **f**) ChIP real-time analysis of chromatin-associated NF-Y, acetyl-H4 and H3K4me3 to TOP2A promoter following 24-h (**e**) and 8-h (**f**) incubation with 30 $\mu$M bDMC. (**g**) Semi-quantitative analysis of the recruitment of NF-Y and acetylated histones on p21 regulatory region cells treated for 24 h with DMSO and 30 $\mu$M bDMC. (**h**) mRNA expression levels of p21 in 24 h bDMC-treated cells

gene promoters, whose deposition is strongly dependent upon the binding of NF-Y.[47,48] Although H3ac was not modified by bDMC, the levels of H4ac were reduced by about 60% on the TOP2A promoter region (Figure 5d). Real-time PCRs highlighted that maximum NF-Y and H4ac reduction were induced after 8 h, while H3K4me3 showed a decrease at 24 h, hinting that NF-Y dissociation could lead to later effects on the chromatin structure of TOP2A promoter and therefore on gene transcription (Figures 5e and f). On the other hand, both H3 and H4 acetylation increased on p21 regulatory region, consistently to its transcriptional activation (Figures 5g and h). Taken together, these data indicate that bDMC induces the transcriptional repression of TOP2A by affecting NF-Y binding to its promoter region.

**bDMC affects NF-YA expression and sub-cellular localization of NF-YB and NF-YC subunits.** We next wondered whether decreased NF-Y binding to TOP2A CCAAT boxes could be ascribed to reduced NF-Y cellular levels upon bDMC treatment. Total extracts were prepared from HCT116 cells treated with DMSO and bDMC for 24 h. Western blot analysis showed a decrease of the DNA binding subunit NF-YA, consistently with mRNA halved levels (Figures 6a and b); no changes were observed in NF-YB and NF-YC expression levels (Figures 6a and b). While NF-YA has been shown to be mainly localized in the nucleus, NF-YB and NF-YC shuttle from the cytoplasm to the nucleus.[49] Therefore, we performed western blot analysis of NF-Y subunits on nuclear and cytosolic fractions of bDMC-treated cells. As shown in Figure 6c, NF-YB and NF-YC were accumulated in the cytoplasm. A time-dependent increase of cytosolic NF-YB and NF-YC was observed following bDMC administration, with a maximum peak after 24 h of treatment (Figure 6d), although nuclear NF-YB and NF-YC were reduced to minimum levels already after 8 h. To discriminate whether nuclear export rather than import was affected by bDMC, we co-treated cells with Leptomycin B (LMB), a known inhibitor of CRM1 exportin: no increase of nuclear NF-YB and NF-YC was observed in co-treated *versus* bDMC-treated cells (Figure 6e). The accumulation of nuclear p53 confirmed the efficacy of LMB treatment on HCT116 cells. These results support the hypothesis that bDMC induces Topo IIα transcriptional repression by decreasing NF-YA levels and retaining NF-YB/NF-YC into the cytoplasm.

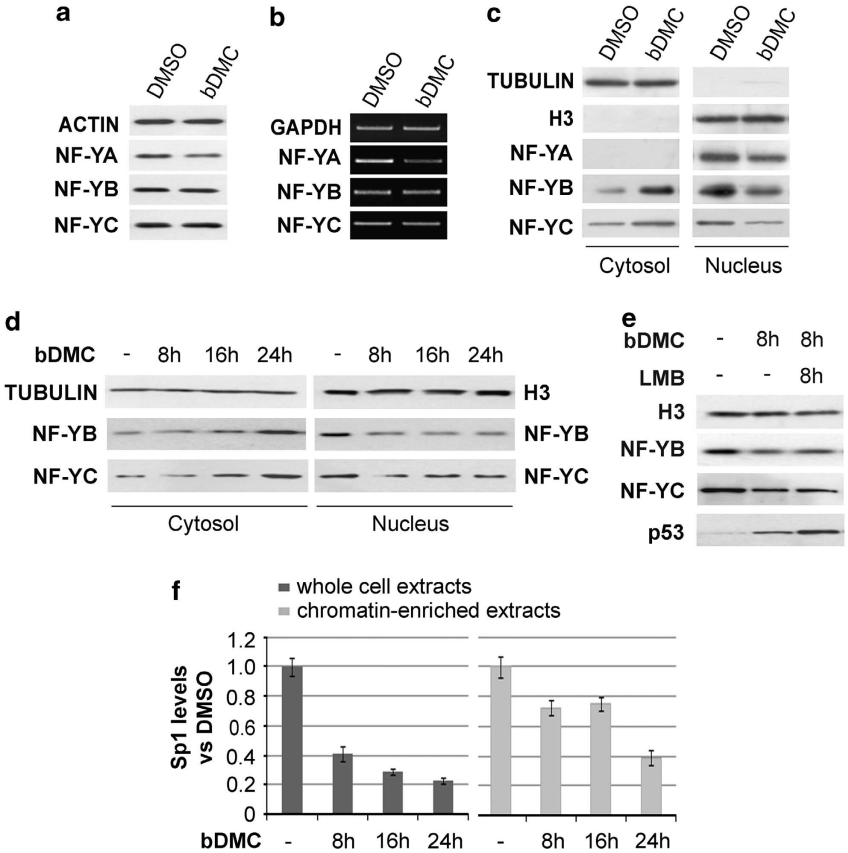


**Figure 6** bDMC affects NF-Y subunits expression and sub-cellular localization. (**a**) Western blot analysis of total extracts of DMSO and bDMC (30 $\mu$M)-treated cells (24 h) with antibodies against the three NF-Y subunits. (**b**) Semi-quantitative RT-PCRs of NF-YA, NF-YB and NF-YC subunits following 24 h treatment with DMSO and 30 $\mu$M bDMC. (**c**) Expression levels of NF-YB and NF-YC in nuclear and cytosolic fractions of HCT116 cells treated with 30 $\mu$M bDMC for 24 h. Tubulin and H3 were used as loading control for cytosolic and nuclear extracts, respectively. (**d**) Time course analysis of NF-Y subunits expression in nuclear and cytoplasmic cellular compartments. (**e**) Nuclear expression levels of NF-YB, NF-YC and p53 following co-incubation of 30 $\mu$M bDMC with LMB for 8 h *versus* bDMC alone. Histone H3 was used as loading control. (**f**) Expression levels of SP1 in total and chromatin-enriched extracts following time course incubation with 30 $\mu$M bDMC

The transcriptional control of TOP2A gene has been shown to be played by NF-Y in cooperation with the transcription factor Sp1.[50] For this reason, we decided to investigate whether also Sp1 could have a role in the time-dependent decrease of TOP2A mRNA levels. Chromatin-enriched and whole-cell extracts were prepared following 4, 8 16 and 24 h exposure of HCT116 cells to bDMC and western blot analysis performed with anti-Sp1 antibody. As shown in Figure 6f, while total Sp1 levels were already reduced at 8 h, bDMC mainly affected Sp1 chromatin recruitment following 24 h.

**Cell death induced by bDMC is mediated by TOP2α enzymatic and transcriptional targeting.** To assess the importance of TOP2A in mediating bDMC apoptotic response, we knocked down TOP2A by transient RNAi. TOP2A protein levels were reduced by $>70\%$ (Figure 7a) and SubG1 events raised from 1.8 to 11.5% after small interfering RNA (siRNA) transfection for 48 h (Figure 7b), highlighting the fundamental role of TOP2A in HCT116 viability. Following bDMC administration, SubG1 events raised to 6.3% in control cells, while no increase was observed in TOP2A-deficient cells (from 11.5 to 8.7%), although TOP2A protein levels were further reduced (Figure 7a). On the other hand, the release from bDMC for additional 24 h resulted in twofold increase of apoptosis also in TOP2A knockdown cells (from 6.3 to 13.7% in control cells and from 8.6 to 16.4% in silenced cells).

These data suggest that both enzymatic and transcriptional TOP2A targeting contributes to bDMC cytotoxic activity. The lack of an additive apoptotic effect of bDMC administration on TOP2A-silenced cells, indicates that within the first 24 h an important role is played by the enzymatic inhibition of TOP2A. Reduced TOP2A levels avoid a further increase of apoptotic events. Differently, TOP2A-depleted cells are still committed to irreversible cell death when bDMC is removed, suggesting that long-term apoptotic effects can be ascribed to TOP2A transcriptional inhibition rather than its poisoning.

## Discussion

High TOP2A levels result in enhanced proliferation rates of many human malignancies and correlate with shortened patient survival.[51–53] These types of tumors are most susceptible to TOP2-targeting chemotherapeutics. For these reasons, TOP2A expression is a double-edged sword: on one side, high TOP2A levels could indicate tumor aggressiveness and poor outcome, on the other side, this could determine a positive response to chemotherapeutic drugs targeting this enzyme.

Our results provide evidence that bDMC suppresses cell proliferation and induces apoptosis, at least in part, by targeting TOP2A, thus encompassing bDMC in the category of TOP2-based DNA-damaging agents. Indeed, bDMC reduces cell viability by inducing DNA breaks and a persistent and irreversible DNA damage response and inhibits TOP2A activity as highlighted by MNase band-depletion and cell-free TOP2A relaxation assays (Figure 4).

Interestingly, bDMC does not cause DNA damage-induced cell death in normal cells, which are less susceptible to bDMC, as highlighted by higher IC50 concentrations (Figure 2). Tumor selectivity of Curcumin and its derivatives has been already attributed to different mechanisms, such as lower drug uptake in healthy cells,[54] rather than increased sensitivity of cancer cells due to lower glutathione levels or constitutive expression of NF-kB.[55] Taking into account that tumor cells have normally higher expression of TOP2A compared with normal cells, our data suggest that one of the molecular basis for bDMC cancer cell selectivity and susceptibility could be dependent on the levels of TOP2A target protein.

TOP2A has a fundamental role in DNA replication, and it has been shown that DNA damage induced by TOP2A poisons is related to their interaction with DNA replication fork progression.[56] Although bDMC delays the progression from early to late S phase,[36] the majority of cells positive for γH2AX following bDMC administration are accumulated in G2/M phase (Figure 3), and chromosome aberrations are observed in mitotic cells (Figure 3). DNA damage response and repair are activated in G2/M cells, as demonstrated by the clear reduction of the G2/M population following pre-treatment with the PI3K-kinases inhibitor WORT (Figure 3). Surprisingly, these cells escaping the G2/M DNA damage checkpoint are not driven to apoptosis but are accumulated in the next G0/G1 phase, suggesting that apoptosis is triggered by a persistent activation of the DNA damage response in G2/M cells.

Although 4- and 8-h treatment with bDMC induces a concurrent inhibition of transcription and activity of TOP2A, prolonged administration for 16 and 24 h results only in reduced gene transcription (Figures 4 and 5). The inability of long-term poisoning of TOP2A by bDMC could be due to the rapid metabolism of the molecule inside the cell. After 24 h, $<0.5\%$ of bDMC was detected inside the cells,[36] and about 7.5% ($\pm 1.5$) and 6.2% ($\pm 0.7$) after 4 and 8 h, respectively (data not shown). These data strongly suggest that the main effects are induced by bDMC within 8 h, consistently with maximum TOP2A enzymatic inhibition and reduced NF-Y activity in 8 h, although the molecular mechanisms triggered by bDMC or its metabolites, leading to TOP2A transcriptional inhibition, could continue for longer time.

To shed light on the contribution of TOP2A poisoning rather than transcriptional inhibition on apoptosis activation, we silenced TOP2A through transient RNAi (Figure 7). TOP2A knockdown leads to about sixfold increase of SubG1 events,

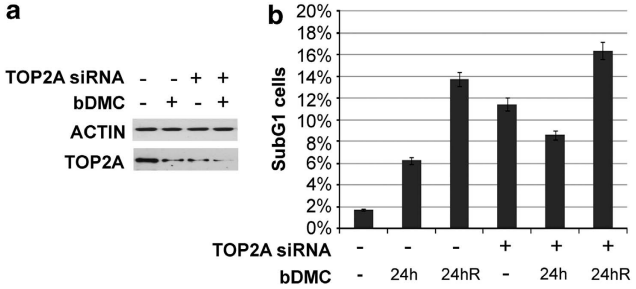


**Figure 7** bDMC cytotoxic activity is mediated by Topoisomerases IIα enzymatic and transcriptional targeting. (**a**) Western blot analysis of TOP2A following siRNA-mediated knockdown of TOP2A and bDMC (30 μM) treatment for 24 h. (**b**) Quantification of SubG1 population upon 30 μM bDMC treatment and release (R) in control and TOP2A-inactivated cells

and bDMC treatment for 24 h is not able to further augment apoptosis, suggesting that direct TOP2A targeting contributes to bDMC pro-apoptotic activity. The inhibition of mRNA levels, and consequently of protein levels of TOP2A, has a major role in the irreversible activation of cell death, observed after drug removal at 24 h.

TOP2A transcriptional inhibition results from decreased recruitment of the transcription factor NF-Y to its regulatory regions (Figure 5), as a consequence of halved NF-YA nuclear levels and NF-YB/NF-YC cytoplasmic retention (Figure 6). Despite a reduction of only 40 and 30% in the binding of NF-YA and NF-YB, respectively, to TOP2A promoter, TOP2A gene transcription is strongly affected by bDMC. This result is consistent with our previous data observed in NF-YB-inactivated cells: although NF-YB knockdown induces a robust decrease of TOP2A levels, NF-YA and NF-YB binding were reduced by about 20% compared with control cells.[57]

Finally, we showed that bDMC induces decreased expression and chromatin recruitment of Sp1, important functional partner of NF-Y in the control of TOP2A gene transcription (Figure 6). These results are in agreement with (i) Sp1 downregulation observed upon NF-Y inactivation by gene expression profiling,[57] and (ii) ChIP-seq analysis (ENCODE Data at UCSC Genome Browser) showing NF-Y binding to Sp1 regulatory regions. All together, these data suggest that NF-Y directly controls Sp1 transcription, and therefore, TOP2A transcriptional downregulation induced by bDMC can be ascribed to reduced NF-Y and, consequently, Sp1 levels.

In addition to the identification of TOP2A as one of the molecular targets of bDMC, our data highlight that NF-Y regulation can be an interesting approach in anti-cancer therapy, taking into consideration that (i) NF-Y is one of the transcription factors orchestrating oncogenic transcriptional changes,[58,59] and (ii) clinical studies correlated upregulated expression of NF-Y target genes to poor clinical prognosis in multiple types of cancer.[60]

## Materials and Methods

**Cell lines and treatments.** Human colorectal carcinoma HCT116 cells were cultured in Iscove's Modified Dulbecco's Medium (IMDM) supplemented with 10% fetal calf serum (FCS). Human hepatic fetal epithelial WRL-68 cells and colon adenocarcinoma LOVO cells were maintained in Dulbecco's Modified Eagle Medium (DMEM) with 10% FCS. Primary human fibroblasts (HF) were grown in DMEM 10% FCS, with Glutamine (2 mM) and Gentamicin (55 mg/l). Doubling time has been estimated of about 16 h for HCT116, LOVO and WRL68 cells, and 24 h for HF cells.

bDMC (1,7-bis[4-hydroxyphenyl]hepta-1,6-diene-3,5-dione) has been synthesized as previously reported[36] and added to warm medium at the indicated concentrations. DMSO (Sigma-Aldrich Srl, Milan, Italy) was used as control. For pharmacological inhibitions, cells were pre-treated for 1 h and then co-incubated with bDMC for the indicated times with 25 $\mu$M Z-VAD-fmk (Enzo Life Sciences, Inc., Farmingdale, NY, USA), 10 $\mu$M WORT (Enzo Life Sciences, Inc.), 1 $\mu$M MG132 (Sigma-Aldrich Srl), 20 mM NAC (Sigma-Aldrich Srl) and 10 ng/ml LMB (Enzo Life Sciences, Inc.).

**Crystal Violet assay.** The inhibition of proliferation was measured by Crystal Violet staining, and the concentration at which cellular growth is inhibited by 50% (IC50) was determined following 24 h treatment with bDMC, as previously reported.[54] Briefly, the cell monolayer was fixed with methanol and stained with 0.05% Crystal Violet solution in 20% methanol for 1 h. After washes, cells were allowed to dry. The incorporated dye was solubilized in acidic isopropanol and determined spectrophotometrically at 540 nm wavelength. The extracted dye was proportional to cell number.

**Flow cytometric analysis.** Cells were harvested after drug treatments at the indicated time points and DNA distribution analysis of propidium iodide (PI)-stained cells was performed by an Epics cytofluorimeter (Beckman Coulter Srl, Milan, Italy).[36] Apoptotic cells were detected by FACS using Annexin V-PE conjugate (BD Biosciences, Becton Dickinson Italia, Milan, Italy) following the protocol of the manufacturer.

Indirect immunofluorescence staining was performed as previously described.[57] Briefly, harvested cells were washed with PBS 1X, fixed in 1% formaldehyde for 10 min at 37 °C and post-fixed with 90% ethanol. After permeabilization with 0.25% Triton X-100 in PBS 1X for 5 min, cells were stained with anti-phospho-H2AX Ser139 (No. 05-636, Millipore Spa, Vimodrone, Italy; 1 : 25) o.n. at 4 °C and with rabbit anti-mouse FITC-conjugated secondary antibody (No. 0313, Dako Italia Spa, Milan, Italy; 1 : 50) for additional 2 h at 4 °C. Following RNAse A treatment for 40 min, cells were incubated with PI (30 mg/ml) for 30 min at 4 °C and analyzed by an Epics cytofluorimeter (Beckman Coulter Srl).

**Chromosome spreads.** DMSO- and bDMC-treated cells were collected, swollen in hypotonic solution (75 mM KCl) and incubated for 10 min at room temperature. After two washes in Fix solution (3 : 1(vol/vol) methanol:acetic acid), the cellular suspension was dropped on a wet ice-cold slide and stained for 15 min in Giemsa stain (No. 32884, Sigma-Aldrich Srl). Slides were washed in distilled water, air-dried and mounted with DPX mountant (No. 44581, Sigma-Aldrich Srl). Chromosomes were analyzed with a Nikon Eclipse 90i microscope (Nikon Instruments Spa, Florence, Italy).

**Immunoblotting.** Whole-cell protein extracts were prepared by resuspending cells into 1X SDS sample buffer (25 mM Tris–HCl pH 6.8, 1.5 mM EDTA, 20% glycerol, 2% SDS, 5% β-mercaptoethenol, 0.0025% Bromophenol blue). Nuclear and cytoplasmic extracts were obtained by resuspending cells in 200 $\mu$l of Solution A (10 mM HEPES pH7.9, 10 mM KCl, 1.5 mM MgCl2, 0.34 M sucrose, 10% glycerol, protease and phosphatase inhibitors), adding 0.1% Triton X-100 and incubating cells for 10 min on ice. The supernatant containing cytoplasmic proteins was collected by centrifugation at 1300 $\times$ *g* for 5 min at 4 °C, and the remaining pellet (nuclei) was disrupted in 1X SDS sample buffer (as above). Chromatin-enriched extracts were prepared as previously described.[57] For immunoblotting, equivalent amounts of cellular extracts were resolved by SDS-PAGE, electro-transferred to PVDF membrane (GE Healthcare Italia, Milan, Italy) and immunoblotted. The following primary antibodies were used: anti-NF-YB and anti-NF-YC purified rabbit polyclonal antibodies; anti-phospo-H2AX (sc-101696), anti-H3 (C16) (sc-8654), anti-p53 (DO1) (sc-126), anti-TOP2A (K19) (sc-5347), anti-PARP1 (F2) (sc-8007), anti-NF-YA (sc-10779), anti-Sp1 (sc-420 X) and anti-actin (I19) (sc-1616) from Santa Cruz Biotecnology, Inc. (Dallas, TX, USA); anti-phospho-ATM Ser1981 (No. 4526), anti-phospho-BRCA1 Ser1524 (No. 9009), anti-phospho-Chk1 Ser296 (No. 2349) from Cell Signaling Technology, Inc. (Danvers, MA, USA); and anti-α-tubulin (T6074) from Sigma-Aldrich Srl. Chemiluminescent detection reagent has been purchased from Millipore Spa (Luminata Classico and Forte Western HRP).

**Immuno-band depletion assay.** Briefly, $6 \times 10^5$ cells were lysed in 50 $\mu$l of alkaline lysis solution (200 mMNaOH, 2 mM EDTA), and the lysate was neutralized by 8 $\mu$l of neutralization buffer (1 M HCl, 600 mM Tris pH 8.0). The neutralized lysate was mixed with 6.6 $\mu$l of 10 $\times$ MNase reaction buffer (50 mM $MgCl_2$, 50 mM $CaCl_2$, 5 mM DTT, 1 mM EDTA, 1 mM PMSF, protease inhibitors) and incubated or not with 60 units of MNase. After 20 min digestion, 60 $\mu$l of 2 $\times$ SDS sample buffer were added to each sample, and the lysates were separated on 8% SDS-PAGE gels and immunoblotted.

**TOP2 decatenation assay.** TOP2 activity was assayed *in vitro* through the Topoisomerse II assay kit (No. TG1001, TopoGEN Inc., Port Orange, FL, USA), following the instructions of the manufacturer. Nuclear extracts containing TOP2 activity were obtained from HCT116 cells following the suggestions of the manufacturer, and the ability to decatenate kDNA was analyzed in the presence of DMSO and bDMC. Briefly, decatenation assay was performed with 50 ng kDNA in a 10-$\mu$l reaction mixture containing 50 mM Tris–HCl (pH 8.0), 150 mM NaCl, 10 mM MgCl2, 0.5 mM dithiothreitol, 2 mM ATP, 30 $\mu$g/ml BSA with DMSO or 30, 60, 120 $\mu$M of bDMC and 0.5 $\mu$g of cell nuclear extract. Reactions were incubated at 37 °C for 30 min and stopped by adding 5 $\mu$l of stop buffer (5% Sarkosyl,

0.125% bromphenol blue and 25% glycerol). Samples were loaded directly onto a 1% agarose gel containing ethidium bromide (0.5 $\mu$g/ml). TOP2 activity was measured by the appearance of decatenated minicircular products and determined as the percentage of DMSO by ImageJ software (Image J, U.S. National Institutes of Health, Bethesda, MD, USA).

**RT-PCR.** RNA was extracted from cells treated with DMSO and bDMC using the Purelink RNA mini kit (Invitrogen, Life Technologies Italia, Monza, Italy) according to the manufacturer's protocol, and 3 $\mu$g of RNA were retro-transcribed with a Moloney murine leukemia virus reverse transcriptase (Promega Italia SrL, Milan, Italy). Semi-quantitative and quantitative real-time PCRs were performed with oligonucleotides designed to amplify the cDNA of: GAPDH (forward 5′-ACAGTCAGCCGCATCTTCTT-3′; reverse 5′-GCCCAATACGACCAAATCC-3′), TOP2A (forward 5′-TGGCAGAGGCAGAGAGAGTT-3′; reverse 5′-TCAAAAAG CACCATAGAGTTGC-3′) and p21 (forward: 5′-TGACCCTGAAGTGAGCACAG-3′; reverse: 5′-GGGAAAAGGCTCAACACTGA-3′). Semi-quantitative PCR results were analyzed by ImageJ software, whereas relative fold change enrichments of real-time PCR samples were calculated with the formula $2^{-(\Delta\Delta Ct)}$, where $-(\Delta\Delta Ct) = -((Ct_{target} - Ct_{GAPDH})_{bDMC} - (Ct_{target} - Ct_{GAPDH})_{DMSO})$.

**siRNA transfection.** HCT116 cells were transfected (Metafectene SI$^+$, Biontex Laboratories GmbH, Martinsried/Planegg, Germany) with 300 nM of paired TOP2A and non-targeting control siRNAs obtained from Sigma-Aldrich Srl. TOP2A sense strand sequence: 5′-AAGACTGTCTGTTGAAAGAA-3′. Cells were analyzed or treated with bDMC 36 h after transfection.

**ChIPs.** ChIPs were performed as previously described.[54] In all, 4 $\mu$g of the following antibodies were added to each IP and incubated overnight at 4 °C on a rotating wheel: anti-H3Ac (No. 06-599, Millipore Spa), anti-H4Ac (No. 06-866, Millipore Spa), anti-H3K4me3 (No. ab8580, AbCam, Cambridge, UK), anti-NF-YA (No. sc-10779, Santa Cruz), anti-NF-YB purified polyclonal antibody and anti-FLAG (No. F7425, Sigma-Aldrich Srl), used as control for non-specific interactions. DNAs were resuspended in TE buffer, and PCR analyses were performed with the following primers: p21 (forward: 5′-GTAAATCCTTGCCTGCCAGAGTG-3′; reverse: 5′-GCTGCCCAGCGCCGAGCCAG-3′) and TOP2A (forward: 5′-CGTCA GAACAGAGGACAGTTTTT-3′; reverse 5′-TGGAAGAGATGGGCTTTGG-3′). Semi-quantitative PCR results were analyzed by ImageJ software. Relative fold change enrichments of real-time quantitative PCR samples were calculated with the formula $2^{-(\Delta\Delta Ct)}$, where $-\Delta\Delta Ct = -((Ct_{sample} - Ct_{input})_{bDMC} - (Ct_{sample} - Ct_{input})_{DMSO})$.

## Conflict of Interest

The authors declare no conflict of interest.

**Acknowledgements**. This work was supported by the Associazione Italiana per la Ricerca sul Cancro to CI (MFAG No. 6192) and Fondazione di Vignola to CI and EF. PB is the recipient of a fellowship from the Fondazione Italiana per la Ricerca sul Cancro (FIRC). We thank Fondazione Cassa di Risparmio di Modena.

1. Yang X, Li W, Prescott ED, Burden SJ, Wang JC. DNA topoisomerase IIbeta and neural development. *Science* 2000; **287**: 131–134.
2. Khelifa T, Casabianca-Pignede MR, Rene B, Jacquemin-Sablon A. Expression of topoisomerases II alpha and beta in Chinese hamster lung cells resistant to topoisomerase II inhibitors. *Mol Pharmacol* 1994; **46**: 323–328.
3. Laemmli UK, Kas E, Poljak L, Adachi Y. Scaffold-associated regions: cis-acting determinants of chromatin structural loops and functional domains. *Curr Opin Genet Dev* 1992; **2**: 275–285.
4. Warburton PE, Earnshaw WC. Untangling the role of DNA topoisomerase II in mitotic chromosome structure and function. *Bioessays* 1997; **19**: 97–99.
5. Akimitsu N, Adachi N, Hirai H, Hossain MS, Hamamoto H, Kobayashi M *et al.* Enforced cytokinesis without complete nuclear division in embryonic cells depleting the activity of DNA topoisomerase IIalpha. *Genes Cells* 2003; **8**: 393–402.
6. Heck MM, Hittelman WN, Earnshaw WC. Differential expression of DNA topoisomerases I and II during the eukaryotic cell cycle. *Proc Natl Acad Sci USA* 1988; **85**: 1086–1090.
7. Woessner RD, Mattern MR, Mirabelli CK, Johnson RK, Drake FH. Proliferation- and cell cycle-dependent differences in expression of the 170 kilodalton and 180 kilodalton forms of topoisomerase II in NIH-3T3 cells. *Cell Growth Differ* 1991; **2**: 209–214.
8. Negri C, Chiesa R, Cerino A, Bestagno M, Sala C, Zini N *et al.* Monoclonal antibodies to human DNA topoisomerase I and the two isoforms of DNA topoisomerase II: 170- and 180-kDa isozymes. *Exp Cell Res* 1992; **200**: 452–459.
9. Hochhauser D, Stanway CA, Harris AL, Hickson ID. Cloning and characterization of the 5′-flanking region of the human topoisomerase II alpha gene. *J Biol Chem* 1992; **267**: 18961–18965.
10. Adachi N, Nomoto M, Kohno K, Koyama H. Cell-cycle regulation of the DNA topoisomerase IIalpha promoter is mediated by proximal CCAAT boxes: possible involvement of acetylation. *Gene* 2000; **245**: 49–57.
11. Falck J, Jensen PB, Sehested M. Evidence for repressional role of an inverted CCAAT box in cell cycle-dependent transcription of the human DNA topoisomerase IIalpha gene. *J Biol Chem* 1999; **274**: 18753–18758.
12. Yoon JH, Kim JK, Rha GB, Oh M, Park SH, Seong RH *et al.* Sp1 mediates cell proliferation-dependent regulation of rat DNA topoisomerase IIalpha gene promoter. *Biochem J* 1999; **344**(Pt 2): 367–374.
13. Mantovani R. The molecular biology of the CCAAT-binding factor NF-Y. *Gene* 1999; **239**: 15–27.
14. Isaacs RJ, Harris AL, Hickson ID. Regulation of the human topoisomerase IIalpha gene promoter in confluence-arrested cells. *J Biol Chem* 1996; **271**: 16741–16747.
15. Joshi AA, Wu Z, Reed RF, Suttle DP. Nuclear factor-Y binding to the topoisomerase IIalpha promoter is inhibited by both the p53 tumor suppressor and anticancer drugs. *Mol Pharmacol* 2003; **63**: 359–367.
16. Wang Q, Zambetti GP, Suttle DP. Inhibition of DNA topoisomerase II alpha gene expression by the p53 tumor suppressor. *Mol Cell Biol* 1997; **17**: 389–397.
17. Turley H, Comley M, Houlbrook S, Nozaki N, Kikuchi A, Hickson ID *et al.* The distribution and expression of the two isoforms of DNA topoisomerase II in normal and neoplastic human tissues. *Br J Cancer* 1997; **75**: 1340–1346.
18. Nitiss JL. Targeting DNA topoisomerase II in cancer chemotherapy. *Nat Rev Cancer* 2009; **9**: 338–350.
19. McClendon AK, Osheroff N. DNA topoisomerase II, genotoxicity, and cancer. *Mutat Res* 2007; **623**: 83–97.
20. Kaufmann SH. Cell death induced by topoisomerase-targeted drugs: more questions than answers. *Biochim Biophys Acta* 1998; **1400**: 195–211.
21. Limbo O, Chahwan C, Yamada Y, de Bruin RA, Wittenberg C, Russell P. Ctp1 is a cell-cycle-regulated protein that functions with Mre11 complex to control double-strand break repair by homologous recombination. *Mol Cell* 2007; **28**: 134–146.
22. Mao Y, Desai SD, Ting CY, Hwang J, Liu LF. 26 S proteasome-mediated degradation of topoisomerase II cleavable complexes. *J Biol Chem* 2001; **276**: 40652–40658.
23. Sartori AA, Lukas C, Coates J, Mistrik M, Fu S, Bartek J *et al.* Human CtIP promotes DNA end resection. *Nature* 2007; **450**: 509–514.
24. Felix CA. Secondary leukemias induced by topoisomerase-targeted drugs. *Biochim Biophys Acta* 1998; **1400**: 233–255.
25. Mistry AR, Felix CA, Whitmarsh RJ, Mason A, Reiter A, Cassinat B *et al.* DNA topoisomerase II in therapy-related acute promyelocytic leukemia. *N Engl J Med* 2005; **352**: 1529–1538.
26. Myers CE, McGuire WP, Liss RH, Ifrim I, Grotzinger K, Young RC. Adriamycin: the role of lipid peroxidation in cardiac toxicity and tumor response. *Science* 1977; **197**: 165–167.
27. Velez JM, Miriyala S, Nithipongvanitch R, Noel T, Plabplueng CD, Oberley T *et al.* p53 Regulates oxidative stress-mediated retrograde signaling: a novel mechanism for chemotherapy-induced cardiac injury. *PLoS One* 2011; **6**: e18005.
28. Chauhan DP. Chemotherapeutic potential of curcumin for colorectal cancer. *Curr Pharm Des* 2002; **8**: 1695–1706.
29. Jiang MC, Yang-Yen HF, Yen JJ, Lin JK. Curcumin induces apoptosis in immortalized NIH 3T3 and malignant cancer cell lines. *Nutr Cancer* 1996; **26**: 111–120.
30. Song G, Mao YB, Cai QF, Yao LM, Ouyang GL, Bao SD. Curcumin induces human HT-29 colon adenocarcinoma cell apoptosis by activating p53 and regulating apoptosis-related protein expression. *Braz J Med Biol Res* 2005; **38**: 1791–1798.
31. Martin-Cordero C, Lopez-Lazaro M, Galvez M, Ayuso MJ. Curcumin as a DNA topoisomerase II poison. *J Enzyme Inhib Med Chem* 2003; **18**: 505–509.
32. Lopez-Lazaro M, Willmore E, Jobson A, Gilroy KL, Curtis H, Padget K *et al.* Curcumin induces high levels of topoisomerase I- and II-DNA complexes in K562 leukemia cells. *J Nat Prod* 2007; **70**: 1884–1888.
33. Magalska A, Brzezinska A, Bielak-Zmijewska A, Piwocka K, Mosieniak G, Sikora E. Curcumin induces cell death without oligonucleosomal DNA fragmentation in quiescent and proliferating human CD8+ cells. *Acta Biochim Pol* 2006; **53**: 531–538.
34. Korwek Z, Bielak-Zmijewska A, Mosieniak G, Alster O, Moreno-Villanueva M, Burkle A *et al.* DNA damage-independent apoptosis induced by curcumin in normal resting human T cells and leukaemic Jurkat cells. *Mutagenesis* 2013; **28**: 411–416.
35. Bielak-Zmijewska A, Sikora-Polaczek M, Nieznanski K, Mosieniak G, Kolano A, Maleszewski M *et al.* Curcumin disrupts meiotic and mitotic divisions via spindle impairment and inhibition of CDK1 activity. *Cell Prolif* 2010; **43**: 354–364.
36. Basile V, Ferrari E, Lazzari S, Belluti S, Pignedoli F, Imbriano C. Curcumin derivatives: molecular basis of their anti-cancer activity. *Biochem Pharmacol* 2009; **78**: 1305–1315.
37. Yodkeeree S, Chaiwangyen W, Garbisa S, Limtrakul P. Curcumin, demethoxycurcumin and bisdemethoxycurcumin differentially inhibit cancer cell invasion through the down-regulation of MMPs and uPA. *J Nutr Biochem* 2009; **20**: 87–95.

38. Anand P, Thomas SG, Kunnumakkara AB, Sundaram C, Harikumar KB, Sung B *et al.* Biological activities of curcumin and its analogues (Congeners) made by man and Mother Nature. *Biochem Pharmacol* 2008; **76**: 1590–1611.
39. Paull TT, Rogakou EP, Yamazaki V, Kirchgessner CU, Gellert M, Bonner WM. A critical role for histone H2AX in recruitment of repair factors to nuclear foci after DNA damage. *Curr Biol* 2000; **10**: 886–895.
40. Bakkenist CJ, Kastan MB. Initiating cellular stress responses. *Cell* 2004; **118**: 9–17.
41. Shiloh Y. ATM and related protein kinases: safeguarding genome integrity. *Nat Rev Cancer* 2003; **3**: 155–168.
42. Asaad NA, Zeng ZC, Guan J, Thacker J, Iliakis G. Homologous recombination as a potential target for caffeine radiosensitization in mammalian cells: reduced caffeine radiosensitization in XRCC2 and XRCC3 mutants. *Oncogene* 2000; **19**: 5788–5800.
43. Block WD, Merkle D, Meek K, Lees-Miller SP. Selective inhibition of the DNA-dependent protein kinase (DNA-PK) by the radiosensitizing agent caffeine. *Nucleic Acids Res* 2004; **32**: 1967–1972.
44. Deplanque G, Ceraline J, Mah-Becherel MC, Cazenave JP, Bergerat JP, Klein-Soyer C. Caffeine and the G2/M block override: a concept resulting from a misleading cell kinetic delay, independent of functional p53. *Int J Cancer* 2001; **94**: 363–369.
45. Kesharwani KR, Misra K. Prediction of binding site for curcuminoids at human toposomerase II a protein; an in silico approach. *Curr Sci* 2011; **101**: 1060–1065.
46. Agostinho M, Rino J, Braga J, Ferreira F, Steffensen S, Ferreira J. Human topoisomerase IIalpha: targeting to subchromosomal sites of activity during interphase and mitosis. *Mol Biol Cell* 2004; **15**: 2388–2400.
47. Ceribelli M, Dolfini D, Merico D, Gatta R, Vigano AM, Pavesi G *et al.* The histone-like NF-Y is a bifunctional transcription factor. *Mol Cell Biol* 2008; **28**: 2047–2058.
48. Fossati A, Dolfini D, Donati G, Mantovani R. NF-Y recruits Ash2L to impart H3K4 trimethylation on CCAAT promoters. *PLoS One* 2011; **6**: e17220.
49. Frontini M, Imbriano C, Manni I, Mantovani R. Cell cycle regulation of NF-YC nuclear localization. *Cell Cycle* 2004; **3**: 217–222.
50. Magan N, Szremska AP, Isaacs RJ, Stowell KM. Modulation of DNA topoisomerase II alpha promoter activity by members of the Sp (specificity protein) and NF-Y (nuclear factor Y) families of transcription factors. *Biochem J* 2003; **374**(Pt 3): 723–729.
51. Romero A, Martin M, Cheang MC, Lopez Garcia-Asenjo JA, Oliva B, He X *et al.* Assessment of Topoisomerase II alpha status in breast cancer by quantitative PCR, gene expression microarrays, immunohistochemistry, and fluorescence in situ hybridization. *Am J Pathol* 2011; **178**: 1453–1460.
52. Zaczek AJ, Markiewicz A, Seroczynska B, Skokowski J, Jaskiewicz J, Pienkowski T *et al.* Prognostic significance of TOP2A gene dosage in HER-2-negative breast cancer. *Oncologist* 2012; **17**: 1246–1255.
53. Miettinen HE, Jarvinen TA, Kellner U, Kauraniemi P, Parwaresch R, Rantala I *et al.* High topoisomerase IIalpha expression associates with high proliferation rate and and poor prognosis in oligodendrogliomas. *Neuropathol Appl Neurobiol* 2000; **26**: 504–512.
54. Basile V, Belluti S, Ferrari E, Gozzoli C, Ganassi S, Quaglino D *et al.* bis-dehydroxy-curcumin triggers mitochondrial-associated cell death in human colon cancer cells through ER-stress induced autophagy. *PLoS One* 2013; **8**: e53664.
55. Ravindran J, Prasad S, Aggarwal BB. Curcumin and cancer cells: how many ways can curry kill tumor cells selectively? *AAPS J* 2009; **11**: 495–510.
56. Hajji N, Pastor N, Mateos S, Dominguez I, Cortes F. DNA strand breaks induced by the anti-topoisomerase II bis-dioxopiperazine ICRF-193. *Mutat Res* 2003; **530**: 35–46.
57. Benatti P, Dolfini D, Vigano A, Ravo M, Weisz A, Imbriano C. Specific inhibition of NF-Y subunits triggers different cell proliferation defects. *Nucleic Acids Res* 2011; **39**: 5356–5368.
58. Goodarzi H, Elemento O, Tavazoie S. Revealing global regulatory perturbations across human cancers. *Mol Cell* 2009; **36**: 900–911.
59. Rhodes DR, Kalyana-Sundaram S, Mahavisno V, Barrette TR, Ghosh D, Chinnaiyan AM. Mining for regulatory programs in the cancer transcriptome. *Nat Genet* 2005; **37**: 579–583.
60. Yamanaka K, Mizuarai S, Eguchi T, Itadani H, Hirai H, Kotani H. Expression levels of NF-Y target genes changed by CDKN1B correlate with clinical prognosis in multiple cancers. *Genomics* 2009; **94**: 219–227.



Supplementary Information accompanies this paper on Cell Death and Disease website (http://www.nature.com/cddis)

OPEN ACCESS Freely available online

PLOS ONE

# bis-Dehydroxy-Curcumin Triggers Mitochondrial-Associated Cell Death in Human Colon Cancer Cells through ER-Stress Induced Autophagy

**Valentina Basile[1], Silvia Belluti[1], Erika Ferrari[2], Chiara Gozzoli[1], Sonia Ganassi[1], Daniela Quaglino[1], Monica Saladini[2], Carol Imbriano[1]***

**1** Dipartimento di Scienze della Vita, Università di Modena e Reggio Emilia, via Campi 213/D, Modena, Italy, **2** Dipartimento di Scienze Chimiche e Geologiche, Università di Modena e Reggio Emilia, via Campi 183, Modena, Italy

## Abstract

***Background:*** The activation of autophagy has been extensively described as a pro-survival strategy, which helps to keep cells alive following deprivation of nutrients/growth factors and other stressful cellular conditions. In addition to cytoprotective effects, autophagy can accompany cell death. Autophagic vacuoles can be observed before or during cell death, but the role of autophagy in the death process is still controversial. A complex interplay between autophagy and apoptosis has come to light, taking into account that numerous genes, such as p53 and Bcl-2 family members, are shared between these two pathways.

***Methodology/Principal Findings:*** In this study we showed a potent and irreversible cytotoxic activity of the stable Curcumin derivative *bis*-DeHydroxyCurcumin (bDHC) on human colon cancer cells, but not on human normal cells. Autophagy is elicited by bDHC before cell death as demonstrated by increased autophagosome formation -measured by electron microscopy, fluorescent LC3 puncta and LC3 lipidation- and autophagic flux -measured by interfering LC3-II turnover. The accumulation of poly-ubiquitinated proteins and ER-stress occurred upstream of autophagy induction and resulted in cell death. Cell cycle and Western blot analyses highlighted the activation of a mitochondrial-dependent apoptosis, which involves caspase 7, 8, 9 and Cytochrome C release. Using pharmacological inhibitions and RNAi experiments, we showed that ER-stress induced autophagy has a major role in triggering bDHC-cell death.

***Conclusion/Significance:*** Our findings describe the mechanism through which bDHC promotes tumor selective inhibition of proliferation, providing unequivocal evidence of the role of autophagy in contrasting the proliferation of colon cancer cells.

**Citation:** Basile V, Belluti S, Ferrari E, Gozzoli C, Ganassi S, et al. (2013) bis-Dehydroxy-Curcumin Triggers Mitochondrial-Associated Cell Death in Human Colon Cancer Cells through ER-Stress Induced Autophagy. PLoS ONE 8(1): e53664. doi:10.1371/journal.pone.0053664

**Editor:** Regine Schneider-Stock, Institute of Pathology, Germany

**Received** June 12, 2012; **Accepted** December 3, 2012; **Published** January 11, 2013



**Funding:** This work was supported by Associazione Italiana per la Ricerca sul Cancro-MFAG (grant number 6192 to CI) and Fondazione Cassa di Risparmio di Vignola to CI and EF. The funders had no role in study design, data collection and analysis, decision to publish, or preparation of the manuscript.

**Competing Interests:** The authors have declared that no competing interests exist.

* E-mail: cimbriano@unimo.it

## Introduction

Apoptosis, also known as type I cell death, is the best described mechanism of cell death and is morphologically characterized by cell shrinkage, membrane blebbing, nuclear condensation, and formation of apoptotic bodies [1]. An energy-dependent cascade of molecular events coordinates the apoptotic process, which can be distinguished into two main pathways: the extrinsic death receptor pathway and the intrinsic mitochondrial pathway. The two pathways seem to be linked and influenced one another, and both trigger the activation of caspases 3, 6 and 7, proteases targeting hundred proteins and leading to cell demolition [2].

Besides apoptosis, autophagy has been described as an alternative self-destructive cellular process. Autophagy has been long known to provide cellular survival following nutrients/growth factors deprivation or other stressful conditions, and only more recently it has been linked to cell death. Also known as type II cell death, autophagy activation is characterized by the presence of autophagic vacuoles in the cytoplasm, and enlargement of the endoplasmic reticulum (ER) and the Golgi apparatus [3]. Double-membraned autophagic vesicles encapsulate cytoplasm and organelles and, after their fusion with lysosomes, autophagolysosomes degrade their contents [4]. The classic autophagy pathway acts downstream of the mTOR (mammalian target of rapamycin) kinase. When this Ser/Thr kinase is associated in mTORC1 protein complex, it is able to suppress the autophagic machinery. 16 autophagy-related (ATG) proteins have been described to participate to the autophagy pathway [5], and the majority of them play a role in the complex process of double-membraned vesicles formation and growth, downstream of mTORC1 [6]. Although the inhibition of mTORC1 pathway is the best known mechanism through which autophagy is induced, many other signaling cascades and transcriptional events can be involved in the activation of the autophagic process. In particular, various

kinases control different steps of this catabolic process, such as AMP-activated protein kinase, Akt, mitogen-activated protein kinase (ERK, p38 and JNK) and protein kinase C [7].

The role of autophagy in cell survival rather than cell death is dependent on cell and tissue context as well as on the nature of the stress stimulus [8].

Apoptotic and autophagic cell death are not mutually exclusive pathways: they can induce cell death simultaneously and cooperatively (for a review see [9]). Autophagic morphologies of cells are observed shortly before or during cell death; although, whether autophagy is the mechanism by which cells actually die and whether cell death is executed by autophagy or with autophagy is still discussed [10].

The distinction between apoptotic and autophagic cell death is even more complicated by two considerations: i) various cellular stresses triggering signal transduction pathways can elicit both apoptosis and autophagy and ii) many proteins essential for autophagy are also involved in apoptotic-cell death, such as ATG5, the transcription factor p53 and the Bcl-2 family members.

p53 is a well known oncosuppressor, activated following a variety of stress stimuli, and responsible for transcriptional regulation of both pro- and anti-apoptotic genes. While the pro-apoptotic genes, such as Bax, Puma and Noxa are up-regulated, the anti-apoptotic ones, as Bcl-2α, are down-regulated by nuclear p53. Also cytoplasmically localized p53 has been shown to be important in controlling the apoptotic response, by inducing Bax oligomerization at the mitochondria or by releasing the pro-apoptotic BH3-only proteins from their anti-apoptotic partners Bcl-2/Bcl-XL [11].

The role of p53 in tumor suppression has been also ascribed to its activity in regulating autophagy. p53-mediated activation of autophagy leads to cell death through transactivation of the autophagy-inducing protein DRAM and inactivation of the mTOR pathway [12,13]. In opposition, pharmacological inhibition and inactivation of p53 suggest a negative regulation of autophagy through transcription-independent mechanisms [14].

In addition to p53, the Bcl-2 family members are common players of apoptosis and autophagy. They are central to the regulation of the outer mitochondrial membrane permeabilization (MMP), which is responsible for the release into the cytoplasm of proteins mediating cell death, such as Cytochrome C. Bcl-2 proteins have been shown to inhibit autophagy by disrupting the Bcl-2/Bcl-XL-Beclin-1 complexes [15]. It is not clear how Bcl-2 proteins participate to the apoptotic *versus* the autophagic process, but the two different functions could be determined by protein localizations at the mitochondria rather than ER [16]. Relative levels of Bcl-2 and Beclin-1 emerged among the multiple cellular factors controlling whether autophagy contributes to cancer inhibition or survival (reviewed in [17]).

Various natural products and drugs are able to induce cancer cell death through the activation of autophagy or by targeting the pathways of autophagy [18]. Tamoxifen, Imatinib, Resveratrol and Curcumin are examples of molecules exerting their cytotoxic activity towards cancer cells *via* induction of autophagic cell death [17,18].

Curcumin, the active component found in the rhizome of *Curcuma longa*, has shown therapeutic activity against various tumors. It can inhibit the initiation, progression and tumor cell survival [19]. In particular, mouse models and human clinical trials demonstrated its chemopreventive potential for colorectal cancer [19]. In colorectal carcinoma cell lines, Curcumin inhibits cell proliferation by inducing a G2/M cell cycle arrest or apoptosis when used at high doses [20,21]. Moreover, the modulation of cellular apoptotic pathways by Curcumin has been recently observed on cancer cells of patients with colorectal cancer [22].

Microarray studies showed that Curcumin-induced apoptosis is regulated by multiple signaling pathways [23,24]. Curcumin up-regulates the pro-apoptotic proteins (Bax, Bim, Bak, Puma and Noxa) and down-regulates the anti-apoptotic ones (Bcl-2 and Bcl-XL) in different cancer cells, triggering the release of Cytochrome C and the activation of caspase 3 [24]. In human melanoma, HL-60 leukemia and gastric cells, Curcumin activates apoptosis through the Fas receptor/caspase 8 pathway [25,26,27]. In addition to the apoptotic activity, Curcumin induces ER stress in various human tumor cells, among which liposarcoma cells [28], non small cell lung cancer cells [29] and leukemia cells [30].

The autophagy process takes part to the anti-proliferative and apoptotic activities of Curcumin, both *in vitro* and *in vivo*: in cancer cells and in a xenograft mouse model, Curcumin and its metabolite Tetrahydrocurcumin inhibit the growth of malignant cells by activating autophagic-cell death *via* Akt/mTOR/p70S6K signaling and ERK1/2 pathways [31,32,33]. In glioma initiating cells, Curcumin administration results in tumor suppression because of autophagy-induced differentiation events [34].

Despite Curcumin inhibition of key molecular pathways of tumorigenesis, clinical trials revealed low bioavailability, limited tissue distribution and rapid metabolism [35]. 90% of Curcumin decomposes rapidly in neutral and basic conditions through oxidation, reduction, glucuronidation and sulfation [28,29]. To overcome these limitations, natural and synthetic analogs have been synthesized, among which *bis*-DeHydroxyCurcumin (bDHC) (Fig. 1A, left panel). Cells administration of bDHC for 72 h at IC50 concentrations resulted in a slight decrease of anti-proliferative activity compared to Curcumin in androgen-dependent and-independent prostate cancer cell lines and in estrogen-dependent and –independent breast cancer cell lines [36,37].

In this report, we investigated the tumor-selective inhibitory efficacy of bDHC on the proliferation of human colorectal cancer cells. Compared to Curcumin, bDHC is more active in inducing an irreversible cytotoxic effect in HCT116 and LOVO cells, but not in human normal cells.

The accumulation of poly-ubiquitinated proteins and the induction of ER stress are upstream signals of autophagy, which triggers mitochondrial-dependent apoptosis. Pharmacological and RNAi-mediated inhibition of ER-stress and autophagy highlights that autophagy potentiates the anti-proliferative effect of bDHC. Our studies demonstrate that bDHC acts as a pro-autophagic cytotoxic drug, unraveling its therapeutic potential in fighting selectively tumor development.

## Materials and Methods

### Cell culture and drugs

Human colorectal carcinoma HCT116, HCT116/E6 and HCT116 Bax −/− were generously provided by Bert Vogelstein (Johns Hopkins University School of Medicine, Baltimore, MD). Cells were cultured in Iscove's Modified Dulbecco's Medium (IMDM), supplemented with 10% fetal calf serum (FCS). Primary human fibroblasts (HF) were grown in DMEM 10% FCS, with Glutamine (2 mM) and Gentamicin (55 mg/L). Hepatic fetal human epithelial WRL68 cells and colon adenocarcinoma LOVO cells were maintained in DMEM medium supplemented with 10% FCS. Doubling time has been estimated to be 16 hours for HCT116 and LOVO tumor cells, and 24 hours for HF and WRL68 normal cells.

Curcumin [1,7-bis[3-methoxy-4-hydroxy-phenyl]hepta-1,6-diene-3,5-dione] and bDHC [1,7-bis[3-methoxy-phenyl]hepta-1,6-

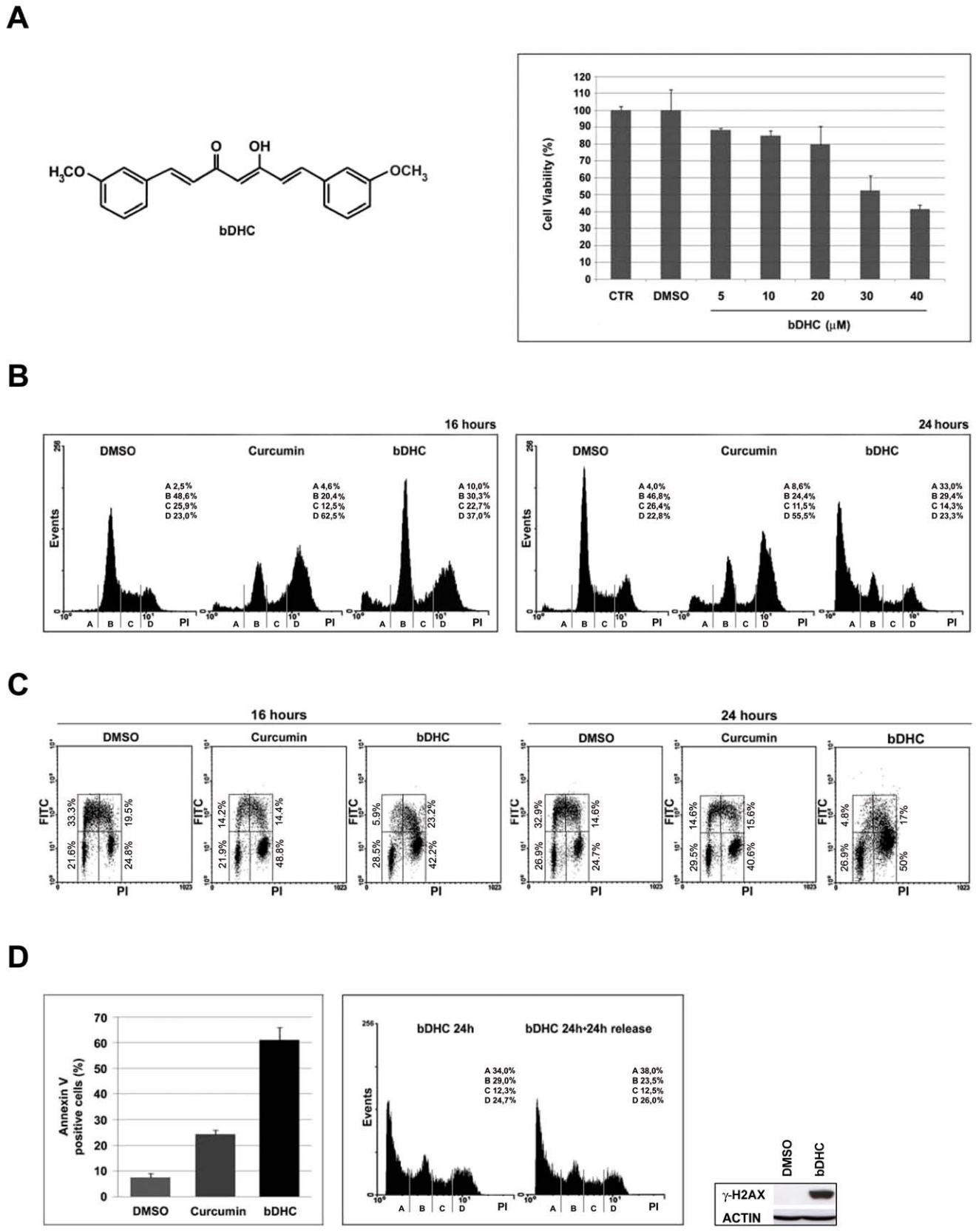


**Figure 1. bDHC induces cell cycle impairment and apoptosis in HCT116 cells. A.** Left panel: Structure of bDHC. Right panel: Dose-response effect of bDHC on cell viability upon 24 hours treatment, compared to control and DMSO-treated cells. **B.** PI/FACS analysis of cell cycle progression after DMSO, Curcumin (10 μM) and bDHC (30 μM) treatments for 16 and 24 hours (left and right panel, respectively). The indicated events are means of ten independent experiments (A = SubG1, B = G0/G1, C = S, D = G2/M). **C.** PI/BrdU bivariate FACS analysis of 16 and 24 hours treatments with

DMSO, Curcumin and bDHC. Analysis was gated to exclude SubG1 population. **D.** Left panel: The percentage of Annexin V positive cells upon 24 hours treatment with bDHC is compared to DMSO- and Curcumin-treated cells. Data are means of three independent experiments −/+ SD. Middle panel: PI/monoparametric cell cycle analysis of bDHC-treated cells *versus* bDHC-cells released for 24 hours in fresh medium. Events are indicated as means of three independent experiments (A = SubG1, B = G0/G1, C = S, D = G2/M). Right panel: γ-H2AX expression levels *versus* actin in cells treated with bDHC for 24 hours.
doi:10.1371/journal.pone.0053664.g001

diene-3,5-dione] were synthesised as previously reported [20]. The purity of synthesized compounds, determined by NMR techniques and combustion analysis, was >98%. Curcumin and bDHC were added to warm medium at 10 μM and 30 μM concentrations, respectively. C3-bDHC was administered to cells at 3 μM concentration. HCT116 cells were incubated with Adriamycin (1.3 μM) for 48 hours. For pharmacological inhibitions, cells were pre-treated for 1 hour and then co-incubated with bDHC for additional 16 or 24 hours with 25 μM ZVAD-fmk (Enzo Life Sciences), 5 μM LEVD-fmk (Enzo Life Sciences), 3 μM Wortmannin (Enzo Life Science), 2 μM Cycloheximide (Sigma Aldrich), 20 μM Chloroquine (Sigma Aldrich), 50 μM Salubrinal (Santa Cruz). Thapsigargin (Sigma Aldrich) was administered to cells for 36 hours at 1 μM concentration.

## Cytometric analysis (FACS)

Flow Cytometric cell cycle analysis was performed as previously described [20]. Indirect fluorescence staining was performed using anti-phospho-Histone H3 (Ser10) (Cell Signaling #9706) and mouse anti-FITC (Dako #F0313) antibodies. Cells were harvested after drug treatments, washed twice with PBS 1×, fixed in 1% formaldehyde for 10 min at 37°C, and post-fixed with 90% methanol o.n. at −20°C. After permeabilization with 0.25% Triton X-100 in PBS 1× for 5 min, cells were stained with primary antibody (1:25) o.n. at 4°C, and secondary antibody (1:50) for additional 2 hours at 4°C. Cells were then treated with RNAse A for 40 min, incubated with Propidium Iodide (30 μg/μl) for additional 30 min at 4°C in the dark and analyzed with cytometer.

Apoptotic cells were identified by FACS using Annexin V-FITC conjugate (Bender MedSystems) following the protocol of the manufacturer.

## Cellular uptake studies

bDHC was extracted from cells and culture medium as previously reported [20].

## Crystal Violet assay

The inhibition of proliferation was measured by Crystal Violet staining and the concentration at which cellular growth is inhibited by 50% (IC50) was determined following 24 hours treatment with bDHC. After removal of cell culture medium, the cell monolayer was fixed with methanol and stained with 0.05% Crystal Violet solution in 20% methanol for 30 min. After washes, cells were allowed to dry. The incorporated dye was solubilized in acidic isopropanol (1 N HCl: 2-propanol, 1:10) and determined spectrophotometrically at 540 nm wavelength. The extracted dye was proportional to cell number. Percentage of cytotoxicity was calculated by comparing the absorbance of treated to untreated cells.

## Acridine Orange staining

HCT116 cells were treated with DMSO and bDHC for 8 and 16 hours. After this, cells were incubated with Acridine Orange (1 μg/ml) for 15 min at 37°C, followed by visualization with a Zeiss AxioSkop 40 fluorescence microscope (Carl Zeiss, Germany).

## Intracellular ATP content

Determination of intracellular ATP content was performed by using ATP bioluminescence assay kit CLSII (Roche), following the manufacturer's protocol.

## Mitochondrial membrane potential

Mitochondrial membrane potential was measured by evaluating the binding of 3,3-Dihexyloxacarbocyanineiodide (DiOC6), a cationic dye that binds to mitochondria with intact membrane potential. Cells were labeled after DMSO or bDHC incubation for 16 and 24 hours with DiOC6 (4 nM) for 40 min at 37°C. Thereafter, cells were washed twice with PBS 1× and the fluorescence intensity was analyzed using Beckman Coulter cytometer.

## Immunoblotting

Cells were lysed in Laemmli sample buffer 1× for total cellular extracts. Nuclear/cytoplasmic extracts were prepared as reported in Ref. [38]. Western blot analysis was performed as previously described [20]. The following primary antibodies were used: anti-p53 DO-1 (Santa Cruz #sc-126), anti-phospo-H3 (Ser10) (Millipore #05-817), anti-H2A acid-patch (Active Motif), anti-p21 (Upstate), anti-actin (Santa-Cruz), anti-PARP1 (Santa Cruz # sc-8007), anti-γH2AX (Millipore, #05-636), anti-GADD153 (F168) (Santa Cruz # sc-575), anti-tubulin (Sigma-Aldrich), anti-cleaved caspases 3, 7, 8, 9 (Cell Signaling), anti-caspase 4 4B9 (Enzo Life Sciences), anti-Bax (N-20) (Santa Cruz #sc-493), anti-Bcl-2 (Santa Cruz #sc-509), anti-Bcl-XL (Santa Cruz #sc-8392), anti-LC3B (Sigma Aldrich #L7543), anti-Ub (Santa Cruz #sc-8017), anti-ATG7 (Sigma Aldrich #A2856), anti-Beclin 1 (Sigma Aldrich #B6061) and anti-H3 (C16) (Santa Cruz #sc-8654). Chemiluminescent detection reagent has been purchased from Millipore (Luminata Classico and Forte Western HRP).

## Isolation of cytosolic fraction by digitonin lysis method

2.000.000 HCT116 cells were washed twice in PBS 1× and then resuspended in digitonin lysis buffer (75 mM NaCl, 1 mM $NaH_2PO_4$, 8 mM $Na_2HPO_4$, 250 mM Sucrose, 190 mg/ml of digitonin, protease inhibitors). Each sample was incubated on ice for 5 minutes and then centrifugated at 15.000×g at 4°C for 30 minutes. The supernatants were collected and used for Western blotting by using anti-Cytochrome C antibody (Santa Cruz # sc-13560).

## Immunofluorescence

Immunofluorescence analysis was performed as previously described [20,39], using anti-p53 DO-1 (Santa Cruz #sc-126) and anti-LC3B (Sigma Aldrich #L7543) antibodies diluted 1:100 in PBS+BSA 1%. p53 cellular localization was examined with Zeiss AxioSkop 40 fluorescence microscope (Carl Zeiss, Jena, Germany), images collected with an AxioCam HRc camera and AxioVision version 3.1 software package. Staining of endogenous LC3B was analyzed by confocal microscopy (Leica DM IRE2).

### Plasmids and transient transfection

HCT116 were transiently transfected with Bcl-2, Bcl-XL or carrier plasmids with FuGENE (Promega). Human Bcl-2 and Bcl-XL expression vectors were kindly provided by M. Priault (CNRS IBGC UMR 5095, Bordeaux, France) [40]. Cells were recovered 48 hours after transfection for Western blot and cell cycle analysis.

### Small interfering RNA (siRNA)

HCT116 cells were transfected (Lipofectamine 2000, Invitrogen) with 200 nM of paired ATG7, BCN1 and non-targeting control small interfering RNAs (Sigma Aldrich), as described by Hoyer-Hansen et al. [41]. CHOP siRNA (HSC.RNAI.N004083.10.2 from IDT) was a kind gift of A. Pietrangelo (University of Modena and Reggio Emilia, Modena, Italy). Total extracts and FACS samples were prepared after 72 h upon siRNA transfection.

### RT-PCR analysis

RNA extraction, retrotranscription and semiquantitative PCRs were performed as previously described [42,43]. Actin and LC3B were amplified with the following oligonucleotides: $Actin_{For}$: 5′-GAGGCCCAGAGCAAGCGT-3′; $Actin_{Rev}$: 5′-GCTCGAAGTCCAGGGCGACG-3′; $LC3B_{For}$:5′-CCTGGAGAAAGAGTGGCATTT-3′; $LC3B_{Rev}$: 5′-GAAGGCAGAAGGGAGTGTGT-3′.

### Scanning electron microscopy (SEM)

Cells grown in monolayer on coverslips were fixed in 1.25% glutaraldehyde in PBS 1× for 30 min R.T. and washed in PBS 1× for three times. After dehydration in graded ethanol solutions, the specimens were critical-point dried with $CO_2$ using a Critical Point Dryer 010 Balzer, mounted on aluminium stubs, and sputter-coated with 10 nm gold-palladium in a Coating Unit E 500 (Polaron). Observations were performed by Philips XL-30 scanning electron microscope.

### Transmission Electron Microscopy analysis

Cells, scraped from Petri dishes, were centrifuged at 12000×g for 5′ at 10°C. The resulting pellets were fixed overnight with 2.5% glutaraldehyde (Agar Scientific, Stensted, UK) in Tyrode's buffer, post-fixed for 2 hours in 1% osmium tetroxide (Agar Scientific), dehydrated and embedded in TLV resin (TAAB, Aldermaston, UK). Semithin sections obtained through the whole thickness of pellets were stained with toluidine blue and observed with a Zeiss Axiophot light microscope (Oberkochen, Germany). Ultrathin sections were stained with uranyl acetate and lead citrate and observed with a Jeol 1200 EXII electron microscope (Jeol, Tokyo, Japan).

### Chromatin Immunoprecipitation (ChIP)

ChIPs were performed with chromatin from DMSO and bDHC treated cells for 24 hours as described in Martens *et al.* [44]. PCR oligonucleotides were previously reported [43].

### Statistical analysis

Results are shown as means of at least three independent experiments +/− SD. Statistical analysis was done using one-way ANOVA, followed by LSD test to determine whether there were differences between specific groups.

## Results

### Effects of bDHC on viability and cell cycle progression of HCT116 cells

Full dose-response experiments were performed in HCT116 cells to identify the ability of bDHC to suppress cell growth. bDHC cytotoxicity was assayed through Crystal Violet vital staining method and the 50% inhibitory concentration for cell growth (IC50) was estimated equal to 30 μM, following 24 hours of treatment (Fig. 1A, right panel).

The effect of bDHC on cell cycle progression was investigated by fluorescent-activated cell sorting (FACS) analysis (Fig. 1B). HCT116 cells were treated for 16 and 24 hours with bDHC and the distribution into cell cycle phases was compared to DMSO and Curcumin treated cells. As previously shown [20], Curcumin arrested cells in G2/M phase and halved the population in G0/G1 and S phase within 16 hours; no significant increase of SubG1 events was detected. Differently, bDHC accumulated cells not only in G2/M (from about 23% of control cells to 37% of treated cells) but also in SubG1 phase (from 2.5% to 10%). With prolonged exposure, SubG1 events slightly raised upon Curcumin (from 4% to 8.6%), while an evident increase was detectable with bDHC (from 4% to 33%).

A cell cycle profile was then created by performing PI/BrdU biparametric analysis and using selective gating excluding SubG1 population (Fig. 1C). As expected, Curcumin halved S phase population and doubled G2/M cells. As well as Curcumin, bDHC-treated cells showed a clear decrease of early S population (from about 33% to 5.9% and 4.8% after 16 and 24 hours, respectively) and an accumulation of G2/M events (from about 25% to about 42% and 50%, following 16 and 24 hours), while no significant changes in G0/G1 percentage were detected.

To discriminate between G2 and mitotic populations, the cells were dual probed with PI and a specific antibody against the mitotic marker phospho-histone H3Ser10 using flow cytometry (Fig. S1A). While about 90% of 4n cells were positive to phospho-histone H3Ser10 following Curcumin treatment, only about 2% were detected as mitotic population upon bDHC administration.

The comparison between monoparametric and biparametric analyses (Fig. 1B and Fig. 1C) highlighted that the main effect of bDHC treatment is a G2 block after 16 hours and cell death upon 24 hours.

Cytotoxic activity of bDHC was examined by SEM analysis (Fig. S1B). Deep morphological alterations of the surface, such as loss or enlarged microvilli, membrane "blebs" and apoptotic bodies were present in bDHC treated cells. Moreover, a strong increase of Annexin V positive cells was detected following 24 hours of bDHC administration (61%) compared to DMSO (7%) and Curcumin (24%) treated cells (Fig. 1D, left panel), suggesting the activation of an apoptotic cell death.

To examine the reversibility of bDHC-growth arrest, HCT116 cells treated for 24 hours with bDHC were then washed to remove dead cells and released for 24 hours into fresh medium. An irreversible effect on cell viability was observed, with a clear accumulation of SubG1 events (38%) and no increase in any other phase of the cell cycle (Fig. 1D, middle panel).

Similarly to HCT116, human colon adenocarcinoma LOVO cells showed an evident increase of SubG1 events following bDHC administration for 24 hours (from 2.6% in DMSO to 27.7% in bDHC treated cells) (Fig S1C).

Consistently with the appearance of cells with hypodiploid SubG1 DNA content, bDHC triggered the phosphorylation of the histone variant H2AX (γ-H2AX), whose function is associated

with DNA fragmentation during apoptosis [45], both in HCT116 and LOVO cells (Fig. 1D, right panel and Fig. S1C, right panel).

## bDHC induces cell death in HCT116 cells but not in human normal cells

We next wondered whether bDHC had a tumor-selective activity. Untransformed human fibroblasts (HF) and hepatic fetal human epithelial normal cells (WRL68), whose doubling time is 24 hours, were treated for 24 and 48 hours with bDHC 30 μM and growth suppressive activity was then investigated by FACS (Fig. 2A and B, left and middle panels). In HF cells, bDHC induced a progressive accumulation of S (from 19.8% to 21.9% and from 11.4% to 17% within 24 and 48 hours, respectively) and G2/M events (from 16.8% to 24.7% within 24 hours, from 8.5% to 34.5% within 48 hours). bDHC administration to WRL68 resulted in an increase of both S and G2/M events as well, but differently from HF cells, maximal effects were detected after 24 hours (from 14% to 20.6% in S phase, and from 19.1% to 33.7% in G2/M phase). Interestingly, neither HF nor WRL68 cells were committed to apoptotic cell death and, coherently, no increase of γ-H2AX expression was observed upon bDHC treatment (Fig. S1D).

To investigate the stability of the cell cycle block induced in normal cells, HF cells were treated with bDHC for 48 hours, then washed and released in drug-free medium for 24 hours. Unlike HCT116, HF cells passed from G2/M to G1 phase (from 48% to 56.3% after the release), and no increase of SubG1 was detected (Fig. 2A, right panel). The reversible effects of bDHC on normal cells were even more evident in WRL68 cells, whose cell cycle distribution after 48 hours and following the release into fresh medium perfectly overlapped that of control cells (Fig. 2B, middle and right panels).

These data hint that bDHC reversibly blocks the cell cycle progression of non-malignant cells without inducing apoptosis.

With the purpose of unraveling the nature of bDHC selectivity towards colon cancer cells rather than normal cells, we performed further studies to estimate the variation of cellular uptake as a function of treatment concentration in HCT116 and HF cell lines. Data were normalized and presented as ng/mg of total proteins (Fig. 2C, upper panels) and culture medium residual amounts (μg) (Fig. 2C, lower panel). Drug uptake increased in a dose-dependent manner in both cell lines, but HCT116 revealed a significant higher uptake as compared to HF cell line at 30 μM : 4575±40 *versus* 2979±21 ng/mg total protein (Fig. 2C, upper right panel).

## bDHC-induced cell death is a caspase-dependent process

To explore the contribution of caspases on the execution of apoptosis, we pre-incubated HCT116 cells with the broad-caspase inhibitor ZVAD before treating cells with bDHC for 24 hours (Fig. 3A, left panel). A dramatic drop of SubG1 events was observed concomitantly to a progressive accumulation of cells in S and G2/M phases (from 11.7% to 24.5% in S phase and from 16% to 40% in G2/M, upon ZVAD pre-treatment). The inhibition of apoptosis by ZVAD determined an evident decrease of phosphorylated H2AX (Fig. 3A, right panel and Fig. S2A). The loss of γ-H2AX in ZVAD-bDHC co-treated cells corroborates the hypothesis that bDHC triggers a caspase-dependent cell death, as γ-H2AX formation has been shown to be an early chromatin modification downstream from caspase activation during apoptosis [45].

Interestingly, apoptosis suppression increased the expression levels of both p53 and p21, key regulators of the cell cycle (Fig. 3A, right panel and Fig. S2A).

The activation of individual caspases was then investigated by Western blot upon 8, 16 and 24 hours of treatment (Fig. 3B, left panel). Caspases 7, 8, 9 but not the executioner caspase 3, were clearly cleaved by 24 hours bDHC-incubation. The treatment with the anti-tumor drug Adriamycin demonstrated a fully functional caspase system, which includes caspase 3, in HCT116 cells.

We then explored the impact of caspases activation on proteolysis of poly (ADP-ribose) polymerase 1 (PARP1) substrate (Fig. 3B, left panel). Although caspase 3 was not detected at 24 hours, the 89 KDa fragment of PARP1 was observed, suggesting a redundancy between the executioner caspases. Pre-treatment of bDHC-cells with ZVAD completely abolished the cleavage of pro-caspases and PARP-1, consistently with apoptosis suppression (Fig. 3B, middle panel).

A major caspase activation pathway is the Cytochrome C-initiated pathway, which is triggered by the permeabilization of the mitochondrial outer membrane. Cellular fractionation followed by Western blot showed Cytochrome C release into the cytoplasm upon 24 hours of bDHC treatment (Fig. 3C and Fig. S2B).

Changes in the mitochondrial potential of bDHC-treated cells have been further investigated by labeling cells with DiOC6, a strong cationic dye that binds to undamaged mitochondria with intact membrane potential [46]. A clear decrease in the binding of DiOC6 was observed in cells treated with bDHC for 16 and 24 hours with respect to control cells, indicating the loss of mitochondrial transmembrane potential ($\Delta\psi$) (Fig. 3D, left panel).

Finally, a time-dependent decrease of intracellular ATP levels was detected (Fig. 3D, right panel), hinting at a compromised bioenergetic function of mitochondria triggered by mitochondrial inner membrane permeabilization with $\Delta\psi$ loss [47].

## Role of the Bcl-2 family members in bDHC-induced apoptosis

The intrinsic pathway of apoptosis is controlled by Bcl-2 family members, which regulate mitochondrial outer membrane integrity.

By RT-PCRs we investigated mRNA levels of the Bcl-2 anti-apoptotic genes: while Bcl-2α decreased in a time-dependent manner, Bcl-XL was mainly reduced upon 8 hours of treatment (Fig. 4A, left panel). A clear decrease of Bcl-2α and Bcl-XL protein levels was detected upon 24 hours treatment (Fig. 4A, right panel and Fig. S2C).

Given the significance of Bcl-2α and Bcl-XL as suppressors of apoptosis, single gene transfections were performed to determine whether either protein can inhibit bDHC-induced cell death. SubG1 events detected upon bDHC treatment were reduced of about 60% in Bcl-2α and 40% in Bcl-XL overexpressing cells, indicating a more important role for Bcl-2α rather than Bcl-XL in bDHC-apoptotic cell death (Fig. 4B).

As to pro-apoptotic genes, while transcription levels of the BH3-only Noxa and Puma raised compared to control cells, no increase was observed for Bax mRNA and protein levels (Fig. 4A, left and right panels). To shed light on the role of Bax in mediating bDHC-cell death process, we switched to HCT116 Bax −/− cells (Fig. 4C). Compared to HCT116, bDHC-induced apoptosis was partially suppressed (from 1% in control cells to only 10% in treated-cells), in behalf of an increase of G2/M phase population (from 24% to 41%), thus indicating that Bax contributes to bDHC induced cell death.

Despite the participation of Bax to the apoptotic process, the lack of its mRNA up-regulation suggests the activation of a p53 transcriptional-independent apoptotic pathway. In fact cytosolic/

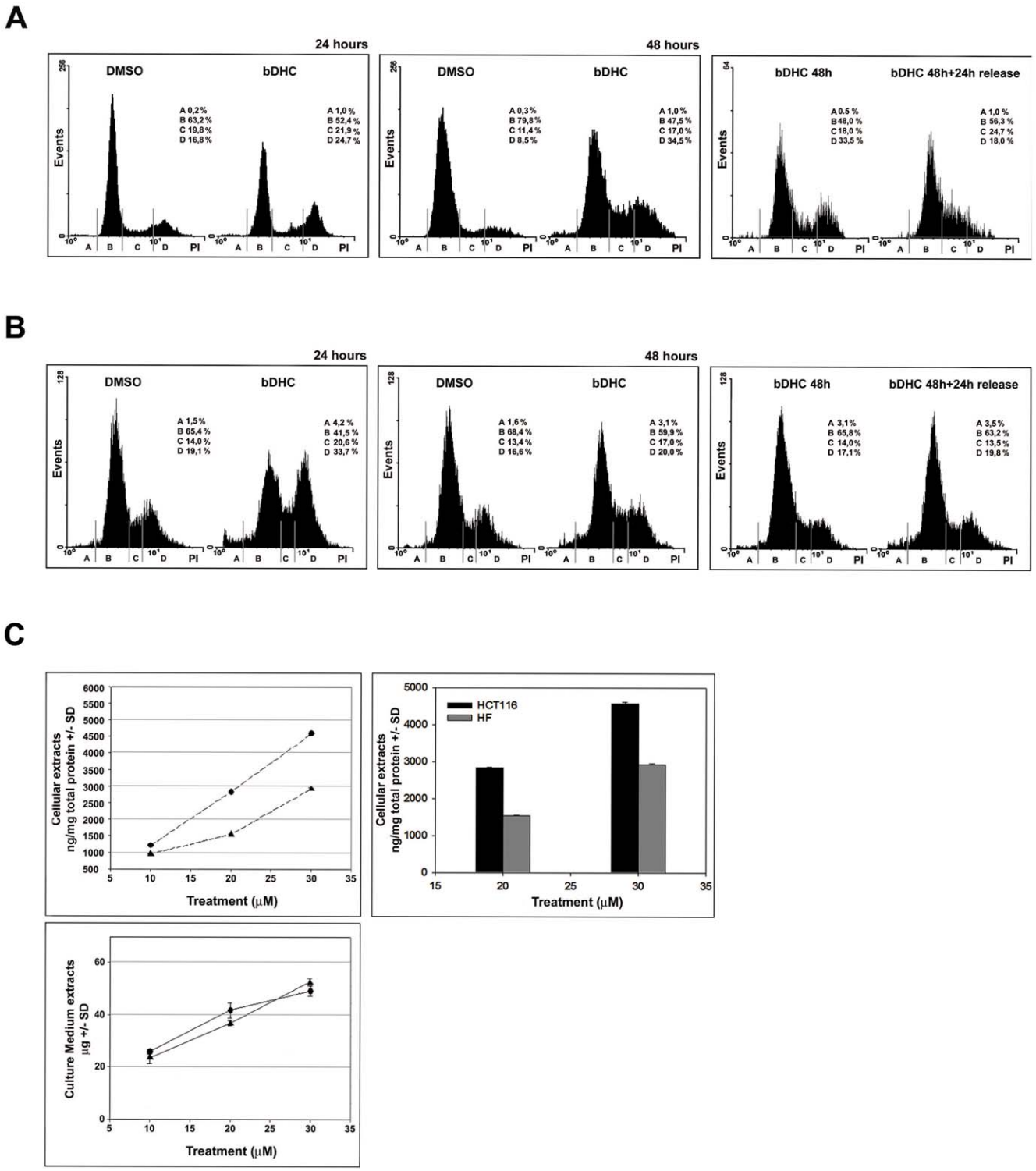


**Figure 2. Reversible anti-proliferative activity of bDHC on human normal cells. A.** PI/FACS analysis of HF cell cycle progression after DMSO and bDHC treatments for 24 and 48 hours (left and middle panel, respectively). PI/monoparametric cell cycle analysis of bDHC-treated cells *versus* bDHC-released cells (right panel) (A = SubG1, B = G0/G1, C = S, D = G2/M). **B.** Left and middle panels: Analysis of cell cycle progression of WRL68 cells following 24 and 48 hours of treatment with DMSO or bDHC. Right panel: PI/FACS monoparametric analysis of WRL68 cells treated with bDHC for 48 hours and then released into fresh medium for additional 24 hours (A = SubG1, B = G0/G1, C = S, D = G2/M). **C.** Quantitative evaluation of bDHC concentration by UV-vis spectroscopy. Upper left panel: bDHC recovered from cell lysates of HCT116 (●) and HF (▲) cells after 24 hours treatment at different concentrations (10, 20 and 30 μM). bDHC recovered from cell pellets (ng) was referred to total cellular proteins (mg), determined using Bradford method. Upper right panel: Comparison of cellular uptake (20 and 30 μM concentrations) in HCT116 (black histograms) and HF cells (grey histograms). Lower panel: bDHC recovered from culture media following incubation of HCT116 (●) and HF (▲) cells with bDHC at 10, 20 and 30 μM concentration. All data were normalized on control (DMSO). Drug amount was determined by reading absorbance at $\lambda_{max} = 393$ nm. Reported values are an average of three independent experiments −/+ SD.
doi:10.1371/journal.pone.0053664.g002

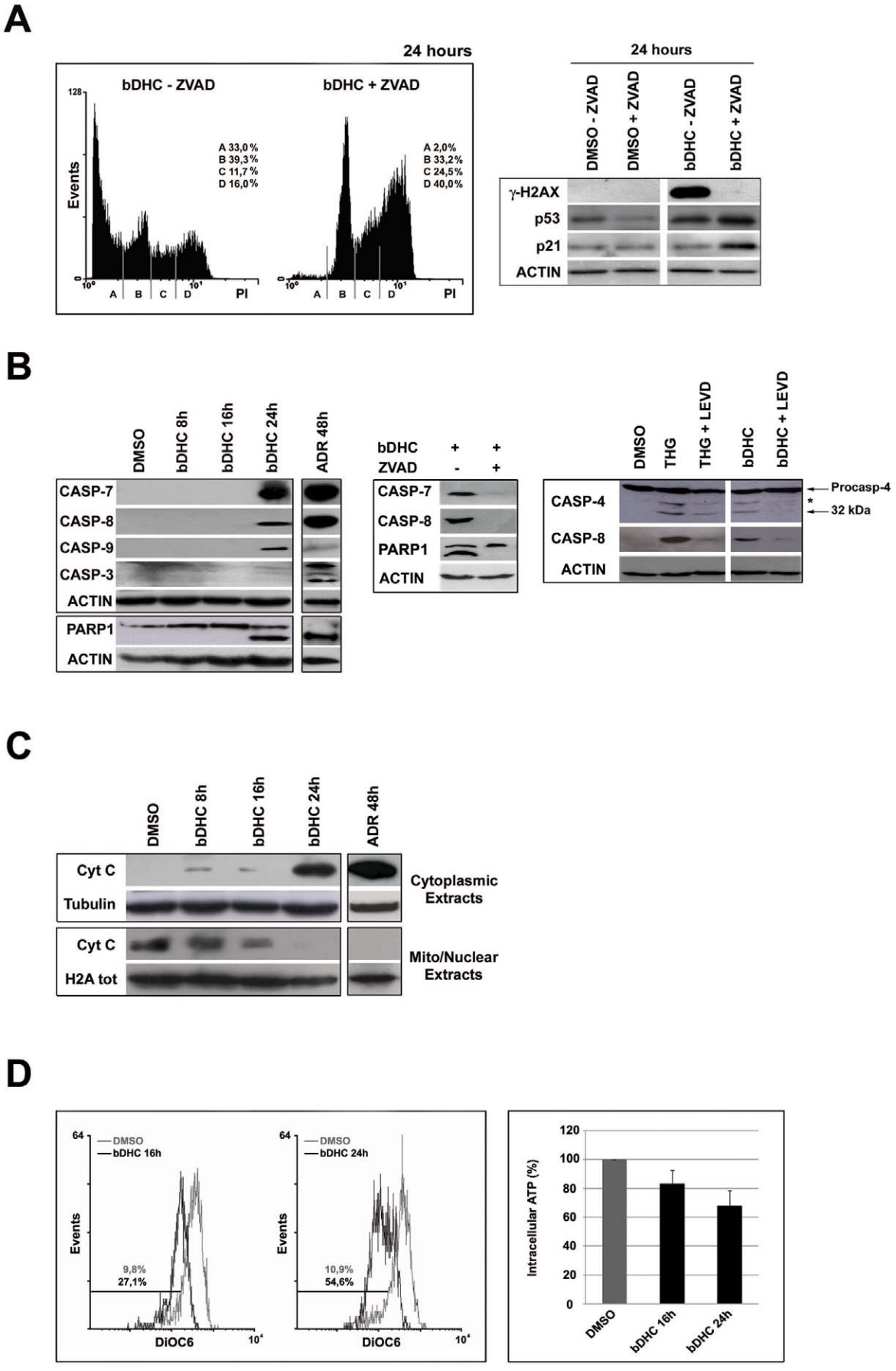
A
24 hours
bDHC - ZVAD
bDHC + ZVAD
Events
A 33,0 %
B 39,3 %
C 11,7 %
D 16,0 %
A 2,0%
B 33,2%
C 24,5%
D 40,0%
PI
24 hours
DMSO - ZVAD
DMSO + ZVAD
bDHC - ZVAD
bDHC + ZVAD
γ-H2AX
p53
p21
ACTIN
B
DMSO
bDHC 8h
bDHC 16h
bDHC 24h
ADR 48h
CASP-7
CASP-8
CASP-9
CASP-3
ACTIN
PARP1
bDHC
ZVAD
THG
THG + LEVD
bDHC + LEVD
CASP-4
Procasp-4
32 kDa
C
Cyt C
Tubulin
Cytoplasmic Extracts
H2A tot
Mito/Nuclear Extracts
D
DMSO
bDHC 16h
bDHC 24h
9,8%
27,1%
10,9%
54,6%
DiOC6
Intracellular ATP (%)

**Figure 3. Caspases activation upon bDHC treatment in HCT116 cells. A.** Left panel: PI/monoparametric analysis of cell cycle progression of bDHC-treated cells with or without ZVAD pre-incubation. The indicated events are means of three independent experiments (A = SubG1, B = G0/G1, C = S, D = G2/M). Right panel: Western blot analysis of the indicated proteins after DMSO and bDHC treatment with or without ZVAD co-incubation. Actin was used as loading control. **B.** Left panel: Expression analysis of cleaved-caspases and cleaved–PARP1 by Western blot following bDHC and Adriamycin administration. Actin was used as loading control. Middle panel: Western blot analysis of cleaved-caspases and PARP1 upon ZVAD pre-treatment compared to bDHC alone. Right panel: Expression levels of cleaved caspase 4 and 8 in HCT116 cells incubated with bDHC for 24 hours and co-treated with LEVD. Thapsigargin (THG) treatment for 36 hours was used as positive control. Protein loading was assessed by probing the blot with anti-actin antibody. The asterisk in caspase 4 blot indicates a band derived from unknown cleavage. **C.** Cytochrome C expression analysis in cytoplasmic and mitochondrial/nuclear extracts from HCT116 treated with bDHC for 8, 16 and 24 hours. Tubulin and total histone H2A were used as loading controls of cytoplasmic and nuclear extracts, respectively. **D.** Left panel: Flow Cytometric analysis of mitochondrial membrane potential ($\Delta\psi$) by measuring DiOC6 binding in HCT116 cells following administration of bDHC for 16 and 24 hours. The percentage of cells with decreased $\Delta\psi$ is indicated. Right panel: ATP content in HCT116 cells following incubation with bDHC *versus* DMSO (arbitrarily set at 100%).
doi:10.1371/journal.pone.0053664.g003

mitochondrial p53 could activate Bax/Bak without direct regulation of gene expression [48]. As it concerns Puma and Noxa, they have been shown to be activated through p53-dependent and -independent mechanisms. Puma can be induced by ER stress [49], and regulated by transcription factors other than p53, including FOXO3a, p73 and E2F [50–52]. Noxa mRNA can be induced by the proteasomal inhibitor MG132, in p53 null human cell lines [53].

To investigate whether p53 could play a role in mitochondrial-dependent apoptosis rather than in the transcriptional control of the apoptotic pathway, we analyzed the expression and cellular localization of endogenous p53 following bDHC administration. Western blot highlighted an increase of p53 levels into cytosolic fractions of cells treated for 16 and 24 hours with bDHC (Fig. 4D). Similarly, cytoplasmic p53 was detected by Immunofluorescence only following 16 and 24 hours of bDHC incubation (Fig. 4E, arrows). The accumulation of p53 protein outside the nuclear compartment suggests an important role of p53 mainly into cytoplasmic molecular mechanisms.

## Activation of the endoplasmic reticulum stress response following bDHC treatment

As well as described for the pro-apoptotic genes, also anti-apoptotic Bcl-2 family members can be transcriptionally regulated in a p53-independent way. The transcriptional down-regulation of Bcl-2α following bDHC treatment could be ascribed to different transcriptional regulators, among which CHOP (C/EBP homologous protein). Indeed, an increase of CHOP expression levels was observed by RT-PCR and Western blot in bDHC-treated cells (Fig. 5A). CHOP is a transcription factor induced under ER stress, which triggers an ER-specific cascade for implementation of apoptosis [54]. mRNA levels of several ER-stress induced genes were studied (Fig. 5A, left panel). We observed a transcriptional increase of the pro-apoptotic CHOP target gene DR-5 (death receptor-5), and of two main CHOP transcriptional activators, ATF6 and the ER-induced spliced variant of XBP1. Other ER-stress markers, such as GRP78, a chaperone that binds to unfolded proteins, and HERPUD1 were up-regulated in a time-dependent manner.

A considerable increase of H3 and H4 acetylation was observed by ChIP in regulatory regions of ER-stress genes, consistently with their transcriptional activation (Fig. 5B).

The analysis of cells treated for 16 hours with bDHC by electron microscope revealed enlargement and dilation of the ER, corroborating the activation of ER stress (Fig. 5C).

Severely damaged ER functions have been shown to induce apoptosis. In addition to CHOP, processing of caspases 12, 4, 3, 6, 7, 8, and 9 has been observed to play a role in ER stress-induced apoptosis. In particular, caspase 12 in rodents and caspase 4 in humans can initiate a specific cascade independent of mitochondria, linking ER stress to apoptosis [55,56,57]. We therefore examined caspase 4 activation following bDHC administration, compared to Thapsigargin (THG), which is able to trigger ER stress-apoptosis in HCT116 cells [58]. Although to a lesser degree with respect to THG, cleavage of caspase 4 (32 kDa subunit) was induced by bDHC and reverted by co-incubation with the caspase 4 inhibitor LEVD (Fig. 3C, right panel). Interestingly, caspase 4 inhibition resulted in a clear decrease of caspase 8 processing, suggesting that caspase 4 acts upstream of caspase 8.

Curcumin-induced proteasomal dysfunction and inhibition were shown to contribute to Curcumin-ER stress activation [59,60]: we therefore examined proteasomal function by Western blot analysis of bDHC-total cellular extracts with anti-poly-ubiquitin antibody. Figure 5D highlights an accumulation of poly-ubiquitinated proteins upon Curcumin administration for 24 hours. Exposure to bDHC, even after 8 hours, resulted in a more robust increase of poly-ubiquitinated proteins than Curcumin, comparable to the effect of the well known proteasome inhibitor MG132.

These data suggest that the proteasome can't degrade the ubiquitinated proteins accumulated in the ER lumen and that the process of ER stress is already maximally stimulated by bDHC upon 8 hours.

## bDHC induces autophagy in p53-positive cells

Phase-contrast microscopy analysis of bDHC-treated cells highlighted the presence of cytoplasmic vacuoles (data not shown). We performed ultrastructural analysis by using electron microscopy to further investigate the morphological changes induced by bDHC upon 16 hours of incubation. Compared to control cells, bDHC treated cells showed double membrane vacuolar structures with the morphological features of autophagosomes (Fig. 6A, arrows).

Formation of autophagolysosomes was also detected by fluorescence microscopy following staining with the lysosomotropic agent Acridine Orange, whose protonated red fluorescent form accumulates in acidic compartments [61]. While control cells showed green fluorescence with minimal cytoplasmic red components, corresponding to lysosomes, bDHC-treated cells displayed considerable red fluorescence, caused by the formation and accumulation of autophagolysosomes (Fig. 6B).

To validate the hypothesis that bDHC could induce autophagy, we monitored by Western blot the formation of LC3-II, which is regarded as autophagy marker [62]. bDHC induced a time-dependent expression of the microtubule-associated protein light chain 3 (LC3-I), and the accumulation of its processed form (LC3-II) (Fig. 6C). Quantification of LC3-II versus actin levels highlighted an increase of about 5 fold of LC3-II in cells treated for 24 hours with bDHC, compared to DMSO (Fig. 6C, right panel). Figure S3A shows the quantification of the conversion of LC3-I into the phosphatidylethanolamine conjugate LC3-II (LC3-II/LC3-I ratio).

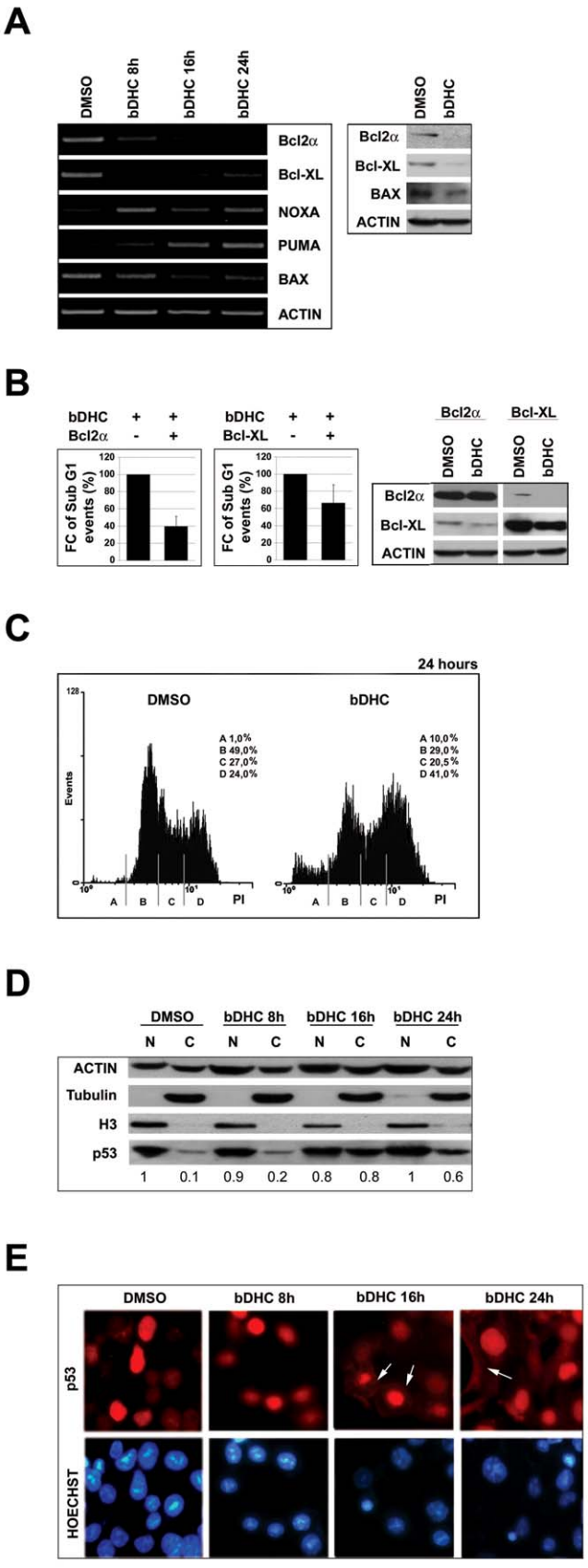


**Figure 4. Role of Bcl-2 family members in bDHC-induced apoptosis. A.** Left panel: RT-PCR analysis of the indicated Bcl-2 family genes upon bDHC treatment for different times *versus* DMSO. Right panel: Protein expression levels of Bcl-2α, Bcl-XL and Bax following 24 hours treatment with bDHC. **B.** SubG1 (left panel) and Western blot analysis (right panel) of HCT116 cells upon transient transfection of Bcl-2α or Bcl-XL and treatment with DMSO or bDHC. Data are reported as fold change (FC) of SubG1 population in transfected cells treated with bDHC relative to bDHC-cells (arbitrarily set at 100%). **C.** PI/FACS analysis of cell cycle progression of HCT116 Bax −/− cells after DMSO and bDHC incubation for 24 hours. **D.** Western blot analysis of p53 expression in nuclear and cytosolic extracts of cells treated with DMSO and bDHC for 8, 16 and 24 hours. Tubulin and histone H3 were used as loading controls of cytosolic and nuclear extracts. The intensity of immunoreactive bands was quantitated to actin (basal nuclear p53 arbitrarily set at 1). Values are means of three independent experiments. **E.** Immunofluorescence analysis of endogenous p53 cellular localization in HCT116 following time-dependent exposure to bDHC. p53 cytoplasmic localization is indicated by white arrows.
doi:10.1371/journal.pone.0053664.g004

Interestingly, bDHC was not able to increase LC3-II in HF cells after 24 and 48 hours (Fig. S4A), suggesting that bDHC-cell death could be related to autophagy activation.

The increase of LC3-II and the appearance of autophagosomes are not measure of the autophagic flux, but can reflect the inhibition of autophagosome clearance [63]. To verify whether autophagic flux was occurring in bDHC-treated cells, we prevented lysosomal degradation by using Chloroquine, that neutralizes the lysosomal pH [64]. As shown by the quantification of LC3-II levels with respect to actin, the amount of LC3-II induced by bDHC strongly increased in the presence of the inhibitor, corroborating a time dependent activation of autophagy (Fig. 6D).

Finally, we monitored bDHC-induced autophagy through Immunofluorescence, measured as an increase in punctuate endogenous LC3. Figure 6E shows the changes in LC3 localization upon incubation with bDHC, compared to HCT116 control cells. LC3-stained autophagic compartments are indicated by arrows. As already observed (Fig. 6D), Chloroquine induced an increase in the level of LC3 puncta in control cells and had an additive effect when administered with bDHC.

p53 has been described to regulate the activation of autophagy: nuclear p53 can participate to autophagy induction, while cytoplasmic p53 inhibits autophagy through a transcriptional-independent mechanism. We therefore analyzed the effects of bDHC administration to HCT116/E6 cells, in which p53 is degraded by the viral E6 protein. Under normal conditions HCT116/E6 showed higher levels of LC3-II compared to HCT116 wt, but no increase was observed following bDHC treatment (Fig. S4B, upper panels). Moreover, HCT116/E6 cells were less susceptible than wt cells to bDHC-induced apoptosis, as indicated by the lower percentage of SubG1 events (from 33% in bDHC-treated HCT116 to 16% in bDHC-HCT116/E6 cells) (Fig. S4B, lower left panel). The high levels of poly-ubiquitinated proteins observed in HCT116/E6 cells suggest that bDHC can induce ER stress also in p53 deficient cells, but it doesn't elicit the activation of autophagy, which can contribute to drug-induced cell death (Fig. S4B, lower right panel).

## Autophagy activation triggered by bDHC potentiates its pro-death activity

To investigate whether autophagy and apoptosis participate independently in parallel pathways or they affect one another, we co-treated cells with bDHC and inhibitors of autophagy or apoptosis.

Inhibition of apoptosis by ZVAD resulted in a conspicuous decrease of SubG1 events and of the apoptotic markers, cleaved-

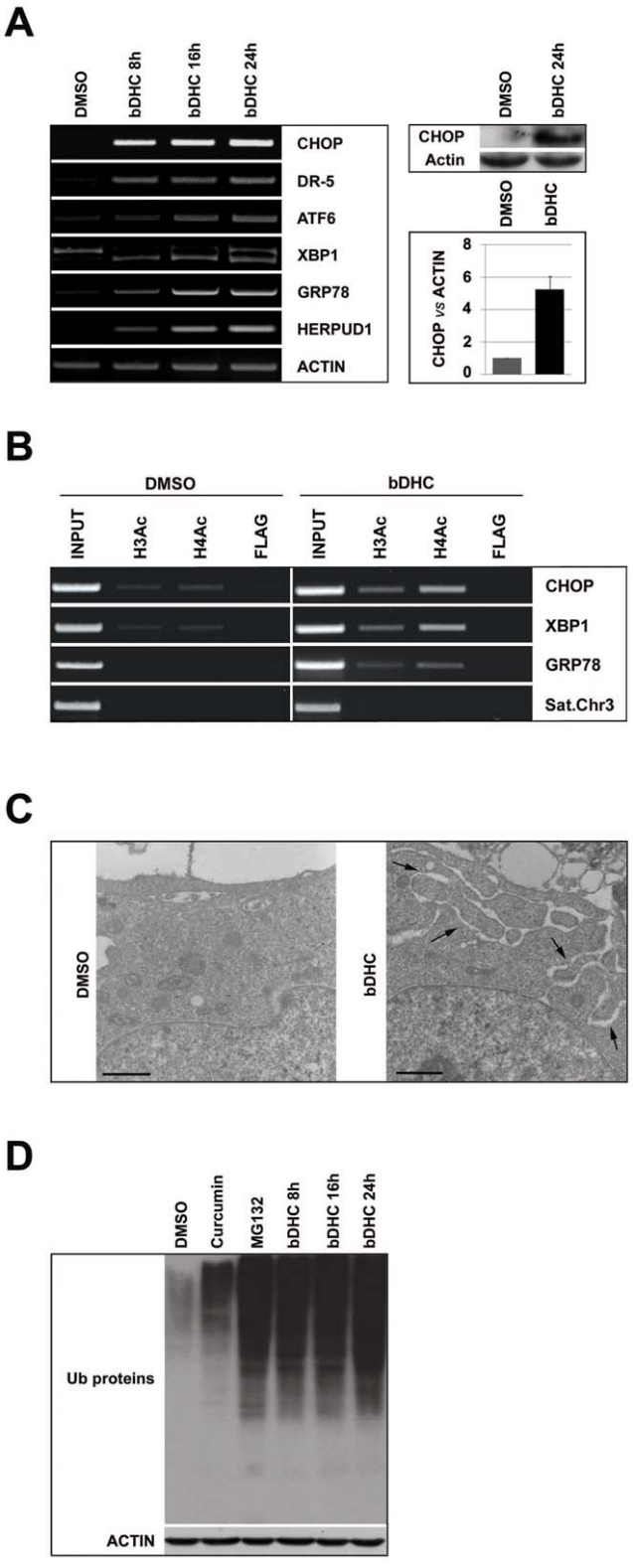


**Figure 5. Activation of ER stress response in bDHC-treated HCT116 cells. A.** Left panel: time-course mRNA expression analysis by RT-PCR of the indicated genes. CHOP protein expression (right upper panel) and quantification (right lower panel) after 24 hours treatment with bDHC *versus* DMSO. **B.** Changes in histones acetylation upon bDHC treatment. Anti-Acetylated histone H3 and H4 have been used for ChIP analysis of the indicated regulatory regions. **C.** Transmission Electron Microscopy analysis of ER in control and bDHC-treated cells. The black arrows indicate the expanded ER. Scale bar: 1 μm. **D.** Increase of protein ubiquitination in Curcumin (24 hours), MG132 (24 hours) and bDHC lysates (8, 16, 24 hours) by Western blot analysis. Actin was used as loading control.

doi:10.1371/journal.pone.0053664.g005

PARP-1 and γ-H2AX (Fig. 7A and Fig. S2D, left panel). Compared to bDHC, ZVAD co-treatment didn't reduce the transcriptional activation of CHOP and DR-5, as well as LC3-II protein levels, indicating that ER stress response and the autophagic process are still active when apoptosis is suppressed (Fig. 7A, middle panels, and Fig. S3B, left panel).

The same analysis was performed following co-treatment of bDHC with the specific caspase 4 inhibitor LEVD (Fig. 7B). As well as observed in ZVAD co-treated cells, no decrease of LC3-II levels was detected, while SubG1 events were significantly reduced by LEVD, hinting at an important role of ER stress-related caspase 4 as initiator of bDHC-induced apoptosis.

Pharmacological inhibition of autophagy by co-treatment with Wortmannin, which blocks the early steps of autophagic degradation, resulted in decreased LC3-II levels (Fig. 7C and Fig. S3B, right panel). Concomitantly, we observed a reduction of PARP-1 cleavage, γ-H2AX expression and SubG1 events, but no effects on ER stress genes activated by bDHC (Fig. 7C and Fig. S2D, right panel). Similarly, co-treatment with Chloroquine reduced SubG1 events of about 70% compared to bDHC-treated cells (Fig. S4C).

To further confirm the effects of autophagy inhibition on bDHC-induced cell death, we specifically knocked down the autophagy-related proteins Beclin1 and ATG7 (Fig. 7D). Western blot analysis showed an efficient silencing of both Beclin1 and ATG7, whose expression levels were reduced to about 10% with respect to control cells (Fig. S2E). Interestingly, while Beclin1 inactivation didn't affect either LC3-II levels or apoptosis upon bDHC administration, ATG7 knock down reduced the formation of LC3-II and decreased SubG1 events of bDHC-cells of about 30% (Fig. 7D and Fig. S3C).

These data suggest a role of Beclin1-independent autophagy in bDHC pro-death activity in HCT116 cells.

As shown in Figure 5, bDHC is able to activate ER stress response and accumulation of poly-ubiquitinated proteins. To investigate whether ER stress activation occurred upstream of bDHC-induced autophagy and apoptosis, we used Salubrinal, an ER stress inhibitor, which can regulate eIF2α phosphorylation [65]. Salubrinal co-treatment with bDHC reduced LC3-II levels and SubG1 events (Fig. 8A). CHOP knock down by RNAi reduced apoptosis as well, suggesting the contribution of ER stress to the apoptotic process (Fig. 8B).

Inhibition of translation through Cycloheximide (CHX) co-treatment reduced ER stress activation, as indicated by the lack of overexpression of ER-stress related genes. CHX concurrently lowered the accumulation of LC3-II, as well as γ-H2AX, cleaved-PARP1 and SubG1 events (Fig. 8C, Fig. S2F and Fig. S3D).

Only the co-administration of CHX to cells completely inhibited the accumulation of poly-ubiquitinated proteins induced by bDHC, suggesting that the increase of unfolded nascent proteins can be one of the main causes triggering ER stress response and autophagic-cell death (Fig. S4D).

Taken together, these results indicate that bDHC-induced ER stress leads to autophagy, which occurs upstream of apoptosis and is not protective for bDHC-treated cells.

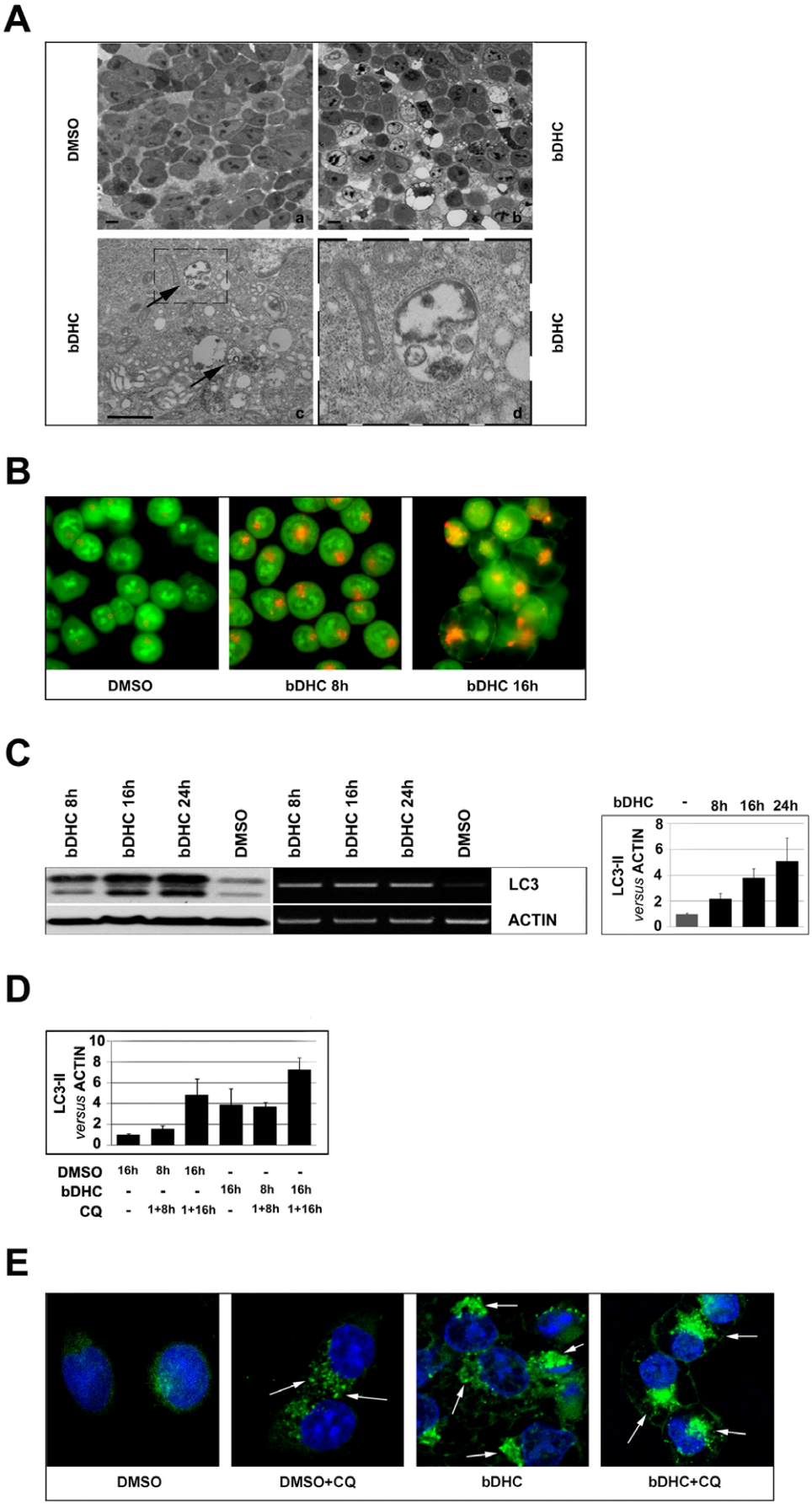
A
DMSO
bDHC
bDHC
bDHC
a
b
c
d
B
DMSO
bDHC 8h
bDHC 16h
C
bDHC 8h
bDHC 16h
bDHC 24h
DMSO
bDHC 8h
bDHC 16h
bDHC 24h
DMSO
LC3
ACTIN
bDHC - 8h 16h 24h
LC3-II versus ACTIN
0
2
4
6
8
D
LC3-II versus ACTIN
0
2
4
6
8
10
DMSO 16h 8h 16h - - -
bDHC - - - 16h 8h 16h
CQ - 1+8h 1+16h - 1+8h 1+16h
E
DMSO
DMSO+CQ
bDHC
bDHC+CQ

**Figure 6. bDHC induces autophagy in HCT116 cells. A.** Optical (*a* and *b* photomicrographs) and Scanning Electron Microscopy (*c* and *d* photomicrographs) representative images of cells treated with DMSO and bDHC for 24 hours. Photomicrograph of panel *c* shows the presence of autophagolysosomes in bDHC treated cells. Enlargement of the dashed box (panel *d*) illustrates a double-membraned autophagosome. Scale bar *a* and *b* panels: 10 μm; *c* panel: 1 μm. **B.** Detection of bDHC-induced autophagosomes formation by fluorescence microscopy following staining with Acridine Orange. **C.** Left panel: Western blot and RT-PCR analysis of LC3 expression at 8, 16 and 24 hours of bDHC exposure in HCT116 cells. Right panel shows the levels of LC3-II *versus* actin following time-dependent incubation with bDHC. Values are mean of six independent experiments −/+ SD. **D.** Quantification of LC3-II detected by Western blot analysis following pre-incubation (1 h) of DMSO and bDHC with Chloroquine (CQ). The levels of LC3-II have been normalized to actin. **E.** Fluorescence staining of endogenous LC3 following incubation of HCT116 cells with bDHC for 24 hours, with or without Chloroquine (CQ). LC3-stained autophagic compartments are indicated by white arrows.
doi:10.1371/journal.pone.0053664.g006

## Discussion

Apoptosis is the major source to oppose uncontrolled growth of cancer cells and to reduce tumor cell population expansion. Although many dietary agents show interesting chemotherapeutic activity, they often produce major side effects. Curcumin has been used through the ages as alternative medicinal agent and it has been classified as safe by health authorities. It is currently in phase II/III clinical trials, although it shows limited application because of its instability in physiological conditions.

In this study, we demonstrated that the stable Curcumin-derivative bDHC is highly cytotoxic towards colon-cancer cells in a dose-dependent manner. At the concentration of 30 μM, bDHC reduces cell proliferation both by inducing a cell cycle block and by activating the apoptotic program (Fig. 1). At the same concentration, Curcumin is not able to induce such a high cell death in HCT116 cells, but only a G2/M arrest can be detected [20]. It could be that the mismatch repair system protects HCT116 cells from Curcumin cytotoxicity, in part by activating the G2/M checkpoint, as recently shown [66].

bDHC exhibits a selective activity towards cancer cells: in human normal cells (HF and WRL68), it reversibly inhibits proliferation, without eliciting a cytotoxic response (Fig. 2). Its tumor-selectivity can be ascribed to lower uptake in normal cells compared to colon cancer cells (Fig. 2C), but we can't rule out that other mechanisms are involved. As hypothesized for Curcumin, it could be that the great efficacy of bDHC in tumor cells is caused by (i) their lower glutathione levels, which enhances drug sensitivity compared to normal cells or (ii) the constitutive expression of active NF-kB in cancer cells, which is one of Curcuminoids targets [67].

Although it remains to be determined why bDHC is particularly active against colorectal carcinoma cells (HCT116 and LOVO cells) rather than other types of cancer cells [36,37, VB and CI unpublished data], this is an encouraging prerequisite for bDHC anti-tumor activity *in vivo*. Indeed, Curcumin and its derivatives show increased bioavailability in the gastrointestinal tract and, consequently, slow the growth of gastrointestinal cancers [68,69].

Our study demonstrates that bDHC-induced apoptosis in colon cancer cells occurs through a mitochondria-dependent pathway (Fig. 3). Mitochondria play an essential role as sensors and amplifiers of death signaling pathways. In particular, the collapse of the mitochondrial membrane potential is considered an irreversible point in the death cascade [70]. Following bDHC treatment, we observed a decrease of mitochondrial transmembrane potential (Fig. 3), and the release into the cytosol of Cytochrome C, which triggers the caspase-activating cell death pathways [71] (Fig. 3C). Cytochrome C is a key player of mitochondria-dependent apoptotic cell death: its release from mitochondria elicits the formation of Apaf-1/caspase 9 apoptosome, which further activates effector caspases 3 and 7, leading to the cleavage of nuclear substrates, such as PARP-1 (Fig. 3B) and lamins, and to oligonucleosomal DNA fragmentation [72].

We showed a major role of caspases as final effectors of bDHC-cell death (Fig. 3B). The inhibition of pro-caspases cleavage by ZVAD completely suppresses bDHC-induced apoptosis, the cleavage of PARP-1 and the phosphorylation of H2AX at Ser139 (Fig. 3A-B and Fig. 7A). Even if the function of γH2AX has been mainly linked to DNA-damage repair [73], this histone plays a key role in programmed cell death. Its formation during apoptosis depends on caspases activation and is concurrent with the initiation of apoptotic endonuclease activation [45], regulating the accessibility of various DNases to DNA [74,75].

The balance between cell proliferation and cell death is controlled by anti- and pro-apoptotic proteins, most of which are known p53 target genes. RT-PCR analysis indicates that bDHC can induce cell death by regulating the expression of the Bcl-2 family members: Bcl-2α and Bcl-XL anti-apoptotic proteins are down-regulated, while the pro-apoptotic Noxa and Puma genes are up-regulated by bDHC (Fig. 4A).

Although the pro-apoptotic Bax doesn't show any transcriptional activation, bDHC treatment of HCT116 Bax−/− cells clearly highlights its contribution to the activation of cell death (Fig. 4A and C). Indeed, Bax-induced mitochondrial membrane permeabilization and the resulting Cytochrome C release into the cytoplasm, can be achieved through Bax translocation from the cytoplasm to the outer mitochondrial membrane, without any p53-transcriptional activation [76]. The analysis of p53 expression and cellular compartmentalization shows that protein levels increase exclusively into the cytoplasm, suggesting a marginal role for p53 in the transcriptional regulation of anti- and pro-apoptotic target genes in response to bDHC (Fig. 4D and E). A p53 transcriptional-independent activation of Bax has been described following the activation of caspase 8 and the up-regulation of Puma [77], consistently with our data from bDHC-treated cells (Fig. 3 and Fig. 4). In addition to Bax, also Puma and Noxa activation can be achieved through p53-independent mechanisms: Puma was shown to be induced by ER stress [49] and Noxa by proteasome inhibition [78], both injuries being observed upon bDHC administration to HCT116 cells (Fig. 5). The increase of p53 expression upon apoptosis inhibition by ZVAD, which results in a G2/M cell cycle arrest, ascribes to the oncosuppressor mainly a role in bDHC-cell cycle block rather than apoptosis (Fig. 3A). The same behavior is observed for p21, which has a fundamental function in maintaining the cell cycle block induced by Curcumin and its derivatives [20].

Administration of bDHC to HCT116/E6 cells partially reduces but doesn't abolish apoptosis, suggesting that a p53-independent-cell death can occur. On the other hand, p53 has come to light as a positive regulator of autophagy, which indeed is not induced by bDHC in HCT116/E6 (Fig. S4B). We believe that the halved percentage of SubG1 population in E6 compared to wt cells could be ascribed to the lack of autophagy activation, which contributes to bDHC-cell death.

RT-PCRs highlight the activation of various genes involved in ER stress response: CHOP, ATF6, GRP78, HERPUD1 and sXBP1 mRNA levels increase already after 8 hours of bDHC

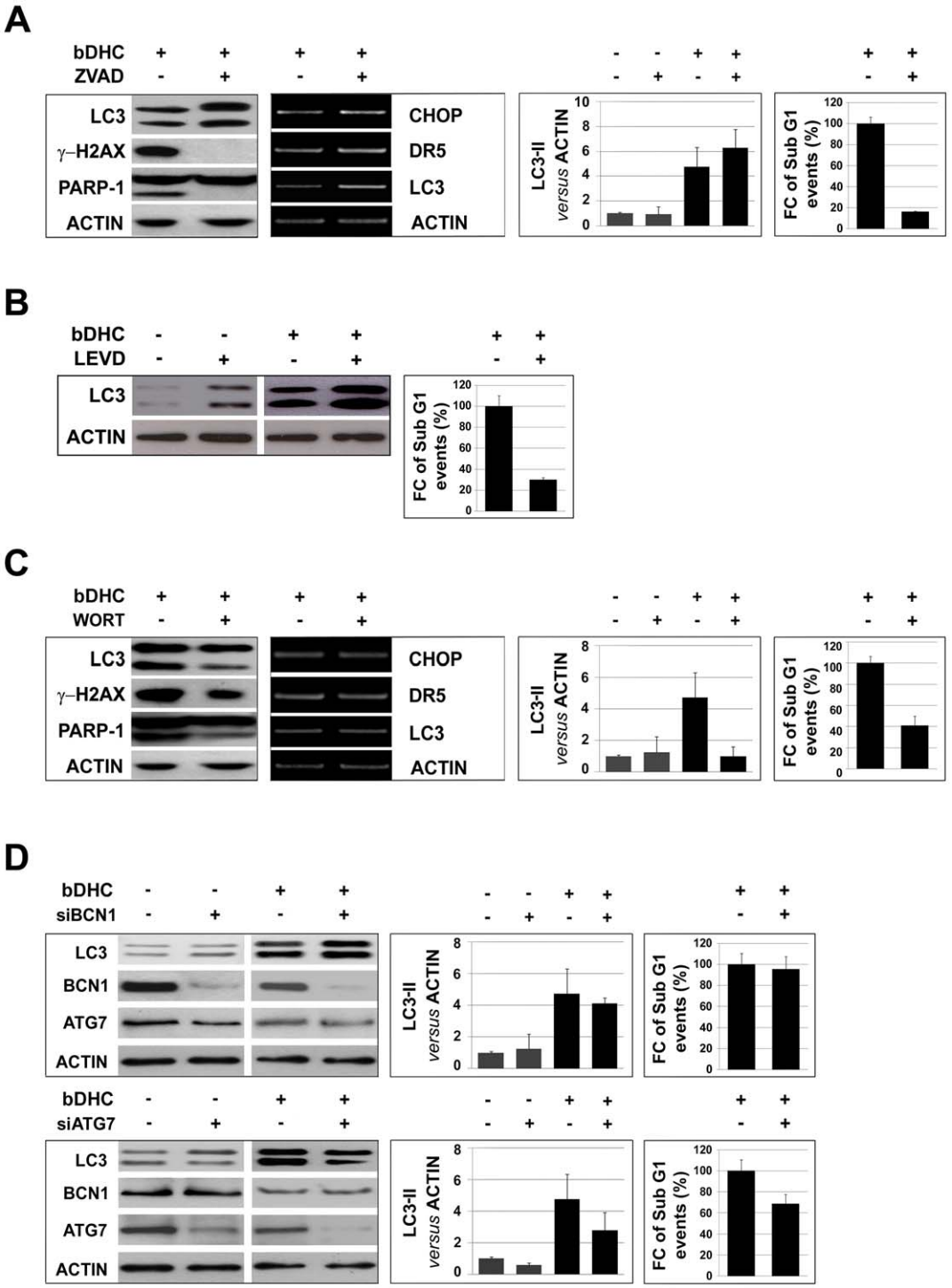


**Figure 7. Autophagy activation leads to cell death. A.** Left panels: LC3, γ-H2AX and PARP1 levels in bDHC cells co-treated with ZVAD. Middle left panel: RT-PCR analysis of the indicated genes normalized *versus* actin mRNA expression. Middle right panel: LC3-II levels *versus* actin with or without co-treatment. Right panels: Flow cytometric analysis of SubG1 events in cells with or without co-treatments. Data are reported as fold change (FC) of SubG1 population relative to bDHC-treated cells (arbitrarily set at 100%). **B.** Left panel: Western blot analysis of LC3 and actin levels following 24 hours co-treatment of DMSO or bDHC with LEVD. Right panel: Fold change (FC) of SubG1 events in cells co-treated with LEVD and bDHC *versus* bDHC-treated cells (arbitrarily set at 100%). **C.** Left panels: LC3, γ-H2AX and PARP1 levels in bDHC cells co-treated with Wortmannin (WORT). Middle left panel: mRNA levels of the indicated genes normalized *versus* actin. Middle right panel: Expression levels of LC3-II normalized to actin with or without co-treatment. Right panels: Flow cytometric analysis of SubG1 events in cells with or without Wortmannin. Data are reported as fold change (FC) of SubG1 population relative to bDHC-treated cells (arbitrarily set at 100%). **D.** Left panels: Western blot analysis of LC3, Beclin1 (BCN1) and Atg7 expression levels in DMSO and bDHC treated cells following BCN1 (upper panel) and Atg7 (lower panel) knock down. Middle panels: LC3-II levels in control, BCN1 and Atg7 inactivated cells have been normalized *versus* actin levels. Values are mean of three independent experiments −/+ SD. Right panels: Fold change (FC) of SubG1 events of BCN1 and Atg7 inactivated bDHC-cells *versus* bDHC-treated cells (arbitrarily set at 100%).
doi:10.1371/journal.pone.0053664.g007

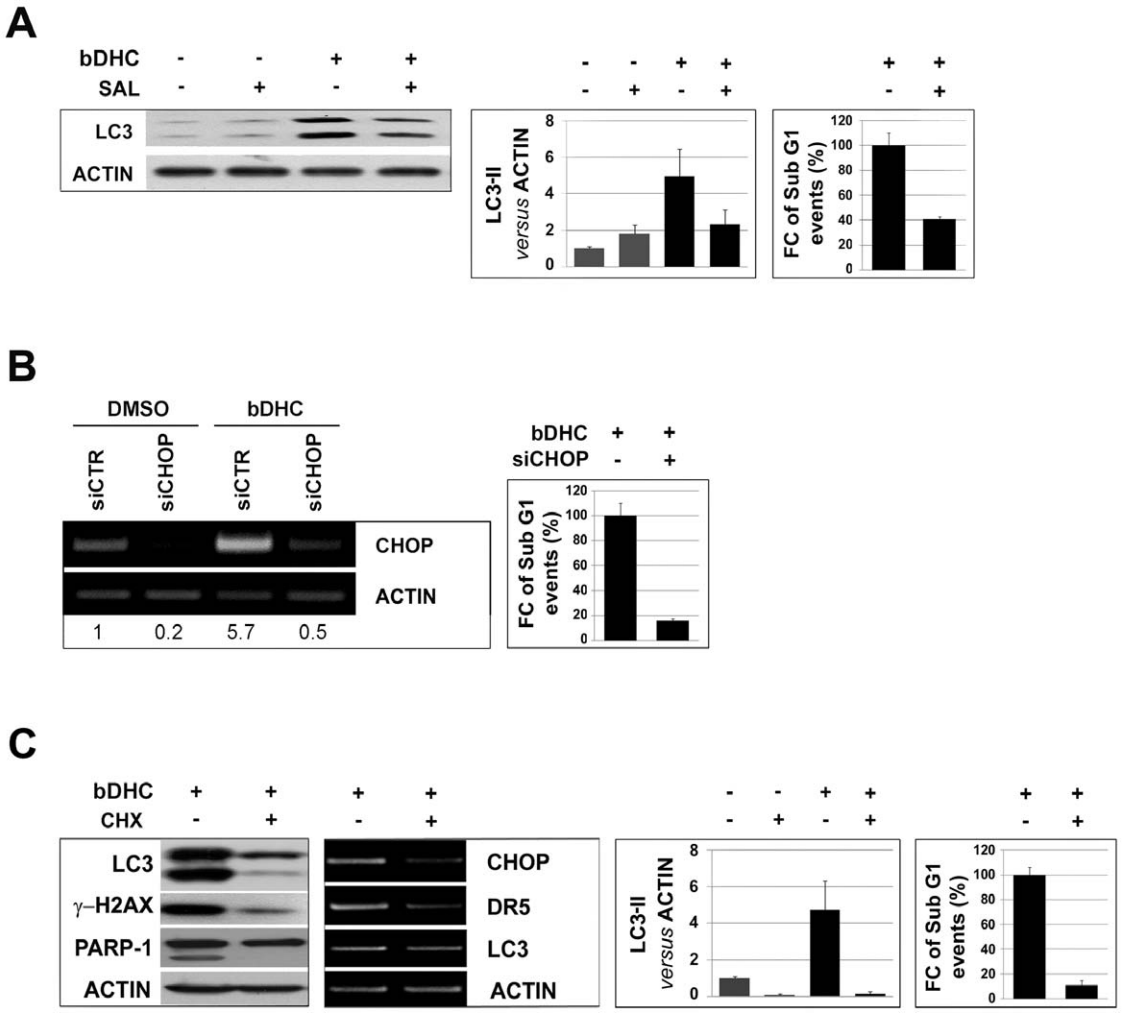


**Figure 8. ER stress precedes autophagy-mediated cell death. A.** Effects of Salubrinal (SAL) on bDHC-treated cells. Protein expression levels of LC3 (left panel) and LC3-II quantification *versus* actin levels (middle panel) in DMSO or bDHC cells co-treated with Salubrinal. Right panel: Fold change (FC) of SubG1 events in co-treated *versus* bDHC-treated cells (arbitrarily considered as 100%). Values are mean of three independent experiments −/+ SD. **B.** Left panel: RT-PCR analysis following CHOP inactivation. Values indicate the quantification of CHOP mRNA levels relative to actin. Right panel: Fold change (FC) of SubG1 events of CHOP inactivated bDHC-cells *versus* bDHC-treated cells (arbitrarily set at 100%). **C.** Effects of co-incubation of bDHC-treated cells with Cycloheximide (CHX). Left and middle left panels: Protein and mRNA expression levels of the indicated genes. Middle right panel: LC3-II levels were quantitated *versus* actin, before and after Cycloheximide co-administration. Right panel: Fold change (FC) of SubG1 events in co-treated *versus* bDHC-treated cells (arbitrarily considered as 100%). Values are mean of three independent experiments −/+ SD.
doi:10.1371/journal.pone.0053664.g008

treatment (Fig. 5). The activation of ER stress response, and in particular of CHOP, could determine the transcriptional down-regulation of the anti-apoptotic Bcl-2, in a p53-independent manner.

Murine caspase 12 and human caspase 4 have been described to be cleaved by ER stress inducing agents, and to participate to ER-induced apoptosis [55,56]. Moreover, human cells treated with siRNA targeting caspase 4 were resistant to ER-stress induced apoptosis [55].

In agreement with these data, we detected the cleavage of caspase 4 following bDHC administration to HCT116 cells, and a clear decrease of apoptosis was determined by preventing its activation with LEVD (Fig. 3C and Fig. 7B). Consistently with recent results demonstrating a novel ER stress-triggered caspase cascade initiated by caspase 4 and involving caspase 8 [79], LEVD co-administration to cells resulted in a decrease not only of cleaved-caspase 4, but also of cleaved-caspase 8, suggesting that ER stress-induced caspase 4 leads to caspase 8 processing in HCT116 cells (Fig. 3C).

Accumulating data indicate that ER stress can trigger autophagy [80,81,82]. In the case of Unfolded Protein Response (UPR), stimulation of autophagy can be required to activate the cell death machinery [83]. The UPR and autophagic process can work independently from each other, or they can share their cytoprotective or cytocidial functions, depending on the type and duration of the cellular stress [84].

The intricate cross-talk between apoptosis and autophagy is crucial to the overall fate of the cell. Indeed, the final outcome of autophagy depends on (i) the stress-inducing stimulus and (ii) the cellular context: autophagy can help ER-stressed cells to survive, contributing to the elimination of unfolded proteins, or can take part to ER stress induced cell death [85].

In this study we have shown that autophagy induced by bDHC is a consequence of ER stress and has an important role in the activation of cell death. In fact, when apoptosis is inhibited

through ZVAD and LEVD, ER stress and autophagy are still active in bDHC-treated cells. On the other hand, following pharmacological inhibition of autophagy by Wortmannin or Chloroquine, apoptosis is strongly attenuated, suggesting that bDHC-induced autophagy occurs upstream of apoptosis (Fig. 7C and Fig. S4C). To better investigate the role of autophagy, we inactivated both Beclin1 and ATG7, known autophagy related genes. The analysis of LC3-II levels upon RNAi in bDHC cells highlights that Beclin1 has a marginal function in bDHC-autophagy, and consequently its inactivation doesn't prevent autophagic cell death. This was quite expected considering that Beclin1 has been mainly involved in starvation- rather than drug-induced autophagy. Moreover, decreased levels of Beclin1 protein observed following bDHC administration are consistent with its exclusion from bDHC-autophagy process (Fig. 7D). In particular, time-course analysis shows that Beclin1 levels are already reduced upon 8 hours of bDHC treatment, before autophagy is activated (data not shown). In contrast to Beclin1, Atg7 silencing results in a significant decrease in LC3-II accumulation and alters cell death response to bDHC.

Although the suppression of autophagy reduces SubG1 population, neither Wortmannin/Chloroquine nor ATG7 knock-down can completely rescue the loss of cell viability caused by bDHC, hinting at an independent apoptotic pathway running parallel to the autophagic-mediated cell death. This is also consistent with the percentage of apoptosis detected in HCT116/E6, which can't activate autophagy (Fig. S4B). Nevertheless, both autophagic-dependent and -independent cell death seems to be triggered by ER stress.

The increase of poly-ubiquitinated proteins in bDHC treated cells, fully suppressed by Cycloheximide (Fig. S4D), hints at a possible activity of bDHC as proteasome inhibitor, as well as reported for Curcumin [59,60]. The lack of p53 doesn't reduce proteins poly-ubiquitination, suggesting once again that p53 has a possible role downstream ER stress response in the activation of autophagic-cell death.

Although bDHC has shown enhanced anti-proliferative activity compared to Curcumin in HCT116 and LOVO cells, its high IC50 concentration could limit its possible development in clinical application. With the purpose to reduce the dose necessary to activate bDHC-cell death in tumor cells, we have recently designed and tested a bDHC-analog, by inserting an alkali group in C-3 position of bDHC backbone (C3-bDHC) [86]. C3-bDHC has improved chemical stability in physiological conditions and it exerts anti-proliferative activity in HCT116 and LOVO cells at 10-fold lower concentration compared to bDHC (IC50 = 3 μM in HCT116 and 4 μM in LOVO cells) [86]. Our preliminary data support that C3-bDHC is able to induce autophagy and cell death in HCT116 even better than its lead compound (Fig. S5).

Overall, we demonstrated that bDHC exerts a selective cytotoxic activity on colon cancer cells, through the activation of ER-stress induced autophagic cell death, providing new evidence that autophagy is an effective inducer of cell death.

Further studies are needed to better characterize bDHC and its derivatives [86,87], new possible candidates for promising therapies to prevent or treat colon cancer diseases through their pro-autophagic activity.

## Supporting Information

**Figure S1** **A.** Percentages of 4n phospho-Ser10H3 positive HCT116 cells (black bars) counted out of a total number of 4n cells (grey bars) after DMSO, Curcumin and bDHC treatments for 16 and 24 hours. **B.** Scanning Electron Microscopy images of control and bDHC-treated HCT116 cells. Scale bar: 5 μm. **C.** Left panel: Distribution of LOVO cells into the different phases of the cell cycle following treatment with DMSO or bDHC for 24 hours. The percentages are means of three independent experiments −/+ SD. Right panel: γH2AX expression levels in LOVO cells treated with bDHC compared to DMSO control cells. Actin was used as loading control. **D.** Western blot analysis of γH2AX expression following bDHC administration to HF (left panel) and WRL68 cells (right panel) for 24 and 48 hours. Actin was used as loading control.
(TIF)

**Figure S2** **A.** Quantification of the expression levels of γH2AX, p53 and p21 *versus* actin in HCT116 cells co-treated with ZVAD or incubated with DMSO and bDHC alone (Western blots shown in Fig. 3A). **B.** Cytoplasmic (left panel) and mitochondrial/nuclear Cytochrome C levels following time-dependent administration of bDHC. Adriamycin (ADR) was used as positive control (Western blots shown in Fig. 3C). **C.** Quantification of the expression levels of Bcl2α, Bcl-XL and BAX *versus* actin in total cellular extracts of DMSO and bDHC treated cells (Western blots shown in Fig. 4A). **D.** Expression levels of γH2AX and cleaved PARP-1 in HCT116 cells co-treated with ZVAD (left panel) or Wortmannin (WORT) and bDHC (Western blot shown in Fig. 7A). **E.** Beclin1 (BCN1) and ATG7 expression levels normalized to actin levels in BCN1 (left panel) and ATG7 (right panel) silenced cells untreated or treated with bDHC (Western blots shown in Fig. 7B). **F.** Quantification of the expression levels of γH2AX and cleaved PARP1 *versus* actin in HCT116 cells treated with bDHC or co-incubated with Cycloheximide (CHX) and bDHC (Western blots shown in Fig. 8C). All the indicated values are mean of at least three independent experiments −/+ SD.
(TIF)

**Figure S3** **A.** Ratio of LC3-II/LC3-I expression levels normalized to actin following DMSO and time dependent exposure of HCT116 cells to bDHC. **B.** LC3-II/LC3-I ratio in DMSO and bDHC cells co-treated with ZVAD or Wortmannin (WORT) *versus* DMSO. **C.** LC3-II/LC3-I ratio in Beclin1 (BCN1) and ATG7 inactivated cells following DMSO or bDHC administration. **D.** Ratio of LC3-II/LC3-I expression levels upon co-incubation of Cycloheximide (CHX) with bDHC compared to DMSO. Basal LC3-II/LC3-I ratio in control cells has been arbitrarily set at 1. All the indicated values are means of three independent experiments, *$P<0.05$, **$P<0.01$.
(TIF)

**Figure S4** **A.** Left panel: Western blot analysis of LC3 expression following 24 and 48 hours of bDHC exposure in HF cells. Right panel indicates the levels of LC3-II *versus* actin following time-dependent exposure to bDHC. Values are means of three independent experiments. **B.** Upper left panels: LC3 expression levels in HCT116/E6 compared to HCT116 cells. Upper right panel: Quantification of LC3-II *versus* actin levels in HCT116/E6 cells incubated with bDHC for 16 and 24 hours. Lower left panel: Distribution of HCT116/E6 cells throughout the different phases of the cell cycle (PI monoparametric analysis), following DMSO and bDHC administration for 24 hours. Lower right panel: Western blot analysis of poly-ubiquitinated proteins in HCT116/E6 after bDHC treatment for 24 hours. **C.** Left panel: LC3, γ-H2AX and PARP1 levels in DMSO and bDHC cells co-treated with Chloroquine (CQ). Actin was used as loading control. Middle panel: LC3-II/LC3-I ratio in DMSO and bDHC cells co-treated with Chloroquine. LC3-II/LC3-I ratio in DMSO cells has been arbitrarily set at 1. Values are means of three independent experiments, *$P<0.05$, **$P<0.01$. Right panel: Fold change (FC)

of SubG1 events of HCT116 cells co-incubated with bDHC and Chloroquine (CQ) compared to bDHC-treated cells (arbitrarily considered as 100%). **D.** Left panel: Western blot with anti-ubiquitin antibody of total cellular extracts of DMSO and bDHC-treated cells co-incubated with ZVAD, Wortmannin, Chloroquine and Cycloheximide. Middle panel: Time-dependent effect of Salubrinal co-treatment on proteins poly-ubiquitination. Actin was used as internal loading control. Right panel: Western blot of poly-ubiquitinated proteins in HCT116 total extracts after CHOP inactivation, with or without bDHC co-treatment.
(TIF)

**Figure S5** Left panel: Western blot analysis of LC3 expression in HCT116 cells treated with DMSO, bDHC and C3-bDHC for 24 hours. Right panel: PI/FACS cell cycle analysis of HCT116 cells following incubation with DMSO and C3-bDHC for 24 hours. Values are means of three independent experiments −/+ SD.
(TIF)

## Acknowledgments

We thank Serena Carra (University of Modena and Reggio Emilia) for helpful comments and suggestions.

## Author Contributions

Conceived and designed the experiments: CI VB. Performed the experiments: VB SB EF CG SG DQ. Analyzed the data: CI SB VB. Contributed reagents/materials/analysis tools: MS. Wrote the paper: CI.

## References

1. Taylor RC, Cullen SP, Martin SJ (2008) Apoptosis: controlled demolition at the cellular level. Nat Rev Mol Cell Biol 9: 231–241.
2. Igney FH, Krammer PH (2002) Death and anti-death: tumour resistance to apoptosis. Nat Rev Cancer 2: 277–288.
3. Cuervo AM (2004) Autophagy: many paths to the same end. Mol Cell Biochem 263: 55–72.
4. Cuervo AM, Macian F (2011) Autophagy, nutrition and immunology. Mol Aspects Med 33: 2–13.
5. Yorimitsu T, Klionsky DJ (2005) Autophagy: molecular machinery for self-eating. Cell Death Differ 12 Suppl 2: 1542–1552.
6. Yang Z, Klionsky DJ (2009) Mammalian autophagy: core molecular machinery and signaling regulation. Curr Opin Cell Biol 22: 124–131.
7. He C, Klionsky DJ (2009) Regulation mechanisms and signaling pathways of autophagy. Annu Rev Genet 43: 67–93.
8. Eskelinen EL (2005) Doctor Jekyll and Mister Hyde: autophagy can promote both cell survival and cell death. Cell Death Differ 12 Suppl 2: 1468–1472.
9. Maiuri MC, Zalckvar E, Kimchi A, Kroemer G (2007) Self-eating and self-killing: crosstalk between autophagy and apoptosis. Nat Rev Mol Cell Biol 8: 741–752.
10. Kroemer G, Levine B (2008) Autophagic cell death: the story of a misnomer. Nat Rev Mol Cell Biol 9: 1004–1010.
11. Green DR, Kroemer G (2009) Cytoplasmic functions of the tumour suppressor p53. Nature 458: 1127–1130.
12. Crighton D, Wilkinson S, O'Prey J, Syed N, Smith P, et al. (2006) DRAM, a p53-induced modulator of autophagy, is critical for apoptosis. Cell 126: 121–134.
13. Feng Z, Zhang H, Levine AJ, Jin S (2005) The coordinate regulation of the p53 and mTOR pathways in cells. Proc Natl Acad Sci U S A 102: 8204–8209.
14. Tasdemir E, Maiuri MC, Galluzzi L, Vitale I, Djavaheri-Mergny M, et al. (2008) Regulation of autophagy by cytoplasmic p53. Nat Cell Biol 10: 676–687.
15. Levine B, Sinha S, Kroemer G (2008) Bcl-2 family members: dual regulators of apoptosis and autophagy. Autophagy 4: 600–606.
16. Eisenberg-Lerner A, Bialik S, Simon HU, Kimchi A (2009) Life and death partners: apoptosis, autophagy and the cross-talk between them. Cell Death Differ 16: 966–975.
17. Singletary K, Milner J (2008) Diet, autophagy, and cancer: a review. Cancer Epidemiol Biomarkers Prev 17: 1596–1610.
18. Zhang X, Chen LX, Ouyang L, Cheng Y, Liu B (2012) Plant natural compounds: targeting pathways of autophagy as anti-cancer therapeutic agents. Cell Prolif 45: 466–476.
19. Hatcher H, Planalp R, Cho J, Torti FM, Torti SV (2008) Curcumin: from ancient medicine to current clinical trials. Cell Mol Life Sci 65: 1631–1652.
20. Basile V, Ferrari E, Lazzari S, Belluti S, Pignedoli F, et al. (2009) Curcumin derivatives: molecular basis of their anti-cancer activity. Biochem Pharmacol 78: 1305–1315.
21. Chen A, Xu J, Johnson AC (2006) Curcumin inhibits human colon cancer cell growth by suppressing gene expression of epidermal growth factor receptor through reducing the activity of the transcription factor Egr-1. Oncogene 25: 278–287.
22. He ZY, Shi CB, Wen H, Li FL, Wang BL, et al. (2011) Upregulation of p53 expression in patients with colorectal cancer by administration of curcumin. Cancer Invest 29: 208–213.
23. Ramachandran C, Rodriguez S, Ramachandran R, Raveendran Nair PK, Fonseca H, et al. (2005) Expression profiles of apoptotic genes induced by curcumin in human breast cancer and mammary epithelial cell lines. Anticancer Res 25: 3293–3302.
24. Reuter S, Eifes S, Dicato M, Aggarwal BB, Diederich M (2008) Modulation of anti-apoptotic and survival pathways by curcumin as a strategy to induce apoptosis in cancer cells. Biochem Pharmacol 76: 1340–1351.
25. Bielak-Mijewska A, Piwocka K, Magalska A, Sikora E (2004) P-glycoprotein expression does not change the apoptotic pathway induced by curcumin in HL-60 cells. Cancer Chemother Pharmacol 53: 179–185.
26. Bush JA, Cheung KJ, Jr., Li G (2001) Curcumin induces apoptosis in human melanoma cells through a Fas receptor/caspase-8 pathway independent of p53. Exp Cell Res 271: 305–314.
27. Moragoda L, Jaszewski R, Majumdar AP (2001) Curcumin induced modulation of cell cycle and apoptosis in gastric and colon cancer cells. Anticancer Res 21: 873–878.
28. Wang L, Song R, Shen Y, Sun Y, Gu Y, et al. (2011) Targeting sarcoplasmic/endoplasmic reticulum Ca(2)+-ATPase 2 by curcumin induces ER stress-associated apoptosis for treating human liposarcoma. Mol Cancer Ther 10: 461–471.
29. Wu SH, Hang LW, Yang JS, Chen HY, Lin HY, et al. (2010) Curcumin induces apoptosis in human non-small cell lung cancer NCI-H460 cells through ER stress and caspase cascade- and mitochondria-dependent pathways. Anticancer Res 30: 2125–2133.
30. Ng AP, Chng WJ, Khan M (2011) Curcumin sensitizes acute promyelocytic leukemia cells to unfolded protein response-induced apoptosis by blocking the loss of misfolded N-CoR protein. Mol Cancer Res 9: 878–888.
31. Aoki H, Takada Y, Kondo S, Sawaya R, Aggarwal BB, et al. (2007) Evidence that curcumin suppresses the growth of malignant gliomas in vitro and in vivo through induction of autophagy: role of Akt and extracellular signal-regulated kinase signaling pathways. Mol Pharmacol 72: 29–39.
32. Pallauf K, Rimbach G (2012) Autophagy, polyphenols and healthy ageing. Ageing Res Rev.
33. Wu JC, Lai CS, Badmaev V, Nagabhushanam K, Ho CT, et al. (2011) Tetrahydrocurcumin, a major metabolite of curcumin, induced autophagic cell death through coordinative modulation of PI3K/Akt-mTOR and MAPK signaling pathways in human leukemia HL-60 cells. Mol Nutr Food Res 55: 1646–1654.
34. Zhuang W, Long L, Zheng B, Ji W, Yang N, et al. (2011) Curcumin promotes differentiation of glioma-initiating cells by inducing autophagy. Cancer Sci 103: 684–690.
35. Anand P, Kunnumakkara AB, Newman RA, Aggarwal BB (2007) Bioavailability of curcumin: problems and promises. Mol Pharm 4: 807–818.
36. Anand P, Thomas SG, Kunnumakkara AB, Sundaram C, Harikumar KB, et al. (2008) Biological activities of curcumin and its analogues (Congeners) made by man and Mother Nature. Biochem Pharmacol 76: 1590–1611.
37. Fuchs JR, Pandit B, Bhasin D, Etter JP, Regan N, et al. (2009) Structure-activity relationship studies of curcumin analogues. Bioorg Med Chem Lett 19: 2065–2069.
38. Benatti P, Dolfini D, Vigano A, Ravo M, Weisz A, et al. (2011) Specific inhibition of NF-Y subunits triggers different cell proliferation defects. Nucleic Acids Res 39: 5356–5368.
39. Basile V, Mantovani R, Imbriano C (2006) DNA damage promotes histone deacetylase 4 nuclear localization and repression of G2/M promoters, via p53 C-terminal lysines. J Biol Chem 281: 2347–2357.
40. Priault M, Hue E, Marhuenda F, Pilet P, Oliver L, et al. (2010) Differential dependence on Beclin 1 for the regulation of pro-survival autophagy by Bcl-2 and Bcl-xL in HCT116 colorectal cancer cells. PLoS One 5: e8755.
41. Hoyer-Hansen M, Bastholm L, Szyniarowski P, Campanella M, Szabadkai G, et al. (2007) Control of macroautophagy by calcium, calmodulin-dependent kinase kinase-beta, and Bcl-2. Mol Cell 25: 193–205.
42. Benatti P, Basile V, Merico D, Fantoni LI, Tagliafico E, et al. (2008) A balance between NF-Y and p53 governs the pro- and anti-apoptotic transcriptional response. Nucleic Acids Res 36: 1415–1428.
43. Donati G, Imbriano C, Mantovani R (2006) Dynamic recruitment of transcription factors and epigenetic changes on the ER stress response gene promoters. Nucleic Acids Res 34: 3116–3127.
44. Martens JH, O'Sullivan RJ, Braunschweig U, Opravil S, Radolf M, et al. (2005) The profile of repeat-associated histone lysine methylation states in the mouse epigenome. EMBO J 24: 800–812.

45. Rogakou EP, Nieves-Neira W, Boon C, Pommier Y, Bonner WM (2000) Initiation of DNA fragmentation during apoptosis induces phosphorylation of H2AX histone at serine 139. J Biol Chem 275: 9390–9395.
46. Bernardi P, Scorrano L, Colonna R, Petronilli V, Di Lisa F (1999) Mitochondria and cell death. Mechanistic aspects and methodological issues. Eur J Biochem 264: 687–701.
47. Kroemer G, Reed JC (2000) Mitochondrial control of cell death. Nat Med 6: 513–519.
48. Moll UM, Wolff S, Speidel D, Deppert W (2005) Transcription-independent pro-apoptotic functions of p53. Curr Opin Cell Biol 17: 631–636.
49. Reimertz C, Kogel D, Rami A, Chittenden T, Prehn JH (2003) Gene expression during ER stress-induced apoptosis in neurons: induction of the BH3-only protein Bbc3/PUMA and activation of the mitochondrial apoptosis pathway. J Cell Biol 162: 587–597.
50. You H, Pellegrini M, Tsuchihara K, Yamamoto K, Hacker G, et al. (2006) FOXO3a-dependent regulation of Puma in response to cytokine/growth factor withdrawal. J Exp Med 203: 1657–1663.
51. Melino G, Bernassola F, Ranalli M, Yee K, Zong WX, et al. (2004) p73 Induces apoptosis via PUMA transactivation and Bax mitochondrial translocation. J Biol Chem 279: 8076–8083.
52. Hershko T, Ginsberg D (2004) Up-regulation of Bcl-2 homology 3 (BH3)-only proteins by E2F1 mediates apoptosis. J Biol Chem 279: 8627–8634.
53. Jullig M, Zhang WV, Ferreira A, Stott NS (2006) MG132 induced apoptosis is associated with p53-independent induction of pro-apoptotic Noxa and transcriptional activity of beta-catenin. Apoptosis 11: 627–641.
54. Faitova J, Krekac D, Hrstka R, Vojtesek B (2006) Endoplasmic reticulum stress and apoptosis. Cell Mol Biol Lett 11: 488–505.
55. Hitomi J, Katayama T, Eguchi Y, Kudo T, Taniguchi M, et al. (2004) Involvement of caspase-4 in endoplasmic reticulum stress-induced apoptosis and Abeta-induced cell death. J Cell Biol 165: 347–356.
56. Nakagawa T, Zhu H, Morishima N, Li E, Xu J, et al. (2000) Caspase-12 mediates endoplasmic-reticulum-specific apoptosis and cytotoxicity by amyloid-beta. Nature 403: 98–103.
57. Szegezdi E, Logue SE, Gorman AM, Samali A (2006) Mediators of endoplasmic reticulum stress-induced apoptosis. EMBO Rep 7: 880–885.
58. Yamaguchi H, Wang HG (2004) CHOP is involved in endoplasmic reticulum stress-induced apoptosis by enhancing DR5 expression in human carcinoma cells. J Biol Chem 279: 45495–45502.
59. Milacic V, Banerjee S, Landis-Piwowar KR, Sarkar FH, Majumdar AP, et al. (2008) Curcumin inhibits the proteasome activity in human colon cancer cells in vitro and in vivo. Cancer Res 68: 7283–7292.
60. Yoon MJ, Kim EH, Lim JH, Kwon TK, Choi KS (2009) Superoxide anion and proteasomal dysfunction contribute to curcumin-induced paraptosis of malignant breast cancer cells. Free Radic Biol Med 48: 713–726.
61. Paglin S, Hollister T, Delohery T, Hackett N, McMahill M, et al. (2001) A novel response of cancer cells to radiation involves autophagy and formation of acidic vesicles. Cancer Res 61: 439–444.
62. Kroemer G, Galluzzi L, Vandenabeele P, Abrams J, Alnemri ES, et al. (2009) Classification of cell death: recommendations of the Nomenclature Committee on Cell Death 2009. Cell Death Differ 16: 3–11.
63. Klionsky DJ, Abeliovich H, Agostinis P, Agrawal DK, Aliev G, et al. (2008) Guidelines for the use and interpretation of assays for monitoring autophagy in higher eukaryotes. Autophagy 4: 151–175.
64. Fass E, Shvets E, Degani I, Hirschberg K, Elazar Z (2006) Microtubules support production of starvation-induced autophagosomes but not their targeting and fusion with lysosomes. J Biol Chem 281: 36303–36316.
65. Boyce M, Bryant KF, Jousse C, Long K, Harding HP, et al. (2005) A selective inhibitor of eIF2alpha dephosphorylation protects cells from ER stress. Science 307: 935–939.
66. Jiang Z, Jin S, Yalowich JC, Brown KD, Rajasekaran B (2010) The mismatch repair system modulates curcumin sensitivity through induction of DNA strand breaks and activation of G2-M checkpoint. Mol Cancer Ther 9: 558–568.
67. Ravindran J, Prasad S, Aggarwal BB (2009) Curcumin and cancer cells: how many ways can curry kill tumor cells selectively? AAPS J 11: 495–510.
68. Ireson CR, Jones DJ, Orr S, Coughtrie MW, Boocock DJ, et al. (2002) Metabolism of the cancer chemopreventive agent curcumin in human and rat intestine. Cancer Epidemiol Biomarkers Prev 11: 105–111.
69. Anand P, Sundaram C, Jhurani S, Kunnumakkara AB, Aggarwal BB (2008) Curcumin and cancer: an ''old-age'' disease with an ''age-old'' solution. Cancer Lett 267: 133–164.
70. Zamzami N, Marchetti P, Castedo M, Zanin C, Vayssiere JL, et al. (1995) Reduction in mitochondrial potential constitutes an early irreversible step of programmed lymphocyte death in vivo. J Exp Med 181: 1661–1672.
71. Donovan M, Cotter TG (2004) Control of mitochondrial integrity by Bcl-2 family members and caspase-independent cell death. Biochim Biophys Acta 1644: 133–147.
72. Baliga B, Kumar S (2003) Apaf-1/cytochrome c apoptosome: an essential initiator of caspase activation or just a sideshow? Cell Death Differ 10: 16–18.
73. Bonner WM, Redon CE, Dickey JS, Nakamura AJ, Sedelnikova OA, et al. (2008) GammaH2AX and cancer. Nat Rev Cancer 8: 957–967.
74. Lu C, Zhu F, Cho YY, Tang F, Zykova T, et al. (2006) Cell apoptosis: requirement of H2AX in DNA ladder formation, but not for the activation of caspase-3. Mol Cell 23: 121–132.
75. Baritaud M, Cabon L, Delavallee L, Galan-Malo P, Gilles ME, et al. (2012) AIF-mediated caspase-independent necroptosis requires ATM and DNA-PK-induced histone H2AX Ser139 phosphorylation. Cell Death Dis 3: e390.
76. Speidel D (2009) Transcription-independent p53 apoptosis: an alternative route to death. Trends Cell Biol 20: 14–24.
77. Kim H, Tu HC, Ren D, Takeuchi O, Jeffers JR, et al. (2009) Stepwise activation of BAX and BAK by tBID, BIM, and PUMA initiates mitochondrial apoptosis. Mol Cell 36: 487–499.
78. Qin JZ, Ziffra J, Stennett L, Bodner B, Bonish BK, et al. (2005) Proteasome inhibitors trigger NOXA-mediated apoptosis in melanoma and myeloma cells. Cancer Res 65: 6282–6293.
79. Rosati E, Sabatini R, Rampino G, De Falco F, Di Ianni M, et al. (2011) Novel targets for endoplasmic reticulum stress-induced apoptosis in B-CLL. Blood 116: 2713–2723.
80. Bernales S, McDonald KL, Walter P (2006) Autophagy counterbalances endoplasmic reticulum expansion during the unfolded protein response. PLoS Biol 4: e423.
81. Ogata M, Hino S, Saito A, Morikawa K, Kondo S, et al. (2006) Autophagy is activated for cell survival after endoplasmic reticulum stress. Mol Cell Biol 26: 9220–9231.
82. Yorimitsu T, Nair U, Yang Z, Klionsky DJ (2006) Endoplasmic reticulum stress triggers autophagy. J Biol Chem 281: 30299–30304.
83. Levine B, Yuan J (2005) Autophagy in cell death: an innocent convict? J Clin Invest 115: 2679–2688.
84. Verfaillie T, Salazar M, Velasco G, Agostinis P (2010) Linking ER Stress to Autophagy: Potential Implications for Cancer Therapy. Int J Cell Biol 2010: 930509.
85. Ding WX, Ni HM, Gao W, Hou YF, Melan MA, et al. (2007) Differential effects of endoplasmic reticulum stress-induced autophagy on cell survival. J Biol Chem 282: 4702–4710.
86. Ferrari E, Pignedoli F, Imbriano C, Marverti G, Basile V, et al. (2011) Newly synthesized curcumin derivatives: crosstalk between chemico-physical properties and biological activity. J Med Chem 54: 8066–8077.
87. Nardo L, Maspero A, Selva M, Bondani M, Palmisano G, et al. (2012) Excited-State Dynamics of Bis-dehydroxycurcumin Carboxylic Acid, a Water-Soluble Derivative of the Photosensitizer Curcumin. J Phys Chem A 116: 9321–9330.